UNIVERSITY OF READING

Department of Meteorology

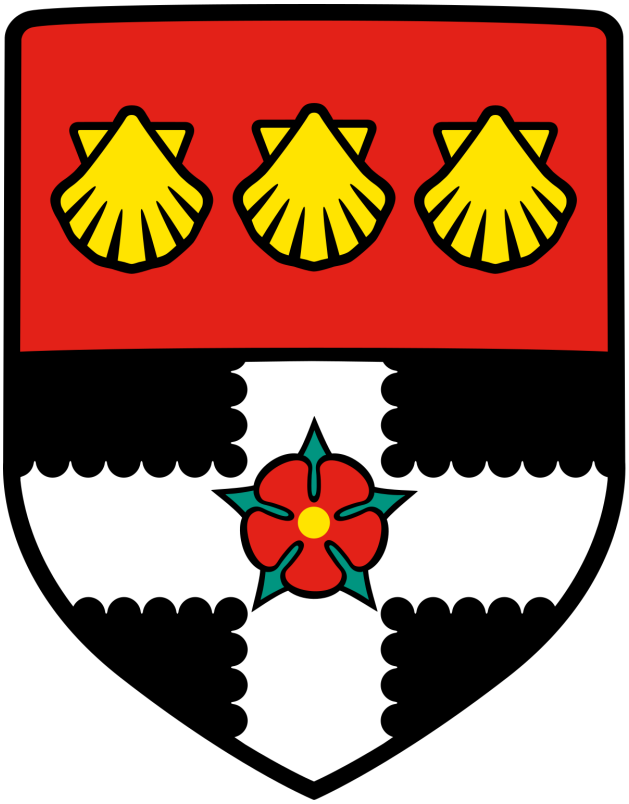

Serial Clustering of Extratropical Cyclones over Western Europe: Dynamics and Associated Impacts

MATTHEW DAVID KENNETH PRIESTLEY

A thesis submitted for the degree of Doctor of Philosophy

March 2019

DECLARATION

I confirm that this is my own work and the use of all material from other sources has been properly and fully acknowledged.

Matthew Priestley

ABSTRACT

Extratropical cyclones are a key process in the atmospheric variability of the North Atlantic and western Europe. They are associated with heavy precipitation and extreme winds which can result in considerable socio-economic impacts. Throughout the winter season these intense extratropical cyclones have been shown to occur in groups (this is known as clustering), which is more prevalent over the eastern North Atlantic and western Europe.

In this thesis the drivers of cyclone clustering are investigated, particularly focussing on the large-scale dynamical mechanisms and the role secondary cyclones. During clustering events the upper-troposphere over the North Atlantic is characterised by a strong and zonally extended jet which steers large numbers of cyclones toward western Europe. The extended jet is associated with anomalous Rossby wave breaking on one or both flanks, with the balance on each flank being associated with changes in the angle of the jet and the latitude at which the clustering occurs.

Secondary cyclones are objectively identified and are shown to contribute approximately 50% to the increase in cyclone numbers during periods of intense clustering. This increase is mainly a result to the large-scale flow steering more secondary cyclones along a similar track toward western Europe with there also being a slight increase in genesis rate near western Europe.

The climate model HiGEM is used to examine the impact of cyclone clustering on seasonal wind damage estimates across Europe. HiGEM is able to represent the large-scale dynamics associated with clustering and a wind speed proxy, the storm severity index, is used to estimate the associated losses. It is found that clustering acts to increase the losses that are experienced across Europe by 10-20% for high return period seasonal losses compared to a random series of cyclones in a season. These results demonstrate the importance of correctly representing clustering in modelling studies and loss estimations.

DECLARATION OF AUTHORSHIP

The following papers have been included in this thesis. Tthe components carried out by the candidate and the other authors are stated below.

Priestley, M. D. K., J. G. Pinto, H. F. Dacre, and L. C. Shaffrey (2017), Rossby Wave Breaking, the Upper Level Jet, and Serial Clustering of Extratropical Cyclones in Western Europe, Geophysical Research Letters, 44, 514-521, doi:10.1002/2016GL071277.

Priestley, M. D. K., J. G. Pinto, H. F. Dacre, and L. C. Shaffrey (2017), The Role of Cyclone Clustering During the Stormy Winter of 2013/2014. Weather, 72, 187-192. doi:10.1002/wea.3025.

Priestley, M. D. K., H. F. Dacre, L. C. Shaffrey, K. I. Hodges, and J. G. Pinto (2018), The Role of Serial European Windstorm Clustering for Extreme Seasonal Losses as Determined from Multi-centennial Simulations of High-resolution Global Climate Model Data, Natural Hazards and Earth System Sciences, 18, 2991-3006, doi: 10.5194/nhess-18-2991-2018.

Priestley, M. D. K., H. F. Dacre, L. C. Shaffrey, S. Schemm and J. G. Pinto (2019), The Role of Secondary Cyclones and Cyclone Families for the North Atlantic Storm Track and Clustering over Western Europe, Quarterly Journal of the Royal Meteorological Society, *Submitted*.

The concept for all of the above studies was developed by all the authors. The analysis, creation of figures, and writing of the text was completed by M. Priestley. The remainder of the authors provided feedback and comments to produce the final manuscript.

ACKNOWLEDGEMENTS

I owe many people so much for helping me through my time doing my PhD and in the writing of this thesis and I am very grateful to all of them.

First of all to my supervisors: Helen Dacre, Joaquim Pinto, Len Shaffrey, and Alexandros Georgiadis. You've all given large amounts of your time and provided excellent support and guidance whenever I have needed it and for that I will always be thankful. It has been a pleasure to work with you all and I hope to do so again in the future. Further thanks to my monitoring committee members Tom Frame and Nick Klingaman. It was great to always have a fresh pair of eyes and useful questions and discussions whenever we met. Also thanks to Aidan and everyone else at Aon who were beyond helpful during the time I spent working with them. Finally, I am very grateful for the discussions had with my two thesis examiners, Gregor Leckebusch and Nick Klingaman.

Working in Reading has been a pleasure this last few years. I owe special thanks to all the other PhDs and members of staff who made it such an enjoyable place to be. Extra thanks to the people who had to share a house with me, those in 1U07, and all the other friends I've made from the department.

I'm most grateful for the support my family have given me throughout my life and continued education and studies. Finally, I also have to thank Lucy. You've been the most supportive and understanding person I could've asked for throughout all of this and I will always be grateful for everything.

Contents

DECLARATION I

ABSTRACT III

DECLARATION OF AUTHORSHIP IV

ACKNOWLEDGEMENTS V

TABLE OF CONTENTS VI

LIST OF ACRONYMS X

LIST OF MATHEMATICAL SYMBOLS XII

1 INTRODUCTION 1

1.1 Motivation . . . 1
1.2 Extratropical Cyclones . . . 2
1.2.1 Models of Evolution . . . 2
1.2.2 Cyclone Structure . . . 3
1.2.3 Cyclone Formation and Intensification Mechanisms . . . 5
1.3 Storm Tracks . . . 8
1.3.1 Eulerian Approach . . . 8
1.3.2 Objective Tracking of Extratropical Cyclones . . . 9
1.3.3 Storm Track Features of the North Atlantic . . . 11
1.4 Classifying Cyclones . . . 12
1.4.1 Upper versus Lower Level Forcing . . . 12
1.4.2 Secondary Cyclones . . . 13
1.5 Impacts Associated with Extratropical Cyclones . . . 16
1.5.1 Precipitation . . . 16
1.5.2 Wind . . . 17
1.6 European Windstorms . . . 19
1.6.1 Large Scale Dynamical Drivers of European Windstorms . . . 20
1.6.2 Modelling Windstorm Impacts . . . 22
1.7 Clustering . . . 25
1.7.1 Quantifying Clustering . . . 26
1.7.2 Differing Perspectives of Clustering . . . 29
1.7.3 Mechanisms for Clustering . . . 29
1.8 Current Knowledge Gaps . . . 32
1.9 Thesis Aims and Structure . . . 33

2 DATA AND METHODS 35

2.1 Datasets . . . 35
2.1.1 ERA-Interim . . . 35

2.1.2 HiGEM . . . 37
2.2 Objective Cyclone Identification and Tracking Methodologies . . . 38
2.2.1 Murray & Simmonds/Pinto Method . . . 38
2.2.2 Hodges Method . . . 39
2.3 Secondary Cyclones . . . 40
2.3.1 Identifying Synoptic Scale Frontal Features . . . 41
2.3.2 Identifying Cyclogenesis on Fronts . . . 42

3 Rossby Wave Breaking, the Upper Level Jet, and Serial Clustering of Extratropical Cyclones in Western Europe 44
3.1 Abstract . . . 45
3.2 Introduction . . . 45
3.3 Data & Methods . . . 46
3.4 RWB and Cyclone Clustering in the Winter of 2013/14 . . . 48
3.5 RWB and Cyclone Clustering in ERA-Interim . . . 50
3.6 The Temporal Evolution of the RWB and the Jet during Clustering . . . 52
3.7 Dynamical Variability of Clustering . . . 53
3.8 Conclusions . . . 56

4 The Role of Cyclone Clustering During the Stormy Winter of 2013/2014 58
4.1 Abstract . . . 59
4.2 Introduction . . . 59
4.3 Data and Methods . . . 61
4.4 Analysis of 2013/2014 . . . 62
4.4.1 Precipitation Associated with Cyclone Tini . . . 62
4.4.2 Identification and analysis of clustering and associated cyclone family . . . 63
4.4.3 Large-scale Dynamics of Observed DJF1314 Clustering . . . 65
4.5 Discussion and Conclusions . . . 67

5 The Role of Secondary Cyclones and Cyclone Families for the North Atlantic Storm Track and Clustering over Western Europe 69
5.1 Abstract . . . 70
5.2 Introduction . . . 71
5.3 Data and Methodology . . . 74
5.3.1 Dataset . . . 74
5.3.2 Cyclone and Front Identification . . . 74
5.3.3 Classifying Secondary Cyclogenesis . . . 75
5.3.4 Large-scale Environmental Variables . . . 76
5.4 Results . . . 78
5.4.1 Climatology of Primary, Secondary+, and Solo Cyclones . . . 78
5.4.2 Structure of a Cyclone Family . . . 82

5.4.3 Large-scale Environmental Conditions at the Time of Primary and Secondary+ Cyclogenesis . . . 86
5.4.4 Secondary+ cyclones and clustering over western Europe . . . 91
5.5 Summary and Discussion . . . 95

6 The Role of Serial European Windstorm Clustering for Extreme Seasonal Losses as Determined from Multi-centennial Simulations of High Resolution Global Climate Model Data 99
6.1 Abstract . . . 100
6.2 Introduction . . . 101
6.3 Data & Methods . . . 103
6.3.1 Datasets . . . 103
6.3.2 Cyclone Identification and Tracking . . . 103
6.3.3 SSI Metric . . . 104
6.3.4 Clustering Measures . . . 106
6.3.5 Return Periods and Statistical Methods . . . 107
6.4 Results . . . 108
6.4.1 Evaluation of Cyclone Clustering in HiGEM . . . 108
6.4.2 Comparison of SSI in ERA-Interim and HiGEM . . . 110
6.4.3 Large Return Period Losses in HiGEM_bc . . . 114
6.5 Discussion & Conclusions . . . 119

7 Discussion and Conclusions 122
7.1 Overview of the Thesis . . . 122
7.2 Key Findings . . . 123
7.2.1 **Q1.** Are clustering events in different locations across western Europe associated with similar large-scale dynamical features? . . . 123
7.2.2 **Q2.** What were the dynamical features that were associated with the clustered winter season of 2013/2014 across the UK? . . . 125
7.2.3 **Q3.** To what extent do secondary cyclones contribute to periods of clustering that affect western Europe? . . . 126
7.2.4 **Q4.** Can windstorm losses associated with extratropical cyclones be represented in climate models for seasonal losses with a return period of 200 years? . . . 128
7.2.5 **Q5.** How important of a contribution does clustering make to the most severe seasons in terms of overall losses? . . . 129
7.3 Implications and Limitations of the Thesis . . . 130
7.3.1 Implications . . . 130
7.3.2 Limitations . . . 131
7.4 Future Work . . . 132
7.5 Key Conclusions . . . 134

Appendix A Changes in Static Stability based on Thermal Wind Balance 136

APPENDIX B CLARIFICATIONS TO THE TEXT **139**

REFERENCES **145**

List of Acronyms

Acronym	Definition
AEP	Annual Exceedance Probability
AEP_random	Randomised Annual Exceedance Probability
CCB	Cold Conveyor Belt
CFSR	Climate Forecast System Reanalysis
CMIP	Coupled Model Intercomparison Project
DI	Dry Intrusion
DI-SSI	Distribution Independent Storm Severity Index
DJF	December, January, February
DJF1314	December, January, February 2013/2014
DWB	Double-Sided Rossby Wave Breaking
EA	East Atlantic Pattern
ECMWF	European Centre for Medium Range Weather Forecasts
ENSO	El Niño Southern Oscillation
ERA	ECMWF Re-Analysis
ERA-I	ERA-Interim
EWP	England-Wales Precipitation Series
GCM	General Circulation Model
GPCP	Global Precipitation Climatology Project
GPD	Generalised Pareto Distribution
HadGEM	Hadley Centre Global Environment Model
HadUKP	Hadley Centre UK Precipitation Series
HiGEM	High-Resolution Global Environment Model
HiGEM_bc	Bias corrected HiGEM
JJA	June, July, August
JRA	Japanese Re-Analysis
MERRA	Modern-Era Retrospective Analysis for Research and Applications
MSLP	Mean Sea Level Pressure
NAO	North Atlantic Oscillation
NCAR	The US National Center for Atmospheric Research
NCEP	The National Centers for Environmental Prediction
NDJFM	November, December, January, February, March
OEP	Occurrence Exceedance Probability

Acronym	Definition
POL	Polar Pattern
PV	Potential Vorticity
PVU	Potential Vorticity Units
RCP	Representative Concentration Pathway
RWB	Rossby Wave Breaking
SCA	Scandinavian Pattern
SJ	Sting Jet
SON	September, October, November
SSI	Storm Severity Index
SST	Sea Surface Temperature
TFP	Thermal Front Parameter
UK	United Kingdom
WCB	Warm Conveyor Belt

LIST OF MATHEMATICAL SYMBOLS

Symbol	Definition	Units
θ	Potential Temperature	K
θ_w	Wet Bulb Potential Temperature	K
θ_e	Equivalent Potential Temperature	K
ρ	Density	kg m^{-3}
f	Coriolis Parameter	rad s^{-1}
p	Mean Sea Level Pressure	hPa
$\nabla^2 p$	Laplacian of Mean Sea Level Pressure	hPa deg.lat.$^{-2}$
ξ	Quasi-Geostrophic Relative Vorticity	s^{-1}
ξ_{850}	Quasi-Geostrophic Relative Vorticity at 850 hPa	s^{-1}
ω	Vertical Velocity	Pa s^{-1}
T	Temperature	K
g	Acceleration due to Gravity	m s^{-2}
τ	Two-Dimensional Thermal Field	K
R	Specific Gas Constant	J kg^{-1} K^{-1}
N^2	Brunt-Väisälä frequency	s^{-2}

Chapter 1:

INTRODUCTION

1.1 Motivation

Across the North Atlantic Ocean and Europe, extratropical cyclones are the most common synoptic-scale weather type. These cyclones can cause significant socio-economic damage when they impact considerably built-up regions of Europe. This damage is exacerbated when many of these intense cyclones pass through the same region in a short period of time. This behaviour is known as clustering and causes elevated economic and insured losses. For example the cyclone series of Anatol, Lothar, and Martin, which affected western and central Europe in December 1999 resulted in $18.7 billion of economic losses ($10.1 billion insured, Munich Re, 2016). Intense cyclones occurring quickly after each other pose significant risks both environmentally and socio-economically, as infrastructure is often more vulnerable following a first event and these sequences can disrupt loss estimations of both insurance and re-insurance companies (Swiss Re, 2016) due to their high monetary impact. Recently the winter season of 2013/2014 was incredibly stormy in the United Kingdom (UK, Kendon and McCarthy, 2015) and resulted in precipitation records being shattered nationally as numerous cyclones propagated across the country throughout the winter season. The occurrence of clustering, and its preferential locations, has been well known in the scientific community for some time (Mailier et al., 2006; Vitolo et al., 2009), but with little attention on the dynamical controls of these events until recently with the analysis of several select events (Pinto et al., 2014). This thesis aims to address the gaps in the knowledge surrounding the clustering of extratropical cyclones across the eastern North Atlantic and western Europe and aims to fully categorise the large-scale atmospheric dynamics associated with these events, and also understand exactly how important the process of clustering is to the damages caused by these cyclones.

The rest of this chapter will evaluate the current state of knowledge surrounding this subject. An overview of extratropical cyclone formation and evolution will be given in section 1.2, with section 1.3 dedicated to a discussion of the mid-latitude storm tracks and specifically focussing on the features of the

North Atlantic storm track. Classifications of extratropical cyclones will be given in section 1.4, with their associated impacts discussed in section 1.5. Section 1.6 reviews the dynamics and impacts of European windstorms, before a discussion on cyclone clustering in section 1.7. Finally, the aims, structure, and science questions addressed in this thesis will be presented in section 1.8.

1.2 Extratropical Cyclones

Extratropical cyclones dominate the day-to-day variability of weather in the mid-latitudes. They are responsible for large amounts of precipitation (Hawcroft et al., 2012) and also cause strong winds which can result in significant damage to infrastructure (Browning, 2004; Leckebusch et al., 2006). They are vitally important for atmospheric energy transport from the tropics to the poles, dominating total atmospheric energy fluxes in the mid-latitudes (Peixoto and Oort, 1992; Kaspi and Schneider, 2013). They also help to reinforce the mean westerly flow in the extratropics through fluxes of momentum and heat (Woollings et al., 2010b; Barnes and Hartmann, 2012). The associated heat-flux of cyclones and the storm track has downstream effects on the latitudinal location of the eddy-driven jet (Novak et al., 2015). These weather systems have been extensively studied for around 100 years. In this section an overview of these weather systems will be given, discussing the methods of formation, and also the cyclone structure and evolution.

1.2.1 Models of Evolution

Extratropical cyclones that dominate the mid-latitudes are known by several names, this can be as already mentioned, or mid-latitude depression, low pressures system, or frontal cyclone, to name but a few. However, the conceptual origin of these systems can be traced back to the work of Bjerknes (1919), and also Bjerknes and Solberg (1922), which present the *"Norwegian Model"* of an extratropical cyclones formation and lifecycle. The work of Bjerknes and Solberg (1922) describes how extratropical cyclones grow on the boundary of a cold and warm airmass, this boundary otherwise being known as the *"polar front"*.

The Norwegian model describes how the two different air masses interact, developing from a near-straight boundary, with cold polar air to the north, and warm tropical air to the south. The model assumes that the two air masses are moving in opposite directions that slowly develops into a wave that bulges on the cold side of the front. The amplitude of this wave increases as the wave propagates eastwards. It is described how precipitation forms on the boundaries between the air masses as the warmer air is forced to rise. With further amplification of this wave, the warm-sector slowly narrows, until the cold air at the rear of the cyclone catches the cold air at the front, causing the warm air to be cut off aloft, and the formation of an occlusion. Eventually the warm air is fully cut-off and a near-symmetric vortex of cold air is then present, which slowly dissipates until cyclone decay.

The model presented by Bjerknes and Solberg (1922) was based on surface observations, and several theoretical studies showed deviations from this model. These differences led to the development of another cyclone formation and development model presented by Shapiro and Keyser (1990). In the *"Shapiro-Keyser model"* the start of the cyclone lifecycle is very similar. However, following this the models differ, with the *"Shapiro-Keyser model"* describing how the warm and cold fronts separate, forming a frontal fracture and a "T-bone" structure. In the final stages the warm air gets wrapped up in the centre of the cyclone, creating a warm seclusion. A comparison of both models is shown in figure 1.1. There is no "one-size fits all" model describing all the lifecycles of all extratropical cyclones, however studies such as Schultz et al. (1998) have shown how some cyclones may be more likely to follow the Norwegian, or Shapiro-Keyser models, depending on whether the flow is more confluent or diffluent.

1.2.2 Cyclone Structure

Both the *"Norwegian"* and the *"Shapiro-Keyser"* models for extratropical cyclones introduce these phenomena as developing from an initial frontal disturbance. Throughout the last ∼100 years these models have been developed further and built on. Extratropical cyclone structure is now commonly referred to using distinct cyclone-relative airstreams. These airstreams have been described in a number of different studies (e.g. Harrold, 1973; Browning and Roberts, 1994; Deveson et al., 2002), with the major airstreams being the warm conveyor belt (WCB), cold conveyor belt (CCB), and dry intrusion (DI). The WCB was first described by Harrold (1973) as a stream of warm moist air, originating at low levels and ahead of the

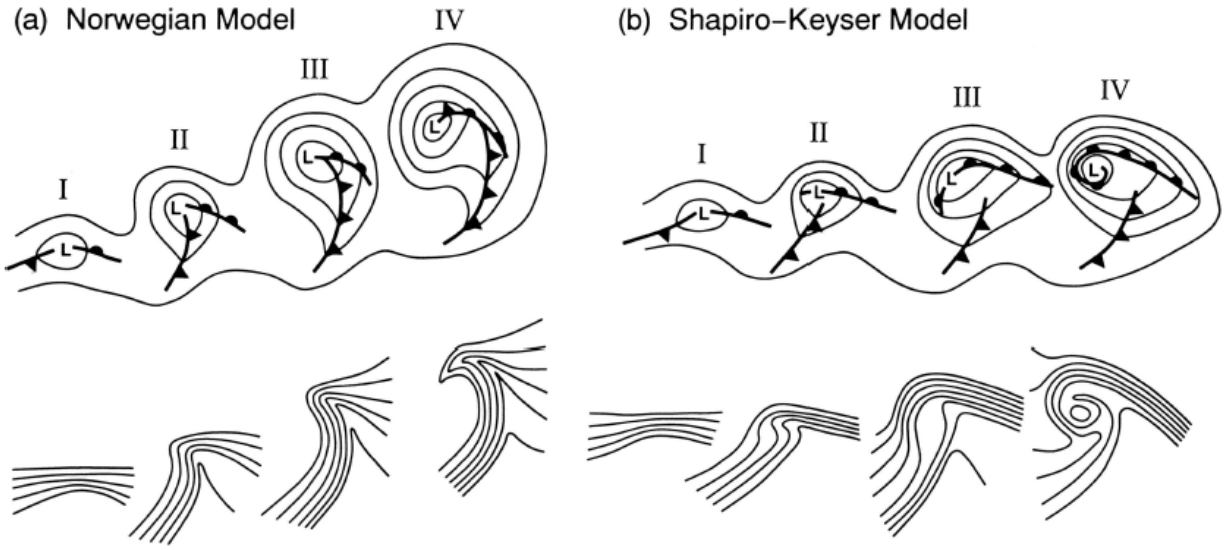

Figure 1.1: *Conceptual models of cyclone evolution showing lower-tropospheric geopotential height and fronts (top), and lower-tropospheric potential temperature (bottom). (a) Norwegian cyclone model: (I) incipient frontal cyclone, (II) and (III) narrowing warm sector, (IV) occlusion; (b) Shapiro-Keyser cyclone model: (I) incipient frontal cyclone, (II) frontal fracture, (III) frontal T-bone and bent-back front, (IV) frontal T-bone and warm seclusion. Figure and caption from Schultz et al. (1998).*

surface cold front. These features then ascend rapidly over a period of 2-3 days, leading to condensation, formation of a cloud head, and precipitation (Eckhardt et al., 2004). This precipitation is on average six times larger than that of other low-level originating airstreams in the extratropics. The WCB then turns either anticyclonically (Carlson, 1980), or cyclonically (Browning and Roberts, 1994) forming the upper branch of the cyclone cloud head. Eckhardt et al. (2004) showed how most wintertime cyclones in the Northern Hemisphere are associated with a WCB, although they are not features of all extratropical cyclones globally. WCBs play an important role in extreme precipitation, with more than 90% of extreme precipitation cases associated with a WCB (Catto et al., 2015).

The CCB initially travels in the opposite direction to the propagation of the cyclone and forms in the cold air mass on the poleward side of the warm front. The CCB was first identified by Carlson (1980) via isentropic analysis to be initially below the WCB before turning anticyclonically and rapidly ascending. Schultz (2001) demonstrated that there are generally two branches to the CCB, one turning anticyclonically (as in Carlson, 1980), and one turning cyclonically around the centre of the low pressure minima, and remaining more in the lower troposphere. On occasion the cyclonically turning CCB can produce a strong winds in the form of a low-level jet as the airstream travels in the same direction as the cyclone on its equatorward flank. The peak winds associated with the low-level jet can be a large driver of windstorm risk and cause large amounts of damage (Smart and Browning, 2014; Hewson and Neu, 2015), but almost only when extratropical cyclones are in their mature phase.

The DI is region of cold dry air which descends behind the cyclone and diverges along the rear of the cold front, some turning cyclonically, some anticyclonically. This air originates near the tropopause and can be associated with a tropopause fold (Browning, 1997) or stratospheric intrusion (Wernli, 1997). The DI helps with the formation of the comma-shaped pattern of the cloud associated with an extratropical cyclone due to the cloud-free nature of the dry air. As the DI descends it can overrun the WCB and cause potential instability (Browning, 1997), often resulting in severe convective activity near to the surface cold front.

A fourth airstream, that is also responsible for strong winds at the surface, is the Sting Jet (SJ). First termed by Browning (2004) the SJ is a region of very strong surface winds between the bent back front and cold front of a *"Shapiro-Keyser"* cyclone. The SJ is distinct from the WCB and CCB (Volonté et al., 2018) and has the unique property that as the air descends, it accelerates (Clark et al., 2005). SJs have been responsible for considerable surface damage in the past, such as the "Great Storm" of 1987 (Hoskins and Berrisford, 1988). A schematic illustrating all of the above described airstreams as in a *"Shapiro-Keyser"* cyclone can be found in figure 1.2.

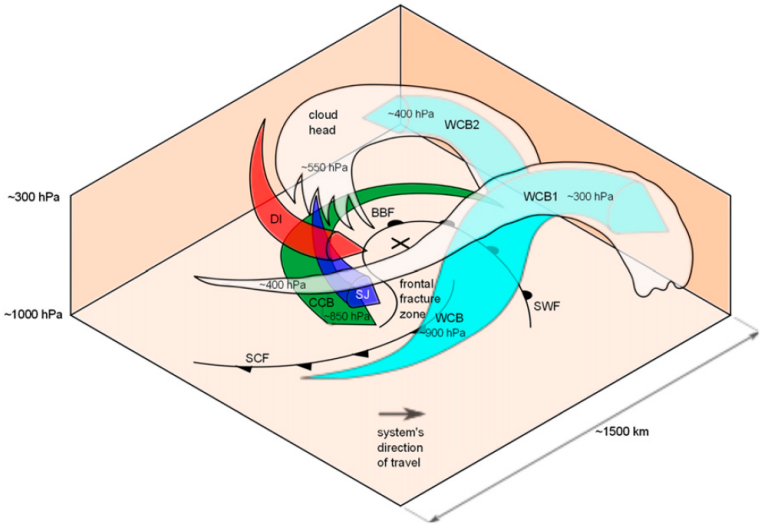

Figure 1.2: *The structure of a Northern Hemisphere Shapiro-Keyser extratropical cyclone. Illustrated are the airstreams of the warm conveyor belt (WCB), cold conveyor belt (CCB), dry intrusion (DI), and the sting jet (SJ). Also shown are the surface warm front (SWF), surface cold front (SCF), the bent back front (BBF), and the cyclone centre (X). Figure from Martínez-Alvarado et al. (2014).*

1.2.3 Cyclone Formation and Intensification Mechanisms

1.2.3.1 Baroclinic Instability

The aforementioned *"Norwegian"* and *"Shaprio-Keyser"* conceptual models all describe the growth of a cyclone from an initial along-front disturbance. One of the primary methods for synoptic-scale wave growth in the mid-latitudes is baroclinic instability (Charney, 1947; Eady, 1949; Holton, 2004). The polar front is an ideal location for high baroclinic instability due to the location of the strong meridional temperature gradient. This temperature gradient is associated with a gradient in the vertical zonal wind, through thermal wind balance. This flow is then unstable to small perturbations and provides an environment that can convert potential energy to kinetic energy through the growth of extratropical cyclones (Holton, 2004).

The Eady model (Eady, 1949) is a mathematical model that describes baroclinic instability. Another similar model is the Charney model (Charney, 1947). Both these models are used as an explanation for mid-latitude cyclogenesis and consists of a basic state with a zonal flow that has constant vertical shear. A small amplitude perturbation is applied to this state to represent an extratropical cyclone. The models differ in their representation of the coriolis force, with the Eady model having a uniform coriolis parameter (f) with latitude (also called f-plane), and the Charney model having a latitudinally varying value of f (also called β-plane). Both these models produce similar baroclinic growth rates. Described in Gill (1982) the fastest growing mode of the Eady model has the following properties:

- The wave on the surface has the warmest air ahead of the surface trough
- The pressure field slopes approximately 90° westwards with height

- The temperature field slopes approximately 90° eastwards with height
- In the mid-troposphere, the warm air moves polewards and ascends, whilst cold air moves equatorwards and descends
- The vertical velocity field tilts westwards with height

The Eady model suggests a reasonable growth rate for cyclones (e-folding time of approx. 1 day), whereas the length scale of this growth is too large. The model suggests a length scale of approximately 2000km, whereas in reality this is likely to be nearer 1000km, with these errors a result of the Eady model not including moist processes (Thorncroft and Hoskins, 1990). The presence of heating, and hence latent heat release in the mid-troposphere acts to create a PV dipole with positive (negative) anomalies below (above) the region of heating (Eliassen and Keinschmidt, 1957; Hoskins et al., 1985; Haynes and McIntyre, 1987; Wernli and Davies, 1997). Emanuel et al. (1987) performed baroclinic lifecycle simulations that included the effects of moisture and found a 250% increase in the growth rate and wavelengths being on average reduced by a factor of 0.6 compared to their dry counterparts. Furthermore Kuo et al. (1991) found that simulations that represented moist processes increased cyclone vertical motion considerably and modified the frontal structure. This increased vertical motion further contributed to an increase in the convergence of moisture into the cyclone. Latent heat release has also been shown to be very important for explosively developing cyclones (Revell and Ridley, 1995), with as much as 50% of the pressure drop in the intensification phase of a cyclone being as a result of the increased latent heat release (Fink et al., 2012; Heo et al., 2015).

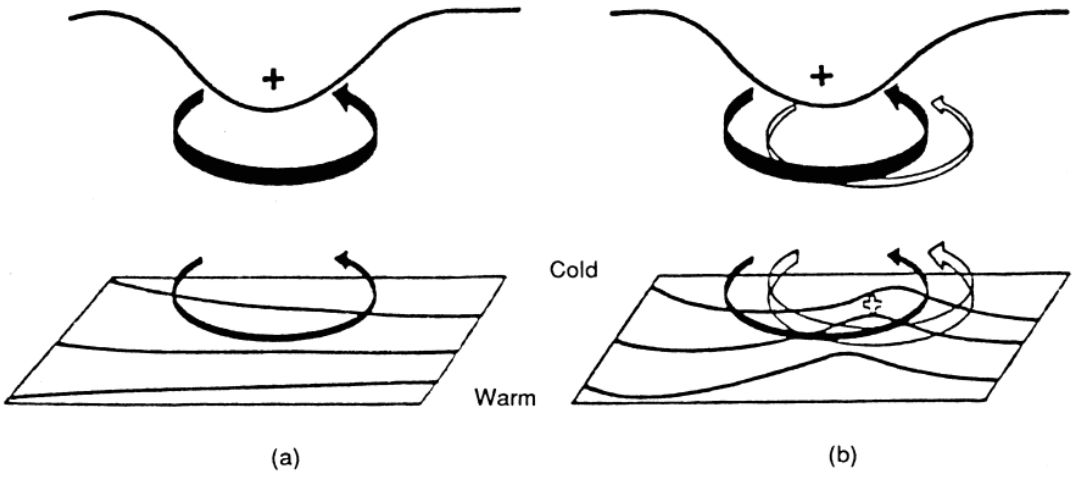

Figure 1.3: *A schematic picture of cyclogenesis associated with the arrival of an upper-level PV perturbation over a lower-level baroclinic region. (a) Lower-level cyclonic vorticity induced by the upper-level PV anomaly. The circulation induced by the PV anomaly is shown by the solid arrows, and potential temperature (θ) contours are shown at the lower boundary. The advection of θ by the induced lower-level circulation leads to a warm anomaly slightly east of the upper-level PV anomaly. This in turn will induce a cyclonic circulation as shown by the open arrows in (b). The induced lower-level circulation will reinforce the original upper-level anomaly and can lead to amplification of the disturbance. Figure and caption from Holton (2004) and adapted from Hoskins et al. (1985).*

A further way of describing baroclinic instability is through the interaction of two counter-propagating Rossby waves (Hoskins et al., 1985). One of these waves is at the surface, and the other at upper-levels (i.e. the tropopause) which grow through mutual amplification. A schematic of this process is shown in figure 1.3. In order to initiate this growth, an upper-level disturbance or trough (i.e. a positive potential vorticity (PV) anomaly) moves over a strong equator-to-pole temperature gradient at the surface. This positive PV anomaly has an associated cyclonic circulation, which through action-at-a-distance, induces a cyclonic circulation at the surface. This circulation then generates positive and negative temperature anomalies at the surface, which in turn have their own cyclonic and anticyclonic circulations respectively. These circulations interact with each other and advect high and low PV air in a manner to enhance and reinforce the circulations at the upper and lower levels. As the upper level and low level anomalies propagate in opposite directions relative to the mean flow, they can become phase locked and unstable wave growth can occur. In cases when these anomalies are no longer in phase the tilting structure where the divergence and convergence are aligned with the surface features is lost. As this occurs the baroclinic system tends toward a barotropic state and starts to decay. This process is illustrated in a composite of 200 intense extratropical cyclones by Dacre et al. (2012) using atmospheric re-analysis (figure 1.4).

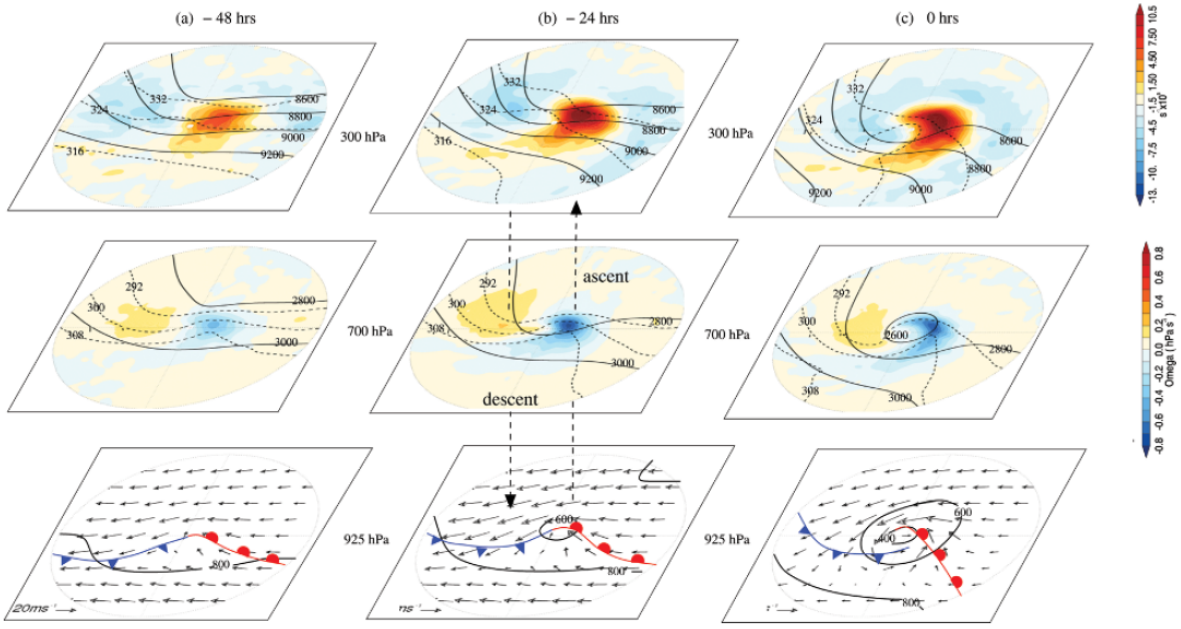

Figure 1.4: *Horizontal composites at (a) 48 and (b) 24 h before the time of maximum intensity, and (c) at the time of maximum intensity. Bottom row: 925-hPa geopotential height (solid lines at 400, 600, and 800 m); system relative wind vectors, and frontal positions. Middle row: 700-hPa geopotential height (solid lines at 2,800 and 3,000 m); equivalent potential temperature (θ_e , dashed lines at 292, 300, and 308 K) and vertical velocity (omega, filled). top row: 300-hPa geopotential height (solid lines at 8,600, 8,800, 9,000, and 9,200 m); θ_e (dashed lines at 316, 324, and 332 K) and divergence (filled). Figure and caption from Dacre et al. (2012).*

1.3 Storm Tracks

1.3.1 Eulerian Approach

The regions of high synoptic activity in the mid-latitudes are known as the storm tracks, which largely consists of variability associated with low pressure centres. Early attempts at classifying this mid-latitude variability was done by Blackmon (1976). In this study, wintertime 500 hPa geopotential height data was band-pass filtered (2.5-6 days). This filtering identified by main regions of storm variance in the Northern hemisphere with two main regions being identified, firstly, extending across the North Atlantic ocean basin, and secondly across the North Pacific (figure 1.5). This analysis method has been used in numerous studies since, for example, Hoskins and Hodges (2002) investigated the band-pass filtered fields of a wide number of atmospheric variables such as mean sea level pressure (MSLP), 850 hPa relative vorticity (ξ_{850}), potential vorticity, temperature, and vertical velocity. The results using all the fields were largely consistent with Blackmon (1976) in picking out the regions of highest synoptic variability, however different variables were slightly better at highlighting smaller scale features (i.e. ξ_{850} for highlighting variability in the Mediterranean).

An Eulerian approach provides a good overview of where in the mid-latitudes synoptic variability is at its largest and provide a good description of this activity. However, it is usually difficult to interpret differences in the number/intensity of systems in causing this variability because this method only provides

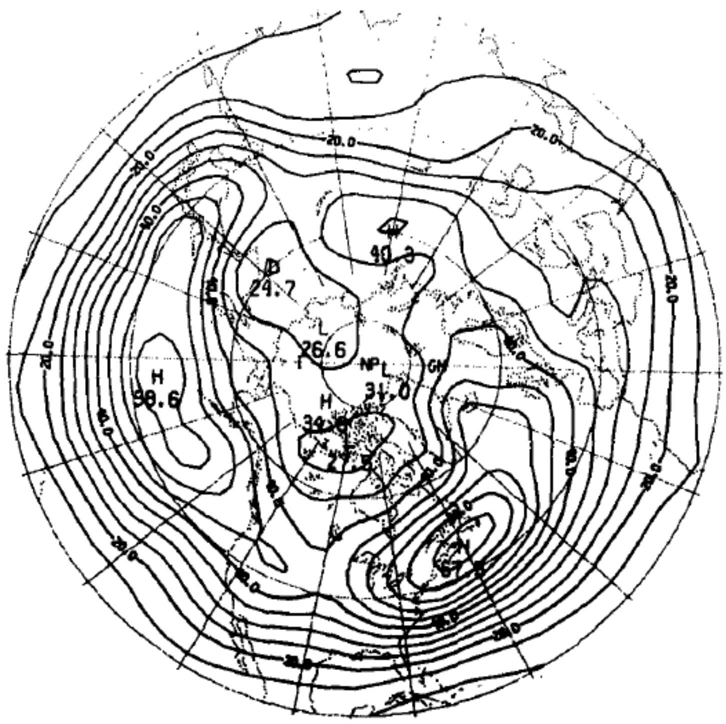

Figure 1.5: *Map of the winter (DJF) bandpass filtered 500 hPa geopotential height variance. Contour intervals are every 2m. Figure from Blackmon (1976).*

and integrated perspective of the synoptic activity. More details can be achieved by taking a more Lagrangian approach to storm track classification, and that is by identification of the cyclonic systems themselves and tracking them throughout their lifetimes.

1.3.2 Objective Tracking of Extratropical Cyclones

The objective tracking of cyclones has generally been the focus of most modern studies into the features of the mid-latitude storm tracks. However, the earliest work done in objectively identifying storm tracks was performed by manually identifying and tracking individual systems on synoptic charts. As this is very time-consuming there have been numerous attempts to objectively identify extratropical cyclones in an automated manner with the greater prevalence of gridded atmospheric data, many of which use different methodologies. The two main methods of identification use either MSLP (e.g. Murray and Simmonds, 1991b,a; Pinto et al., 2005; Wernli and Schwierz, 2006), or low-level relative vorticity (e.g. Sinclair, 1994; Hodges, 1994, 1995, 1999) as they both focus on synoptic scale features, but at opposite ends of the synoptic scale range. These methods (along with many more) have been applied for numerous different studies to look at the behaviour of the whole storm track (e.g. Hoskins and Hodges, 2002; Bengtsson et al., 2006; Raible et al., 2008; Chang et al., 2012; Zappa et al., 2013b), or individual features (e.g. Dacre and Gray, 2009; Catto et al., 2010; Fink et al., 2012; Pinto et al., 2014).

A comparison of tracking using MSLP and ξ_{850} was performed by Hoskins and Hodges (2002) using the method of Hodges (1994, 1995, 1999) for extratropical cyclones in the Northern Hemisphere in the ERA-15 reanalysis (Gibson et al., 1997). Both methods identified consistent features with maxima in track densities across the North Pacific and also the North Atlantic. These features are consistent with the Eulerian analysis of Blackmon (1976), however, much finer-scale features are able to be identified such as high values around Iceland, and also the Mediterranean storm track. The main differences between using MSLP and ξ_{850} are that the track densities are much larger when using ξ_{850} (figure 1.6). This is due to the fact that features are identified earlier when using ξ_{850} (as they may have no distinct pressure minima at this time), and ξ_{850} is also more sensitive to small scale features (Hodges et al., 2003), however this is all dependent on the scale of spatial filtering used to identify features and the thresholds applied (e.g. Zappa et al., 2014).

Further comparisons between methods have been performed by Raible et al. (2008), Neu et al. (2013), and Pinto et al. (2016). These studies applied different identification methods in a number of re-analysis products (e.g. NCEP-NCAR, ERA-I; Saha et al., 2010; Dee et al., 2011) and found that all methods were largely consistent in the large scale representation of the storm tracks. Neu et al. (2013) showed how 15 different methods were generally in better agreement for cyclones in the Northern Hemisphere, those in the

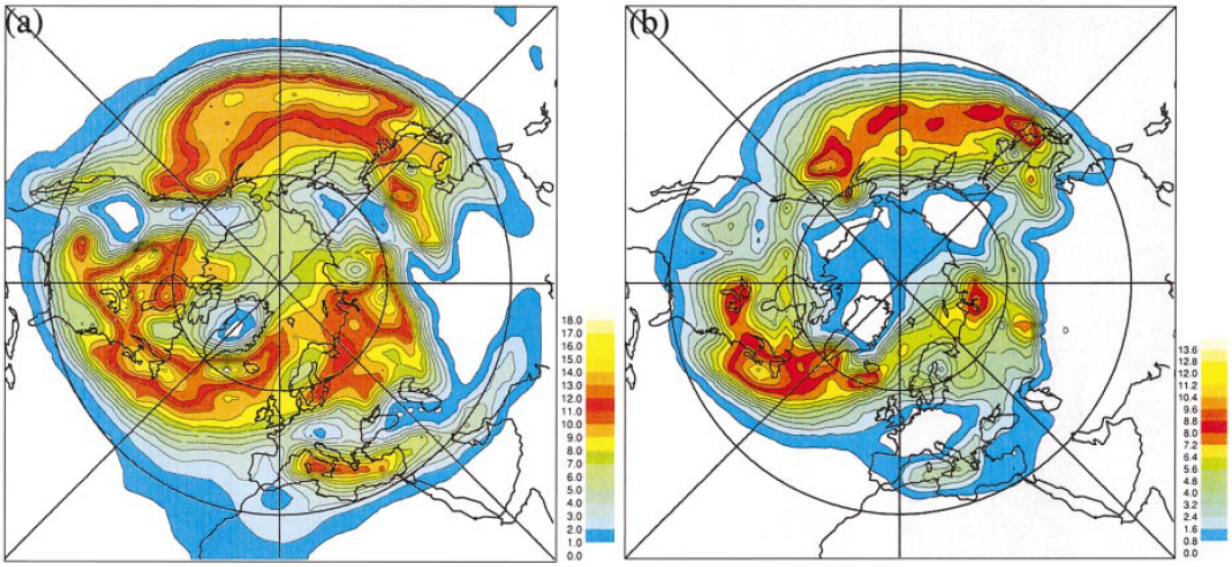

Figure 1.6: *The NH DJF (a) ξ_{850} and (b) MSLP cyclonic track density climatologies. Track densities are in units of number density per month per unit area. Figure and caption from Hodges et al. (2003).*

winter rather than the summer, and those that were more intense systems. Neu et al. (2013) also showed how the numbers of cyclones could vary largely between methods, reasons for this could be differences in the variable of choice for identification, differences in the minimum distance criteria between systems, differences in how the method treats systems over high orography, and finally, the exclusion of cyclones without a closed pressure contour in some methods could cause discrepancies.

It is also important to consider how a method performs when applied to different datasets as different data may provide different representations of the storm track. Hodges et al. (2003) found a good agreement between different re-analysis products for cyclones in the Northern Hemisphere, with differences being more pronounced for cyclones in the Southern Hemisphere. A follow up study (Hodges et al., 2011) with more recent re-analysis products found similar results, but with much better agreement for cyclones occurring in the Southern Hemisphere as a result of improved resolution and data assimilation of observations in the newer generation re-analyses.

Despite the similarities between re-analyses it is also important to note differences between datasets that extend back in time more than 50 years. Befort et al. (2016) and Bloomfield et al. (2018) showed how in the early 20th century re-analyses varied in their number of cyclones and also the trend of cyclone numbers in various geographic areas. Both studies showed much improved agreement between re-analyses for more recent years, especially beyond 1979 and the start of the satellite era with improved observations.

1.3.3 Storm Track Features of the North Atlantic

As the focus of this thesis is on extratropical cyclones that impact Europe, an overview will now be given of the North Atlantic storm track. Whittaker and Horn (1984) and Wernli and Schwierz (2006) showed how cyclones that propagate over western and central Europe most commonly form over the North Atlantic ocean and are part of the North Atlantic storm track. The main features of the North Atlantic storm track were summarised by Dacre and Gray (2009), with their findings being consistent with the previous studies of Whittaker and Horn (1984) and Hoskins and Hodges (2002). It is summarised in Dacre and Gray (2009) how North Atlantic cyclones commonly form downstream of the Rocky mountains, with the main cyclogenesis region being over the Gulf stream on the east coast of North America. In this region the strong sea surface temperature (SST) gradient, coupled with the cold continental air over the North American continent, make this a baroclinic environment very favourable for cyclone development. Cyclones forming in this region generally propagate in a northeasterly direction, which is a result of the unique shape of the North American continent and also the deflection of westward moving air masses by the Rocky mountains (Brayshaw et al., 2009). The largest cyclolysis regions in the North Atlantic are the central and eastern North Atlantic at high latitudes (above 60°N), near Iceland and over the Nordic seas.

Further insights into the North Atlantic storm track are gained by subsetting to cyclones forming in specific regions. Both Hoskins and Hodges (2002) and Dacre and Gray (2009) looked at cyclones forming over the Gulf stream, and also the eastern North Atlantic and found that those forming over the Gulf stream rarely travel the entire length of the storm track, and commonly dissipate over a broad area covering the entire North Atlantic. Conversely, those that form over the eastern North Atlantic commonly travelled nearer to western Europe and had a more dominant influence over the eastern North Atlantic (also Wernli and Schwierz, 2006). These different genesis locations of western and eastern North Atlantic cyclones also hint at different formation mechanisms of these cyclones, as the eastern North Atlantic is not characterised by the same strongly baroclinic environment as near the Gulf stream. Dacre and Gray (2009) hypothesise that these eastern North Atlantic cyclones may be cyclones that form on the trailing fronts of decaying western North Atlantic cyclones. These studies further confirm the statement by Whittaker and Horn (1984) that extratropical cyclones rarely travel the entire length of the storm track, and so the mean perspective of the North Atlantic storm track is often not representative of the behaviour of individual cyclones. An overview of the above characteristics is shown in figure 1.7.

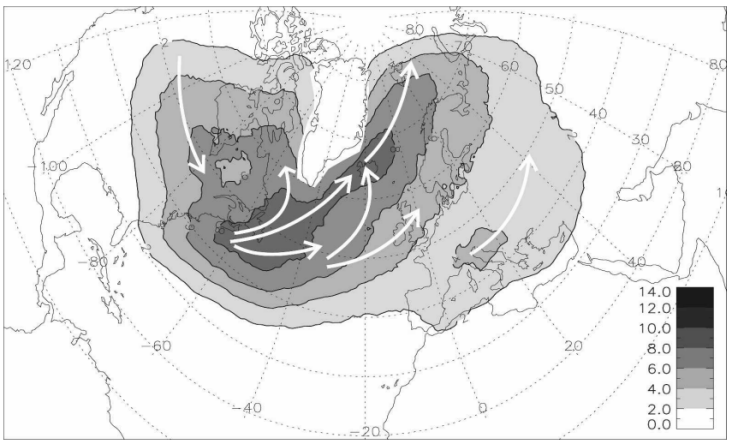

Figure 1.7: *Schematic of cyclone track paths plotted over track density for cyclones over the North Atlantic. Contours every 2 cyclones* $(10^6\ km^2\ )^{-1}\ month^{-1}$. *Figure and caption from Dacre and Gray (2009).*

1.4 Classifying Cyclones

1.4.1 Upper versus Lower Level Forcing

Extratropical cyclones can visually appear very different and have very different characteristics. The *"Norwegian"* and *"Shaprio-Keyser"* models that were described earlier aim to generalise cyclone formation and development, yet it is very rare that a cyclone will strictly follow the lifecycle highlighted by one of these models. Therefore it can be difficult to classify similar cyclones consistently. One way in which this has been done is to examine the synoptic conditions that lead to the formation of a cyclone. This was initially investigated by Petterssen and Smebye (1971) and later by Deveson et al. (2002) who used a height-attributable version of the quasi-geostrophic omega (ω) equation. These initial classifications, termed *"Type A"* and *"Type B"*, distinguish between a dominance in either upper-level, or low-level forcing respectively.

"Type A" cyclones have been shown to form in a baroclinic zone with a surface frontal feature. These cyclones are associated with minimal vorticity advection at upper-levels, but large amounts of thermal advection at low-levels during their initial development. These cyclones do not tend to be associated with an upper-level feature at cyclogenesis, yet one may develop with the cyclone, and the tilt between the surface and upper-level features remains constant with development. *"Type A"* essentially describes an amplifying synoptic wave that forms embedded in a region of high near-surface baroclinicity. Growth is dominated by low-level features.

"Type B" cyclones form when an upper-level feature (commonly a trough) moves over a region of warm advection. These cyclogenesis cases have large amounts of vorticity advection at upper-levels associated with the trough, and minimal temperature advection at low-levels. The tilt between the upper and

lower level features generally decreases with the development of the cyclone. These cyclones are strongly driven by upper-level features.

These classifications were extended to a further class named *"Type C"* by Deveson et al. (2002) and later by Plant et al. (2003). *"Type C"* cyclones have a strong dominance of upper-level forcing, with very minor temperature advection at lower levels. The tilt of *"Type C"* cyclones either remains constant or increases with cyclone development. These cyclones are also strongly associated with strong mid-level latent heating and the diabatic heating is crucial in aiding the development of these cyclones (Plant et al., 2003; Ahmadi-Givi et al., 2004).

Gray and Dacre (2006) examined a number of cyclones in the North Atlantic sector and found preferential regions for each cyclone type to form. *"Type A"* cyclones were found to dominate cyclogenesis to the east of the Rocky mountains, *"Type B"* cyclones dominated cyclogenesis near the east coast of the United States, and finally *"Type C"* cyclones dominated cyclogenesis that was occurring in oceanic regions. Gray and Dacre (2006) also showed how *"Type A", "Type B",* and *"Type C"* made up 30%, 38%, and 32% of the total cyclones in the North Atlantic respectively. In classifying cyclones in either the western or eastern North Atlantic sectors Dacre and Gray (2009) showed how *"Type B"* cyclones were more dominant in the western North Atlantic, and *"Type C"* cyclones were more dominant in the eastern North Atlantic and had slightly shorter lifetimes as well. These eastern North Atlantic cyclones identified by Dacre and Gray (2009) also intensified quicker and developed in regions of weak baroclinicity and reduced static stability.

As well as these classes of cyclones there are also specific types of cyclone that have been observed and modelled, such as Lee cyclones (e.g. Chung et al., 1976; McGinley, 1982) and also Polar lows (e.g. Emanuel and Rotunno, 1989; Zahn and von Storch, 2008). However, these classes are beyond the scope of this thesis and so are not discussed any further.

1.4.2 Secondary Cyclones

Following on from the cyclone classifications discussed above (Petterssen and Smebye, 1971; Deveson et al., 2002; Plant et al., 2003), it was hypothesised by Dacre and Gray (2009) that the cyclones forming over the eastern North Atlantic (commonly *"Type C"* cyclones) were actually cyclones that form on the trailing cold fronts of more mature cyclones. These cyclones are commonly termed *"Secondary"* cyclones and have been discussed as early as the work by Bjerknes and Solberg (1922). The overall picture of extratropical cyclones that was discussed in section 1.2.1 generally refers to that of *"Primary"* cyclones, these being those that go through a generic baroclinic lifecycle as described by the Charney (1947) and Eady (1949) models and form in the strong baroclinic region over the Gulf stream for those that are part of

the North Atlantic storm track. These *"Primary"* cyclones generally fall into the classifications of *"Type B"* (Petterssen and Smebye, 1971) and have been subject to extensive numerical simulations and studies of their lifecycles (Simmons and Hoskins, 1978; Emanuel et al., 1987; Thorncroft et al., 1993), therefore this process can be said to be well understood. As the lifecycles and initiation phases of secondary cyclones do not follow the aforementioned descriptions (Parker, 1998), it is accepted that a wider range of dynamical and mesoscale drivers contribute to along-front cyclogenesis.

Secondary cyclones have been observed in numerous cases (Joly and Thorpe, 1990a; Chaboureau and Thorpe, 1999), with these cyclones often being associated with severe impacts (e.g. The *"Great Storm"* of 1987, as described by Hoskins and Berrisford (1988), and Storm Kyrill in 2007, as discussed by Ludwig et al. (2015)). Thorncroft and Hoskins (1990) performed dry baroclinic simulations of cyclogenesis occurring on a mature cold front associated with a primary baroclinic cyclone in which they find cyclogenesis is commonly initiated by the interaction of the surface front with an upper-level PV anomaly that is commonly of stratospheric origin. These high PV anomalies are often associated with regions of lower tropopause heights, also called tropopause folds, allowing regions of very high PV to interact with, and amplify, low-level baroclinic features (Reed, 1955; Browning, 1997). Explosive cyclogenesis and cases of frontal wave cyclogenesis (Iwabe and da Rocha, 2009) have been shown to be associated with the influence of tropopause folds that are associated with very high PV air aloft. Further theoretical work describing frontal wave instability explains the mechanism of secondary cyclone growth (Joly and Thorpe, 1990b; Schär and Davies, 1990). It is described how an along front PV or potential temperature (θ) anomaly that is aligned with a frontal feature can initiate frontal wave growth as the anomalies can trigger instability. The driver of the along-front anomalies is commonly a result of deformation strain along the front (Bishop and Thorpe, 1994b; Renfrew et al., 1997; Rivals et al., 1998; Chaboureau and Thorpe, 1999; Dacre and Gray, 2006). This process was described by Dacre and Gray (2006) as follows (see also figure 1.8):

1. Build up of a deformation strain causes a tightening of the along-front temperature gradient and ascending motion on warm side of front. The ascending moist air releases latent heat, creating a positive PV strip along the length of the front.
2. Following a reduction of the deformation strain, the along-front PV strip breaks up into individual positive PV anomalies. Each anomaly has an associated cyclonic circulation which results in the formation of frontal waves.

It has been shown in numerous studies that this reduction in the deformation strain is essential for the frontal waves to form (Renfrew et al., 1997; Dacre and Gray, 2006), and that a deformation strain that is too large can inhibit along-front wave growth (Bishop and Thorpe, 1994b; Rivals et al., 1998; Dacre and Gray, 2006). As well as deformation strain numerous other processes have been shown to be important for the development and intensification of cyclones forming on fronts; such as frontal shear (Chaboureau

and Thorpe, 1999), latent heat release/moist processes (Shutts, 1990; Plant et al., 2003; Ahmadi-Givi et al., 2004), and also friction in the boundary-layer (Adamson et al., 2006). As a result of all these contributing factors, the development of these frontal wave cyclones are notoriously hard to forecast, with Parker (1998) stating that only approximately 50% of waves will have a significant pressure deepening.

The development of objective cyclone and front identification and tracking schemes has allowed secondary cyclones to be specifically identified as a separate class of cyclones. The studies of Schemm and Sprenger (2015) and Schemm et al. (2018) combined the cyclone identification and tracking scheme of Wernli and Schwierz (2006) with the front identification scheme of Hewson (1998) (adapted by Schemm et al., 2015). Schemm and Sprenger (2015) found that along-front cyclogenesis was most common over the Gulf stream/western North Atlantic and mainly in the September/October/November (SON) and December/January/February (DJF) seasons where it largely makes up between 6-14% of all cyclogenesis events. This study also confirmed theoretical assumptions (Joly and Thorpe, 1990b; Schär and Davies, 1990) by providing evidence for low-level, along-front PV structures that are associated with reduced static stability. It was also shown how cyclones forming in the eastern North Atlantic had a stronger phase locking between the upper and lower level PV anomalies (as well as stronger anomalies), aiding the rapid development and intensification in the eastern North Atlantic which is largely consistent with the mechanism for *"Type C"* cyclogenesis (Plant et al., 2003). Schemm et al. (2018) demonstrated that over

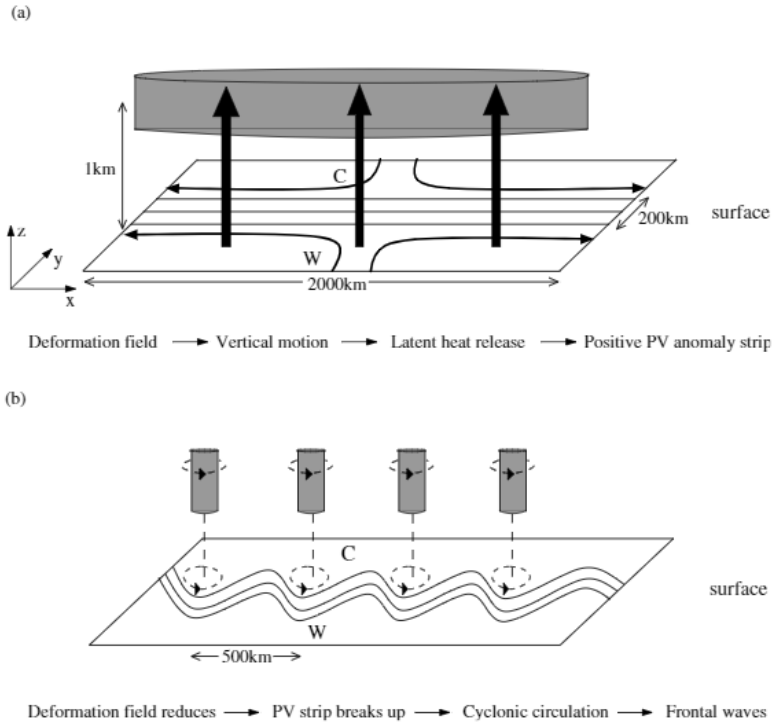

Figure 1.8: *A conceptual model for barotropic frontal-wave development. (a) First stage of frontal-wave development - formation of PV strip, (b) second stage of frontal-wave development - break-up of PV strip. Contours are isotherms, shading is positive PV anomaly. Thin arrows represent the deformation strain flow, thick arrows represent vertical ascent and dashed arrows represent horizontal circulations. Figure and caption from Dacre and Gray (2006).*

20% of all cyclones in the central and eastern North Atlantic form along fronts, and that these are also a common feature of the central North Pacific storm track. These studies have demonstrated the possibility for secondary cyclones to be identified in reanalysis, and that they are occasionally very intense weather systems and features that are common in the eastern North Atlantic. As most cyclones that impact western Europe form in the eastern North Atlantic (e.g. Wernli and Schwierz, 2006), it is likely that secondary cyclones are a strong contributor to the weather system variability here, although this is something that is yet to be quantified.

1.5 Impacts Associated with Extratropical Cyclones

Extratropical cyclones have significant impacts associated with them, regardless of their classification or formation mechanisms. Across Europe, these impacts are commonly in the form of extreme precipitation, wind damage, coastal surges, or a combination of the above. The precipitation and wind impacts will be discussed further in this section.

1.5.1 Precipitation

It has long been documented that extratropical cyclones are strongly associated with precipitation in the mid-latitudes (Bjerknes and Solberg, 1922). Extratropical cyclones play a significant role in global moisture transport, this is mainly done through poleward transport of moisture as part of the WCB (Carlson, 1980). This poleward moisture flux rises as it moves along moist isentropes, this ascending motion results in the condensation of moisture and then the formation of clouds and precipitation (Browning, 1986). It was also shown by Field and Wood (2007) how cyclone strength (measured as mean surface wind speed) is correlated to the amount of precipitation produced by a cyclone, this is because stronger cyclones are generally associated with stronger vertical motion and hence condensation of moisture. With regards to precipitation from extratropical cyclones in the UK, this most commonly occurs in the winter months (DJF), and over a timescale of between 6 hours and 3 days, with summer rainfall often being convective and over shorter timescales (Hand et al., 2004). Heavy precipitation events can have a considerable impact on society (Easterling et al., 2000), with numerous events reporting widespread damage as a result of flooding and even documented losses of life as a consequence (Ulbrich et al., 2003; Sibley, 2010; Kendon and McCarthy, 2015).

In recent years there have been numerous attempts to attribute the precipitation experienced globally to extratropical cyclones, or specific features of extratropical cyclones. Hawcroft et al. (2012) utilised the cyclone identification and tracking algorithm of Hodges (1994, 1995) to associate precipitation to individual cyclones. They found that $\geq$70% of precipitation in northern and western Europe was from extratropical

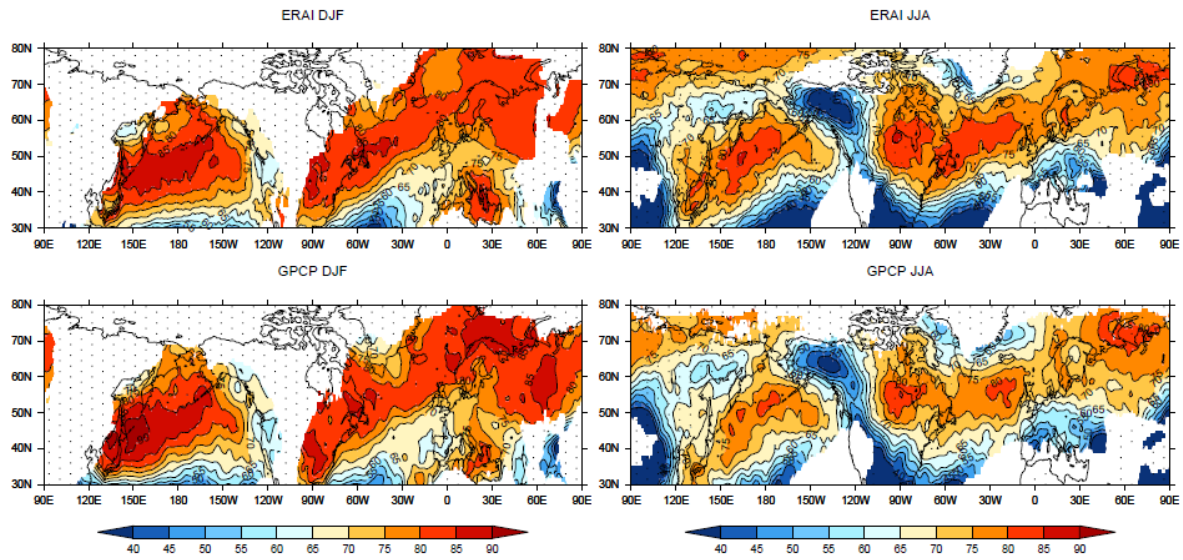

Figure 1.9: *Contribution of storm associated precipitation to the total precipitation (%) from ERA-I and GPCP. The masked and stippled areas are where the total climatological precipitation is less than 1 mm/day. Figure and caption from Hawcroft et al. (2012).*

cyclones in DJF, with this also being the case for a large part of the northern extratropics and also contributions being slightly lower during the summer months (JJA). Local maxima over parts of the oceanic basins exceeded 90% of precipitation coming from extratropical cyclones (figure 1.9). A further study from Pfahl and Wernli (2012) associated extratropical cyclones to precipitation extremes (those exceeding local 99th percentile) in a similar manner to that done by Hawcroft et al. (2012). Contributions from cyclones were slightly reduced compared to findings in Hawcroft et al. (2012), although more than 60% of precipitation extremes were from extratropical cyclones across the North Atlantic storm track region and also the UK and Scandinavia. Some local maxima were again showing more than 90% contribution of extratropical cyclones to precipitation extremes.

1.5.2 Wind

The association between extratropical cyclones and severe wind events has been noted for a considerable period in the scientific literature (Hoskins and Berrisford, 1988; Lamb, 1991), with cyclones that cause this severe wind often being termed windstorms. With regards to the damage caused in Europe, windstorms are by far the most important natural hazard (Della-Marta et al., 2010; Haylock, 2011), they cause an average of $2 billion (USD) per year with the winter seasons of 1990 and 1999 causing $14.6 billion and $12.2 billion of losses respectively (Schwierz et al., 2010). Europe is particularly susceptible to severe windstorm events such as these as it is situated at the end of the North Atlantic storm track where intense extratropical cyclones are commonly found (Wernli and Schwierz, 2006). The most damaging events commonly cause over $1 billion of insured losses (see table 1.1) and are a major impact from both a socio-economic and environmental perspective. Most of the severe windstorms are experienced during the winter months, this is

when the number of cyclones is at its peak and the cyclones are most intense (Hoskins and Hodges, 2002)

Many severe European storms are commonly embedded in a very strong north-south pressure gradient (e.g. Ulbrich et al., 2001; Fink et al., 2009), with the strong pressure gradient providing the strong winds via geostrophic balance (Ackerman and Knox, 2007). Strong winds are most commonly found on the equatorward flank of the cyclone, as here the dynamical wind speed is added to the translational speed of the cyclone, resulting in a stronger total wind field. Strong pressure gradients commonly drive strong wind speeds around the location of the cold front, however the strongest gusts associated with cyclones are often a result of mesoscale instabilities generated within the cyclone (Schultz and Schumacher, 1999; Volonté et al., 2018).

The wind damage that results from an extratropical cyclone is commonly associated to one of the three aforementioned airstreams discussed previously. Those causing damage are the WCB, CCB, and SJ. Hewson and Neu (2015) provided a conceptual model for how the different airstreams/zones of an extratropical cyclone contribute to damages at different stages of their lifetime, and how strong/how much damage may be associated with each one (note Hewson and Neu (2015) refer to the WCB as the warm jet, WJ, and the CCB as the cold jet, CJ). Their conceptual model is shown in figure 1.10. Hewson and Neu (2015) describe the features associated with each of the different airstreams. Strong gusts from the WCB/WJ are generally aligned with the cold front and have peak strengths of 50-70 knots. These strong gusts tend to occur early in the life of the cyclone and can typically last for 24-48 hours. The damage caused by these features can have a footprint of 200-500 km in width and extend for nearly 1000 km. Surface gusts from the CCB/CJ are commonly stronger than those from the WCB/WJ and can often reach 60-80 knots over a periods of 12-36 hours. These commonly occur to the south of the cyclone centre when a cyclone is at peak intensity, and also are stronger for cyclones that have a much faster meridional propagation as this is

Table 1.1: *Top 10 costliest windstorm loss events in Europe 1980-2015 (ordered by insured losses). Table adapted from Munich Re (2016).*

Event	Dates	Overall losses (billion USD)	Insured losses (billion USD)	Fatalities
Storm Lothar	26/12/1999	11.5	6.2	110
Storm Kyrill	18-20/1/2007	10	5.8	49
Storm Daria	25-26/1/1990	7	5.4	94
Storm Xynthia	26-28/2/2010	6.1	3.1	65
Storm Erwin	7-9/1/2005	6	2.6	18
Great Storm of 1987	15-16/10/1987	5.3	3.1	18
Storm Klaus	24-27/1/2009	5.1	3.0	26
Storm Martin	27/12/1999	4.1	2.5	30
Storm Vivian	25-27/2/1990	3.4	2.0	52
Storm Anatol	3-4/12/1999	3.1	2.4	20

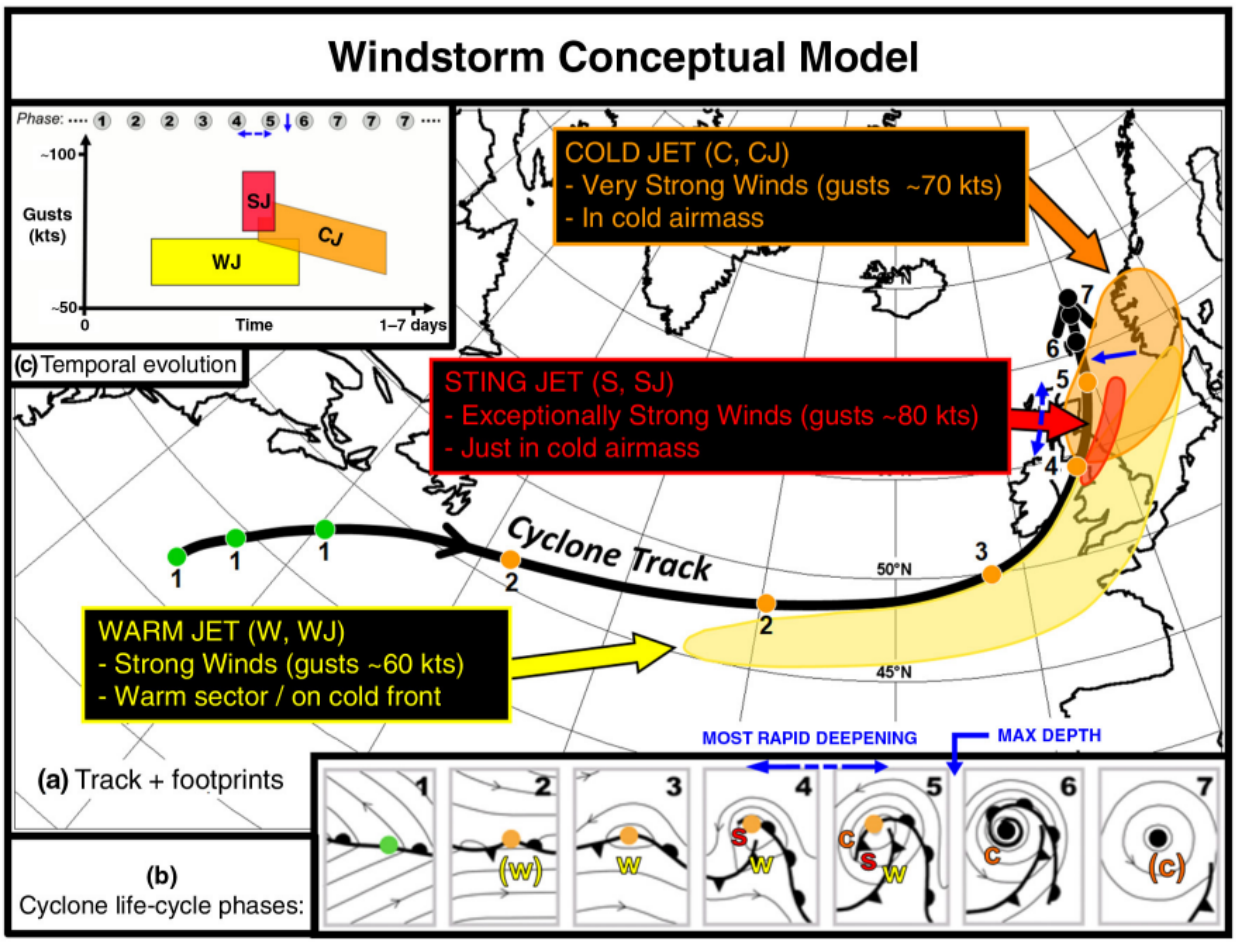

Figure 1.10: *Conceptual model of an extratropical cyclonic windstorm. Panel (a) shows the cyclone track (black), with spots denoting positions equally separated in time, and numbered according to the cyclone life-cycle phases in panel (b). Coloured dots relate to objective typing of the cyclone with green being a diminutive frontal wave, orange a frontal wave cyclone, and black a barotropic low. Shading denotes the footprints, or nominal damage swathes, attributable to the warm jet (yellow), the cold jet (orange) and the sting jet (red). Panel (b) shows the synoptic-scale evolution of fronts and isobars around the cyclone, with added letters denoting relative locations of the strong wind features. Panel (c) denotes the temporal evolution of gust strength for each jet zone, with numbers cross-referencing phases on panel (b). On each panel, a dashed blue line denotes the period of most rapid deepening, whilst the solid blue arrow shows the time of maximum depth. Figure and caption from Hewson and Neu (2015).*

additive with the cyclone gust speed. Finally the SJ is the airstream that provides the strongest gusts with peak strengths of typically 70-90 knots, but over a very short time period of only 1-6 hours. These are rarely observed features due to their small scale and transient nature that only appear in a specific set of cyclones, impacts of a SJ only affect a very small area that is often between 20 and 200 km wide.

1.6 European Windstorms

It was described by Wernli and Schwierz (2006) how most severe cyclones that make their way to the European continent actually form much closer to western Europe than the majority of North Atlantic cyclones, and have their genesis in the eastern North Atlantic. This was also observed by Dacre and Gray (2009) for cyclones that are rapidly intensifying and for many case studies of high impact windstorms

(Lothar and Martin; Ulbrich et al., 2001). Herein, the drivers of windstorms impacting Europe will be explored and also methods for modelling their impacts.

1.6.1 Large Scale Dynamical Drivers of European Windstorms

One very intense storm that has received a lot of attention is that of Lothar (e.g. Ulbrich et al., 2001; Wernli et al., 2002; Rivière et al., 2010), which affected large parts of western and central Europe from 25-27 December 1999 and caused over $10 billion economic damage (Munich Re, 2016). It was found that Lothar was associated with a very large pre-existing low pressure system that was situated over Ireland and drove a strong steering flow toward western Europe. Ulbrich et al. (2001) discuss how the associated jet streak at 300 hPa had peak wind speeds of over 120 m s^{-1} and Lothar caused surface wind speeds in excess of 55 m s^{-1} inland over central Switzerland (Wernli et al., 2002). Further studies have generalised the pattern seen during windstorm Lothar to apply to a broader set of European windstorms.

With regards to the large steering low situated over Iceland that observed during windstorm Lothar (Wernli et al., 2002), the association between large scale pressure patterns and severe cyclones has long been known. The North Atlantic Oscillation (NAO) is a weather pattern that describes the most variability in North Atlantic MSLP (e.g. Hurrell et al., 2003). The NAO is measured as the normalised pressure difference between Iceland and the Azores, with a positive NAO phase being associated with lower than average pressure centred over Iceland, and higher than average pressure centred over the Azores, with the reverse being true during the negative phase. The NAO index is essentially a measure of the strength of the westerly zonal flow across the North Atlantic (Woollings et al., 2008). Serreze et al. (1997) discuss

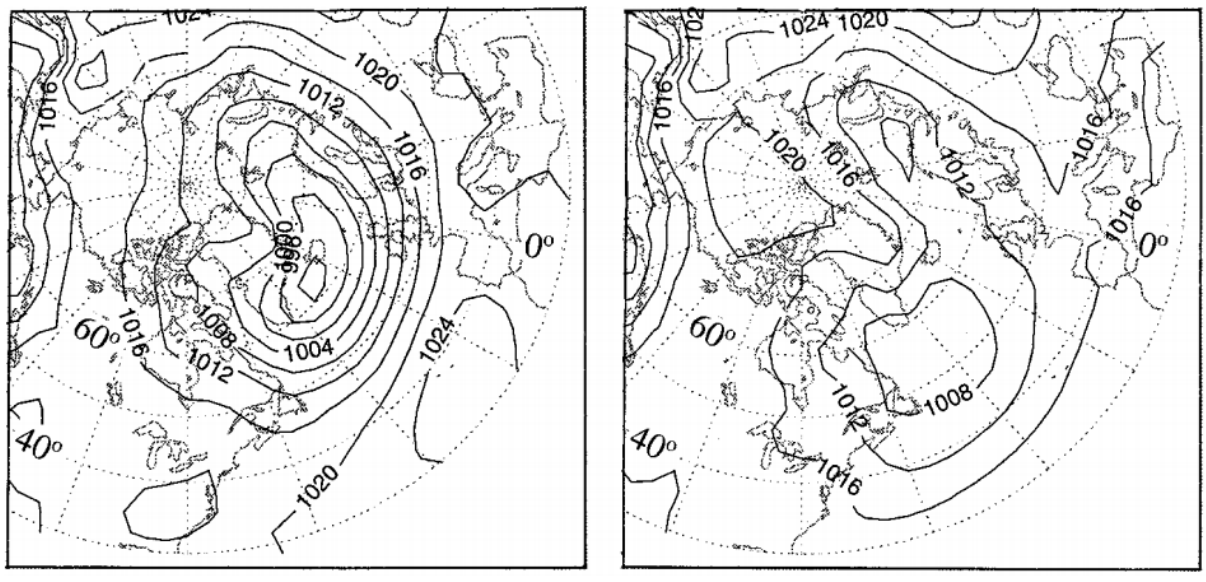

Figure 1.11: *Cold season MSLP associated with positive (a) and negative (b) extreme phases of the NAO. Figure and caption from Serreze et al. (1997).*

how during the positive phase the Icelandic low is stronger and more poleward than the negative phase (figure 1.11) and that cyclones in the North Atlantic are more intense and poleward than in the negative phase. The positive phase features a stronger north-south pressure gradient, driving a stronger zonal flow toward Europe. The link between the NAO phase and severe windstorms in Europe was further confirmed by Pinto et al. (2009) and Donat et al. (2010). In these studies it was found that extreme windstorms are more common over Europe when the NAO is in a positive phase due to the larger area of conditions that are favourable for cyclone growth. They found that the NAO affects the tracks of cyclones through changes in the location of the maximum pressure gradient, and also that the cyclones have a longer lifetime, deeper core pressure, and also longer track length (Pinto et al., 2009).

The NAO itself can dynamically be represented as an oscillation in the occurrence of Rossby wave breaking (RWB) events in the upper troposphere (Benedict et al., 2004; Kunz et al., 2009). RWB is the process of the deformity of PV or θ surfaces at the upper-troposphere, leading to mixing (McIntyre and Palmer, 1983). RWB is commonly associated with mid-latitude blocks (Pelly and Hoskins, 2003) and the barotropic decay of eddies (Barnes and Hartmann, 2012) and has been shown to be connected to shifts in the speed and the location of the mid-latitude jet stream (Rivière and Orlanski, 2007; Woollings et al., 2008). Rossby waves can break either cyclonically or anticyclonically and represent an irreversible mixing of the upper atmosphere. Both RWB orientations have been linked to extratropical cyclones, with Thorncroft et al. (1993) linking the phases to differing cyclone baroclinic lifecycles and shear environments. Woollings et al. (2008) describe how the positive phase of the NAO is often marked by an absence of large scale RWB over the core of the North Atlantic ocean, but slightly increased frequencies in the northern and southern latitudes, with the reverse being true for the negative phase of the NAO. It was confirmed by Hanley and Caballero (2012) that the positive phase of the NAO is strongly associated with destructive windstorms through their analysis of 25 of the most severe cases in the ERA-40 re-analysis. They find that the NAO reaches a maximum in the positive phase approximately 2 days prior to when their 25 severe windstorms are at their most intense and over Europe, with this subsequent decrease commonly following a long period of build-up of the NAO index. This decrease is due to an eastward shift of the NAO pressure dipole that is associated with the occurrence of cyclonic and anticyclone RWB to the north and south of the jet axis respectively (often termed double-sided RWB, DWB). This RWB and shift of the pressure pattern results in an elongated and very strong jet at upper levels, which steers the severe windstorms into Europe. This pattern is also favourable for the rapid intensification of windstorms, via increased baroclinicity resulting from the concentration of the temperature gradient from the breaking waves on either side of the jet, and also the left exit region of the jet being associated with strong divergence that is beneficial for rapid intensification (Rivière and Joly, 2006a,b).

The importance of this double-sided RWB for intensifying cyclones was further noted by Gómara et al. (2014a) in their study of explosively developing cyclones over the North Atlantic. In their subset of events of rapidly deepening cyclones they find that those preceded by double-sided RWB result in faster deepening and higher intensities than those preceded by single-sided RWB. The double-sided RWB is generally located over eastern Greenland and the subtropical North Atlantic and results in an intensification of the eddy-driven jet. This intensification of the jet when flanked by RWB is also noted by Barnes and Hartmann (2012), with the presence of RWB acting to flux momentum into the jet core, resulting in an acceleration. A dominance of RWB on the southern (northern) flank of the jet will also result in a shift of the jet in the poleward (equatorward) direction (Barnes and Hartmann, 2012). This pattern was recently confirmed by Messori and Caballero (2015) who further note the key role of double-sided RWB in intensifying and extending the eddy-driven jet and increasing the chance of destructive windstorms impacting Europe. They further state how the RWB occurring in the eastern North Atlantic is vitally important as double-sided RWB in the eastern North Atlantic almost doubles the climatological likelihood of destructive windstorms in western Europe. This is due to double-sided RWB in the eastern North Atlantic acts to intensify and zonalise the westerly flow across the basin, whereas the reverse is true for double-sided RWB in the western North Atlantic. This double-sided RWB mechanism for driving severe windstorms and cyclones toward Europe was summarised in a schematic by Messori et al. (2018) and is shown in figure 1.12.

1.6.2 Modelling Windstorm Impacts

As previously discussed, windstorms pose significant threat to European countries in terms of insured losses. The exact loss data associated with these storms are often not readily available for academic or public use, and hence several studies have been undertaken to attempt to develop empirical relationships or models

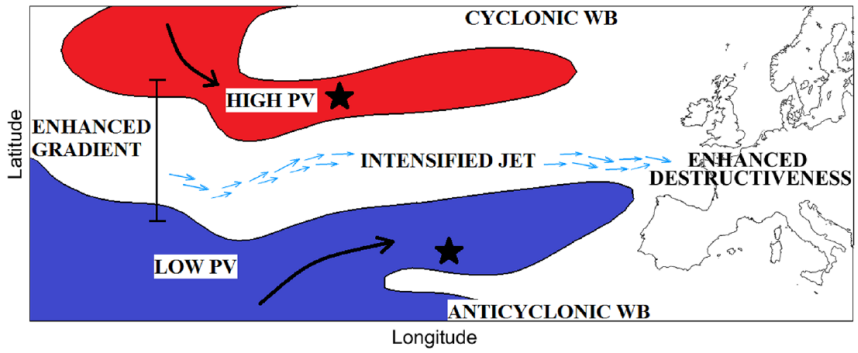

Figure 1.12: *Schematic illustrating the impact of DWB on the large scale flow. The thin black lines show idealised PV contours. The simultaneous anticyclonic RWB and cyclonic RWB result in a strengthened meridional PV gradient, which leads to an intensified zonal jet. This, in turn, favours enhanced wind destructiveness downstream of the DWB. Figure and caption from Messori et al. (2018), adapted from Messori and Caballero (2015).*

of the monetary damages associated with these events based on readily available meteorological data. As damage associated with extratropical cyclones arises primarily from surface winds, and that the damage is highly sensitive to variations in the surface wind, a damage function must be able to represent these variations accurately.

Observational studies and empirical evidence has illustrated that the relationship between wind speed and on the ground damage being strongly non-linear. Both Palutikof and Skellern (1991) and Lamb (1991) suggested that the loss is proportional to the cube of the maximum windspeed (i.e. $V_{max}^3 \propto loss$), with this being supported by loss data from the severe storm series of 1990 (Munich Re, 1993). The cubic relationship between the wind speed and damage is also proportional to the advection of kinetic energy by the flow and is seen as a good approximation for wind loss (Palutikof and Skellern, 1991; Powell and Reinhold, 2007). Despite this, empirical evidence of storm series in 1999 (Lothar and Martin, Munich Re, 2002) suggested that the the relationship may be higher order and loss proportional to either the fourth or fifth power of the maximum wind speed, especially for areas experiencing the most extreme gusts.

One of the first storm loss models developed was that by Klawa and Ulbrich (2003), who use the cubic relationship. This cubic relationship is applied to a gust value that has been normalised by a local threshold, this being the 98th percentile of the wind speed climatology at that point. This normalisation is because damage does not occur for all wind speeds, and damages generally only occur on 2% of days (Palutikof and Skellern, 1991). Using a local threshold means that it is adapted to areas that generally experience higher wind speeds and have infrastructure that is more resilient to the environmental conditions that it experiences. This wind loss model from Klawa and Ulbrich (2003) utilised wind gust speed from 24

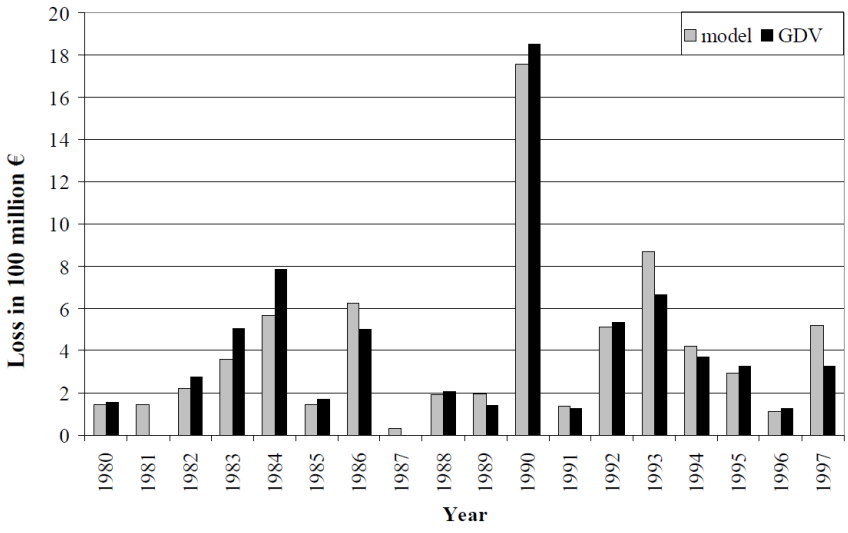

Figure 1.13: *Insured annual accumulated losses in Germany. Comparison between detrended loss data (basic year = 1990) reported by the German Insurance Association (GDV), and loss estimations by the loss model. Figure and caption from Klawa and Ulbrich (2003).*

weather stations and was shown to compare very well to insured losses in Germany for a period covering 1980-1997, with a correlation of 0.96. A year-by-year comparison of insured losses and their model results is shown in figure 1.13.

This model was further adapted and modified to work with gridded meteorological data and termed the storm severity index (SSI) (Leckebusch et al., 2007, 2008). The SSI of Leckebusch et al. (2008) is applied European wide and provides a single loss value for a pre-defined area, or a specific event (an example application is shown in figure 1.14). Its formulation is described in equation 1.1. The area SSI, takes the wind field across a pre-defined area and hence more than one synoptically distinct event can often contribute to the SSI value. The event SSI involves the specific tracking of synoptic events and calculates an SSI that is specific to the regions affected by that event. The original formulation of the SSI from Leckebusch et al. (2008) in equation 1.1 (which can be applied as either the area or event SSI) relates the maximum wind speed at a given location and in a specified time ($v_{k,t}$), to the 98th percentile of the wind speed in that location ($v_{98,k}$). A localised scaling coefficient (A_k) is commonly applied for each grid point, and the resultant field is summed over the time period of interest (T), and over the geographical region of interest (K). Some variants of the SSI do not integrate the losses over the duration of the windstorm as in equation 1.1 and instead use the peak wind speed at each grid point throughout the duration of the windstorm (e.g. Pinto et al., 2012; Karremann et al., 2014a).

$$SSI_{T,K} = \sum_{t}^{T} \sum_{k}^{K} \left[\left(max \left(0, \frac{v_{k,t}}{v_{98,k}} - 1 \right) \right)^3 * A_k \right] \tag{1.1}$$

The area SSI has been widely used to evaluate European windstorms for a number of different purposes (e.g. Leckebusch et al., 2007; Pinto et al., 2007; Donat et al., 2011; Pinto et al., 2012; Karremann et al., 2014a; Pantillon et al., 2017). It can either be used to calculate a normalised loss for events, or scaled to replicate monetary losses (as in Klawa and Ulbrich, 2003). There are limitations to this model, as have been highlighted in Prahl et al. (2015), where they demonstrate there is no upper bound to the losses from the

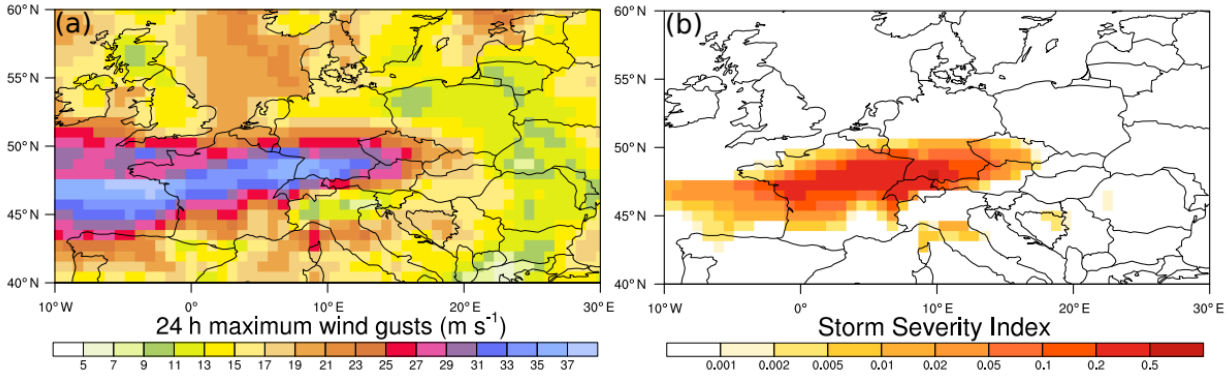

Figure 1.14: *Example of the daily maximum wind gusts (a) and daily Storm Severity Index (b) for storm Lothar in ERA-Interim on 26 December 1999. Figure and caption from Pantillon et al. (2017).*

model and they would not saturate with increasing gust speed. This is unrealistic as eventually a maximum amount of damage will occur in a particular location. Furthermore, the same loss function is applied to all locations. Klawa and Ulbrich (2003) showed that it is a good approximation for all of Germany, and it has been applied successfully to large parts of Europe (especially those that experience frequent severe windstorms such as the northwest corner of the continent).

The SSI has been shown to perform poorly for regions where severe windstorms are less frequent, and extreme wind speeds are experienced less often (such as Iberia and southern Europe) due to differences in the shape of the tail of the wind speed distribution compared to commonly impacted regions. One approach to resolving this is an adjustment to the 98th percentile threshold being made in some regions where the calculated value is not a suitable value (Karremann et al., 2014a; Karremann, 2015). For example, in parts of Iberia and southern Europe the average wind speed is very low, and as a result the 98th percentile in some data products is less than 5 m s^{-1}. This threshold is too low to cause damage to any building, as a result Karremann et al. (2014a) investigated an otherwise suitable threshold instead of the 98th percentile and found that using 9 m s^{-1} was a suitable replacement. Another approach was by Walz et al. (2017) who formulated the distribution independent SSI (DI-SSI). The DI-SSI deals with events occurring in regions outside the main storm track and Walz et al. (2017) highlight how when applying the standard SSI to areas such as Iberia it can lead to erroneously large loss values. The DI-SSI provided better loss estimates for rarely impacted regions by rescaling the tail of the wind speed distribution and defines severity in a more climatological perspective, as a result it is harder to implement than the standard SSI.

As well as the above method from Klawa and Ulbrich (2003) and Leckebusch et al. (2008), there are other storm loss models that have also been developed and implemented for similar purposes, albeit using slightly different methodologies. These models use formulations such as an exponential relationship (e.g. Dorland et al., 1999; Prettenthaler, Franz and Albrecher, Hansjörg and Köberl, Judith and Kortschak, Dominik, 2012; Murnane and Elsner, 2012), a power law combined with damage thresholds (e.g. Heneka et al., 2006; Heneka and Ruck, 2008), and also a power law sigmoid curve (Prahl et al., 2012). Some windstorm loss models have been compared by Roberts et al. (2014) and Prahl et al. (2015) and each of model was demonstrated as having its own benefits, with the SSI of Klawa and Ulbrich (2003) performing well for extreme loss cases and also generally being the easiest to implement (Prahl et al., 2015).

1.7 Clustering

One particular feature of extratropical cyclones over Europe, particularly severe windstorms, is their tendency to occur in clusters. Clustering is the behaviour of cyclones occurring in groups and is something that has been observed numerous times in recent history, particularly for cyclones that cause significant

damage. This behaviour was noted in part of December 1999 when windstorms Anatol, Lothar, and Martin caused total economic damage of $18.7 billion ($10.1 billion insured) with Lothar and Martin impacting both western and central Europe just two days apart (Ulbrich et al., 2001). Further to this, the months of January 1993 (Pinto et al., 2014), January 2007 (Fink et al., 2009), and the winter season of 2013/2014 have demonstrated the behaviour of the recurrent influence of many extratropical cyclones. The DJF of 2013/2014 was particularly impactful for the United Kingdom (Kendon and McCarthy, 2015), breaking precipitation records across the whole country and being classed as the stormiest on record and hence the stormiest in over 140 years for the country (Matthews et al., 2014). Intense cyclones occurring quickly after each other poses significant risks socio-economically, as infrastructure is often more vulnerable following a first event and these sequences can disrupt loss estimations of both insurance and re-insurance companies (Swiss Re, 2016).

Recently, the study from Economou et al. (2015) listed three reasons extratropical cyclones may cluster. The reasons are:

1. Purely by chance: Storm impacts may occur in a random order, and some are bound to occur shortly after a previous event in this situation.
2. Through modulation by large-scale atmospheric patterns: Background conditions can cause increases or decreases in the rate of cyclone passages in particular locations (i.e. NAO positive phase causes an increase in the intensity and number of cyclones near Europe; Pinto et al., 2009; Donat et al., 2010).
3. A dependence between successive storms: Cyclones can occur in families (Bjerknes and Solberg, 1922; Parker, 1998) which if repeated could result in a larger number of cyclones than may otherwise be expected.

Presently it is unclear what the relative importance of each of the three factors is toward clustering, and the current state of knowledge will be discussed below.

1.7.1 Quantifying Clustering

Mailier et al. (2006) investigated cyclone transits and the presence of clustering by observing cyclone passages through latitude bands. The occurrence of individual events can be modelled using a point poisson process (Cox and Isham, 1980), which models the occurrence of random events in times and hence assumes that the arrival of any event is independent of the number of event previously and the amount of time since the previous event. Mailier et al. (2006) use a dispersion statistic derived from a variable rate poisson process to model the cyclone passages. For such a poisson distribution with fixed rate λ, the probability of a number of occurrences (N) during a time interval (ΔT) is formulated as:

$$P(N = n) = \frac{(\lambda \Delta T)^n e^{-\lambda \Delta T}}{n!},\ n = 0, 1, 2, ... \tag{1.2}$$

With the dispersion (ψ) being:

$$\psi = \left(\frac{\sigma^2}{\mu}\right) - 1 \tag{1.3}$$

where σ^2 and μ are the variance and mean of the number of occurrences respectively at any grid point. Using the formulation in equation 1.3 a value of $\psi = 0$ equates to a homogenous poisson process, that being the occurrences are completely random. For values of $\psi > 0$ the occurrences are more clustered than random and are overdispersive, for values of $\psi < 0$ the occurrences are less clustered than a random process and hence they are underdispersive.

Following this Mailier et al. (2006) calculated the dispersion on a grid point basis to identify regions that were more clustered relative to a random process, and those that were more regular. The exit of the North Atlantic storm track was shown to be a preferential region for the clustering of cyclones, with the entrance region being an area where cyclone counts were more regular (figure 1.15). The entrance of the storm track as an area characterised by increased regularity can be explained through the persistent baroclinic nature of this region and cyclones regularly forming with little external influence. It is also discussed in Mailier et al. (2006) that clustering/overdispersion near the exit of the storm track is likely a combination of two processes, firstly via modulation by large-scale patterns, and secondly via the occurrence of coherent wave packets or groups of cyclones that are often formed of primary and secondary cyclones. They hypothesise that the genesis of secondary cyclones in the eastern North Atlantic is increasing the number of cyclones in a wave packet and contributing to the overdispersion in these regions.

Mailier et al. (2006) also illustrate that clustering may be stronger for more intense cyclones, as they performed a similar analysis to that shown in figure 1.15 with cyclones that exceed a vorticity threshold of 6×10^{-5} s^{-1} and found increases in ψ of at least 50% over the UK and North Sea. The increase of the magnitude of dispersion with cyclone intensity was also identified in several other studies (Vitolo et al., 2009; Pinto et al., 2013; Cusack, 2016), with Vitolo et al. (2009) also finding that clustering increased with aggregation period and the geographical area that is considered. This also aligns with the findings of Hunter et al. (2016), who found that winter seasons in Europe that are characterised by a greater number of cyclones generally featured cyclones that were of a higher intensity.

The pattern of clustering with overdispersion on the flanks and downstream of the North Atlantic storm track, and underdispersion in the entrance of the storm track is something that appears robust both to the definition of a cyclone by different identification methods (Pinto et al., 2016), and also in a number of different re-analyses (Pinto et al., 2013). However, it should be noted that some general circulation models (GCMs) have shown issues when representing the patterns of dispersion (Mailier, 2007; Kvamstø et al.,

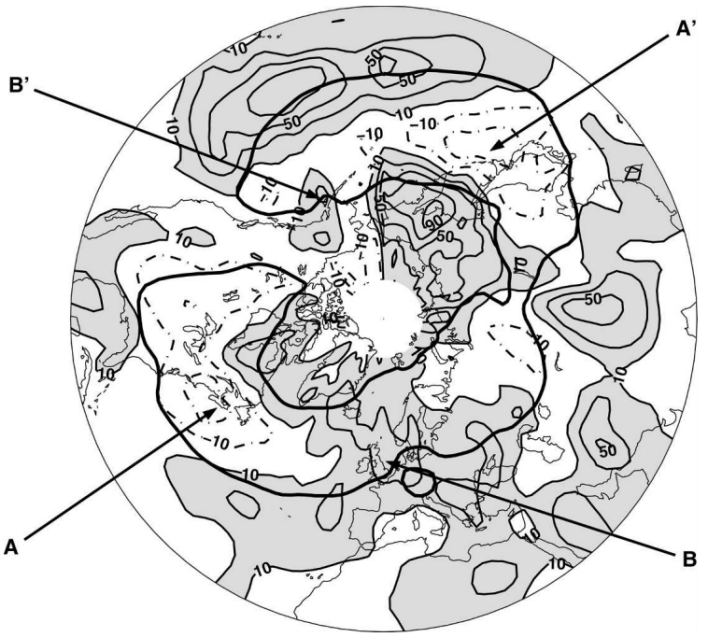

Figure 1.15: *Estimated dispersion statistic ψ (%) of the monthly number of cyclone transits. Solid (dashed) lines indicate positive (negative) values. Contours start at 10%, contour intervals of 20%. Areas where $\psi > 10\%$ are shaded. Thick dark lines representing the boundaries of the regions where number of cyclones it at least 5 per month have been added for easy reference to the storm tracks. Figure and caption from Mailier et al. (2006).*

2008). More recently Economou et al. (2015) showed how a selection of 17 CMIP5 models were able to broadly capture the pattern of dispersion noted in the re-analyses. Both Pinto et al. (2013) and Economou et al. (2015) performed analysis on climate change simulations in an attempt to quantify how the pattern of dispersion may be affected in the future. Pinto et al. (2013) found evidence for a slight reduction in dispersion in the exit of the North Atlantic storm track, however this was also associated with considerable sampling variability between simulated ensemble members. The multi-model mean of the CMIP5 models used by Economou et al. (2015) showed some agreement with the reduction in dispersion found by Pinto et al. (2013), however they also showed considerable variation and hardly any agreement between each of the models considered. Therefore, the effect of climate change on the pattern of dispersion is very unclear with little confidence in a specific response.

The dispersion statistic has been widely used to assess clustering in a number of studies discussed above. Raschke (2015) and Cusack (2016) highlighted some issues with the formulation of ψ presented in equation 1.3 as ψ tends to be proportional to the number of cyclones being considered and so reflects both the intensity of the clustering and the size of the sample. A new formulation was proposed by Raschke (2015) that isolates the intensity of clustering from the number of cyclones via a normalisation by the mean number of cyclones (μ). It is formulated in Cusack (2016) as :

$$\beta = \frac{\psi}{\mu} \tag{1.4}$$

Using the formation of β shown in equation 1.4, Cusack (2016) used large length observational datasets to quantify the how severe clustering was for years with more severe cyclones. It was found that years with more severe cyclones generally had higher values of normalised dispersion (β) (i.e. they are more clustered; consistent with Vitolo et al., 2009; Pinto et al., 2013), but that their estimates were associated with considerable sampling errors. Large differences in the value of β were noted for southern European countries when the exceptionally stormy winter season of 1989/1990 was removed from the timeseries, and hence demonstrated a need for very long length datasets in order to reduce sampling variability and fully assess the strength of clustering for severely stormy seasons.

1.7.2 Differing Perspectives of Clustering

Some differences can arise in the definition of clustering based on various perspectives. One such perspective is that of dispersion that was discussed above and introduced by Mailier et al. (2006). The dispersion perspective essentially describes the deviation of monthly cyclone passages from a point poisson process in a spatial manner. This essentially describes in which locations cyclones are more likely to occur in groups and at irregular intervals compared to a random sequence on a seasonal basis. A further perspective focusses more on the synoptic behaviour of cyclones over a time-period of approximately 7 days. One such example of this is the study of Pinto et al. (2014) who identify short time periods that have a significantly above average number of cyclones that exceeds a pre-defined threshold. These periods of above average number of cyclones are classed as synoptic periods of clustering. This synoptic perspective is the one that will be used through this thesis, with further details given later in this chapter and the ones that follow. A final perspective is one that is often applied by the insurance industry. The insurance perspective defines clustering as an above average number of cyclones in a season, and focusses on longer timescales than the synoptic definition (e.g. Swiss Re, 2016). These various definitions often result in confusion as to how clustering is explicitly defined for all perspectives. However, despite these differences, common events/seasons are often identified, with the seasons of 1990 and 1999 all being identified and discussed by Mailier et al. (2006); Pinto et al. (2014); Swiss Re (2016), all of which address clustering from these different perspectives.

1.7.3 Mechanisms for Clustering

It was discussed in Mailier et al. (2006) that the observed clustering of cyclones is likely to be produced by a combination of an inhomogenous poisson process (that is the varying effect of large-scale factors modulating the passage of cyclones in time), and also a cluster process (this being cyclones that are clustered in space and time as part of a continuous wave packet). The modulation of cyclone transits and intensities in the North Atlantic by large-scale patterns is well documented (e.g. Serreze et al., 1997; Hurrell et al., 2003; Pinto et al., 2009; Donat et al., 2010), and the presence of cluster processes dates back to the work of

Bjerknes and Solberg (1922) and their observed cyclone families.

As one of the main drivers of North Atlantic windstorm intensity and propagation direction is the NAO, several studies have focussed on its role in explaining the variability of the over/underdispersion pattern. Economou et al. (2015) found that the NAO was responsible for explaining a large majority of the variability in cyclone counts across a number of datasets, particularly in the regions to the North and South of the main storm track. Pinto et al. (2016) also found the NAO responsible for explaining the overdispersion near Europe for their tests using a number of different cyclone tracking and identification schemes. Both Economou et al. (2015) and Pinto et al. (2016) state that the NAO is responsible for a large amount of the variability in dispersion (locally >50%), but does not explain all of it. Mailier et al. (2006) used a poisson regression model to infer which leading large-scale patterns were contributing to the variability in the under/overdispersion present in the North Atlantic. They investigated 10 different large-scale patterns, and found that the NAO, East Atlantic Pattern (EA), and Scandinavian Pattern (SCA) all contributed to the variability in cyclone counts in different geographic regions across the North Atlantic. They state how the positive and negative phases of NAO control whether cyclones track in a more northerly or southerly latitude and also create an enhanced pressure and baroclinic gradient favourable for the formation and propagation of cyclones toward Europe. The EA contributes as it can be associated with enhanced cyclogenesis in the eastern North Atlantic, causing cyclones to track in a more central latitude. The SCA is responsible for decreasing cyclone counts over central and western Europe, and can be thought of as a barrier to cyclone propagation resulting in a reduced distance between cyclones as their rate of movement is slowed. These

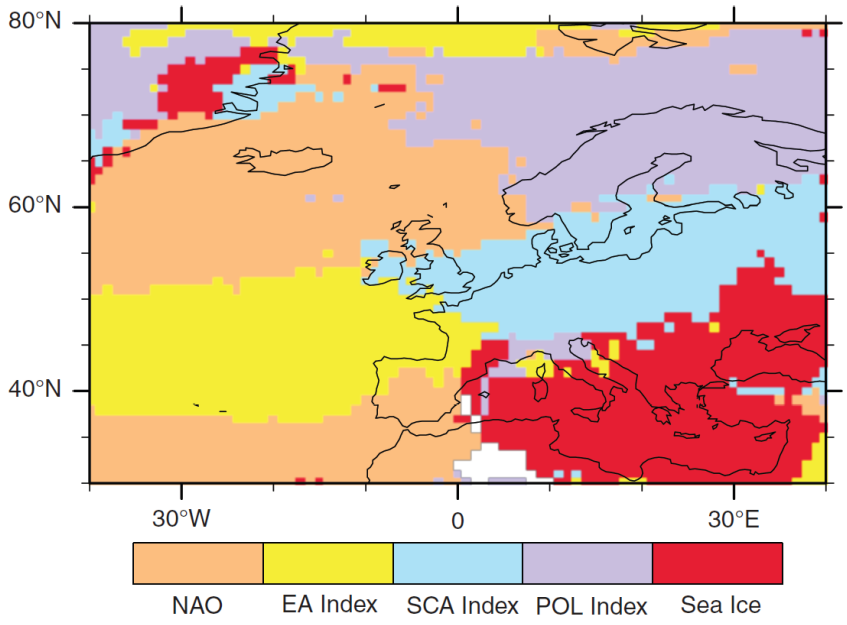

Figure 1.16: *Most dominant teleconnection patterns explaining the inter-annual variability of windstorm counts per grid cell from 1901 to 2008 identified by a Poisson generalised linear model. Patterns identified are the North Atlantic Oscillation (NAO), East Atlantic Pattern (EA), Scandinavian Pattern (SCA), Polar pattern (POL), and the influence of Sea Ice. Figure and caption from Walz et al. (2018).*

results were further confirmed by the study of Walz et al. (2018), who conducted a similar study with a longer timeseries. Their results agree well with the previous literature and also find the NAO, EA, and SCA to be important drivers of windstorm activity and the variability of their occurrence (figure 1.16).

Cyclone families were noted as being a feature of the North Atlantic atmosphere by Bjerknes and Solberg (1922) where one cyclone forms on the trailing front of a predecessor, creating a temporal connection between events. This method was hypothesised as contributing to clustering in Mailier et al. (2006). Pinto et al. (2014) objectively identified periods of clustering as when more than 4 intense cyclones passed through a 700 km radius region centred over the UK at 55°N, 5°W during 4 pre-selected months (February 1990, January 1993, December 1999, and January 2007). They found that the identified periods of clustering were all associated with an much stronger eddy-driven jet that was zonally extended across the North Atlantic, and that the jet was associated with RWB on both its poleward and equatorward flanks, helping to maintain this state. This setup is consistent with that identified by Hanley and Caballero (2012) and Gómara et al. (2014a) for individual extreme cyclones, and it appears that its persistence is associated with this clustered behaviour for these select few cases. During these identified periods of clustering Pinto et al. (2014) also noted a strong presence of upstream cyclone development in all their identified cases (this being secondary cyclogenesis as was discussed earlier) with secondary cyclones forming in the right entrance of the jet streak as a downstream parent cyclone matured. They developed a conceptual model for clustering (figure 1.17), with the large-scale pattern fixing the location of cyclones along a similar track, and then cyclone families continuously passing between the areas of anomalous RWB and affecting the same region downstream.

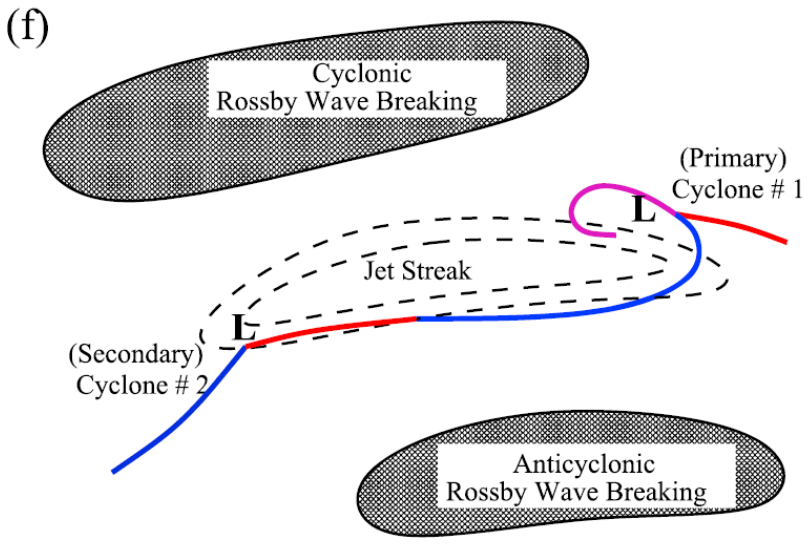

Figure 1.17: *Schematic summary showing relative positions of clustering cyclones with respect to jet streak location and location of RWB. Figure and caption from Pinto et al. (2014).*

In summary, it is clear to see that the occurrence of clustering across Europe is related to the large-scale atmospheric pattern, with a leading driver being the phase of the NAO (e.g. Mailier et al., 2006; Economou et al., 2015; Pinto et al., 2016), but also other patterns such as the EA and SCA (e.g. Mailier et al., 2006; Walz et al., 2018). In addition, the large-scale dynamical pattern of the eddy-driven jet flanked by co-occurring RWB has also been shown to be important for several periods of clustering (Pinto et al., 2014), but this has not been characterised for all events of varying magnitude. Furthermore, the contribution of upstream development (secondary cyclogenesis; Parker, 1998) has been shown to be important in the cases identified by Pinto et al. (2014), but this has also not been characterised for a larger number of clustering events.

1.8 Current Knowledge Gaps

The clustering of extratropical cyclones is a significant socio-economic threat as demonstrated by the winter months of February 1990 and December 1999 (Ulbrich et al., 2001) each resulting in $10 and $18 billion of insured losses respectively (Munich Re, 2016). Both Mailier et al. (2006) and Economou et al. (2015) state that clustering is likely a combination of a modulation of cyclone tracks by large-scale patterns, and also a connection between successive primary and secondary cyclones. Both have been shown to be important (e.g. Pinto et al., 2014), yet the relative role of each mechanism has yet to be explored. The large-scale dynamical drivers of these events has been partially explored in the study of Pinto et al. (2014), however a full characterisation of these events needs to be made and it remains to be seen if all clustering events are associated with a similar set of dynamical conditions. Furthermore, the recent extremely stormy season of 2013/2014 in the UK was associated with numerous intense extratropical cyclones. It is yet to be determined if this season was also characterised by recurrent periods of clustering, and if so, if the periods of clustering were associated with consistent dynamical features. The contribution of secondary cyclones for clustering has also been noted by Pinto et al. (2014) and these cyclones have significant impacts on western Europe (Dacre and Gray, 2009; Schemm and Sprenger, 2015). There have been extensive studies of secondary cyclones in the North Atlantic (e.g. Schemm and Sprenger, 2015; Schemm et al., 2018), however, none have related their impact on periods of clustering, or their geographical relation to the primary cyclones that spawn them. Finally, many studies have illustrated that severely stormy seasons tend to be characterised by an increase of clustering (Vitolo et al., 2009; Pinto et al., 2013; Cusack, 2016), however these estimations have been shown to be affected considerably by sampling variability, and no robust estimations exist for the most extreme seasons due to the limited availability of observational data products.

1.9 Thesis Aims and Structure

The aim of this thesis is to address the knowledge gaps and questions highlighted above, the main questions that will be answered are as follows:

Q1. Are clustering events in different locations across western Europe associated with similar large-scale dynamical features?
Q2. What were the dynamical features that were associated with the clustered winter season of 2013/2014 across the UK?
Q3. To what extent do secondary cyclones contribute to periods of clustering that affect western Europe?
Q4. Can windstorm losses associated with extratropical cyclones be represented in climate models for seasonal losses with a return period of 200 years?
Q5. How important is clustering for the most severe seasons in terms of overall losses?

Following the above science questions, the rest of this thesis will be structured as follows:

Chapter 2. In this chapter the main datasets used for analysis will be discussed. In addition the cyclone and front identification and tracking methods applied will be discussed.
Chapter 3. A climatological analysis of all identifiable periods of clustering is performed with the associated upper-level, large-scale dynamics characterised. The analysis is performed for clustering occurring in numerous geographic locations to test if there are any variations with the associated upper-level features. This chapter was published in full in *Geophysical Research Letters* as Priestley et al. (2017a).
Chapter 4. Here the winter season of 2013/2014 is investigated. This season was characterised by the repeated influence of may extratropical cyclones and the methods utilised by Pinto et al. (2014) is applied to identify if any periods of clustering are identifiable. Furthermore, it is investigated if these events are consistent with the conceptual model introduced by Pinto et al. (2014) and the findings of chapter 3. This chapter was published in full in *Weather* as Priestley et al. (2017b).
Chapter 5. Secondary cyclones, and the process of frontal wave cyclogenesis is discussed with relation to its importance on clustering in western Europe. Furthermore, a climatological perspective of secondary cyclones is also presented. This chapter has been submitted to *Quarterly Journal of the Royal Meteorological Society* and is currently in review as Priestley et al. (2019).
Chapter 6. The importance of clustering for seasonal wind based losses in Europe is examined. Tests are carried out to investigate how important the process of clustering is for seasons of varying loss magnitudes out to a return period of over 200 years. This chapter was published in full in *Natural Hazards and Earth System Sciences* as Priestley et al. (2018).
Chapter 7. Here the main results of the thesis are discussed. The main conclusions are summarised and

avenues for future work are proposed.

Chapter 2:

DATA AND METHODS

This chapter introduces the main tools and methods used to answer the questions that were posed at the end of chapter 1. Firstly, an overview of the relevant datasets is presented in section 2.1, with both ERA-Interim and HiGEM discussed in sections 2.1.1 and 2.2.2 respectively. Following this, the objective cyclone identification and tracking algorithms used are introduced and discussed in section 2.2. Finally, the synoptic front identification scheme and secondary cyclone identification method is discussed in section 2.3.

2.1 Datasets

For assessing meteorological phenomena, spatially and temporally homogenous data is the most suitable. This mostly comes in the form of gridded datasets that are arranged on latitude-longitude grids. Two forms of this data are used in this thesis and are described in this section. The first is a set of pseudo-observations, this data represents the historical state of the atmosphere and is the re-analysis product ERA-Interim (ERA-I). Secondly, a general circulation model (GCM) will be used, which simulate atmospheric and oceanic conditions based on representative atmospheric forcings and does not resemble historical events, this will be done using the UK High-Resolution Global Environment Model (HiGEM).

2.1.1 ERA-Interim

ERA-I is a meteorological re-analysis produced by the European Centre for Medium Range Weather Forecasts (ECMWF; Dee et al., 2011). Re-analyses are commonly used in the meteorological community as they are homogenous in space and time and provide a ”best guess” as to the historical state of the atmosphere. Re-analyses are created by constraining an atmospheric model to observations through data assimilation. They use a consistent model version and assimilation scheme throughout the entire length of the available data, however, the number of observations utilised in the data assimilation changes over their period of availability.

The data from ERA-I covers the period from January 1979 until the end of December 2018. However, in all the analysis that follows only the period of January 1979 - December 2015 will be considered. ERA-I has a spatial resolution of approximately 80km in the midlatitudes (T255 spectral resolution) and has 60 vertical levels with an atmospheric top at 0.1 hPa. The model physics for ERA-I come from the ECMWF's Integrated Forecast System (IFS) cycle Cy31r2 that was operational in 2006. Observations are used to constrain the state of the model using a 4-dimensional variational (4D-var) assimilation scheme in a 12 hourly analysis window, with this being most important in constraining the state of the upper-atmosphere (Dee et al., 2011). Nearly 10^7 observations were assimilated each day by ERA-I for the data covering the period of 2010, with most of these coming from satellites (figure 2.1).

Numerous variables are outputted by ERA-I, with the evolution of these being constrained by the observations provided. Some observations are not directly analysed or used in the assimilation steps, such as precipitation, turbulent fluxes, and soil moisture (Dee et al., 2011). For example, the precipitation outputs are produced by the model combining the temperature and humidity observations that are assimilated, with the accuracy of the output depending on the competence of the underlying model to correctly represent these phenomena.

ERA-I follows ERA-40 (Uppala et al., 2005) as the main re-analysis produced by the ECMWF. ERA-I has many improvements over its predecessor, this is mainly an improvement in the horizontal resolution from

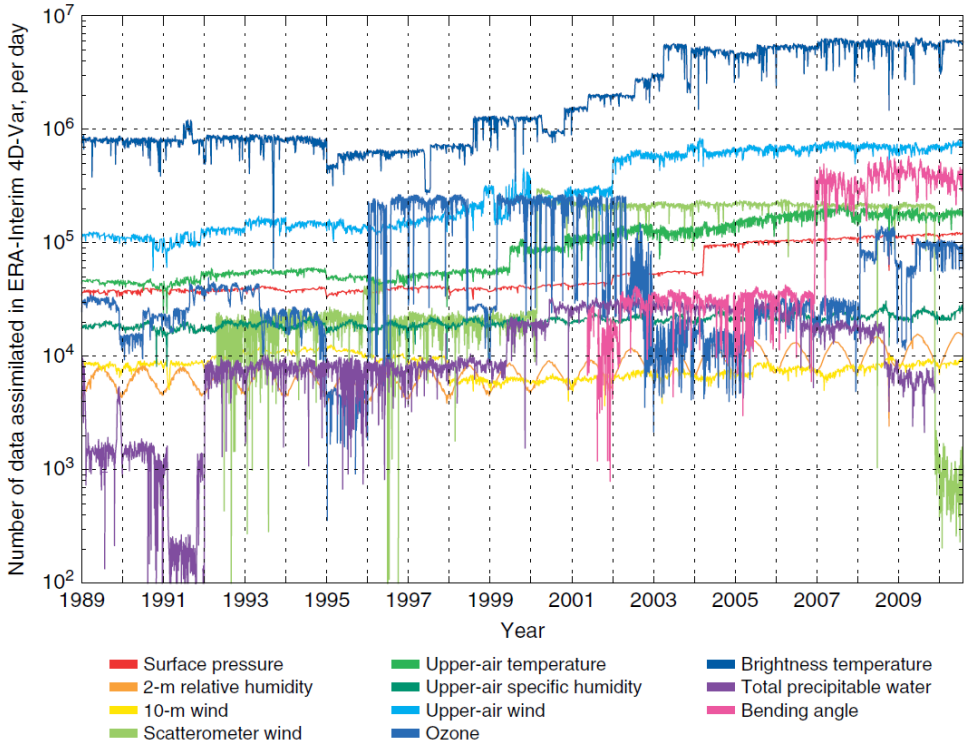

Figure 2.1: *Daily counts, on a logarithmic scale, of observations assimilated in the atmospheric analysis component of ERA-I. Figure and caption from Dee et al. (2011).*

T150 to T255 (approx. 125 km to approx. 80 km) and also a much better representation of precipitation (Dee et al., 2011). ERA-I has been very widely used in the meteorological community for numerous different purposes (e.g. Trenberth et al., 2011; Turner and Annamalai, 2012; Barnes, 2013; Pinto et al., 2014; Rhodes et al., 2015). There are of course numerous other re-analysis products available for use, such as: MERRA 2 (Gelaro et al., 2017a), NCEP-CFSR (Saha et al., 2010), and JRA-55 (Kobayashi et al., 2015a). All of these re-analyses are multi-decadal in length and extend back to before 1980. Of those listed above, ERA-I has the lowest spatial resolution, but has been shown to be a very good data product with regards to the representation of the northern hemisphere storm tracks and storm statistics (Hodges et al., 2011). This, along with its wide use in meteorological analysis demonstrate it to be a suitable product for the work presented in this thesis.

2.1.2 HiGEM

The GCM chosen for use in the analysis in this thesis is the High Resolution Global Environment Model (HiGEM; Shaffrey et al., 2009). HiGEM is based on the Hadley Centre Global Environment Model, HadGEM1 (Johns et al., 2006a; Martin et al., 2006), which was developed as part of the CMIP3 ensemble of models. A full description of HiGEM is presented in Shaffrey et al. (2009) and essentially represents a higher resolution version of HadGEM1.

HiGEM is a fully coupled atmosphere-ocean model and has an atmospheric resolution of 0.83° latitude x 1.25° longitude (N144), with an increase from the 1.25° x 1.875° (N96) resolution of HadGEM1. This is comparable to approximately 90km resolution in the mid-latitudes and is very similar to the resolution of ERA-I. This resolution is generally higher than those included in the CMIP5 ensemble of models, which tend to have a horizontal resolution of 100-300 km. There are 38 atmospheric levels up to 39km, hence the stratosphere is not very well resolved. Furthermore, all of the parameterisations and atmospheric physics are very similar to that of HadGEM1. In the ocean the resolution is $\frac{1}{3}$° x $\frac{1}{3}$°, an increase from 1° x 1 ° in HadGEM1, with the remainder of the physics being consistent with HadGEM1, as in the atmospheric component. This resolution is again higher than would be expected from models in the CMIP5 ensemble, with these resolution increases yielding an improved representation of small-scale phenomena, a reduction in SST biases, and also an improvement in the representation of the El Niño Southern Oscillation (ENSO), when compared to HadGEM1 (Shaffrey et al., 2009).

The HiGEM data analysed in this thesis comes from a series of decadal ensemble hindcasts, as described in Shaffrey et al. (2017). The configuration of HiGEM used in this analysis is consistent with that described in Shaffrey et al. (2009). The decadal ensemble hindcasts consist of 4 members that are initialised every 5 years from 1960 to 2005, inclusive. These ensembles are initialised via the relaxation

of anomalies in ocean temperature and salinity to observed values and is forced with the Historical CMIP5 RCP forcing. Alongside these ensembles, there are several transient runs of HiGEM, which cover the period from 1957 to 2015. These are initialised in 1957 using historical forcings and then greenhouse gases, aerosols, solar radiation, volcanic forcings, and ozone are prescribed throughout the duration of the runs, with no assimilation of observations.

Both the control run of HiGEM, and the decadal ensembles have been used in numerous studies (e.g. Shaffrey et al., 2009; Catto et al., 2010, 2011; Hawcroft et al., 2016; Shaffrey et al., 2017; Robson et al., 2017). The model has shown good ability in capturing the structure of the North Atlantic storm track in terms of its magnitude and variability of the number of cyclones, as well as the cyclones that make up the storm track. In addition the representation of large scale patterns of variability is very good (e.g. ENSO signal and response, Shaffrey et al., 2009), and the spatial patterns/magnitudes of precipitation from extratropical cyclones. Therefore, this is an ideal tool for analysing European windstorms as the model has a proven record for representing these phenomena successfully. Furthermore, as HiGEM has a resolution that is of a similar scale to that of ERA-I, it makes for a good comparison between the two data products.

2.2 Objective Cyclone Identification and Tracking Methodologies

In order to analyse extratropical cyclones and the North Atlantic storm track, objective cyclone identification and tracking methodologies are used. These methods require spatially and temporally homogenous data of a good enough resolution to be able to sufficiently identify and track unique features. There are many different variations on these methodologies, which often yield different results. Comparisons of tracking methodologies was performed by Neu et al. (2013) and Pinto et al. (2016) and is discussed in chapter 1, most methods generally commonly use mean sea level pressure (MSLP) or the geostrophic relative vorticity ξ for identification (Neu et al., 2013). Most methodologies generally perform similarly, with this particularly being the case for intense cyclones, which are more easily identifiable. The two methods that are utilised for the analysis in this thesis will be discussed. The first to be discussed will be the method of Murray and Simmonds (1991b), that was adapted by Pinto et al. (2005) for northern hemisphere cyclones. The second to be discussed will be the TRACK algorithm developed by Hodges (1994, 1995, 1999).

2.2.1 Murray & Simmonds/Pinto Method

In this section the cyclone identification and tracking algorithm of Murray and Simmonds (1991b,a), that was adapted for Northern Hemisphere cyclones by Pinto et al. (2005) is discussed. This algorithm works like all others in that individual cyclonic features must first be identified in a gridded datasets at specific times. These features must then be identified at subsequent times and connected together to form coherent cyclone tracks. This method identifies cyclones using the MSLP field. This method first identifies cyclones

as maxima in the laplacian of the MSLP field ($\nabla^2 p$), which is a good proxy for the local relative vorticity (ξ), as shown in equation 2.1, where ρ and f represent the density and coriolis parameter respectively. Murray and Simmonds (1991b) discuss how mid-latitude cyclones are generally better represented by a cyclonic vorticity maximum, rather than a MSLP minimum.

$$\xi = \frac{1}{\rho \cdot f} \nabla^2 p \tag{2.1}$$

Once the maximum in $\nabla^2 p$ have been found, the true centre of the cyclone is identified as the nearby MSLP minima, hence associating the identified features with "real" low pressure systems. If no MSLP minima is found, the point with the lowest pressure gradient is used. A filtering of cyclones is performed to remove spurious features in this initial stage. Firstly, any cyclones that are at surface points over 1500 metres are discarded due to issues with interpolating to the MSLP grid. Secondly, to eliminate the presence of multiple systems in a confined region, as is often presented near orographic boundaries, or along frontal zones, only the strongest system within a radius of 3° latitude is included.

Following the identification of a cyclonic system at a set time, it must then be connected with the same feature at subsequent times. This is done through the prediction of the subsequent position and core pressure of the cyclone at the following timestep. The cyclonic features that are identified within the vicinity of the new predicted location are examined and the best match chosen. Any features that are not associated with a similar feature at a subsequent or preceding timestep are said to have either just formed (cyclogenesis), or just decayed (cyclolysis). Following the creation of the tracks a further filtering is performed via a set of thresholds to remove any spuriously identified features. Firstly, a cyclone must last for at least 24 hours. It must also be classed as a close and intense system, that is having a distinct pressure minima, and also a value of $\nabla^2 p$ that is larger than 0.6 hPa deg.lat.$^{-2}$ at some point in its lifetime. Several thresholds as applied by Pinto et al. (2009) are also applied. The first being a minimum intensification rate, whereby the cyclone must have a $\frac{d}{dt}\left(\nabla^2 p\right)$ of at least 0.3 hPa deg.lat.$^{-2}$ day^{-1}. And also the minimum pressure of the cyclone must at some point in its lifetime be less than 1000 hPa.

2.2.2 Hodges Method

The method known as TRACK (Hodges, 1994, 1995, 1999) differs from the method of Murray and Simmonds (1991b) and Pinto et al. (2005) in that cyclones are identified using 850 hPa relative vorticity (ξ_{850}) and not MSLP. It is argued in Hoskins and Hodges (2002) that the use of ξ_{850} over MSLP results in more small scale features being identified, and also those that are identified being identified sooner as there is no criteria for a distinct pressure minima to be present, as in the previously discussed method. Furthermore, using ξ_{850} does not require any extrapolation to sea level over high orography, as in the previous method, and is computed straight on the model pressure levels.

In order to identify cyclonic systems, the ξ_{850} field is first of all spectrally truncated to T42 and any wavenumbers less than or equal to 5 are removed. This ensures that regardless of model resolution, tracking is always performed on the same resolution data, and the removal of the planetary scale wavenumbers removes large-scale noise and ensures that only the synoptic scale features are focussed on. The cyclonic features are then identified as maxima in ξ_{850} in the spectrally truncated and filtered fields.

Once the cyclonic features have been identified in the gridded data, they need to be grouped into tracks. This is initially done using a nearest neighbour approach to initialise the tracks, which imposes a maximum distance between which feature points may be located. Following this the tracks are refined and smoothed through the minimisation of a cost function that is subject to adaptive constraints which depend on the speed and direction of features (see Hodges, 1999). Following these steps the tracks are filtered further to those that travel at least 500km and have a lifetime that is at least 24 hours. This ensures that all the cyclones develop for a period of time, with these thresholds being chosen to be consistent with the thresholds in the previously discussed method. The movement criteria also ensure any quasi-stationary cyclones are not identified, but as the focus of this thesis is cyclones moving from the North Atlantic across Europe from the main storm track, this should not limit the cyclones that are identified. Further environmental fields can be associated to tracks (fields such as MSLP or 10-metre wind speed), with this being done via a minimisation technique within a 5° spherical cap centred on the location of the cyclone (Bengtsson et al., 2009).

Both the methods discussed above have been used countless times for studying extratropical cyclones (e.g. Hoskins and Hodges, 2002; Bengtsson et al., 2006; Donat et al., 2010; Hodges et al., 2011; Hawcroft et al., 2012; Catto and Pfahl, 2013; Zappa et al., 2013a; Pinto et al., 2014). These methods have been shown to compare well with other available methods (e.g. Sinclair, 1994; Wernli and Schwierz, 2006; Raible et al., 2008; Neu et al., 2013; Pinto et al., 2016), especially for strongly intensifying systems and those which reach a very high peak intensity.

2.3 Secondary Cyclones

A section of analysis in this thesis focusses on secondary cyclones and cyclone families in the North Atlantic. These are cyclones that form on the trailing fronts of another primary cyclone. Identifying these cyclones is a two step process. First of all, synoptic scale frontal features must be identified in meteorological data. Secondly, the secondary cyclone must be identified near to a front that is associated with a primary cyclone. This two step process is described below.

2.3.1 Identifying Synoptic Scale Frontal Features

The method applied is that used by Schemm et al. (2015) and Schemm and Sprenger (2015), and is based on the thermal detection method of Hewson (1998). The basis of this method lies in identifying gradients of a two-dimensional thermal field (τ). The thermal field that is examined for the location of fronts is defined as the thermal front parameter (TFP), and is formulated in equation 2.2.

$$TFP = -\nabla \left|\nabla\tau\right| \cdot \frac{\nabla\tau}{\left|\nabla\tau\right|} \tag{2.2}$$

The TFP can be expressed as the gradient of the magnitude of the gradient of a thermodynamic scalar quantity, resolved into the direction of the gradient of that quantity (Renard and Clarke, 1965) and the front is commonly placed where TFP = 0. The variable used for τ is commonly either the wet bulb potential temperature (θ_w; e.g. Hewson, 1998; Berry et al., 2011), or the equivalent potential temperature (θ_e; e.g. Jenkner et al., 2010; Schemm et al., 2015; Schemm and Sprenger, 2015), with θ_e being used for the calculations in this thesis. Moist temperature variables are seen as good for this purpose as they are highly conservative properties that follow airmass origins closely. In addition gradients of θ_e are much steeper than gradients of θ in frontal zones due to diabatic modification of air surrounding frontal zones (Hewson, 1998; Jenkner et al., 2010).

In the calculation of TFP a minimum value of $|\nabla\theta_e|$ is applied, in order to remove any weak thermal gradients. In equation 2.2, $|\nabla\theta_e|$ >3.5 K(100km)$^{-1}$ is used as a threshold, and this is evaluated at 850 hPa. The surface is not used as frontal features are often smoothed out by boundary layer processes (Jenkner et al., 2010), therefore 850 hPa is a good choice for near-surface features and has been widely used in other frontal detection studies (Hewson, 1998; Berry et al., 2011; Schemm et al., 2015).

Further criteria are applied to filter out small scale features. Following Schemm et al. (2015) and feature must be at least 500km long following a cubic spline interpolation of the identified grid points. In the studies of Schemm et al. (2015) and Schemm and Sprenger (2015) a minimum advection speed criteria of 3 m s^{-1} was also applied in order to remove unphysical, quasi-stationary features such as land and topographic boundaries. However, this criteria is not applied as this study focusses on cyclones forming along persistent frontal features, some of which have been shown to be quasi-stationary (see Pinto et al., 2014).

There are of course other methods to identify synoptic scale frontal features. The main other method used is that developed by Simmonds et al. (2012). This method identifies directional changes in the 10-metre or 850 hPa wind speed, with it changing from being from the northwest to the southwest quadrant for

cyclones in the southern hemisphere, and vice versa for cyclones in the northern hemisphere. This shift would also have to be associated with an increase of the meridional wind speed by more than 2 m s^{-1}. This method also applies a minimum length criteria of 500km. This method was shown to be particularly good for fronts that are meridionally oriented and of significant length. However, it occasionally struggles with zonally oriented features (Schemm et al., 2015). A comparison of several methods by Hope et al. (2014) found the wind shift method to be broadly consistent with other methods, however it was also susceptible to identifying cut-off lows and pre-frontal troughs as synoptic scale frontal features. A further comparison of the thermal and wind methods by Schemm et al. (2015) showed that the wind shift method was more suited to regions of strong convergence, or those with significant wind shear. Whereas the thermal method was much better for fronts in strong baroclinic situations and agreed well with manual analyses.

2.3.2 Identifying Cyclogenesis on Fronts

The frontal wave cyclogenesis method is Schemm and Sprenger (2015) is broadly followed in the analysis presented in this thesis. Slightly different parameters are used to classify the different types of cyclone. Firstly, for a cyclone to be identified as forming on a trailing front, it must be located within 200km of any of the frontal grid points, this differs from the 100km specified in Schemm and Sprenger (2015). Furthermore, for the trailing front to be connected to another cyclone, it must have one front grid point within 500km of the cyclone centre. In Schemm and Sprenger (2015), the front had to intersect a closed MSLP contour of the associated cyclone. This association was made simpler due to the tracking algorithm of Wernli and Schwierz (2006) that was being applied, and this algorithm providing information regarding the outermost closed MSLP contour. However, as the method of Murray and Simmonds (1991b) and Pinto et al. (2005) will be applied, and provides no information regarding closed MSLP contours, the 500km criteria is chosen for simplicity.

Based on the above methodology, cyclones will be classed into one of three categories, which are as follows:

1. Primary: Cyclones associated with a frontal feature as some point during their lifetime. During this connection the front is then subsequently associated with the cyclogenesis of another cyclone. These cyclones are the first in a family.
2. Secondary+: Cyclones that form within 200km of a pre-existing front that are in turn associated to a previously identified cyclone. These cyclones are any that are not the first in a family.
3. Solo: These cyclones may be associated with fronts during their lifetime, but these fronts will not be associated with cyclogenesis. In addition they may not be associated with a front at all.

Furthermore, the Primary and Secondary+ classes will on occasion be grouped together to form the 'Family'

class of cyclones.

Chapter 3:

Rossby Wave Breaking, the Upper Level Jet, and Serial Clustering of Extratropical Cyclones in Western Europe

It was described in Chapter 1 how the day-to-day variability of weather across western Europe, and specifically the UK, is dominated by the presence of extratropical cyclones (Della-Marta et al., 2010). The clustering of extratropical cyclones has been shown to occur numerous times for a geographical region surrounding the UK, as was shown in Pinto et al. (2014). In these select cases these events were associated with a very strong and zonally extended eddy-driven jet that was flanked by the occurrence of Rossby wave breaking on both the northern and southern edges. The aim of this chapter is to explore these phenomena further and to see if all clustering events are associated with these dynamical features, or if it is just a property of the previously studied very intense clustering periods. It will also be examined if clustering events occurring in different geographic locations in western Europe are also associated with similar dynamical features, or there is some sort of geographical dependence. This chapter will summarise and characterise all similar events and assess the variability of the various dynamical features. The research question that will be addressed in this chapter is as follows:

Q1. Are clustering events in different locations across western Europe associated with similar large-scale dynamical features?

This text and figures that follow have been published in *Geophysical Research Letters* (Priestley et al., 2017a).

Citation

Priestley, M. D. K., J. G. Pinto, H. F. Dacre, and L. C. Shaffrey (2017), Rossby wave breaking, the upper level jet, and serial clustering of extratropical cyclones in western Europe, Geophysical Research Letters, 44, 514-521, doi:10.1002/2016GL071277.

Author Contributions

The concept for this study was initially developed by J. Pinto, H. Dacre, and L. Shaffrey. The development of the analysis and concept was completed by all the authors. The analysis, creation of figures, and writing of the text was completed by M. Priestley. The remainder of the authors provided feedback and comments to produce the final manuscript.

3.1 Abstract

Winter 2013/14 was the stormiest on record for the UK and was characterized by recurrent clustering of extratropical cyclones. This clustering was associated with a strong, straight and persistent North Atlantic jet and was also associated with Rossby wave breaking (RWB) on both flanks, pinning the jet in place. The occurrence of RWB and cyclone clustering is further studied in 36 years of the ERA-Interim Reanalysis. Clustering at 55°N is associated with an extended and anomalously strong eddy-driven jet flanked on both sides by RWB. However, clustering at 65(45)°N has a dominance of RWB to the south (north) of the jet, deflecting the jet northward (southward). A positive correlation was found between clustering and RWB occurrence to the north and south of the jet. However, there is considerable spread in these relationships.

3.2 Introduction

Intense extratropical cyclones are the primary natural hazard affecting Western and Central Europe (Della-Marta et al., 2010) and are responsible for 70-85% of precipitation in these regions (Hawcroft et al., 2012). Cyclone clustering can lead to greater impacts than those which would have occurred from individual cyclones (Vitolo et al., 2009), since the capacity to respond and the resilience of society is weakened with each subsequent event. Consequently, the clustering of extratropical cyclones is of great interest to insurance industry, civil protection and policy-makers.

Observations suggest that winter 2013/14 was the stormiest in over 20 years with record-breaking amounts of rainfall (165% of the UK average) (Matthews et al., 2014; Kendon and McCarthy, 2015). The season was characterised by clusters of cyclones affecting the UK. Similar behaviour has been identified in other winter months (e.g. January 2007) (Pinto et al., 2014). Previous studies have found that the

trajectories of intense North Atlantic cyclones were commonly influenced by Rossby wave-breaking (RWB) on both sides of the North Atlantic jet (Hanley and Caballero, 2012; Gómara et al., 2014a; Pinto et al., 2014; Messori and Caballero, 2015). Cyclonic RWB is most commonly found on the northern flank of the jet, with anticyclonic RWB mostly on the southern flank (Nakamura and Plumb, 1994). Barnes and Hartmann (2012) showed how this presence of RWB acts to flux eddy momentum into the core of the jet, resulting in an acceleration of the upper-level flow between these two regions. Large scale modes of atmospheric variability, such as the NAO (North Atlantic Oscillation, Hurrell et al. (2003)), have also been shown to be related with the clustering of extratropical cyclones (Mailier et al., 2006; Vitolo et al., 2009). Woollings et al. (2010a) found that an NAO+(-) pattern is associated with the jet being in a more northerly (southerly) position, which then controls the location and direction of cyclone tracks over the North Atlantic (Pinto et al., 2009).

Pinto et al. (2014) investigated mechanisms associated with cyclone clustering. They found that clustering events influencing the UK were associated with a zonally extended eddy-driven jet flanked by RWB to the north and south. Clustering can also be influenced by mesoscale processes, for example Pinto et al. (2014) also highlighted the importance of secondary cyclogenesis during clustering. Secondary cyclones can be very destructive (Dacre and Gray, 2009) and commonly form in trailing cold fronts of extratropical cyclones. However, the development of secondary cyclones is more unpredictable and is influenced by other mechanisms such as the associated deformation strain (Renfrew et al., 1997), frontal shear (Chaboureau and Thorpe, 1999), latent heat release (Joly and Thorpe, 1990a) and boundary layer friction (Adamson et al., 2006).

The aim of this study is to characterise the clustering of extratropical cyclones over the North Atlantic and their relationship with RWB and the upper level jet. We focus on clustering not just for the UK, but also at two other regions of Western Europe to the North and South of the UK. Section 3 investigates clustering during winter 2013/14, while clustering across a 36 year period is investigated in section 4. Section 5 examines the temporal evolution of RWB and the jet anomalies during clustering, with the variability of RWB and jet examined in section 6. We will conclude our findings in section 7.

3.3 Data & Methods

In this study, the European Centre for Medium-Range Weather Forecasts Interim Re-Analysis (ERA-Interim) dataset (Dee et al., 2011) is used. ERA-Interim has a horizontal resolution of T255 and 60 vertical levels. We use all December, January and February (DJF) months from 1979/80-2014/15. To identify extratropical cyclones, the cyclone tracking algorithm of Murray and Simmonds (1991a) is applied to ERA-Interim. Cyclones are identified by the Laplacian of mean sea level pressure (MSLP)(∇^2p).

The nearest MSLP minima is located to the maxima in the ∇^2p field. The tracking algorithm used was adapted for Northern Hemisphere cyclones by Pinto et al. (2005) and performs similarly to other tracking methodologies (Neu et al., 2013). Following Pinto et al. (2009) cyclones are only selected if they adhere to the following criteria:

1. cyclone lifetime $\geq$ 24 hours
2. minimum MSLP $<$ 1000 hPa
3. maximum $\nabla^2 p >$ 0.6 hPa degree latitude^{-2}
4. maximum $\frac{d}{dt}\nabla^2 p \geq$ 0.3 hPa degree latitude^{-2} day^{-1}

We follow the definition of Pinto et al. (2014) for cyclone clustering. An area is defined with a 700 km radius about a latitude-longitude point, and cyclones that adhere to the criteria above and pass through this area are counted. The cyclones are recorded when at peak intensity within this area, with the intensity measured as minimum MSLP. To ensure that only the most intense cyclones are considered, we discard any cyclones with a pressure in the highest 95% of MSLP climatology at that latitude-longitude point. A day is identified as clustered if the 7-day running sum of the remaining cyclones is greater than or equal to 4. We perform this analysis for three locations along 5^{o}W, with the radius centred at 55^{o}N, 5^{o}W; 45^{o}N, 5^{o}W; and 65^{o}N, 5^{o}W (figure 3.1), hereafter denominated as 55^{o}N; 45^{o}N; and 65^{o}N. The 95th percentiles used as an intensity threshold are 999 hPa at 45^{o}N, 984 hPa at 55^{o}N, and 972 hPa at 65^{o}N. We have also compared the results of the above method with one based on 850 hPa relative vorticity (Hodges, 1995), with consistent cyclone numbers and clustering periods found across both methods, with the conclusions being unaffected by the method (not shown).

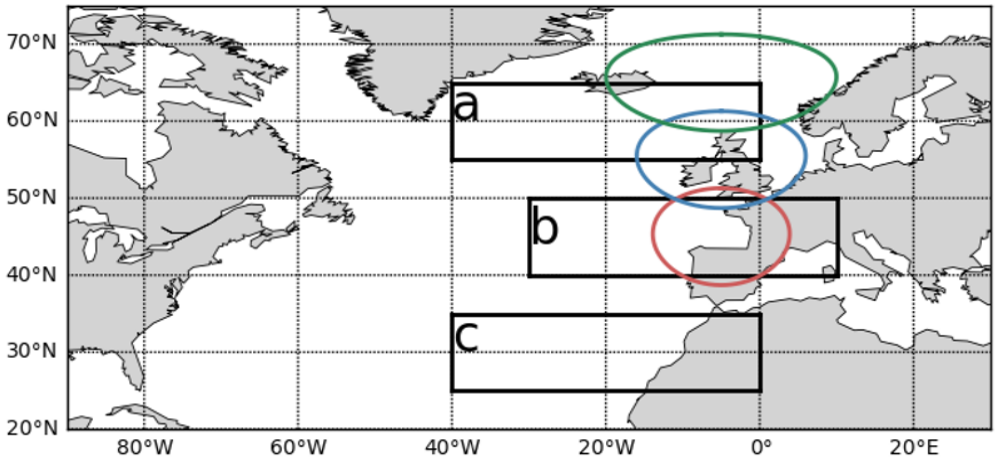

Figure 3.1: *Locations of the three boxes used in the jet and RWB analysis. Boxes a and c are used for the RWB analysis. Box a is 55-65^{o}N, 40-0^{o}W, Box c is 25-35^{o}N, 40-0^{o}W. Box b is used in the jet analysis and is from 40-50^{o}N, 30^{o}W-10^{o}E. Box b is shifted 10^o north and south for the latitudinal areas to the north and south of the UK respectively. The three coloured circles represent the three areas used for cyclone identification. The are centred at 45^{o}N, 5^{o}W(red), 55^{o}N, 5^{o}W(blue) and 65^{o}N, 5^{o}W(green)*

An adapted version of the jet latitude method from Woollings et al. (2010a) is used to analyse the behaviour

of the eddy-driven jet. The original metric uses the daily zonal mean zonal wind at 850 hPa from 25-75^{o}N, 60-0^{o}W. We performed tests for several longitudinal extensions, with each providing consistent results and robust conclusions. However, to focus on the Eastern North Atlantic and Western Europe, we use 40-0^{o}W in our analysis. To generate the anomaly field a long-term daily climatology of the zonal wind is removed with the resulting field being low-pass filtered (Lanczos, 10-day cutoff (Duchon, 1979)) to remove any synoptic influences. The jet latitude on each day is the latitude of maximum wind speed following the removal of the climatology and filtering.

To define and identify RWB, we use the 2-D B-index from Masato et al. (2013), which was originally defined by Pelly and Hoskins (2003). The B-index uses the potential temperature (θ) field on the 2 PVU surface (dynamical tropopause; 1 PVU = $1 \times 10^{-6} Km^2 kg^{-1} s^{-1}$) which is used as a daily average. The B-index is a field that identifies where the meridional gradient of θ is reversed with positive values indicating the presence of RWB. No persistence criteria is applied in order to identify RWB at each 6-hourly interval. Analysis is also performed on a zonally averaged field; this being from 25-75^{o}N, 40-0^{o}W. As with the eddy-driven jet metric, conclusions were found to be insensitive to the exact choice of longitudinal extent.

3.4 RWB and Cyclone Clustering in the Winter of 2013/14

The winter season of 2013/14 was the stormiest on record in the UK (Matthews et al., 2014). Figure 3.2a shows the 39 cyclone tracks that passed within 700 km of 55^{o}N throughout January and February 2014; with 26 of these exceeding the local 95th percentile of MSLP. The enhanced cyclone activity is made further apparent when examining the anomaly in cyclone days per month for January and February 2014 (Figure 3.2b). A statistically significant anomaly of over 12 cyclone days month^{-1} degree latitude^{-2} can be seen near the west coast of Scotland. A majority of the UK had an increase of at least 6 cyclone days per month. In this context 1 cyclone day month^{-1} degree latitude^{-2} corresponds to that latitude square being characterised by cyclonic activity on one day of the month.

A number of clustered days are identified for 55^{o}N during DJF of 2013/14. These are 20-30 December; 3-4, 15-18 January; and 2-14, 22-23 February. These dates are indicated by the blue dashes below figure 3.2d. Figure 3.2c shows that the latitude of the 850 hPa jet varies only a little during Jan/Feb 2014, with the latitude being between 40^{o}N and 50^{o}N on 71% of days. It is also anomalously strong, with anomalous speeds of 24 m s^{-1} in early January, whilst for the majority of DJF 2013/14 speeds are above 10 m s^{-1} greater than the climatology. This is in contrast with late Autumn 2013 and early Spring 2014, when the jet is weaker and varies more latitudinally.

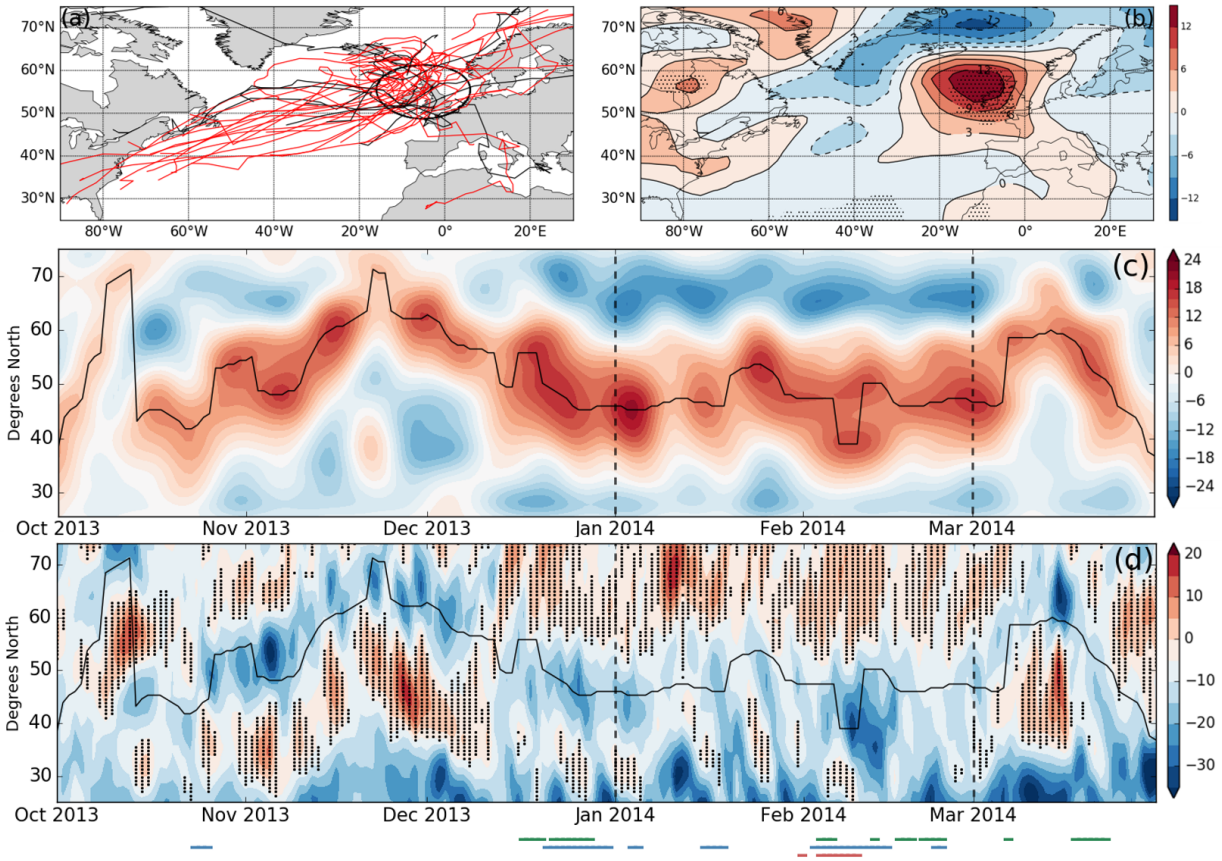

Figure 3.2: *(a) Tracks of cyclones that pass within 700 km of 55°N (black circle) during January and February 2014. Tracks that exceed the 95th percentile of MSLP are red, others are black. (b) Anomalous track density for January and February of 2014 compared to the climatology. Units are cyclone days month^{-1} degree latitude^{-2}. (c) The eddy-driven jet for October-March 2013/14. Shaded contours are the anomalous wind speeds (m s^{-1}). The black line represents the jet latitude. (d) RWB in the North Atlantic for October-March 2013/14. Shaded contours represent the zonally averaged B-index on each day, black dots indicate positive values. The black line is the jet latitude. The vertical dashes in (c) and (d) indicate the period used in (a) and (b). The green dashes below the figure indicate clustering for tracks that pass within 700 km of 65°N, blue are for 55°N, red are for 45°N (see Fig. 3.1).*

RWB occurrence over the North Atlantic shows a clear distinction between clustered and non-clustered periods. Clustering at 55°N is consistently accompanied by RWB on both the northern and southern flanks of the eddy-driven jet (Figure 3.2d). RWB to the south is more intermittent (similar to Pinto et al. (2014); their Fig. 3), with the RWB to the north being more persistent for much of DJF 2013/14. The presence of RWB to both the north and the south will act to enhance the thermal gradient in the upper troposphere, allowing for a more intense jet extended toward western Europe. This extension will steer cyclones further toward western Europe, which can cause significant impact and losses if landfall occurs.

We have repeated this analysis for different latitudes. The 700 km radius was moved both 10° north and south of 55°N. The dashes at the bottom of figure 3.2d show when we identify clustering at 65°N (green) and 45°N (red). The clustering at these latitudes occurs at different times, however there are some periods of overlap which may be as a result of slight overlap of the 700 km radii (see figure 3.1). The green dashes (65°N) are often associated with the jet in a more northern position (mid December 2013, early-mid

March 2014), and also with a greater presence of RWB to the south (e.g. mid-March 2014). Clustered periods for 45^{o}N (red) appear to coincide with the clustering at 55^{o}N. However, the jet has a very large latitudinal range for the period in early February 2014, with peak speeds occurring nearer to 40^{o}N. Hence the more southerly jet latitude would be steering some of the cyclones further south.

3.5 RWB and Cyclone Clustering in ERA-Interim

The results presented above for 2013/14 are consistent with findings from Pinto et al. (2014), which were based on the analysis of four other winters. We now extend this analysis to investigate if the dynamical patterns identified for clustering in winter 2013/14 are valid for all clustered periods in ERA-Interim.

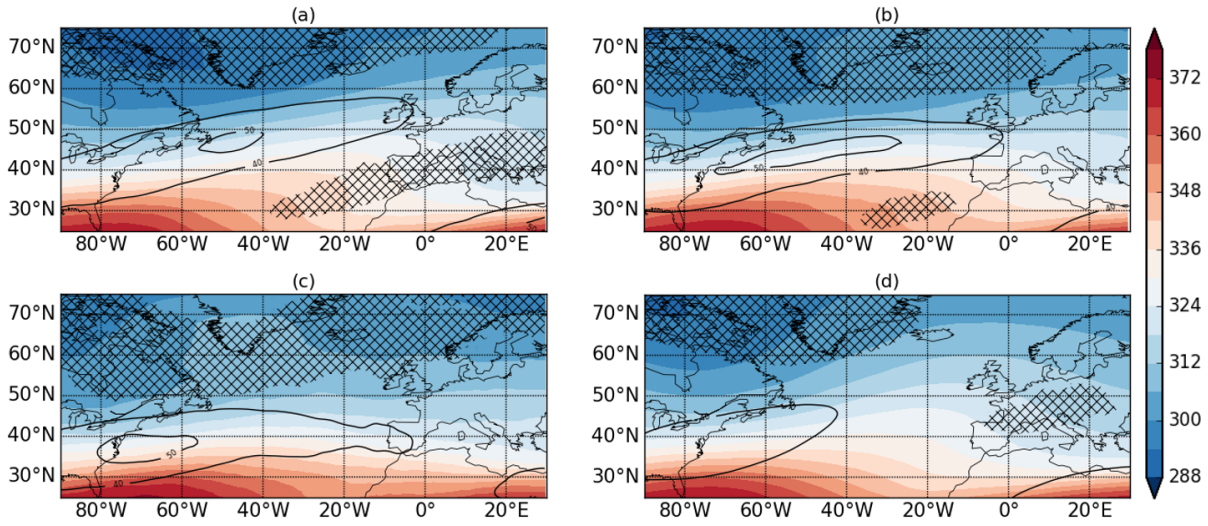

Figure 3.3: *Composites of clustered days at (a) 65^{o}N, (b) 55^{o}N, (c) 45^{o}N. (d) Climatology. For all panels the coloured contours are θ on the 2 PVU surface (K). Black contours are the 250 hPa wind speed from 40 m s^{-1} and every 10 m s^{-1} above. The crossed hatchings are where RWB was occurring on at least 30% of days.*

An upper troposphere composite for clustered days ($\geq$4 intense cyclones in 7 days) in the DJF season from 1979/80-2014/15 (387 out of 3240 days) at 55^{o}N can be seen in figure 3.3b. It shows an eastward extended and intensified jet that is also straighter than would normally be seen (figure 3.3d). This jet is flanked by RWB on both sides, with a sharper thermal gradient between the two regions of RWB than is present in the same region of figure 3.3d. It is apparent from figure 3.3b that this pattern will cause cyclones that form in the North Atlantic or off the east coast of the USA to be steered eastward along the axis of the jet. This pattern resulted in very stormy conditions at 55^{o}N, as was seen in winter 2013/14 and is consistent with that identified in figure 3.2 and also the schematic in figure 7f of Pinto et al. (2014).

The composite image for clustering at 65^{o}N (figure 3.3a) (450 out of 3240 days) demonstrates a different pattern to that shown in figure 3.3b. For clustering at 65^{o}N, the jet is much more tilted from SW-NE, with more RWB to the south and less to the north when compared to figure 3.3b. For clustering

at 45^{o}N (figure 3.3c) (183 out of 3240 days) the jet is zonal until the exit region and is then tilted from NW-SE. Figure 3.3c is also characterised by a large amount of RWB to the north, with little RWB to the south. Finally, when days are classed as non-clustered at 55^{o}N (figure 3.4) (2853 out of 3240 days) the jet is not extended beyond the western North Atlantic and is also weaker than the clustered days. It is characterised by a large area of RWB across western Europe, indicative of anticyclonic blocking, which will steer cyclones to the north or south of western Europe.This is very similar to figure 3.3d and also the non-clustered composites for 45^{o}N and 65^{o}N (figure 3.4).

Figure 3.3 shows that clustering at different latitudes is associated with different dynamical patterns in the North Atlantic. The presence of RWB in various locations in the eastern North Atlantic is associated with the tilt and latitudinal location of the jet, and hence the direction in which the cyclones are steered. This is consistent with findings in previous studies (Benedict et al., 2004; Woollings et al., 2010a; Franzke et al., 2011).

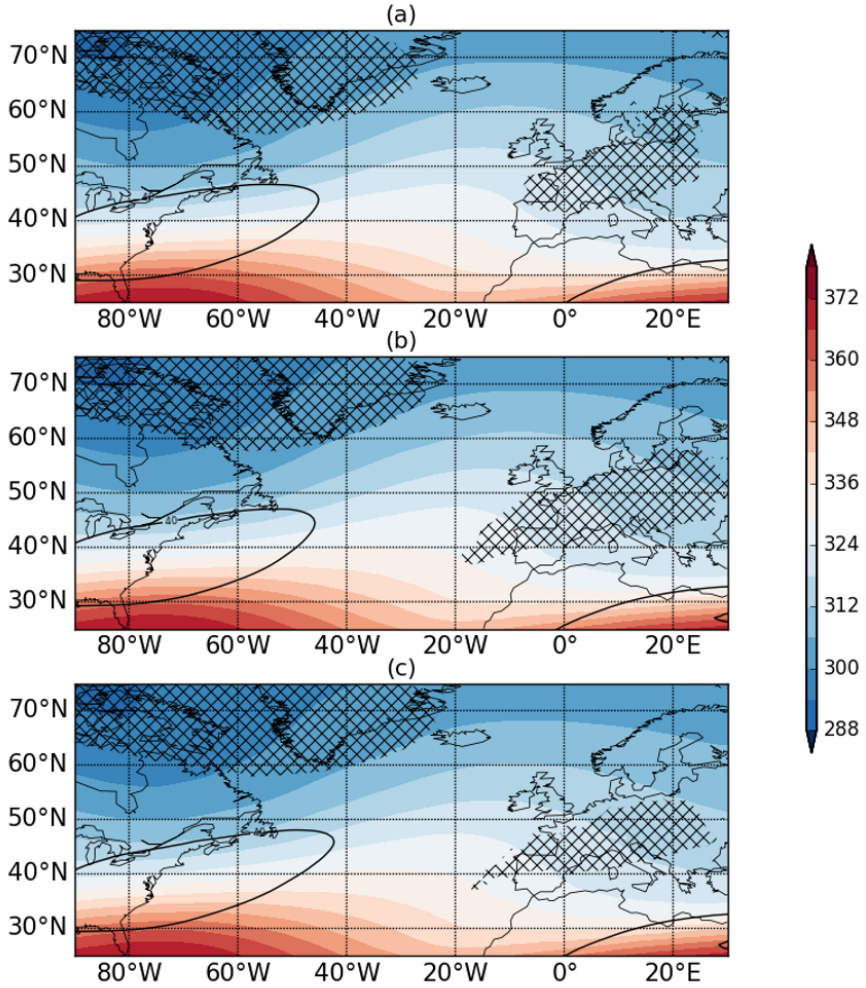

Figure 3.4: *Composite images of non-clustered days (<4 cyclones in 7 days) at (a) 65^{o}N, (b) 55^{o}N and (c) 45^{o}N. (a), (b) and (c) are made up of 2790, 2853 and 3057 days respectively.*

3.6 The Temporal Evolution of the RWB and the Jet during Clustering

Figure 3.5 shows how the RWB and jet anomalies develop in the days before and after clustering at 55^{o}N. A lagged composite analysis of clustered days further highlights the importance of anomalous RWB in the eastern North Atlantic for clustering. We lag to the clustered days identified for 55^{o}N to infer how the dynamical features develop. At lag -8 days jet anomalies are weak, with only isolated regions greater than 5 m s^{-1}. The RWB flanking the jet is also similar to climatology (fig 3.3d), although some increases of up to 10% are present in the regions of box a and box c (see figure 3.1). At lag -4 days the jet has accelerated further with localised anomalies over 10 m s^{-1} and a further increase in RWB with up to 15% more RWB in the eastern North Atlantic. RWB activity reaches its maxima at lag -2 days with anomalies of 15-20% and jet speeds similar to those previously. The jet anomaly peaks on lag 0 days with speeds of more than 15 m s^{-1}. Patterns are consistent at lag 2 days, however, by lag 4 days the presence of RWB and the wind speeds begin to decrease. At lag 8 days the presence of RWB in the eastern North Atlantic has almost disappeared, with anomalous wind speeds nearer to 0 m s^{-1}. Figure 3.5 suggests that RWB activity in the eastern North Atlantic peaks before the anomalies in the jet speed. This is consistent with RWB enhancing the upper tropospheric thermal gradient at lag -2 days, which will strengthen wind speeds at 250 hPa and extend the jet eastwards; which peaks at lag 0 days. This acceleration can be thought of as a convergence of eddy momentum in the jet core from the RWB on each flank, which is consistent with Barnes and Hartmann (2012).

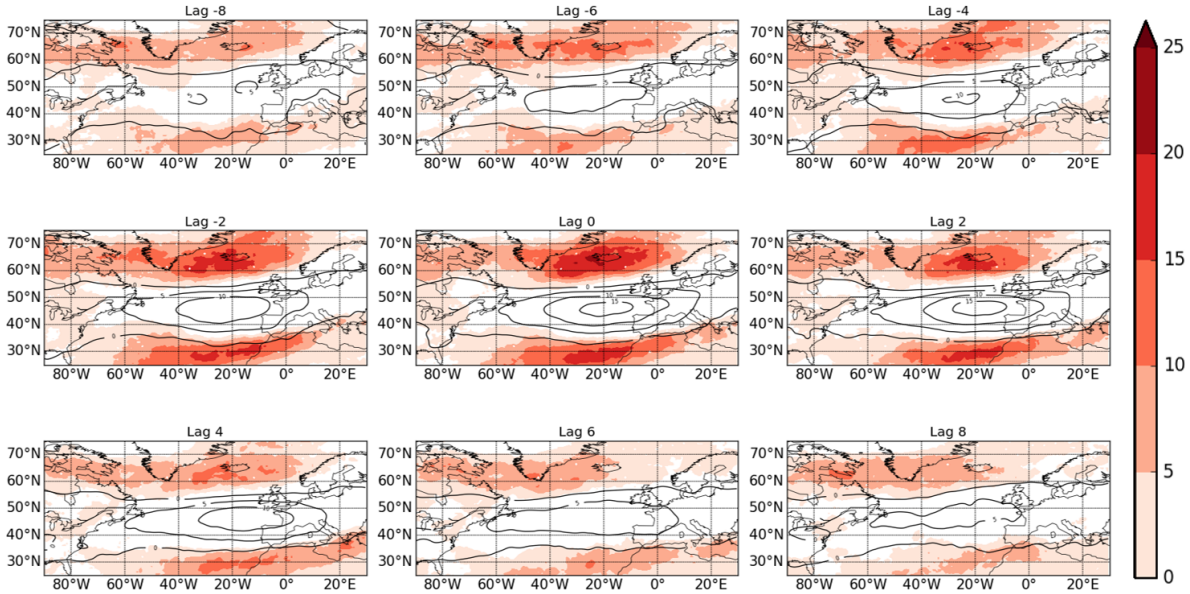

Figure 3.5: *Composite images of North Atlantic RWB and jet anomalies on days lagged to clustered days at 55^{o}N. The red shading is the percentage increase in the B-index compared to climatology (fig 3.3d). Black contours are the 250 hPa wind speed anomalies (m s^{-1}). Shown is from lag -8 days to lag +8 days at 2 day intervals.*

Similar patterns to figure 3.5 are found when we inspect the lagged composite for clustering at 45^{o}N and 65^{o}N (Figures 3.6 and 3.7). In both instances the increases in RWB reaches values of up to 20% above climatology (fig 3.3d) at lag -2 days, which then broaden by lag 0 days and even marginally increase. The RWB in figure 3.6 does not peak as clearly at lag -2 days as in figures 3.5 and 3.4. As with figure 3.5 both figures 3.6 and 3.7 also see peak wind speeds at lag 0 days.

The composites on lag 0 days also further illustrates the preferential positions of RWB for clustering that can influence western Europe that we identified from figure 3.3. Figure 3.5 suggests that the presence of RWB on one or both sides of the jet is highly important for controlling the strengthening of the upper level jet toward any of our clustering latitudes, and hence is a precursor for the observed clustering. This provides a more robust conclusion to the results of Pinto et al. (2014) as analysis was performed using a considerably larger dataset.

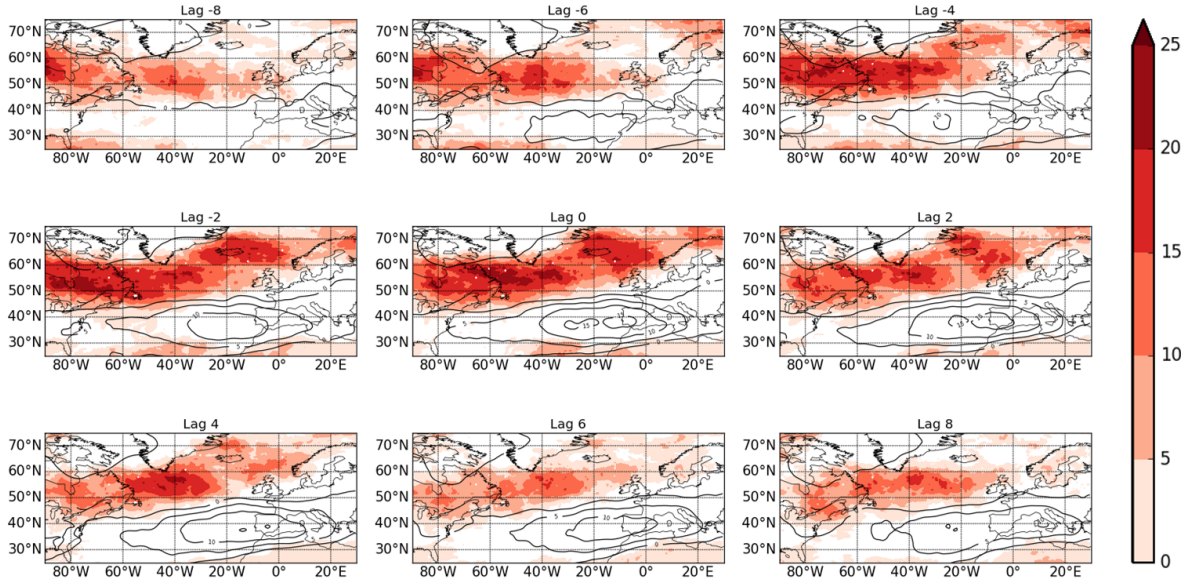

Figure 3.6: *Composite images of North Atlantic RWB and jet anomalies on days lagged to clustered days for clustering at 45^{o}N, 5^{o}W. The red shading is the percentage increase in the B-index compared to climatology. The black contours are the 250 hPa wind speed anomalies (m s^{-1}). Shown is from lag -8 days to lag +8 days at 2 day intervals.*

3.7 Dynamical Variability of Clustering

Composites such as in figure 3.3 and figure 3.5 focus on averages. To examine the relationship between the jet and clustering at the different latitudes we define an area from 40-50^{o}N, 30^{o}W-10^{o}E (box b in figure 3.1; chosen based on examination of figure 3.3) and take an average of the 250 hPa wind speed within this. This box is shifted 10^o south(north) for the jet relationship with clustering at 45^{o}N (65^{o}N) (A full description of

this can be found in the caption of figure 3.1).

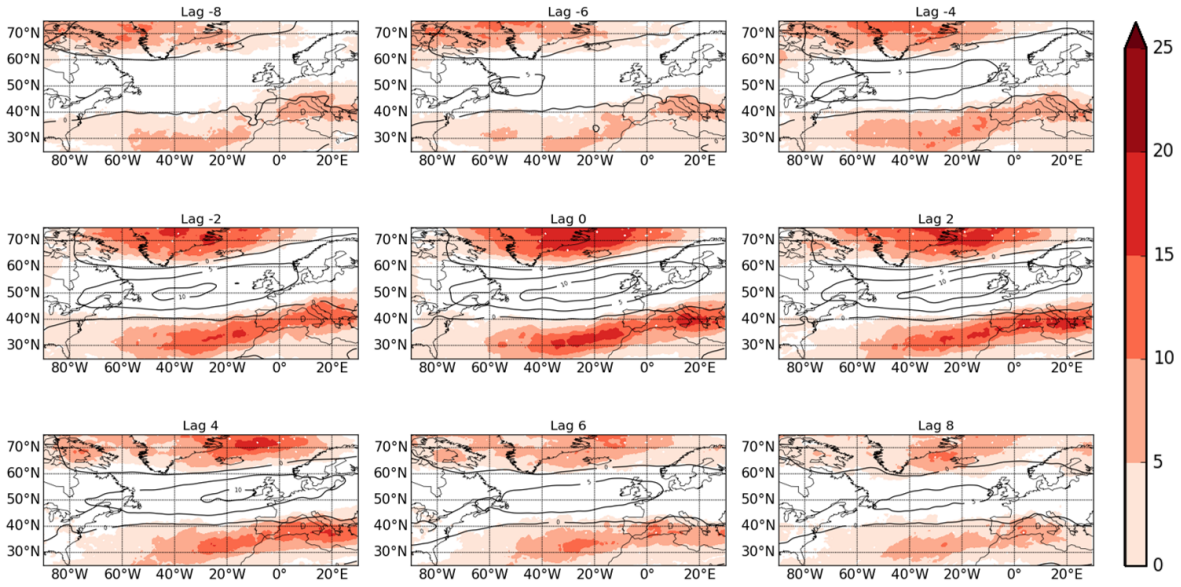

Figure 3.7: *Composite images of North Atlantic RWB and jet anomalies on days lagged to clustered days for clustering at 65^{o}N, 5^{o}W. The red shading is the percentage increase in the B-index compared to climatology. The black contours are the 250 hPa wind speed anomalies (m s^{-1}). Shown is from lag -8 days to lag +8 days at 2 day intervals.*

Figure 3.8b illustrates the relationship between the 250 hPa wind speed and clustering at 55^{o}N. A positive correlation (r=0.69) is apparent with increasingly clustered activity being associated with stronger 250hPa wind speeds. Mean 250hPa wind speeds increase from approximately 25 m s^{-1} on days with no cyclones, to around 40 m s^{-1} for the most clustered days. This is consistent with a stronger and more extended jet directing cyclones eastward across the North Atlantic. There is considerable spread in this relationship (which can be inferred from the size of the box and whiskers in figure 3.8b). Consequently, a strong and extended jet may not always be associated with clustered cyclone activity.

The jet relationship for 45^{o}N (65^{o}N) can be seen in figure 3.8a (3.8c). As in figure 3.8b a positive correlation is apparent (r=0.45 for 45^{o}N, r=0.54 for 65^{o}N (all latitudes are statistically significant)), with days that are associated with the clustering of cyclones also being characterised by a stronger and extended jet. However, there is still considerable spread in these relationships, as in figure 3.8b. There is also considerably less cases at the more clustered end of the axis, so this part of the relationship may not be as robust.

The differences in RWB between non-clustered and clustered days is also examined. To achieve this we define two further areas, the first being from 55-65^{o}N, 40-0^{o}W (box a in figure 3.1) and the second from

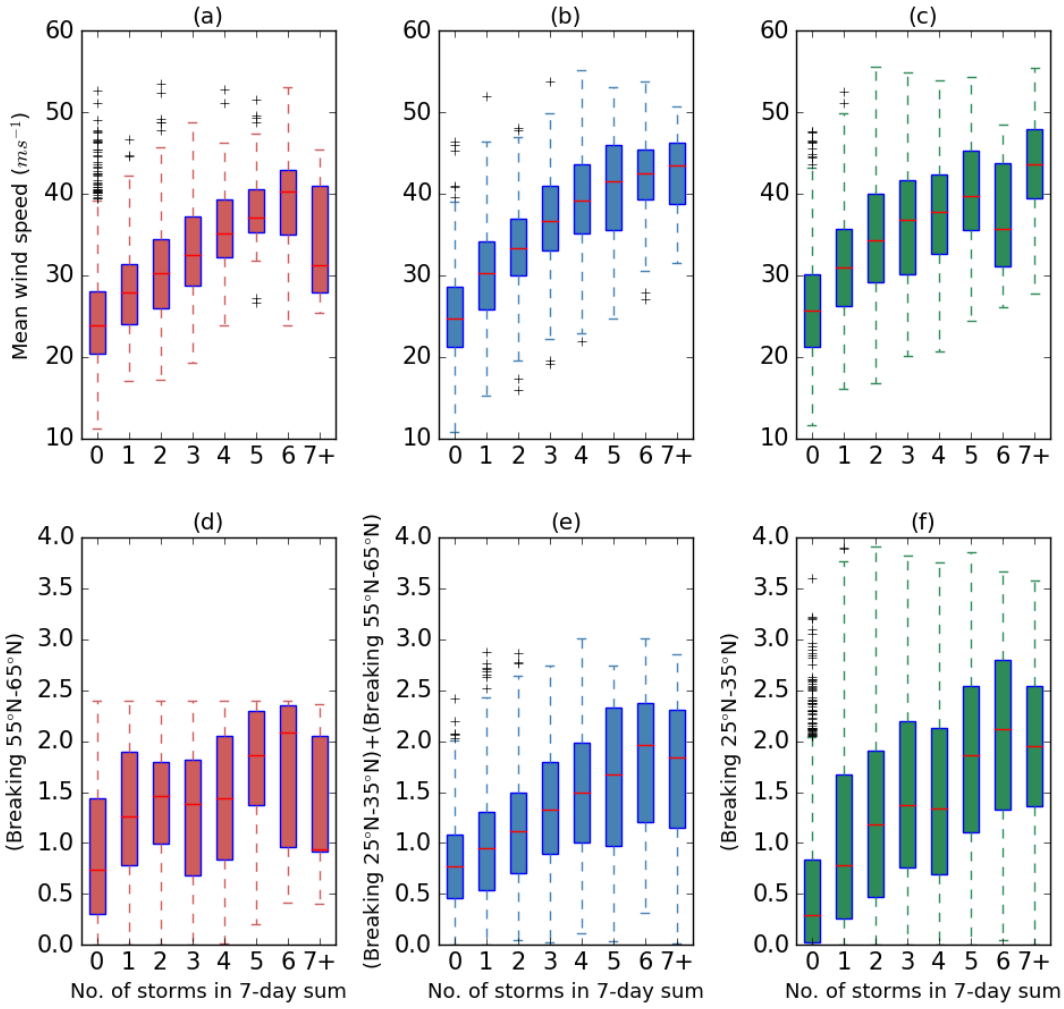

Figure 3.8: *(a) - (c) Average wind speeds at 250 hPa in box b of figure 3.1 (for 55^{o}N) ± 10^o latitude (for 45^{o}N/65^{o}N) against the number of cyclones in each days 7-day sum. (d) - (f) The amount of RWB that takes place in a combination of boxes a & c in figure 3.1. (a) and (d) are for 45^{o}N. (b) and (e) are for 55^{o}N. (c) and (f) are for 65^{o}N. The red lines represents the medians, with the edges of the boxes being the upper/lower quartiles. The whiskers extend to either 1.5 times the interquartile range or the value furthest from the median. Crosses are outliers.*

25-35^{o}N, 40-0^{o}W (box c in figure 3.1). These boxes were chosen as they capture the areas of RWB to the north and south across all three latitudes (figure 3.3). The amount of RWB in each box is calculated by determining the number of latitude-longitude points with a positive B-index on each day, and then normalising this relative to climatology. Using this method a value of 1 relates to a climatological amount of RWB. For clustering at each latitude we take contributions from different boxes based on where RWB is most likely from an examination of figure 3.3. For clustering at 45^{o}N we use box a, for clustering at 55^{o}N we use the average of boxes a and c after they have been normalised, and finally for 65^{o}N we use only box c.

Figures 3.8d-f suggest that given a large amount of RWB in either box a or box c (or a combination of the two) is associated with an environment that is favourable for clustering, although this is less clear

for 45^{o}N. These preferential locations for RWB have been previously identified to be associated with an enhanced jet and intense cyclones propagating toward western Europe (Gómara et al., 2014a; Messori and Caballero, 2015). This pattern was identified in Pinto et al. (2014), but this is the first time such activity has been linked to all clustering events in a 36-year dataset. However, as with the jet (Figs. 3.8a-c) these are dominated by large spread.

It is seen in figure 3.8 how the conditions that are favourable for clustering may often be achieved without the presence of multiple cyclones near western Europe. This may be as a result of other properties that are not directly associated with the normal development mechanism of baroclinic instability. For example, the development of secondary cyclones that contribute to clustering have been shown to be dependent on factors such as deformation strain rate, frontal shear, latent heat release and boundary layer friction. If any of these properties are not favourable for secondary cyclone formation then this may not result in the presence of the multiple cyclones needed to satisfy our clustering criteria, despite the presence of a favourable large-scale environment. However, this is not investigated in this study.

3.8 Conclusions

The aim of this study is to characterise the clustering of extratropical cyclones over the North Atlantic and their relationship with RWB and the upper level jet. Using the ERA-Interim reanalysis, cyclone clustering in the North Atlantic and its relationship with RWB has been specifically investigated for the winter 2013/14 and more generally for the winter seasons of 1979/80-2014/15. The following are the main conclusions of the study:

1. Cyclone clustering at 55^{o}N is associated with an extended and anomalously strong eddy-driven jet flanked on both sides by RWB. However, for clustering at 65^{o}N there is a dominance of RWB to the south of the jet, deflecting the jet exit northwards and tilting the jet SW-NE tilt. Conversely for clustering at 45^{o}N, there is more RWB to the north of the jet and the jet has a slight NW-SE tilt in its exit, deflecting cyclones further south.
2. RWB activity in the eastern North Atlantic peaks 2 days before before the occurrence of clustering and the strongest anomalies in the 250hPa jet speed. This is consistent with RWB enhancing the upper tropospheric thermal gradient and extending the North Atlantic jet eastwards, resulting in cyclone clustering.
3. A positive correlation was identified between the 250 hPa wind in the jet exit and extent of cyclone clustering for 36 winters of ERA-Interim data. A positive correlation was also identified with the RWB when assessing how much RWB was occurring to the north and south of the jet. All latitudes showed an increase in jet speed and RWB activity when there was a greater presence of cyclones.

However, there is considerable spread in all of these relationships.

Future research directions include exploring the projected changes in clustering under future climatic conditions in global circulation models (e.g. Economou et al. (2015)) and specifically the role of the RWB dynamics we have identified in any potential clustering changes. Additional research directions include exploring the role of secondary cyclogenesis during clustering and the various mesoscale processes that are associated with the development of these cyclones.

Chapter 4:

The Role of Cyclone Clustering During the Stormy Winter of 2013/2014

It has already been established that extratropical cyclones have a tendency to cluster (occur in groups) across the eastern North Atlantic and western Europe (Mailier et al., 2006), and several of these clustering events have been associated with a specific set of upper-tropospheric dynamical conditions by Pinto et al. (2014). Previously, in chapter 3, a full characterisation of clustering events for western Europe was made (Priestley et al., 2017a). Recently, the UK has experienced the incredibly stormy season of 2013/2014, which has been classified as the stormiest in 143 years by Matthews et al. (2014). In this chapter, the winter of 2013/2014 in the UK will be investigated to see if the high number of cyclones was a result of clustering, and if the upper-tropospheric dynamics associated with these events are consistent with the features characterised in chapter 3. The research question addressed in this chapter is as follows:

Q2. What were the dynamical features that were associated with the clustered winter season of 2013/2014 across the UK?

This text and figures that follow have been published in *Weather* (Priestley et al., 2017b).

Citation

Priestley, M. D. K., J. G. Pinto, H. F. Dacre, and L. C. Shaffrey (2017), The role of cyclone clustering during the stormy winter of 2013/2014. Weather, 72, 187-192. doi:10.1002/wea.3025.

Author Contributions

The concept for this study was developed by all the authors. The analysis, creation of figures, and writing of the text was completed by M. Priestley. The remainder of the authors provided feedback and comments to produce the final manuscript.

4.1 Abstract

The winter season of 2013/2014 was the stormiest on record for the British Isles. In this article we show that there was an unprecedented amount of cyclone clustering during this season, corresponding to an average of one intense cyclone affecting the country every 2.5 days. An intensely clustered period from 6 to 13 February 2014 that was associated with one specific cyclone family is analysed in detail. This cyclone family is shown to be associated with a strong and straight upper level jet that is flanked by Rossby wave breaking on both its northern and southern sides for the duration of the clustering event. This mechanism is also identified for other periods in this season. The persistence of these conditions resulted in the clustered cyclone activity, and it was accompanied by record-breaking rainfall, widespread flooding and large socio-economic losses.

4.2 Introduction

Extratropical cyclones are the primary natural hazard affecting western Europe. They are associated with strong winds and rainfall (Lamb, 1991) which can result in significant societal impacts. For example, windstorms Anatol, Lothar and Martin in 1999 resulted in approximately €16 billion of total insured losses (Swiss Re, 2016). Cyclones contribute to more than 70% of the precipitation that falls over northwest and central Europe in winter (Hawcroft et al., 2012).

Extratropical cyclones in the North Atlantic tend to travel in a northeasterly direction, forming off the east coast of North America and dissipating over the northeastern Atlantic Ocean or Nordic Sea. Clustering of extratropical cyclones is often defined as the passage of multiple high intensity cyclones through one geographical region within a relatively short period of time (Pinto et al., 2014). It has been statistically shown that extratropical cyclones cluster in the exit region of the storm track and in the vicinity of northwestern Europe (Mailier et al., 2006). The physical mechanisms behind the observed clustering that affected western Europe for several high impact months across various winter seasons was initially explored by Pinto et al. (2014) and expanded on by Priestley et al. (2017a). The latter study looked at all clustered events for 36 winter seasons from 1979/1980 to 2014/2015 and found that a typical clustering event affecting the British Isles was associated with a very strong and straight jet stream in the North Atlantic, with the jet being flanked to the north and south by Rossby wave breaking (RWB).

It is hypothesised that the physical mechanisms leading to clustering include steering by the large-scale

flow, which orientates storms in the same direction and provides the conditions necessary for rapid intensification (Mailier et al., 2006; Hanley and Caballero, 2012). An additional mechanism is secondary cyclogenesis, in which new cyclones form on the cold fronts of more mature cyclones (Parker, 1998); this allows for the occurrence of many storms in a short period of time. The combination of these mechanisms results in clustering (Pinto et al., 2014), that is the large-scale flow allows for all cyclones that form in a region to follow the same direction; in addition, the occurrence of secondary cyclogenesis ensures that the time gap between the passage of these cyclones is reduced.

Figure 4.1: *Images of storm impacts from DJF1314. (a) Breached sea defences and collapsed train line at Dawlish, Devon on 6 February 2014. (Source: Network Rail.) (b) The flooded Somerset Levels on 2 February 2014. (Source: Tim Pestridge.) (c) Large waves at Porthcawl, Wales on 5 February 2014. (Source: Karl Baker.)*

December, January and February of 2013/2014 (DJF1314) was one of the most extreme DJF periods in the British Isles and the stormiest in 143 years (Matthews et al., 2014). The season was known for its persistent wet weather. The average precipitation accumulation across England and Wales was 456mm for the DJF1314 season according to the England-Wales precipitation (EWP) series (Alexander and Jones, 2001), which corresponds to 175% of the seasonal average and is the wettest such period since the record began in 1766 (Kendon and McCarthy, 2015). Several intense storms affected the British Isles during this period (such as Bernd, Dirk, Erich and Tini; all named winter storms herein were named by Freie Universität Berlin: http://www.met.fu-berlin.de/adopt-a-vortex/historie/), which brought high winds and intense rainfall to large parts of the country. The storminess persisted from early December through to late January and early-mid February (Kendon and McCarthy, 2015). This continuously unsettled and severe weather made coastal areas particularly vulnerable (Figure 4.1c), with the main rail line from Exeter to Plymouth collapsing at Dawlish (Figure 4.1a) and the flooding of the Somerset levels being a persistent

feature of this season (Figure 4.1b).

Since highly clustered seasons such as DJF1314, 1990/1991 and 1999/2000 are clearly able to cause large-scale environmental and socio-economic impacts, it is important to understand the atmospheric drivers causing them. The aim of this study is to investigate a short period in the DJF1314 season to determine if one anomalously stormy period follows the dynamical framework identified in previous clustering studies (e.g. Priestley et al., 2017a). The precipitation associated with these storms and how clustering acts to contribute to high values of accumulated precipitation is also investigated.

4.3 Data and Methods

Cyclones are tracked and identified in the European Centre for Medium-Range Weather Forecasts Interim Re-Analysis dataset (ERA-Interim; Dee et al., 2011) using an objective tracking algorithm first developed by Murray and Simmonds (1991b). Full details can be found in Priestley et al. (2017a).

The method of Pinto et al. (2014) and Priestley et al. (2017a) was followed to calculate clustering. The method defines a circular area with a radius of 700km centred at 55°N, 5°W (i.e. focussed around the British Isles) and identifies cyclones when they pass through this area. A day is classed as clustered for the British Isles if four or more intense cyclones pass through the area in the surrounding 7-day period, centred on the day of interest. An intense cyclone is defined as one whose minimum pressure within the 700km radius exceeds the local 95th percentile of sea level pressure climatology; this is 984 hPa at 55°N, 5°W during DJF (see Pinto et al. (2014) and Priestley et al. (2017a) for more details).

ERA-Interim data are also used to determine the location of RWB in the North Atlantic. Following the method of Masato et al. (2013) RWB is identified as a meridional overturning in the potential temperature (θ) field on the tropopause (2 PVU surface; 1 PVU = $1 \times 10^{-6} Km^2 kg^{-1} s^{-1}$). If the normal equator–pole gradient of high θ to low θ values is not present, then RWB is identified at that latitude/longitude point. ERA-Interim 250 hPa winds are also used for the jet analysis.

The precipitation output from ERA-Interim is used to examine accumulations from individual storms. Precipitation observations are not assimilated into ERA-Interim, and so precipitation is used from the short-term forecast in the assimilation cycle (Dee et al., 2011). An additional precipitation climatology is obtained from the daily and seasonal observations taken from the Hadley Centre UK regional precipitation series (HadUKP) England-Wales precipitation (EWP) dataset and sub-regions within (Alexander and Jones, 2001). The EWP data uses area averaged rain gauge data, with daily data dating back to the start of 1931.

4.4 Analysis of 2013/2014

4.4.1 Precipitation Associated with Cyclone Tini

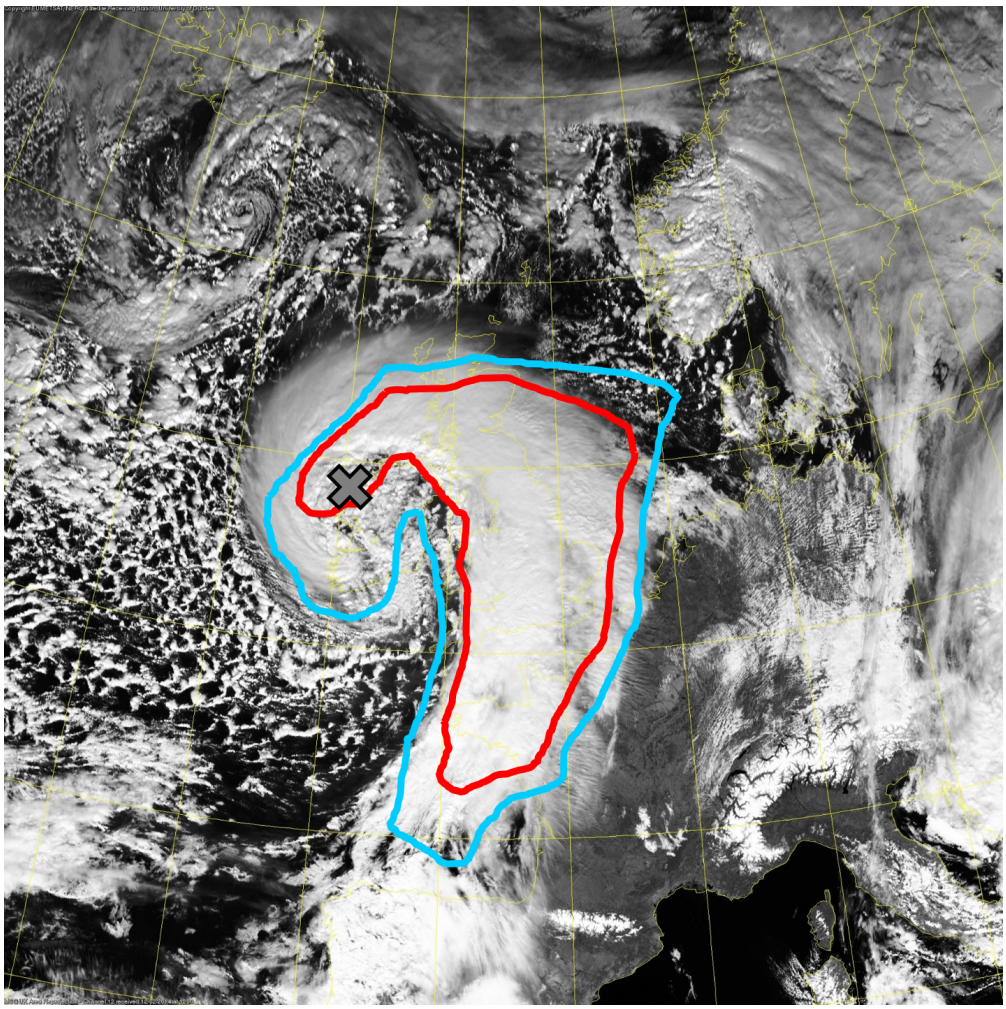

Figure 4.2: *Meteosat SEVIRI visible satellite image of cyclone Tini at 1200 UTC on 12 February 2014, centred over the British Isles. Also shown are 2mm (blue) and 4mm (red) contours of precipitation accumulation from 1500 to 2100 UTC from ERA-Interim. The grey cross indicates the cyclone centre at 1200 UTC. (Source: NEODAAS/University of Dundee.)*

Figure 4.2 shows cyclone Tini [1] as it passes over the British Isles in a Meteosat SEVIRI visible satellite image on 12 February 2014 at 1200 UTC. A comma-shaped cloud pattern is identifiable from this image, and overlaid is the 1500-2100 UTC precipitation accumulation field from ERA-Interim. A broad area of $>$2mm accumulation encompasses most of the cloud band and the British Isles, with the exception of far northern Scotland. The 2mm contour extends beyond the northeast boundary of the cloud and into the North Sea. This mismatch between the accumulation and the cloud area is a result of the different time frames of the two fields and the precipitation being accumulated 3-9h after the image was taken. The red

[1] Storm Tini was named Darwin in Ireland

contour marks the area of at least 4mm precipitation accumulation, which also covers a large portion of the cloud band and most of the British Isles.

The close association of the precipitation accumulations with the cloud structure of cyclone Tini shown in Figure 4.2 demonstrates how large amounts of precipitation over a wide area are directly associated with extratropical cyclones. With the passage of many cyclones in a short period, precipitation accumulation will increase. Despite the accumulations from this 6h-period being relatively small, the accumulations could increase rapidly through two mechanisms. Firstly, if many cyclones were to pass over the British Isles in quick succession each would bring further precipitation, contributing to high accumulations; secondly, if any of these cyclones were to stall and move slowly across the British Isles, this would increase the duration for which they could precipitate over land (Hand et al., 2004).

4.4.2 Identification and analysis of clustering and associated cyclone family

Including Tini, 57 storms passed through the 700km radius surrounding the British Isles in the 90-day DJF1314 period, with 37 of these exceeding the local minimum sea-level pressure threshold. This corresponds approximately to one intense cyclone every 2.5 days, which is more than twice the climatological average of one intense cyclone every 5.5 days. Many of these arrived as part of a cluster, with Figure 4.3 showing a time series of the accumulated number of clustered days throughout DJF1314. During DJF1314 there were 32 clustered days, which is the highest of any DJF period from 1979/1980 to 2014/2015 (the next highest is DJF0607, with 30 days). There are only five DJF periods in the 1979/1980 - 2014/2015 period with greater than 20 clustered days.

Two periods of intense clustered activity can be identified in Figure 4.3 (20 - 30 December 2013 and 2 - 14 February 2014). Consequently, DJF1314 has almost three times the climatological value of 11 clustered days. Each of the two longer clustered periods in DJF1314 are equal in length to the climatological average, further highlighting just how unusual this season was. From the EWP data in Figure 4.3, it can be seen how the national average precipitation accumulation of 460mm, like the clustering, is considerably greater than the climatological value of 235mm. The time series of DJF1314 precipitation accumulation closely mirrors the number of clustered days (as suggested from Figure 4.3), demonstrating the expected link between the clustering of intense cyclones and the floods that impacted the British Isles in this season. Clustered days are associated with an average of 6.25mm of precipitation, whereas non-clustered days receive an average of 3.78mm (the variances are 30.4 and 14.6mm respectively). Using a Welch's t-test the difference in precipitation accumulation between clustered and non-clustered days is statistically significant at the 95% level in both the regional and subregional HadUKP datasets

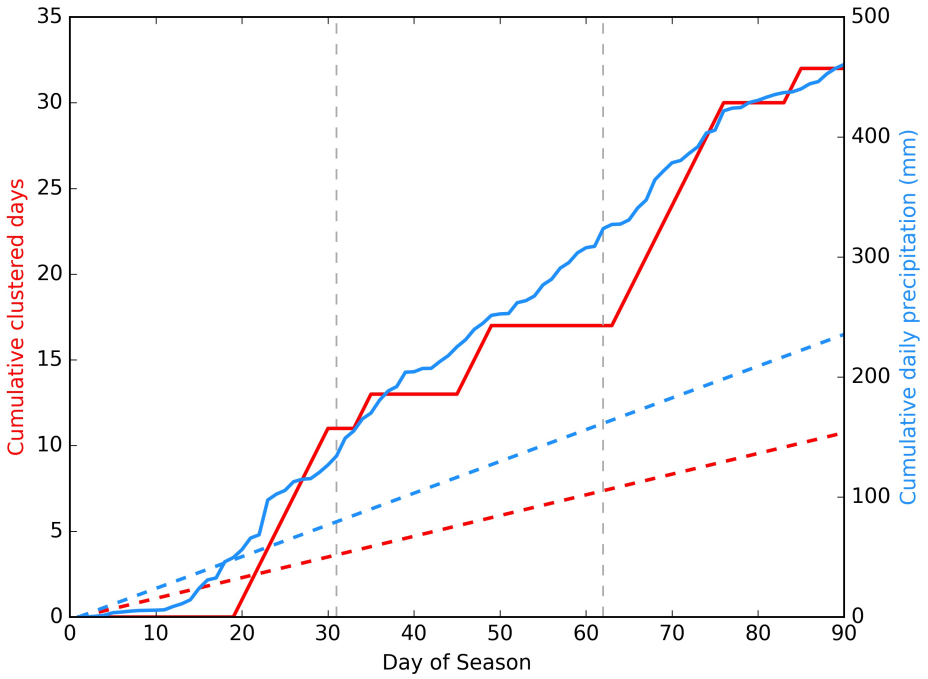

Figure 4.3: *Cumulative clustered days during DJF1314 (red), with the climatological cumulative clustered days for DJF 1979/1980 - 2014/2015 being represented by the dashed red line. The cumulative daily precipitation (mm) in DJF1314 for the EWP region from HadUKP is in blue. The EWP HadUKP DJF climatology from 1766/1767 to 2015/2016 is the dashed blue line. 31 December 2013 and 31 January 2014 are indicated by the vertical dashed grey lines.*

(not shown). The recurrent presence of high-pressure systems over Scandinavia and eastern Europe also contributed to the high precipitation accumulation: as cyclones were unable to move eastwards, they had a tendency to stall over the British Isles (see charts in Figure 4.4 and for the remainder of the DJF1314 season).

From the two intense periods of clustering mentioned above, we will focus on the latter occurring between 2 and 14 February 2014. This period was characterised by many intense cyclones such as Nadja (30 January 2014); Okka (2 February 2014); Petra (3 February 2014); Qumaria (4 February 2014); Ruth (6 February 2014); Stephanie (8 February 2014); Tini (10 February 2014); and Ulla (12 February 2014; the dates are the days on which the storms were named).

The selected time period and cyclones named above were specifically chosen as they form one cyclone family. A cyclone family is identified when secondary cyclogenesis occurs on the trailing cold front of a main cyclone, with the main cyclone acting as the parent cyclone to the secondary cyclone. This process may then repeat as the secondary cyclone replaces the main cyclone and then acts as the parent cyclone.

The development and propagation of these cyclones can be seen in Figure 4.4. Here we show 6-hourly synoptic analysis charts from the Met Office for 6 - 13 February 2014 in order to identify which cyclones

form on the trailing cold front of a parent cyclone and hence are part of one cyclone family; however, only one chart from each day is shown. All of the cyclones that contribute to the observed clustering are labelled with coloured circles, with the same colour on subsequent days corresponding to the same cyclonic system. Hereafter the cyclones will be referred to by their assigned names, with the exception of the green, brown and pink cyclones, which are unnamed. The period in early February 2014 was cyclonically very active over the North Atlantic, with multiple fronts, troughs and cyclones, as can be seen from the crowded and complex nature of all the charts in Figure 4.4. However, not all the cyclones identified pass over the British Isles, with Stephanie passing slightly to the south, and the green storm curving away from the British Isles before it reaches the west coast of Ireland.

From Figure 4.4, a timeline of storms for this particular cyclone family is as follows: Petra - Qumaria - Ruth - Stephanie - Green - Tini - Ulla.

4.4.3 Large-scale Dynamics of Observed DJF1314 Clustering

Using the Murray and Simmonds (1991b) identification and tracking algorithm, we can visually display each cyclone's path across its entire lifecycle. Only the storms that pass within 700km of 55°N, 5°W are shown; hence the omission of Stephanie, which from Figure 4.4 can be seen to track much further to the south of the British Isles. There are also two other tracks in Figure 4.5 which have not yet been mentioned: the brown track (Figure 4.4a) and the pink track (Figure 4.4a and 4.4b). Neither of these systems is part of the observed cyclone family in the North Atlantic and was assigned a name in this winter period; however, as they passed through our area of interest they did contribute to the observed clustering and so have been included in Figure 4.5.

In addition, we can examine the associated upper-level dynamics by compositing fields for this time period. A strong and straight upper-level jet stream was present during the entirety of the period from 6 to 13 February 2014, as can be seen from the values of 250 hPa wind in the composite of Figure 4.5. The jet core across the majority of the North Atlantic is located between 40°N and 50°N, with peak speeds of over 70 ms^{-1}, which is well above the DJF average of 30 - 40ms^{-1}. It is also more zonal than would be seen normally (not shown). Regions to the north and south of the jet are characterised by anomalously large areas of RWB. The dynamical pattern of a strong, straight upper-level jet between areas of RWB on either side has been associated with extratropical cyclone clustering in the studies of Pinto et al. (2014) and Priestley et al. (2017a), and this is further apparent for this intensely clustered period of early February 2014 (the climatological states of both the RWB and jet can be seen in Figure 2d of Priestley et al. (2017a)).

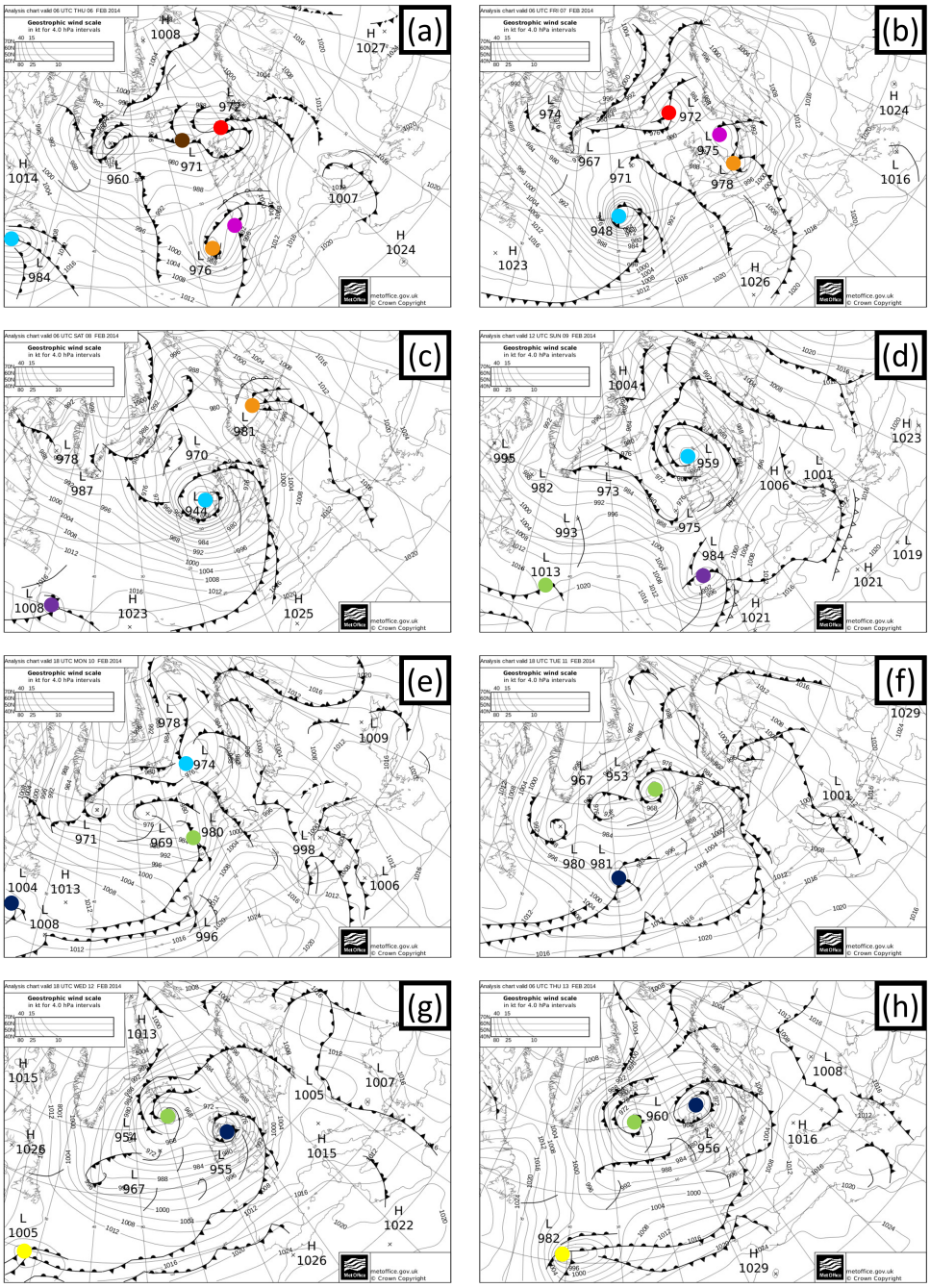

Figure 4.4: *Daily Met Office surface weather charts from 6 February 2014 (a) to 13 February 2014 (h). Related cyclones that impact the British Isles have been coloured: Petra (Red), Qumaria (Orange), Ruth (Cyan), Stephanie (Purple), Tini (Dark Blue), Ulla (Yellow) and three unnamed storms (Brown, Pink, Green). Colours are consistent for cyclones across multiple days. Charts are as follows: (a) 0600, 6 Feb 2014, (b) 0600, 7 Feb 2014, (c) 0600, 8 Feb 2014, (d) 1200, 9 Feb 2014, (e) 1800, 10 Feb 2014, (f) 1800, 11 Feb 2014, (g) 1800, 12 Feb 2014, (h) 0600, 13 Feb 2014.*

The presence of RWB on either side of the jet acts to converge momentum into the region of the jet core (Barnes and Hartmann, 2012), resulting in an acceleration of the wind speeds and an extension of the jet towards western Europe and the British Isles. The presence of these features for the entire 8-day period of 6 - 13 February 2014 allows for the jet to remain in the same place and the cyclones that form to propagate in the same direction and follow a similar track (Figure 4.5), resulting in cluster ing over the

British Isles. The above-mentioned mechanisms of a strong and straight jet flanked by RWB on both sides can also be found for other clustered periods during the season (not shown).

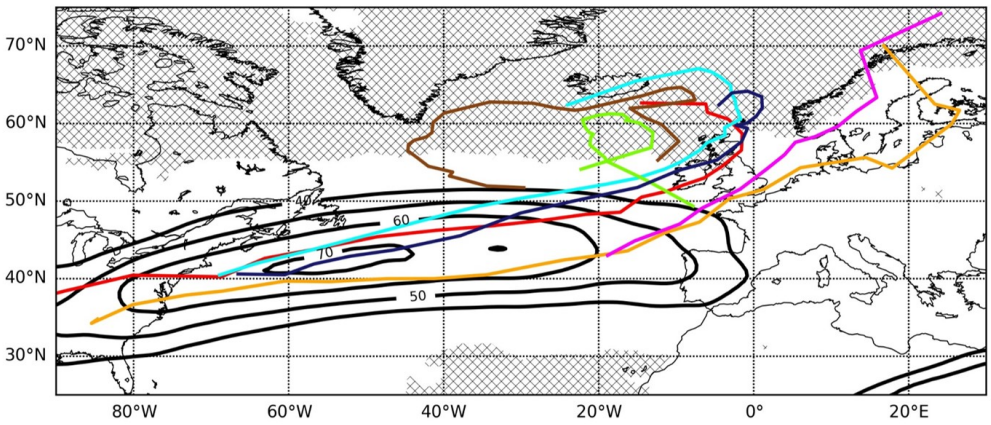

Figure 4.5: *Dynamical composite in the North Atlantic for 6 - 13 February 2014. Thick black contours depict 250 hPa wind (ms^{-1}). Coloured lines are the cyclone tracks identified as influencing the British Isles in this period. The track colours are consistent with cyclones in Figure 4.4: Petra (Red), Qumaria (Orange), Ruth (Cyan), Tini (Dark Blue), and three unnamed storms (Brown, Pink, Green). Crossed regions are where RWB is occurring on at least 30% of days.*

4.5 Discussion and Conclusions

The DJF1314 season was one of the most extreme winter seasons on record. It was a season dominated by the clustering of extratropical cyclones, with an average of one intense cyclone every 2.5 days. This study has focussed on one particularly clustered period in this stormy season: 6 - 13 February 2014. This period had several intense cyclones affecting the British Isles, including cyclones Ruth and Tini.

All the storms that passed over the British Isles in this 8-day period were part of one cyclone family and were connected through secondary cyclogenesis. Multiple secondary cyclogenesis events were accompanied by persistent dynamical features in the North Atlantic. A very strong and extended jet stream observed at 250 hPa was kept in place due to the presence of RWB on its northern and southern flanks. This persistent jet allowed for multiple cyclones to track in the same direction and cluster over the British Isles, resulting in major impacts for the British Isles and other parts of western Europe.

Some recent studies have investigated possible remote influences that may have resulted in such a cyclonically active winter season in the North Atlantic. For example, Slingo et al. (2014) and Huntingford et al. (2014) hypothesise that the high sea surface temperature in the tropical West Pacific and/or the reduced Arctic sea ice may be linked to the stormy activity. However, no clear causal link has yet been identified. An interesting future direction for work in this area would be to examine any potential link between these

teleconnections and RWB in the North Atlantic, and how these remote influences may have contributed to the observed storminess in DJF1314.

Chapter 5:

The Role of Secondary Cyclones and Cyclone Families for the North Atlantic Storm Track and Clustering over Western Europe

It has been shown in chapter 3 and chapter 4 how clustering events in western Europe are associated with a very specific set of large scale features. For these events Rossby wave breaking (RWB) is present on one or both sides of the zonally extended and intense jet, controlling its latitude and hence the latitude of the cyclones that impact Europe. There was shown to be some variability associated with this (figure 4.8), and hence these conditions are a necessary but not sufficient criteria. Therefore, it is hypothesised that increases in the number of cyclones during clustering is a result of increased secondary cyclogenesis and an increased presence of cyclone families. Both Pinto et al. (2014) and Priestley et al. (2017b) showed how cyclone families, and specifically cyclones forming on trailing fronts (secondary cyclones) were frequently present in the North Atlantic during these clustered periods. They have also been shown to commonly occur across the eastern North Atlantic (Schemm and Sprenger, 2015). Therefore, it will be investigated how important a role these secondary cyclones play in periods of clustering for western Europe. Furthermore, the environmental conditions leading to the formation of these cyclones will be explored. The main research question that will be addressed in this chapter is as follows:

Q3. To what extent do secondary cyclones contribute to periods of clustering that affect western Europe?

This text and figures that follow have been submitted to *Quarterly Journal of the Royal Meteorological*

Society and is currently in review (Priestley et al., 2019).

Citation

Priestley, M. D. K., H. F. Dacre, L. C. Shaffrey, S. Schemm, and J. G. Pinto (2019), The role of secondary cyclones and cyclone families for the North Atlantic Storm Track and clustering over western Europe, Quarterly Journal of the Royal Meteorological Society, *Submitted*.

Author Contributions

The concept for this study was developed by MP, HD, LS, and JP. SS provided assistance with the front identification and secondary cyclone classification method. The analysis, creation of figures, and writing of the text was completed by M. Priestley. The remainder of the authors provided feedback and comments to produce the final manuscript.

5.1 Abstract

Secondary cyclones are those that form in association with a pre-existing primary cyclone with this commonly being along a trailing cold front. In previously studied cases they have been shown to cause extreme damage across Europe, particularly when multiple cyclones track over the same location in rapid succession (known as cyclone clustering). To determine the dynamical relationship between primary and secondary cyclones, a frontal identification algorithm is partnered with a cyclone identification method to objectively identify secondary cyclones in 35 extended winter periods using re-analysis data. Cyclones are grouped into 'cyclone families' consisting of a single primary cyclone and one or more secondary cyclones.

Secondary cyclones are shown to occur most frequently in the central and eastern North Atlantic, whereas primary cyclones are more often found over the western North Atlantic. Cyclone families have their strongest presence over the North Atlantic Ocean and contribute more than 50% of cyclones over the main North Atlantic storm track. A final category, Solo cyclones, are most commonly identified over continental regions and also the Mediterranean Sea. Primary cyclones are associated with the development of an environment that is favourable for Secondary cyclone growth. Enhanced Rossby wave breaking following the primary cyclone development leads to an increase of the upper-level jet speed and a decrease in low-level stability. Secondary cyclogenesis commonly occurs in this region of anomalously low stability, close to the European continent.

For Secondary cyclones impacting central Europe, enhanced Rossby wave breaking on both sides of the jet results in a zonally orientated upper-level jet exit, extending towards central Europe. This accelerated jet steers the secondary cyclones rapidly along a similar track resulting in cyclone clustering. Overall,

secondary cyclones are responsible for approximately 50% of the total number of cyclones over western Europe during periods of extreme clustering.

5.2 Introduction

The original conceptual model for extratropical cyclones is the *Norwegian Model* (Bjerknes and Solberg, 1922), which describes how cyclones form and develop throughout their lifetime. The Norwegian model also describes how "cyclone families" can form along the polar front with each successive cyclone forming slightly to the south and west of the one preceding it. This phenomena of cyclone families and specifically cyclogenesis along fronts has been studied and observed in previous case studies (e.g. Rivals et al., 1998; Chaboureau and Thorpe, 1999), with cyclones forming on the trailing fronts of pre-existing cyclones commonly being called *"Secondary"* cyclones.

Secondary cyclones often develop explosively and have a tendency to cause large amounts of damage, such as the Great Storm of 1987 (Hoskins and Berrisford, 1988), Storms Lothar and Martin in 1999 (Pearce et al., 2001; Wernli et al., 2002), and also Kyrill in January 2007 (Ludwig et al., 2015). These secondary cyclones tend to form from frontal wave instabilities along fronts associated to a pre-existing cyclone (often termed *Primary* cyclones), however, in some cases ($\sim$ 50%) these frontal wave instabilities do not develop into cyclones (Parker, 1998), making secondary cyclones difficult to forecast. *Cyclone families* are made up of these primary and any subsequent secondary cyclones.

Secondary and Primary cyclones can be very different in terms of their formation mechanisms. The general formation mechanisms of primary cyclones is well understood as these systems commonly form through baroclinic instability that occurs via the interaction of Rossby waves (Hoskins et al., 1985). With regards to the North Atlantic storm track, this cyclogenesis often occurs near the coast of the North American continent and arises from the strong temperature gradients provided by the SST gradient of the Gulf Stream and the contrasting temperatures of the North American continent (Brayshaw et al., 2009, 2011). For the formation mechanism of secondary cyclones it has been shown that there are many more processes contributing to wave growth.

The theoretical understanding for wave growth comes from Schär and Davies (1990) and Joly and Thorpe (1990b) who describe how a potential temperature (θ) or potential vorticity (PV) anomaly along a frontal feature can generate frontal instability and hence wave growth. The analytical model of Bishop and Thorpe (1994a,b) predicted that frontal wave growth was very unlikely for stretching/deformation rates above 0.6-0.8$\times 10^{-5}$ s^{-1}, something which was later confirmed by Schemm and Sprenger (2015). Dacre and Gray (2006) demonstrated that a relaxation of the frontal strain following the generation of the

PV/θ was crucial for the generation of individual frontal waves, and summarised the process as follows: a deformation flow along the front drives upward motion which results in latent heat release and forms a PV anomaly strip. This deformation then relaxes, causing a breakdown of the PV strip into smaller anomalies, which may then develop further via interaction with an upper-level wave, this being consistent with Type C cyclogenesis (Plant et al., 2003). This further development is not guaranteed (Parker, 1998) with many other contributing factors modulating further growth such as frontal shear (Chaboureau and Thorpe, 1999), latent heat release (Hoskins and Berrisford, 1988; Plant et al., 2003), and also friction in the boundary layer (Adamson et al., 2006).

The differing formation mechanisms of extratropical cyclones can generally be classified into three different types dependent on the dominant forcing, with these commonly being termed Type A, B, or C (Petterssen and Smebye, 1971; Deveson et al., 2002; Plant et al., 2003). Type A cyclones dominate cyclogenesis to the east of the Rocky mountains and are characterised by strong low-level forcing. Type B cyclones are characterised by a dominance of upper-level forcing and these cyclones generally have their genesis near the east coast of North America (Dacre and Gray, 2009). The primary cyclones discussed above are generally classed as Type B cyclones. Type C cyclones are very strongly forced by upper-level features with no low-level forcing and are most prevalent in oceanic regions (Gray and Dacre, 2006). Type C cyclones are also the most dominant cyclone type in the eastern North Atlantic (Dacre and Gray, 2009). Dacre and Gray (2009) hypothesised that identified Type C cyclones that have their genesis in the eastern North Atlantic may commonly be secondary cyclones that have formed on the trailing fronts of primary cyclones that formed near the coast of North America. Dacre and Gray (2009) also observed an overlap of the genesis and lysis regions of east Atlantic and west Atlantic cyclones respectively (their figure 4b), further suggesting a temporal connection connection between these two subsets of cyclones. Cyclones forming in the eastern North Atlantic have been shown to be sensitive to their low-level environment and have been shown to be associated with a reduced low-level static stability (Wang and Rogers, 2001).

There have been previous attempts to identify secondary cyclogenesis occurring on fronts. The key requirement for identifying these events is the presence of a pre-existing synoptic scale front. There are two main methods for identifying fronts in gridded meteorological data. The first is a thermodynamic method that uses a low-level thermal gradient (commonly equivalent potential temperature) to identify frontal features. This method is mainly based on the framework presented by Hewson (1998) and has been used in a number of studies for the purpose of identifying synoptic-scale fronts (Berry et al., 2011; Catto and Pfahl, 2013; Schemm et al., 2018). A second method of identifying fronts is based on the directional shift and acceleration of the 10-metre wind, as described by Simmonds et al. (2012). This method has also been used in other studies (Papritz et al., 2014). These two methods were compared by Hope et al.

(2014) and Schemm et al. (2015). The methods were found to be consistent by Hope et al. (2014), however, Schemm et al. (2015) found the thermodynamic method much better suited to fronts in strongly baroclinic situations (i.e. mid-latitude weather systems), with the wind method being more suited to regions of strong convergence or wind shear, and also for elongated, meridionally oriented fronts.

Schemm and Sprenger (2015) used the thermodynamic method to identify synoptic fronts and the cyclone identification and tracking methodology of Wernli and Schwierz (2006) for finding the cyclogenesis associated with them. This study found that approximately 8-16% of all cyclogenesis events in the western North Atlantic were secondary cyclone events in the December, January, February (DJF) period of 35 winter seasons (1979/80-2013/14), and this was slightly lower at 6-10% in the central North Atlantic. Schemm and Sprenger (2015) also showed how secondary cyclones in the eastern North Atlantic were associated with neutral to negative anomalies in low-level static stability surrounding the cyclone at the time of genesis, consistent with Wang and Rogers (2001) and Dacre and Gray (2009), however, they did not investigate the evolution of the environment surrounding secondary cyclones prior or after genesis. A follow up study by Schemm et al. (2018) found that the tracks of secondary cyclones tended to be located more in the central and eastern parts of the North Atlantic ocean (their figure 5b) and not above the Gulf stream, as would be expected when looking at all cyclones (Hoskins and Hodges, 2002). The identified secondary cyclones in Schemm et al. (2018) make up more than 20% of all cyclones in the central and eastern North Atlantic during DJF. Despite the comprehensive analysis of secondary cyclones by Schemm and Sprenger (2015) and Schemm et al. (2018) they did not objectively identify and compare the related primary cyclones, or quantify any differences in their preferential locations of genesis, track, and lysis.

Extratropical cyclones have been shown to cluster across western Europe (Mailier et al., 2006; Vitolo et al., 2009; Pinto et al., 2014; Priestley et al., 2017a,b), whereby many more cyclones impact a particular geographic region than one would normally expect. Economou et al. (2015) hypothesised that there are three main reasons as to why extratropical cyclones may cluster across the North Atlantic. Firstly, purely by chance. Secondly, through modulation by large-scale atmospheric patterns, such as the North Atlantic Oscillation (NAO). And finally, through a dependence between successive cyclones (i.e. cyclone families). Mailier et al. (2006) and Economou et al. (2015) both showed how the phase of the NAO was associated with a large amount of the variability of clustering across in the North Atlantic. Walz et al. (2018) further highlighted the importance of the NAO, but also the East Atlantic (EA), and Scandinavian (SCA) patterns in playing a role in modulating the inter-annual variability of serial clustering. The presence of cyclone families during periods of clustering was first highlighted by Pinto et al. (2014), and also in the case study of the 2013/2014 winter season in the UK by Priestley et al. (2017b). Both of these periods were accompanied by a strong and zonally extended jet that was flanked by Rossby wave breaking (RWB) on

either flank, steering intense cyclones and cyclone families downstream toward Europe (see also Hanley and Caballero, 2012; Gómara et al., 2014a; Messori and Caballero, 2015). It has yet to be established what causes the increase in cyclone numbers during periods of clustering and whether secondary cyclogenesis plays a relatively more important role.

In this study some of the gaps in the literature presented above are addressed. Particularly identifying the differences between secondary and primary cyclones in the North Atlantic and how secondary cyclones contribute to periods of clustering across western Europe. The questions to be answered are as follows:

1. What is the spatial relationship in the genesis and track density of Primary and Secondary cyclones in the North Atlantic?
2. How do the upper and lower level environments evolve during the formation of the Primary and Secondary cyclones?
3. To what extent do Secondary cyclones contribute to the increase in the number of cyclones during clustered periods?

This paper is laid out as follows. In section 2 the data and methodology used in the study is presented. Following this results are discussed in section 3. This will start with a climatological discussion of the track/genesis/lysis densities of the different classes of cyclones, questions 1 and 2 will be addressed in sections 3.1 and 3.2 respectively. Following this the role of the upper-level environment in cyclogenesis is addressed and question 3 is answered in section 3.3. Finally, a discussion of the role of secondary cyclones on clustering, with question 4 being answered in 3.4. In section 4 the key findings are discussed and summarised.

5.3 Data and Methodology

5.3.1 Dataset

For all of the analysis, the European Centre for Medium-range Weather Forecasts (ECMWF) ERA-Interim re-analysis is used (Dee et al., 2011). The extended winter period of November, December, January, February, and March (NDJFM) from the season of 1979/1980 to 2014/2015 inclusive is used. The horizontal resolution of ERA-Interim is T255 ($\sim$80km in mid-latitudes), with 60 vertical levels, and 6-hourly temporal resolution.

5.3.2 Cyclone and Front Identification

To identify and track extratropical cyclones we use the methodology of Murray and Simmonds (1991b) that was adapted for Northern Hemisphere cyclones by Pinto et al. (2005). Cyclones are identified using the

Laplacian of mean sea level pressure (MSLP) ($\nabla^2 p$), which is a proxy for the local geostrophic vorticity. The cyclone location is then identified as the minimum in MSLP that is closest to the maximum in $\nabla^2 p$, in order to relate the identified feature to a "real" low-pressure core. Tracks are filtered to remove weak (maximum ∇^2p $>$ 0.6 hPa deg.lat^{-2}), short-lived (cyclone lifetime $\geq$ 24 hours), and non-developing (maximum $\frac{d}{dt}\nabla^2$p $\geq$ 0.3 hPa deg.lat^{-2} day^{-1}) cyclones based on the criteria from Pinto et al. (2009). This method has been shown to compare well to other tracking schemes in terms of individual tracks (Neu et al., 2013), and also for seasonal track statistics (Pinto et al., 2016). The track, genesis, and lysis density statistics are calculated on a seasonal basis following the method of Hoskins and Hodges (2002). Density statistics are calculated as the number density per month per 5° spherical cap. Track densities are calculated across the whole lifetime of all tracks, with genesis and lysis densities using the first and last time step of each track respectively.

In order to identify cyclogenesis on synoptic fronts, the fronts themselves must first be identified. To do this the method of Schemm and Sprenger (2015) and Schemm et al. (2015) is followed. This method identifies fronts as having a minimum gradient in equivalent potential temperature (θ_e) at 850 hPa of at least 3.5K per 100km. Furthermore, all fronts must have a minimum length of 500km. This ensures only synoptic scale features and not weak, baroclinic zones are identified. A further filter is applied to the data so that any frontal features within 2° latitude/longitude of another front are classified as the same feature. This method for identifying synoptic scale features has been tested and validated for all types of front in the Northern Hemisphere (Schemm and Sprenger, 2015; Schemm et al., 2015, 2018). There are other methods that can be used for frontal identification (i.e. Simmonds et al., 2012), and other choices of thermal parameter used in a method such as the one used in this study (e.g. θ, Thomas and Schultz (2019); θ_w, Berry et al. (2011)). In Schemm et al. (2018) it was shown that the use of θ, or θ_e produced consistent results, with θ_e being preferred due to its conservation for moist adiabatic motion, and use in operational frontal identifications Hewson (1998).

5.3.3 Classifying Secondary Cyclogenesis

To identify cyclogenesis on pre-existing fronts a similar method to that of Schemm et al. (2015) is used. The process described herein is also summarised in the decision tree in figure 5.1. In order to identify secondary cyclogenesis an objectively identified cyclone must first have its genesis point within 200km of a frontal feature. This front must also be connected to a pre-existing cyclone in order for the cyclone to be classed as secondary. The front is connected to another cyclone if it is located within 500km the cyclone. In situations when there are multiple cyclones within 500km of a front which all satisfy the criteria to be a primary cyclone, only the closest cyclone to the front is taken as the primary cyclone. This ensures there is a

one-to-one correspondence between primary cyclones and secondary cyclones. All cyclones that are classed as secondary or those that satisfy both the primary and secondary cyclone criteria (i.e. a secondary cyclone that later in its life is the primary cyclone to another secondary cyclone) are then classed as Secondary+ cyclones. This ensures that each cyclone family has one primary cyclone associated with it, but potentially multiple secondary cyclones. The first cyclone in a family is always classed as the Primary cyclone with any subsequent cyclones in a family being termed Secondary+ cyclones. Any cyclones that do not satisfy the criteria of being a Primary or a Secondary+ cyclone are classed as Solo cyclones. Solo cyclones may or may not be associated with fronts at some point in their lifecycle, if so, no cyclogenesis is occurring on any connected front.

Based on the above methodology three different types of cyclones are classified.

1. Primary: Cyclones associated with a frontal feature at some point during their lifetime, with the front subsequently being associated with the cyclogenesis of another cyclone. These are the first cyclones in a cyclone family.
2. Secondary+: Cyclones that form within 200km of a pre-existing front that are in turn associated with a previously identified cyclone. These cyclones are any that are not the first in a family.
3. Solo: These cyclones may be associated to fronts during their lifetime, but these fronts are not associated with cyclogenesis along them. Alternatively, they may have no associated frontal features at any point in their lifetime.

In parts of this study ”Family” cyclones are also referred to. These cyclones are simply the sum of Primary and Secondary+ cyclones.

5.3.4 Large-scale Environmental Variables

To evaluate the state of the large-scale environment at times of Secondary+ cyclogenesis several variables are investigated. First of all the upper-level jet, which is taken as the 250 hPa wind speed anomaly from the 1979-2015 NDJFM climatology. Another upper-level feature investigated is that of the Rossby wave breaking (RWB). The method of Masato et al. (2013) is used to identify regions of RWB on the dynamical tropopause (2 potential vorticity unit (PVU) surface: 1 PVU = 1×10^{-6} K m^2 kg^{-1} s^{-1}). RWB is diagnosed as the reversal of the climatological meridional gradient in θ and will be expressed as an anomaly of the frequency of RWB in a particular location relative to the local background climatology (i.e. a frequency of 0.33 in a location where the climatology is 0.3 would have an anomaly value of 1.1).

Furthermore, the environment of the lower atmosphere is investigated, specifically the low-level static stability (800-950 hPa averaged). The Brunt-Väisälä frequency (N^2) is calculated, which has been formulated in pressure (p) co-ordinates and and it is expressed as a relative anomaly to the NDJFM

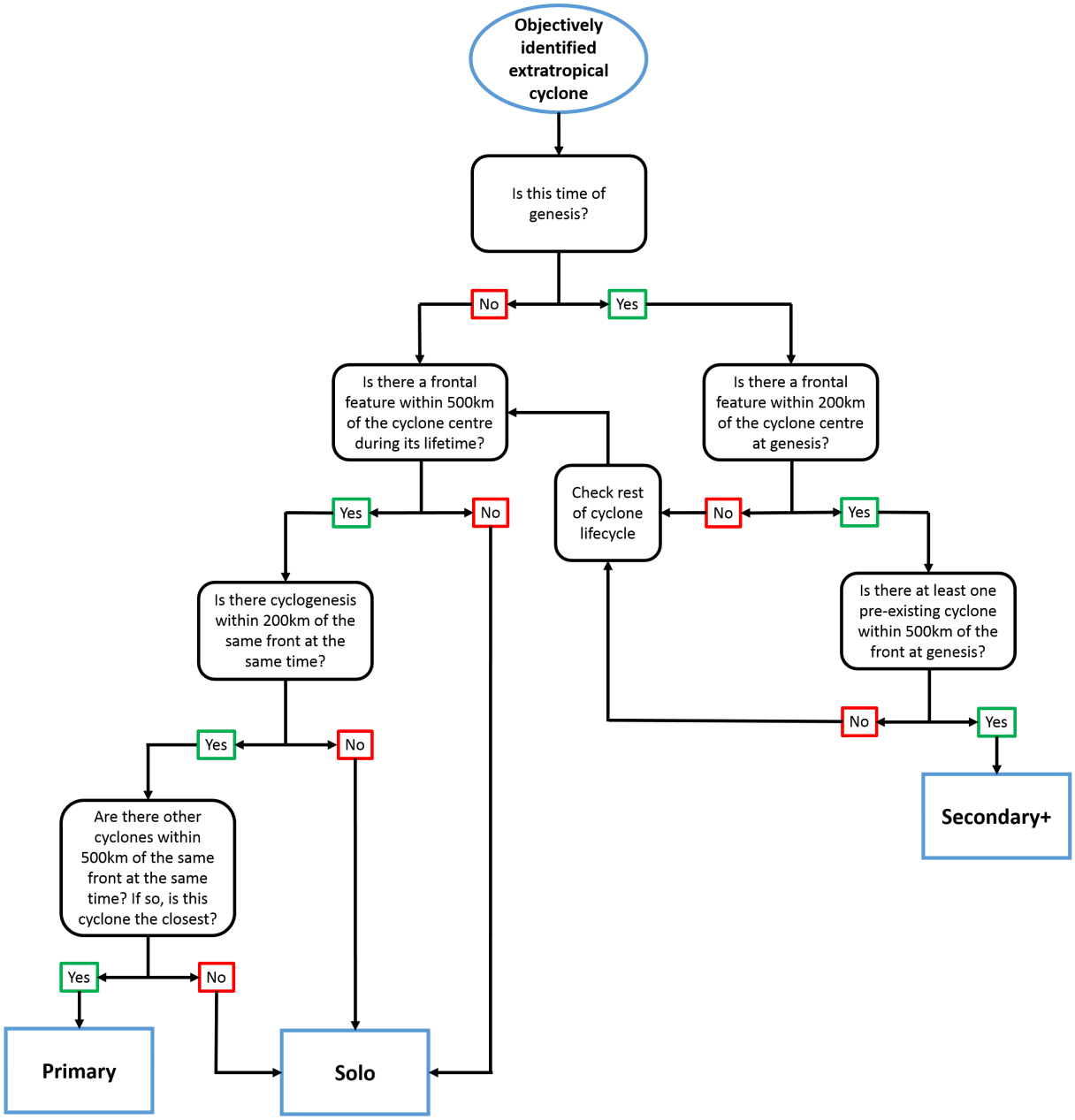

Figure 5.1: *A decision tree for classifying the different types of cyclones that make up a cyclone family. Each cyclone can only be classified once.*

climatology. The formulation for N^2 used is shown in equation 5.1 and is the local change of θ with pressure (p), that is also scaled by gravity (g), the mean layer temperature (T), and the specific gas constant (R).

$$N^2 = -\frac{pg^2}{RT\bar{\theta}}\frac{\partial\theta}{\partial p} \tag{5.1}$$

5.4 Results

5.4.1 Climatology of Primary, Secondary+, and Solo Cyclones

Applying the identification criteria laid out in section 5.3.3 to 36 extended winters, an overview of the properties of the different types of cyclones is performed. Figure 5.2a shows the total NDJFM track density of all cyclones and has a characteristic southwest-northeast tilt that extends from the eastern coast of North America toward the coast of Norway and the Nordic Seas. There is a maximum in the density of cyclone tracks in the region between the tip of Greenland and western Iceland, with values up to 20 cyclones per month. Higher track densities are identified across the central Mediterranean with a maxima of 10-13 cyclones per month downstream of the Gulf of Genoa.

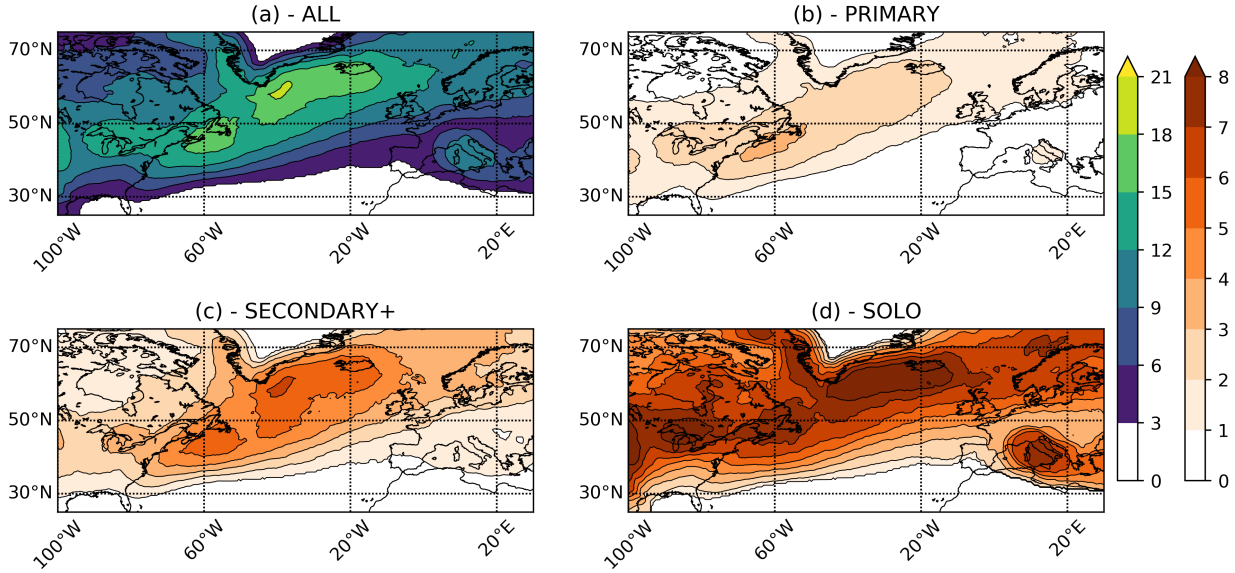

Figure 5.2: *Track densities of (a) All cyclones, (b) Primary cyclones, (c) Secondary+ cyclones, and (d) Solo cyclones. Units of the densities are cyclones per month per 5° spherical cap. Lowest contour intervals are not coloured and regions less than 3 cyclones per month^{-1} per 5° spherical cap are masked out.*

The Primary cyclone class track density is shown in figure 5.2b. The mean spatial features of figure 5.2b are similar to that of figure 5.2a. For example, there is a characteristic SW-NE tilt in the North Atlantic, but the tracks are now concentrated closer to the east coast of North America, with values of approximately 3-4 cyclones per month in this region. Primary cyclones do not travel as far to the NE as in figure 5.2a, with relatively lower track densities beyond 20°W.

The track density of the Secondary+ cyclone class is shown in figure 5.2c. Again a SW-NE tilt is observed as in figure 5.2a and 5.2b. However, for Secondary+ cyclones the maxima in the track density covers a broader region of the North Atlantic (from approx. 40-10°W), with values of 5-7 cyclones per

month. This suggests a difference in the preferential geographical location of Primary vs. Secondary+ cyclones in terms of the overall North Atlantic storm track. The Secondary+ cyclones may be further east than Primary cyclones due to Primary cyclones having to propagate downstream somewhat before the genesis of the Secondary+ cyclones, as was observed by Schemm et al. (2018).

The final cyclone class is that of Solo cyclones (figure 5.2d). Solo cyclones exhibit different mean locations in track density than the Primary and Secondary+ classes. Firstly, the characteristic SW-NE tilt of the track density is less pronounced. The largest densities are not confined to the ocean basin as for Primary and Secondary+ cyclones, with a relatively large number of tracks present over the North American continent. The largest densities are in zonal band between the tip of Greenland and Iceland. The final dominant region for Solo cyclones is in the Mediterranean (>7 cyclones per month), which is a large increase compared to the other classes.

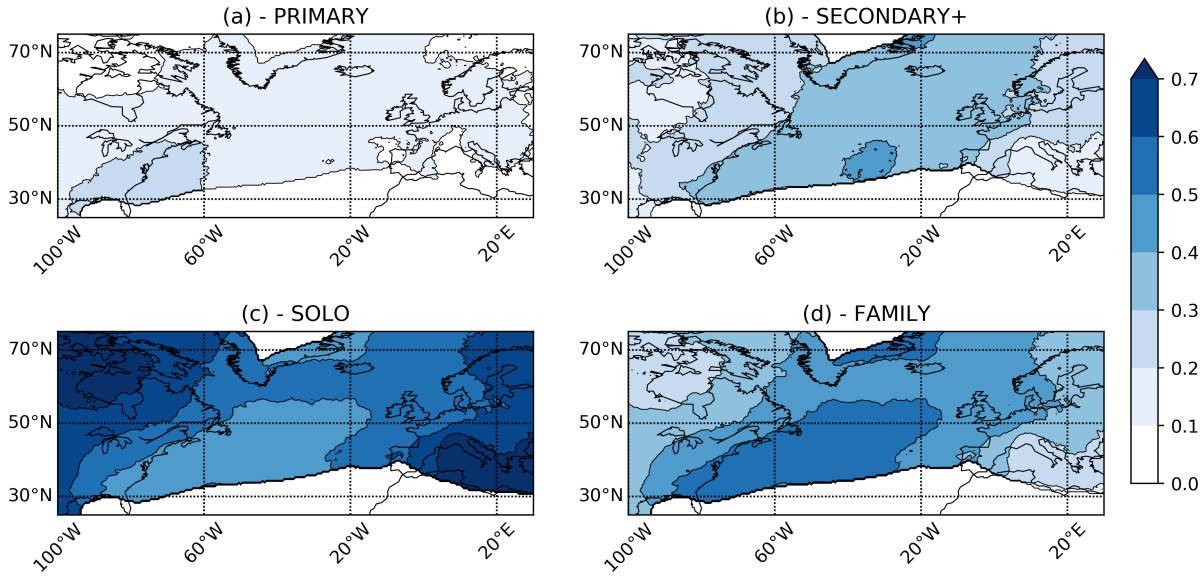

Figure 5.3: *Fractional track density of each cyclone class compared to the overall track density for (a) Primary, (b) Secondary+, (c) Solo, and (d) Family (Primary + Secondary+) cyclones. Regions where the total track density is less than 3 cyclones per month are masked out in each figure.*

The relative contribution of the different cyclone classes to the total track density is shown in figure 5.3. Primary cyclones are more prevalent in the western North Atlantic (figure 5.3a) and over the eastern coast of North America. They are dominant in the entrance region of the North Atlantic storm track where they make up 20-30% of all cyclones.

Conversely, Secondary+ cyclones (figure 5.3b) have their largest contribution to the storm track across the

central and eastern North Atlantic and extending NE toward the Nordic Seas. They make up 40-50% of all cyclones in the central North Atlantic and 30-40% of all cyclones across most of the rest of the North Atlantic basin and northwestern Europe. This pattern is somewhat similar to the findings from Schemm et al. (2018) (their figure 5b), however they found that cyclones forming on a trailing front made up 20-30% of all cyclones in the central/eastern North Atlantic. These differences are likely due to the differences in track densities between the cyclone identification and tracking schemes applied in these studies.

Grouping these two classes together results in the Family class (figure 5.3d). This illustrates how Family cyclones are most dominant in the main storm track region (figure 5.2a) and contribute up to 60% of all storm in the North Atlantic. The Family cyclones are strongly linked to the oceanic regions, with minimum values over continental regions, and are most prevalent across what one may consider to be the wintertime North Atlantic storm track.

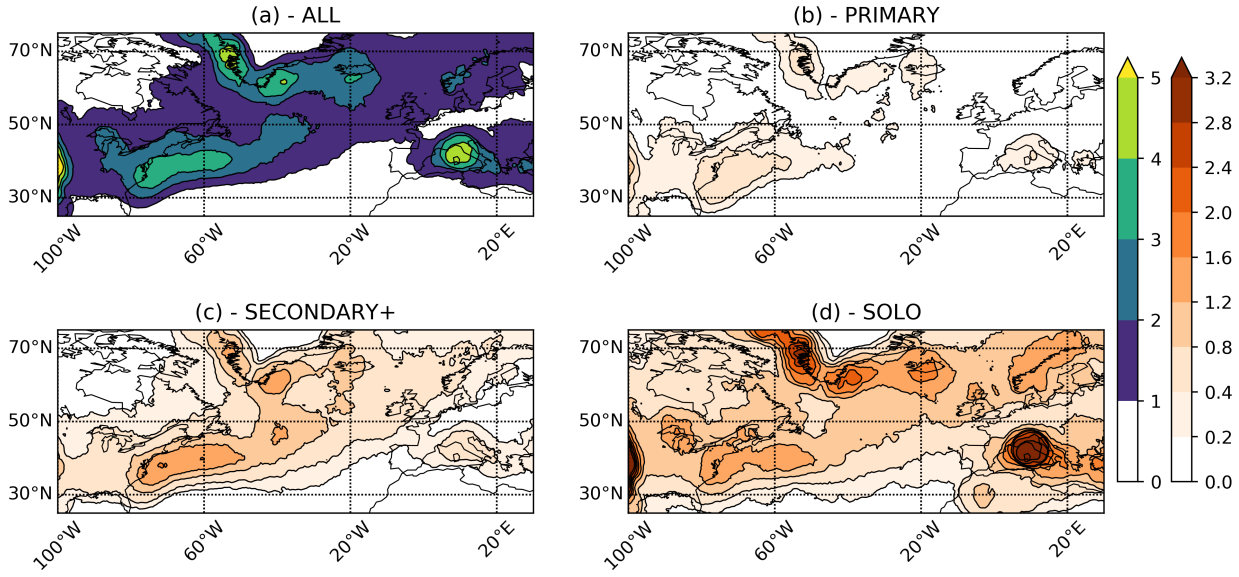

Figure 5.4: *Genesis densities of (a) all cyclones, (b) Primary cyclones, (c) Secondary+ cyclones, and (d) Solo cyclones. Units of the densities are cyclones per month per 5° spherical cap. Lowest contour intervals are not coloured.*

Solo cyclones dominate different locations to Family cyclones. The relative contributions for Solo cyclones to the total density of cyclones (figure 5.3c) are North America, specifically northern Canada, and also the Mediterranean Sea. In both these regions Solo cyclones make up >70% of all cyclones. Solo cyclones are by definition the opposite of Family cyclones and are a smaller fraction of the total number of cyclone tracks across the North Atlantic (<50% of all cyclones across most of this region).

Further insight into the differences between the different classes of cyclone can be inferred from an

examination of their genesis density climatologies (figure 5.4). One of the main genesis locations for all cyclones (figure 5.4a) is close to the eastern coast of North America and over the Gulf stream. This is to be expected as the quasi-permanent temperature gradient in this location generates baroclinic instability that is the dominant driver of mid-latitude cyclone formation. Other main regions for cyclogenesis are surrounding the tip of Greenland, over the Gulf of Genoa, and downstream of the Rocky Mountains.

For Primary cyclones (figure 5.4b), the dominant cyclogenesis region is over the Gulf stream. There are also Primary cyclones that form near the tip of Greenland and over the Mediterranean, but with fewer cyclones forming per month than over the Gulf stream. Secondary+ cyclones (figure 5.4c) also tend to form near the coast of North America, but also in the central North Atlantic. This difference in genesis density of Secondary+ and Primary cyclones can be understood as follows. Any Primary cyclone that forms over the Gulf stream then propagates in a SW-NE direction with the subsequent Secondary+ cyclone then forming on a trailing front, which is likely to be downstream of the Gulf stream.

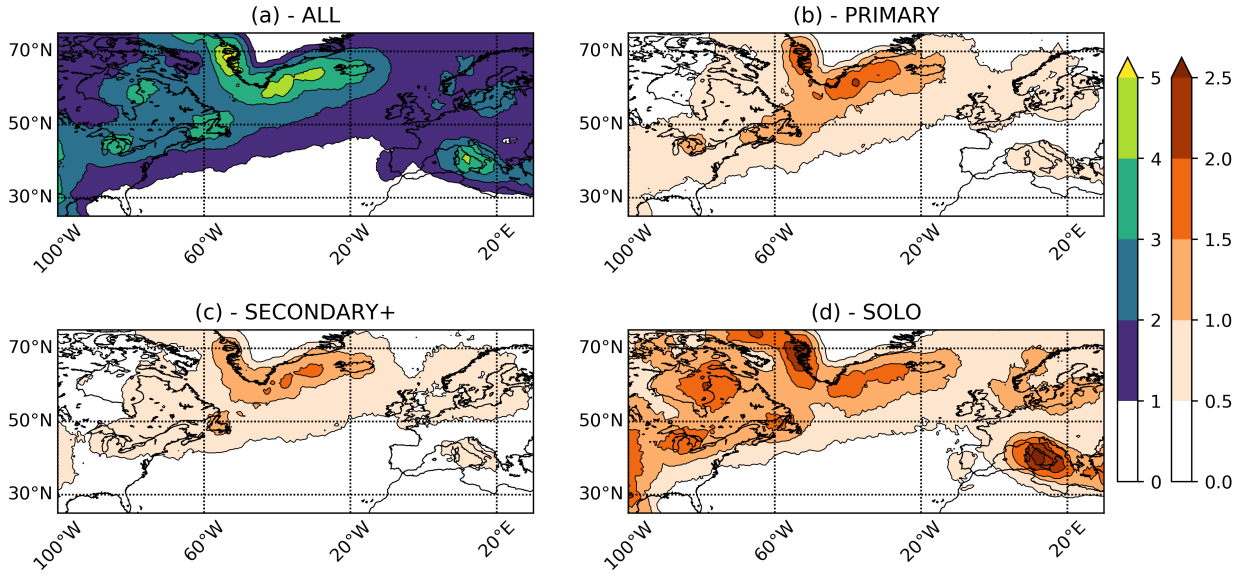

Figure 5.5: *Lysis densities of (a) all cyclones, (b) Primary cyclones, (c) Secondary+ cyclones, and (d) Solo cyclones. Units of the densities are cyclones per month per 5° spherical cap. Lowest contour intervals are not coloured.*

The Solo cyclone class (figure 5.4d) has some cyclogenesis near the coast of North America and the western North Atlantic, however, unlike the other classes this is not the dominant region. The main regions are in the Mediterranean, the Lee of the Rocky mountains (not shown), and also surrounding the tip of Greenland. Given the mean location of Solo cyclogenesis it is possible that Solo cyclones are quite different from Family cyclones and could be more influenced by processes such as lee cyclogenesis.

The lysis densities of the different cyclone classes has also been investigated as part of this study. The lysis is shown in figure 5.5. The characteristics for the Primary and Secondary+ cyclone classes are very similar and both tend to have their lysis in the region between Greenland and Iceland (this is consistent with the lysis for all cyclones). Solo cyclones tend to have their lysis across the Mediterranean, and also parts of North America and the region between Greenland and Iceland.

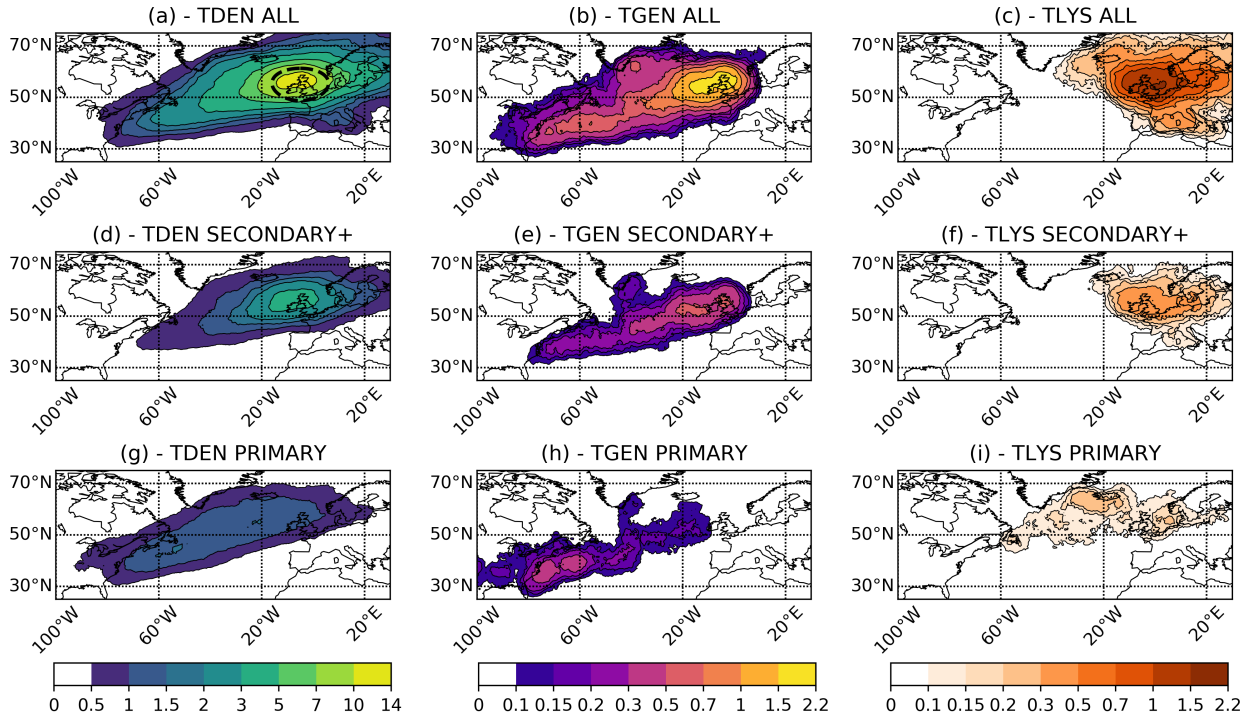

Figure 5.6: *Density plots for all cyclones (a)-(c), Secondary+ cyclones (d)-(f), and the associated Primary cyclone of the Secondary+ cyclones (g)-(i) that pass through the 55°N region. (a,d,g) Track densities. (b,e,h) Genesis densities. (c,f,i) Lysis densities. The lowest contour intervals are not coloured. Units of the densities are cyclones per month per 5° spherical cap. The black dashed region in (a) represents the 700km region that cyclones must pass through.*

5.4.2 Structure of a Cyclone Family

To examine the temporal and spatial relationships between Primary and Secondary+ cyclones, specific Secondary+ cyclone events are examined. To select these events only cyclones that track through a 700km radius centred at 55°N, 5°W are included (black dashed region in figure 5.6a). This area selection is consistent with Priestley et al. (2017a) and allows for a focus on cyclones that are affecting specific regions of western Europe.

For all storms that pass through the 55°N region, the track density (figure 5.6a) is of a more zonal orientation than the total storm track (figure 5.2a). Most cyclones are located between 50-60°N and east of 40°W. This is further apparent when looking at the genesis of these cyclones (figure 5.6b) as most of the cyclones that pass through 55°N form very close to this region (east of 20°W). The average lysis of these

cyclones (figure 5.6c) is to the east of the UK and mainly extending further east toward Denmark and across northern Europe. This suggests that a majority of cyclones tracking over the UK are short-lived features that form close to the European continent, propagate eastwards in a zonal direction before dissipating shortly afterwards (consistent with Dacre and Gray, 2009).

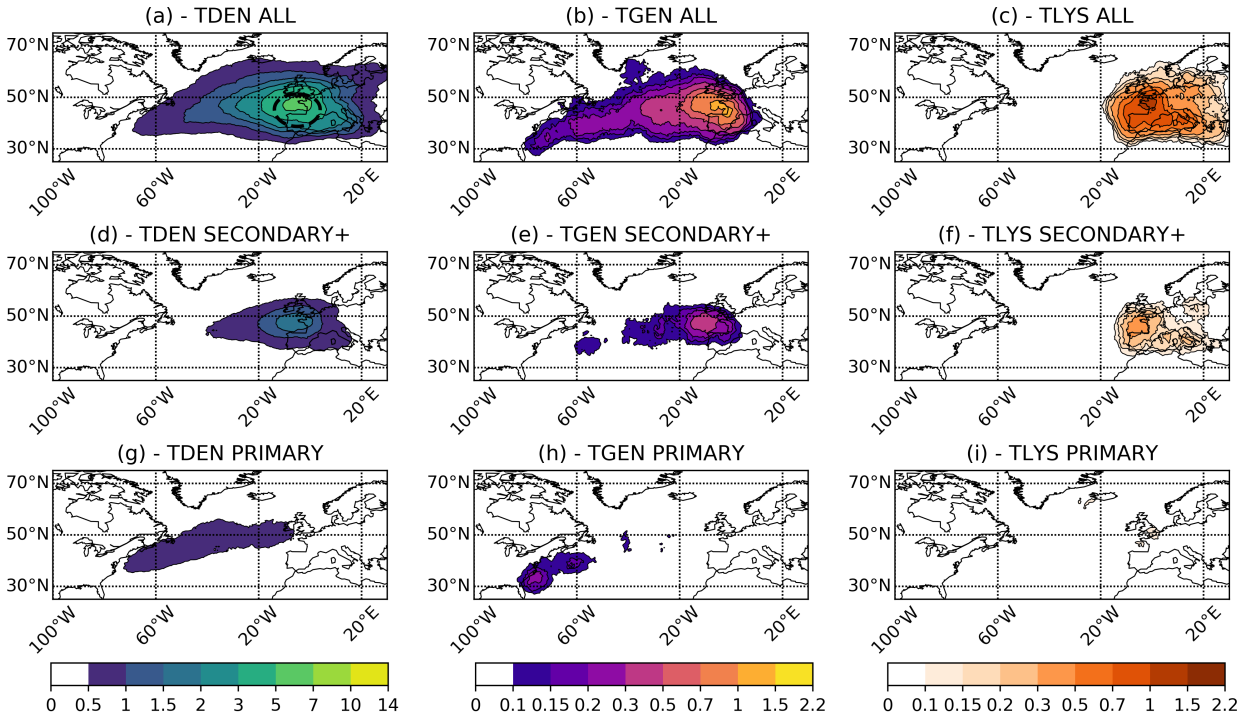

Figure 5.7: *Density plots for all cyclones (a)-(c), Secondary+ cyclones (d)-(f), and the associated Primary cyclone of the Secondary+ cyclones (g)-(i) that pass through the 45°N region. (a,d,g) Track densities. (b,e,h) Genesis densities. (c,f,i) Lysis densities. The lowest contour intervals are not coloured. Units of the densities are cyclones per month per 5° spherical cap. The black dashed region in (a) represents the 700km region that cyclones must pass through.*

Similar density patterns are found when investigating the Secondary+ cyclones that pass through 55°N (figure 5.6d,e,f). These cyclones also form close to the UK and Europe (figure 5.6e), although, as in figure 5.6b, there are also cyclones that form over the western North Atlantic. The pattern of track density (figure 5.6d), is more zonal than the total track density for all storms (figure 5.2a) , before undergoing lysis to the east of the UK and over the North Sea and surrounding countries.

A different picture emerges when looking at the density pattern for the Primary cyclones that are in the same family and hence precede the Secondary+ cyclones analysed in figures 5.6d-f. Unlike the Secondary+ cyclones, which are constrained to pass through the 55°N region (figures 5.6d-f), the Primary cyclone of the family do not have this requirement. The average track density for these Primary cyclones (figure 5.6g) is different to those shown in figures 5.6a,d. The Primary cyclones exhibit the SW-NE tilt seen in figure 5.2b with a maxima in the density of cyclone tracks near the coast of North America, and also to the south of Iceland. It is interesting to note that the track density of Primary cyclones (figure 5.6g), and

the genesis density of Secondary+ cyclones (figure 5.6e) exhibit a similar tilt with the Secondary+ genesis density being at a more southern latitude across the North Atlantic. A majority of the Primary cyclones have their genesis over the strong baroclinic zone off the east coast of North America (figure 5.6h), unlike the more downstream genesis locations of the Secondary+ cyclones. Finally, the lysis locations (figure 5.6i) for Primary cyclones is in the region between the tip of Greenland and Iceland. This suggests that these Primary cyclones do not travel near the European continent and are mainly constrained to longitudes west of 20°W. The similarity in the lysis longitude of the Primary cyclones (figure 5.6i) and the genesis of the Secondary+ cyclones (figure 5.6e) goes some way to confirm the hypothesis from Dacre and Gray (2009) that eastern North Atlantic cyclones are commonly Secondary+ cyclones.

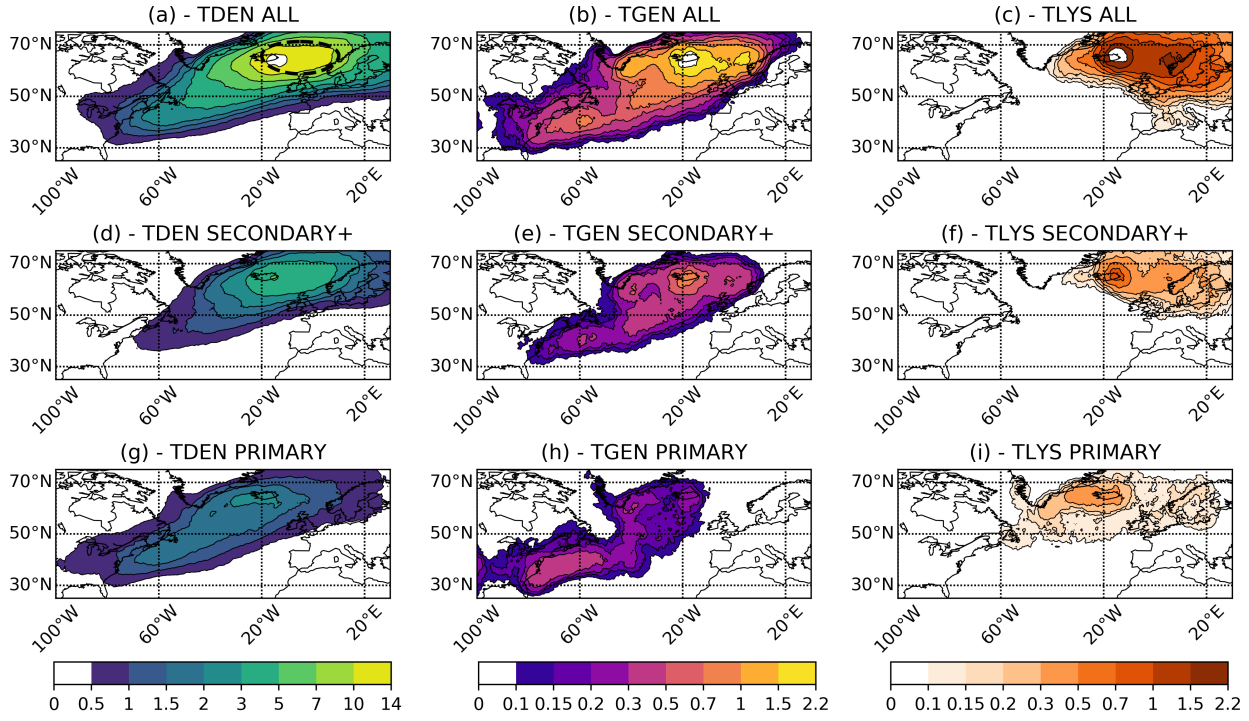

Figure 5.8: *Density plots for all cyclones (a)-(c), Secondary+ cyclones (d)-(f), and the associated Primary cyclone of the Secondary+ cyclones (g)-(i) that pass through the 65°N region. (a,d,g) Track densities. (b,e,h) Genesis densities. (c,f,i) Lysis densities. The lowest contour intervals are not coloured. Units of the densities are cyclones per month per 5° spherical cap. The black dashed region in (a) represents the 700km region that cyclones must pass through.*

In summary, the Primary cyclone tends to form over the Gulf stream and near the coast of North America before travelling in a NE direction across the North Atlantic. These cyclones then have their lysis to the east of Greenland, near Iceland. During their lifetime cyclogenesis occurs along an associated frontal feature, with this generally being located in the central to eastern North Atlantic and at a latitude of 50-60°N and to the south of the Primary cyclone. These Secondary+ cyclones then propagate in a much more zonal direction across the UK in this case before dissipating over the UK or the North Sea and its surrounding countries. This illustrates how these different cyclone classes tend to be preferentially located in different parts of the North Atlantic and also the North Atlantic storm track (as was suggested from figure 5.3). The

results of figure 5.6 further highlights the misleading nature of mean track densities as noted by Whittaker and Horn (1984) due to the fact that cyclones rarely travel the length of the entire storm track and the mean storm track is made up of several different types of cyclone.

This analysis has also been performed for Secondary+ cyclones that pass through two other geographic regions for western Europe at 45°N, 5°W, and 65°N, 5°W, as defined in Priestley et al. (2017a) (see figure 5.7 and figure 5.8). The results of this was very similar to that presented in figure 5.6, with the main difference being northward/southward shift in the genesis/lysis latitude of the Secondary+ cyclones dependent on the latitude of interest. With this, there are only very minor shifts in the angle of the Primary cyclone mean track density. There are clear differences between the two classes for Secondary+ cyclones at all latitudes, with Primary cyclones having a more poleward component to their track the Secondary+ cyclones that follow. However, it is interesting to note that despite there being large differences in the latitude of Secondary+ cyclogenesis, the tracks of the Primary cyclones that precede them are so similar.

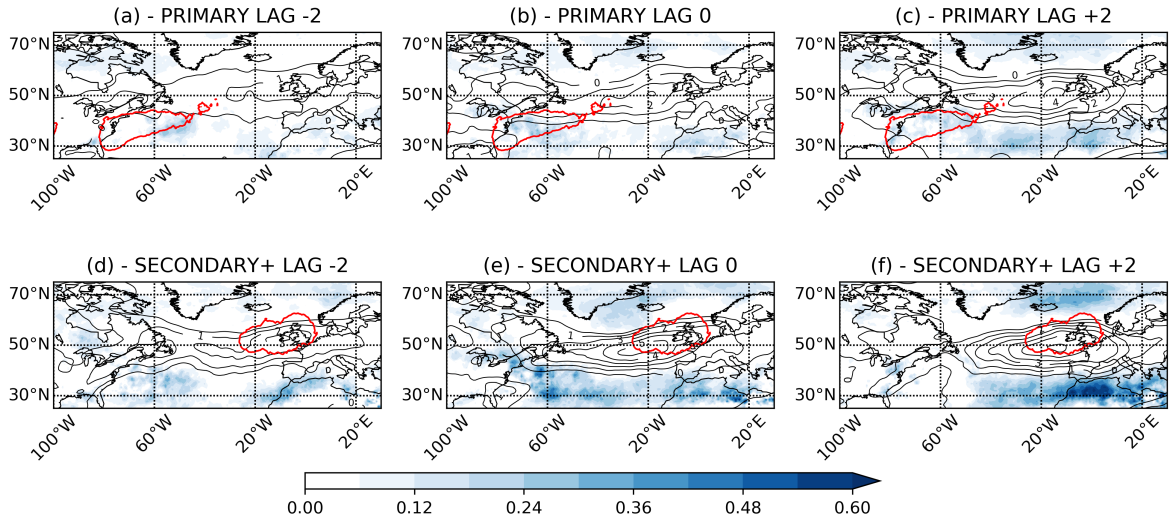

Figure 5.9: *Composites of Rossby wave breaking (RWB) and the upper-level jet for Secondary+ cyclones that pass through the 55°N region and their respective Primary cyclones. Composites are at time of Primary cyclogenesis (b) and Secondary+ cyclogenesis (c). Also shown are composites at lag -2 days (a,d) and lag +2 days (c,f). Red contours in (a-c) are a contour of Primary cyclogenesis (at lag 0 days) that is 50% of the maximum value. Red contours in (d-f) are the same as (a-c) but for Secondary+ cyclones. RWB is expressed as an anomaly in the frequency of RWB at that location relative to the local climatological frequency. The upper-level jet is an anomaly in the 250 hPa wind field to the local climatology in m/s.*

5.4.3 Large-scale Environmental Conditions at the Time of Primary and Secondary+ Cyclogenesis

5.4.3.1 Upper-level Jet and Rossby Wave Breaking

As illustrated in figure 5.6, the Secondary+ cyclones that pass through 55°N, and their respective Primary cyclones, form in different locations and are also likely to form under different environmental conditions. To understand any differences, the upper-level features that are associated with these cyclones at their time of genesis is analysed (figure 5.9). As has been established in several studies, cyclones that impact western Europe are commonly associated with an anomalously strong upper-level jet and RWB on one or both sides of the jet (Hanley and Caballero, 2012; Gómara et al., 2014a; Pinto et al., 2014; Messori and Caballero, 2015; Priestley et al., 2017a), and therefore the same fields will be analysed herein.

The first focus is the time of cyclogenesis for Secondary+ cyclones passing through our 55°N region (figure 5.9e), and the cyclogenesis time of their respective Primary cyclones (figure 5.9b). These will be referred to as lag 0 days. Firstly, for the Primary cyclones (figure 5.9b), it is seen that anomalies in the upper-level jet and RWB frequency are very small. Jet anomalies are less than 3 m s^{-1}, with RWB frequency anomalies generally less than 10%, with some localised regions being $\sim$20% above the climatological frequency. The cyclones are mostly all forming off the east coast of North America, near the right entrance of the jet, and the environment at this time can be mostly described as climatological, with minor positive anomalies.

At the time of Secondary+ cyclone genesis (figure 5.9e) the upper-level environment is very different. There are anomalies in the upper-level jet of over 5 m s^{-1} and anomalous RWB frequencies of up to 40% above the climatological frequency. Both fields have increased anomalies compared to the time of cyclogenesis of the Primary cyclones. This environment is representative of what was described in the aforementioned studies (Pinto et al., 2014; Priestley et al., 2017a), with anomalous RWB either side of an zonally extended and strong jet being favourable for the formation and presence of intense cyclones in the eastern North Atlantic. At the time of cyclogenesis, the Secondary+ cyclones are forming either on the jet axis or the left exit region of the jet, this suggests that conditions are favourable for cyclogenesis via upper-level divergence provided by the ageostrophic circulations in the left exit region of the jet (Rivière and Joly, 2006a,b).

Through inspection of the lag plots, further insight is gained into the connection between the Primary and Secondary+ cyclones. At lag 2 days after Primary cyclone formation (figure 5.9c) there is an amplification of the anomalies from lag 0 (figure 5.9b) downstream of cyclogenesis and around Iceland and the Nordic

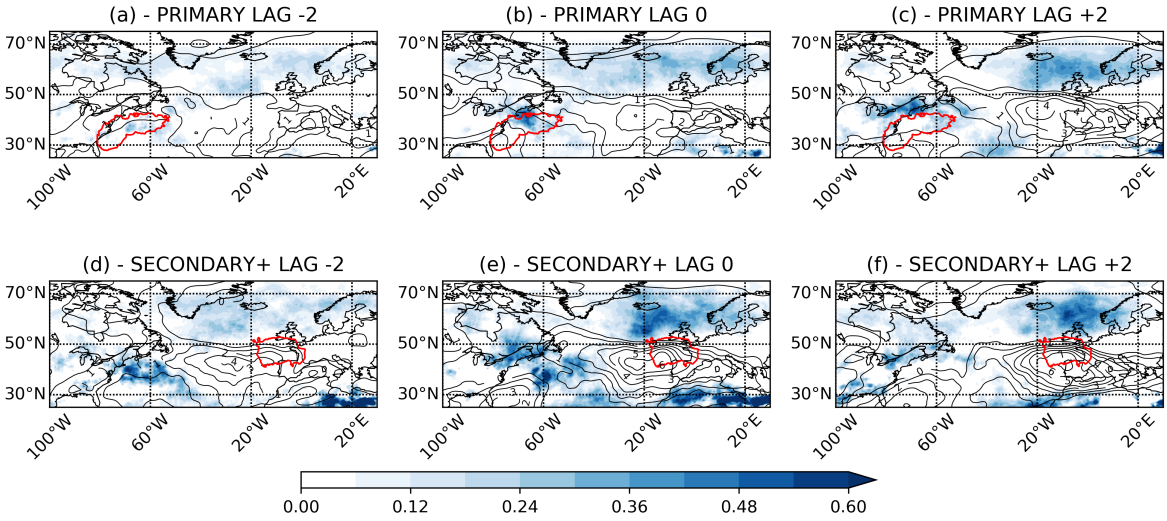

Figure 5.10: *Composites of Rossby wave breaking (RWB) and the upper-level jet for Secondary+ cyclones that pass through the 45°N region and their respective Primary cyclones. Composites are at time of Primary cyclogenesis (b) and Secondary+ cyclogenesis (c). Also shown are composites at lag -2 days (a,d) and lag +2 days (c,f). Red contours in (a-c) are a contour of Primary cyclogenesis (at lag 0 days) that is 50% of the maximum value. Red contours in (d-f) are the same as (a-c) but for Secondary+ cyclones. RWB is expressed as an anomaly in the frequency of RWB at that location relative to the local climatological frequency. The upper-level jet is an anomaly in the 250 hPa wind field to the local climatology in m/s.*

Seas. These anomalies are associated with the presence of the Primary cyclone in this region as it is likely to have propagated toward the NE from its genesis region. The presence of the Primary cyclone is associated wit the development of anomalous RWB, which then in turn causes an acceleration in the jet (see figure 3 Priestley et al., 2017a) through the convergence of eddy momentum (Barnes and Hartmann, 2012). The state of the environment in figure 5.9c, is similar to that at Secondary+ cyclogenesis time (figure 5.9e), albeit with slightly reduced RWB anomalies, suggesting that the Primary cyclone might be key in creating an upper-level environment that is favourable for the formation of Secondary+ cyclones. Further evidence for this is provided in figure 5.9d. 2 days prior to Secondary+ cyclogenesis the upper-level environment has very small anomalies in RWB and the jet, which is very similar to figure 5.9b, and anomalies are almost zero 2 days prior to Primary cyclogenesis (figure 5.9a), suggesting that the anomalies are associated with the development and propagation of the Primary cyclone in the days prior to Secondary+ cyclogenesis. Anomalies are then amplified to an even greater extent as the Secondary+ cyclone develops and moves downstream (figure 5.9f), with anomalies of RWB more than 60% above the climatology and a very anomalous jet at 250 hPa (> 6 m s^{-1}).

As with figure 5.6, this analysis is repeated for Secondary+ cyclones passing through two other geographic regions at 45°N and 65°N (figures 5.10 and 5.11). Similar results as those presented in figure 5.9 are found, yet with a different balance of the RWB to being more dominant on either the northern or southern flank, and hence a shift in the latitude of the jet anomalies, for cyclones impacting 45°N (figure 5.10) and 65°N (figure 5.11) respectively, as seen in Priestley et al. (2017a). These differences in RWB and Primary

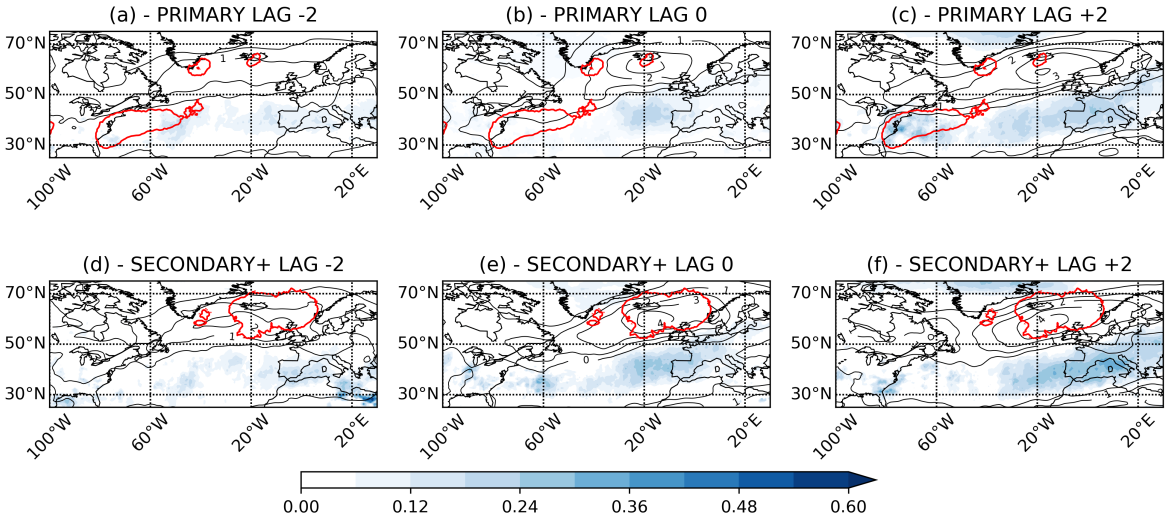

Figure 5.11: *Composites of Rossby wave breaking (RWB) and the upper-level jet for Secondary+ cyclones that pass through the 65°N region and their respective Primary cyclones. Composites are at time of Primary cyclogenesis (b) and Secondary+ cyclogenesis (c). Also shown are composites at lag -2 days (a,d) and lag +2 days (c,f). Red contours in (a-c) are a contour of Primary cyclogenesis (at lag 0 days) that is 50% of the maximum value. Red contours in (d-f) are the same as (a-c) but for Secondary+ cyclones. RWB is expressed as an anomaly in the frequency of RWB at that location relative to the local climatological frequency. The upper-level jet is an anomaly in the 250 hPa wind field to the local climatology in m/s.*

cyclone genesis/lysis could be interpreted through the two different baroclinic lifecycles (LC1/LC2) as first discussed by Thorncroft et al. (1993). Primary cyclones that spawn the 65°N Secondary+ cyclones may be more like the LC1 lifecycle. The Primary cyclone appears to form under more anticyclonic shear (figure 5.11b). LC1 cyclones are associated with anticyclonic RWB on the equatorward flank of the jet and a northward displacement of the jet, which is similar to what is seen in figure 5.11. The lysis of these 65°N Primary cyclones (see figure 5.15a) also occurs close to the jet axis, with part of the lifecycle even being on the equatorward side of the anomalous jet, further suggesting this could be propagating under the LC1 lifecycle. Conversely, the 45°N Primary cyclones appear to form under relatively neutral/cyclonic shear (figure 5.10b). The LC2 lifecycle results in a large amount of cyclonic RWB and a southward displacement of the jet, as is suggested in figure 5.10. The lysis of the 45°N cyclones also occurs quite far from the jet axis (figure 5.15c), indicating these Primary cyclones may be more like the LC2 lifecycle. These results suggest that the environment surrounding the Primary cyclone at the time of genesis is associated with differing lifecycles and RWB structures downstream, therefore affecting the latitude of Secondary+ cyclogenesis and latitude of propagation into western Europe.

5.4.3.2 Low-level Static Stability

As cyclones forming in eastern North Atlantic are associated with a low stability environment (Dacre and Gray, 2009; Wang and Rogers, 2001), and that Secondary+ cyclones are also associated with reduced low-level stability anomalies (Schemm et al., 2015), the evolution of the low-level stability field at the time of Secondary+ cyclogenesis is investigated. Their respective Primary cyclones will also be analysed.

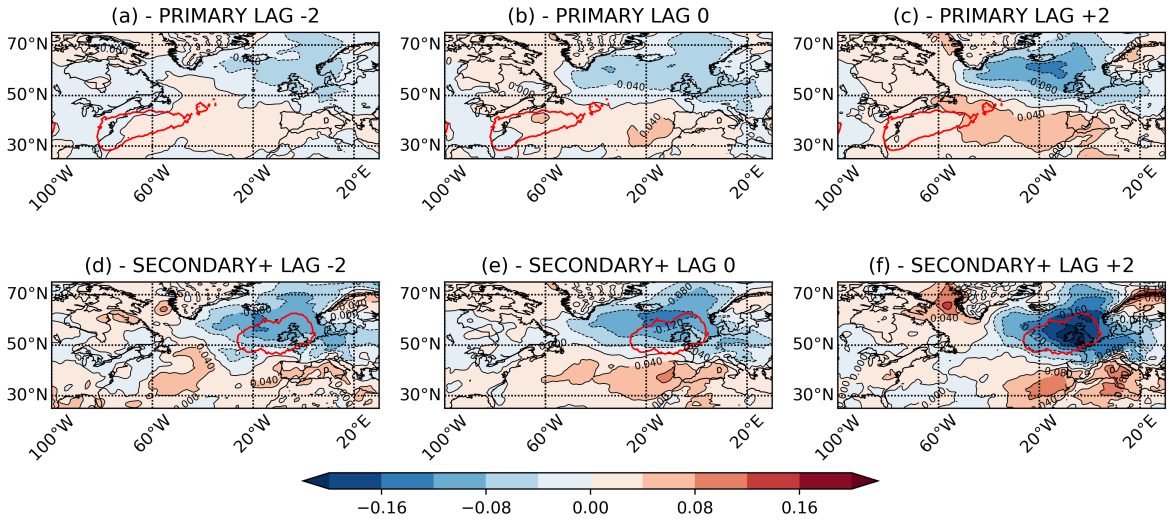

Figure 5.12: *Composites of low-level static stability (N^2) for Secondary+ cyclones that pass through the 55°N region and their respective Primary cyclones. Composites are at time of Primary cyclogenesis (b) and Secondary+ cyclogenesis (c). Also shown are composites at lag -2 days (a,d) and lag +2 days (c,f). Red contours in (a-c) are a contour of Primary cyclogenesis (at lag 0 days) that is 50% of the maximum value. Red contours in (d-f) are the same as (a-c) but for Secondary+ cyclones. Anomalies are expressed as percentage changes relative to the local climatology.*

At the time of cyclogenesis (lag 0 days) for the Primary cyclone (figure 5.12b) there are minimal anomalies (<5%) in static stability across the North Atlantic, with some indication of a N-S dipole between 0-20°W, across 50°N. In the region of Primary cyclone formation anomalies are very weak and do not exceed ±4%. This near-climatological stability indicates that the Primary cyclones forming in this region are rather insensitive to the stability of the low-level environment for formation. This process is likely to not be influenced by the stability as it is common for cyclones forming in this region to be Type B cyclones (Gray and Dacre, 2006) that are driven by an upper-level feature interacting with the quasi-persistent temperature gradients (Petterssen et al., 1955; Davis and Emanuel, 1991).

Conversely, at the time of Secondary+ cyclone formation (figure 5.12e), the dipole in anomalous N^2 is much larger, with negative anomalies of more than 12% from the local climatology in the northeastern North Atlantic. It is in this region of lower N^2 that the Secondary+ cyclones are forming. Cyclogenesis in low N^2 environments of the eastern North Atlantic has been previously studied (Wang and Rogers, 2001; Dacre and Gray, 2009), however it is interesting the note that as in figure 5.9, the anomalies in N^2 are much stronger at the time of Secondary+ cyclogenesis, compared to Primary cyclogenesis. As the Secondary+ cyclones are forming in a strongly anomalous low N^2 region, it appears that this low stability is important for Secondary+ cyclones to form.

As in figure 5.9, an amplification of the anomalies associated with the Primary cyclones from lag 0 days

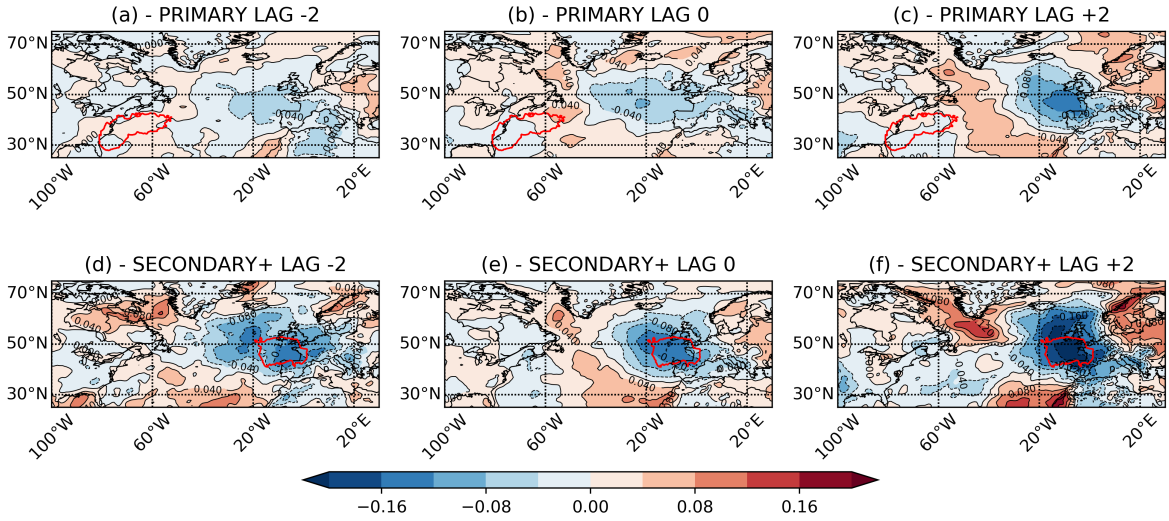

Figure 5.13: *Composites of low-level static stability (N^2) for Secondary+ cyclones that pass through the 45°N region and their respective Primary cyclones. Composites are at time of Primary cyclogenesis (b) and Secondary+ cyclogenesis (c). Also shown are composites at lag -2 days (a,d) and lag +2 days (c,f). Red contours in (a-c) are a contour of Primary cyclogenesis (at lag 0 days) that is 50% of the maximum value. Red contours in (d-f) are the same as (a-c) but for Secondary+ cyclones. Anomalies are expressed as percentage changes relative to the local climatology.*

to lag 2 days is seen (figure 5.12b,c), and an increase in the anomalies from lag -2 days to lag 0 days for Secondary+ cyclogenesis (figure 5.12d,e). This increase in the anomaly magnitude is again likely associated with the propagation of the Primary cyclone downstream and in a northeasterly direction over a period of approximately 2 days. This amplification of the anomalies in N^2 can be understood through interpreting the thermal wind balance equation. As the magnitude of wind shear increases with height, there is also an associated increase in the meridional temperature gradient and also of the vertical potential temperature gradient. This will be associated with an increase in the meridional gradient of static stability. Therefore as the Primary cyclone propagates NE, it is associated with an increase in RWB and hence an acceleration of the jet. This jet speed increase is then associated with an enhanced temperature gradient across the jet axis and a stronger stability dipole. This results in a stability minima at low-levels on the northern flank of the jet. This anomalously low stability environment is then helpful for the formation and intensification of Secondary+ cyclones in this region. This environmental development is associated with the downstream propagation, development, and presence of the Primary cyclone in the 2-3 days prior to the Secondary+ cyclogenesis. A further explanation of this process is given in Appendix A.

As with figures 5.6 and 5.9, this analysis was repeated for Secondary+ cyclones passing through our regions at 45°N and 65°N (figures 5.13 and 5.14). Similar results are found with the dipole in stability anomalies closely following the jet axis and moving south or north for Secondary+ cyclones impacting 45°N (figure 5.13) and 65°N (figure 5.14) respectively. The role of the jet anomalies in driving the latitude of the stability anomalies is clear, with the evolution of the anomalies with the downstream propagation of the Primary

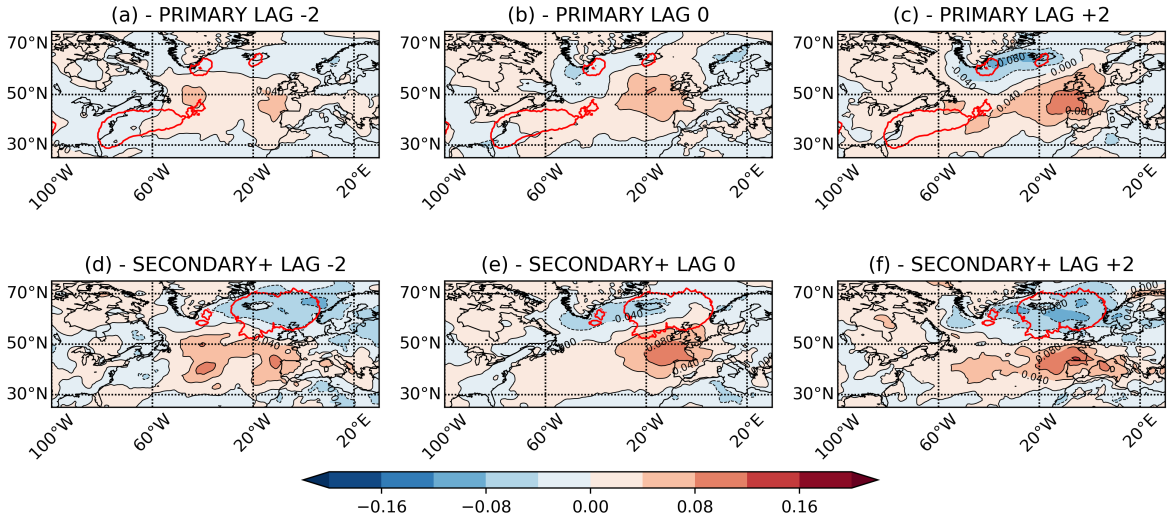

Figure 5.14: *Composites of low-level static stability (N^2) for Secondary+ cyclones that pass through the 65°N region and their respective Primary cyclones. Composites are at time of Primary cyclogenesis (b) and Secondary+ cyclogenesis (c). Also shown are composites at lag -2 days (a,d) and lag +2 days (c,f). Red contours in (a-c) are a contour of Primary cyclogenesis (at lag 0 days) that is 50% of the maximum value. Red contours in (d-f) are the same as (a-c) but for Secondary+ cyclones. Anomalies are expressed as percentage changes relative to the local climatology.*

cyclone also being further apparent.

The relationships identified in sections 5.4.2 and 5.4.3 are brought together, illustrated, and summarised in figure 5.15. It is shown in figure 5.15 how for Secondary+ cyclones passing through the different geographical regions (65°, 55°, 45°N) the Secondary+ cyclones form close to the European continent, with their preceding Primary cyclones forming over the Gulf stream and near the coast of North America and having their lysis over the central North Atlantic. The occurrence of RWB on one or both sides of the jet affects the tilt of the jet in the exit region and is could be a result of different baroclinic lifecycles of the Primary cyclones. These anomalies are then associated with changes in the genesis latitude and subsequent track of the Secondary+ cyclones toward western Europe.

5.4.4 Secondary+ cyclones and clustering over western Europe

In this section of the paper the importance of Secondary+ cyclones for periods of clustering is investigated. The aim is to understand the relative roles of Secondary+ cyclogenesis and steering by the large-scale flow on the increase in the number of cyclones during these periods. Following Pinto et al. (2014); Priestley et al. (2017a), clustering is defined to be more than 4 cyclones in a 7 day period for cyclones that pass through the 55°N region. The results of this are shown in figure 5.16.

For all of the cyclone classes shown in figure 5.16 there is an increase in the number of cyclones in

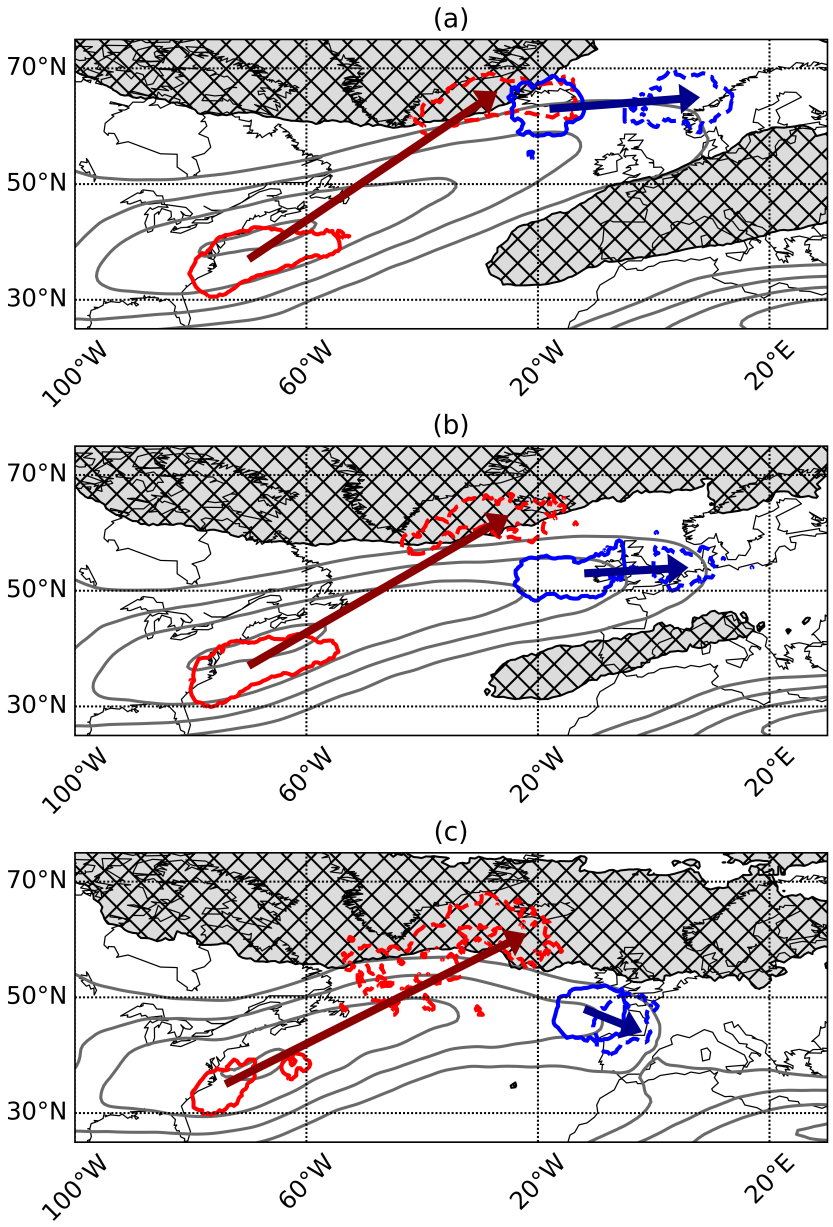

Figure 5.15: *A summary figure illustrating the genesis (solid contours), lysis (dashed contours), and idealised tracks (arrows) of Primary cyclones (red) and their subsequent Secondary+ cyclones (blue) that pass through the (a) 65°N region, (b) 55°N region, and (c) 45°N region. Also shown are contours of the 250 hPa wind speed (grey contours, every 5 m s^{-1} above 30 m s^{-1}) and regions of RWB (grey hatching) averaged throughout the lifetime of the Secondary+ cyclones.*

each class as cyclones pass through the 700km 55°N region more frequently. However, the rate of increase is different for each of the classes. Firstly, the number of Secondary+ cyclones (figure 5.16a) increases almost linearly from less than 1 cyclone in 7-days for non-clustered periods, to an average of 4 cyclones in 7-days during the most intensely clustered periods. A similar relationship is seen for Solo cyclones (figure 5.16b). There is ∼1 cyclone in 7-days in non-clustered periods, with a mean of ∼5 in 7-days for the most clustered events. A different relationship is found for Primary cyclones (figure 5.16c). There is still an increase in the mean number of Primary cyclones as the intensity of clustering increases, yet the total number is much lower. There are at most 2 Primary cyclones in 7-days, with the average during

non-clustered periods being ∼0.2 cyclones per 7-days, and an average of ∼1.5 cyclones in 7-days during the most clustered periods.

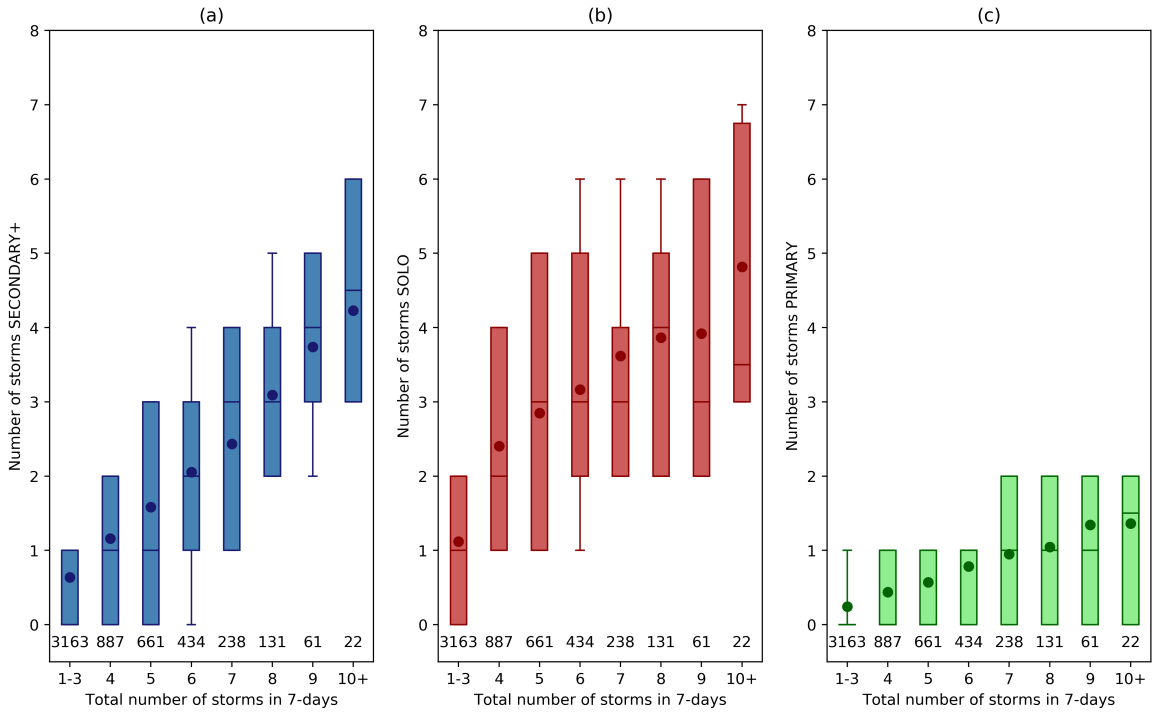

Figure 5.16: *Number of Secondary+ (a), Solo (b), and Primary (c) cyclones compared to the total number of cyclones passing through the 55°N region in a period of 7-days. Boxes show the inter-quartile range, with the lines in the boxes representing the median and the dots being the mean. Whiskers extend to the 20th and 80th percentiles. Numbers below each box represent the number of data points in that bin.*

On average Secondary+ cyclones make up ∼50% of cyclones during severely clustered periods when more than 10 cyclones are passing through the 55°N region in one week. From figure 5.16 it is also interesting to note the difference in the increase in the Secondary+ and Solo cyclones with the intensity of clustering, compared to the lesser absolute increase in Primary cyclones. This could be due to an increase in cyclogenesis near the UK of Secondary+ cyclones that would be assisted by the reduced stability environment associated with the development and propagation of the prior Primary cyclone (figure 5.12). This would result in more Secondary+ cyclogenesis occurring and an increased contribution from cyclone families as the intensity of clustering increases. Alternatively, the amount of cyclogenesis may not be increasing, and the large-scale flow (figure 5.9) may be much more dominant in steering all the cyclones along a similar track. This would lead to a large increase in the number of Secondary+ cyclones with a minimal increase in the number of Primary cyclones as these rarely interact with western Europe.

To understand if the dominant influence is an increase in cyclogenesis or the result of large-scale

steering the Secondary+ cyclones that form in the North Atlantic during clustering periods (including 3 days prior to allow for propagation across the UK), and those during non-clustered periods are inspected. The results are shown in figure 5.17. Genesis densities of all Secondary+ cyclones that form during non-clustered periods are shown in figure 5.17a. This picture is very similar to the climatology of Secondary+ cyclogenesis (figure 5.4c), as non-clustered days make up ∼90% of the total number of days in our dataset. Therefore, the main regions of cyclogenesis are over the Gulf stream, but also the central and eastern North Atlantic between 40°N and 60°N.

During periods of clustering, the main cyclogenesis regions of Secondary+ cyclones (figure 5.17b) is the same as for non-clustered periods with the peak region being near the Gulf stream and the central North Atlantic. In the eastern North Atlantic there is an increase in the number of cyclones with a peak increase of 0.6 cyclones per month (area average 0.13 cyclones per month) in the region nearest to the UK (20°W-0°W, 40°N-60°N), compared to non-clustered periods. Further to this there is also a reduction in cyclogenesis in the latitudes to the North of the UK and near Iceland compared to non-clustered periods. The increase is likely associated with shifts in the genesis regions by the presence of the large-scale RWB (figure 5.9d-f) and also the reduced static stability at low-levels (figure 5.12d-f). It is also of interest to note that the relative number of cyclones forming per day is higher for non-clustered days compared to clustered days. This suggests that as the cyclogenesis rate near the Gulf stream is the same, the increase in cyclogenesis near the UK during clustered periods is simply a result in a shift of the dominant cyclogenesis region slightly to the south instead of an increase of the total number of Secondary+ cyclones forming.

There is a change in the track density of Secondary+ cyclones during clustered periods (figure 5.17d) compared to non-clustered periods (figure 5.17c). The track density is more zonal, particularly in the eastern North Atlantic, with minimal activity north of 60°N. The cyclones are likely being steered along a similar zonal path by the presence of the RWB, resulting in an increase in the numbers of Secondary+ cyclones. The increase in Secondary+ cyclones during clustered periods over the UK is by approximately 3 cyclones per month, an increase of over 100%. The latitudinal shift of the main genesis region and the steering of the cyclones by the jet anomaly and the presence of the RWB is likely a driver of this. This increase in the track density between non-clustered and clustered periods aligns well with the results from figure 5.16a. Changes in the presence of Secondary+ cyclones over the UK are a result of downstream effects on the storm track, hence why all the differences present in figure 5.17 are east of 40°W. Approximately 70% of the changes in the track density in figure 5.17c and 5.17d are a result of the cyclones that form east of 40°W (not shown).

Furthermore, there are minimal changes in the genesis rates of Primary or Solo cyclones (not shown) during clustered periods compared to non-clustered periods, and also an increase in track density over the 55°N

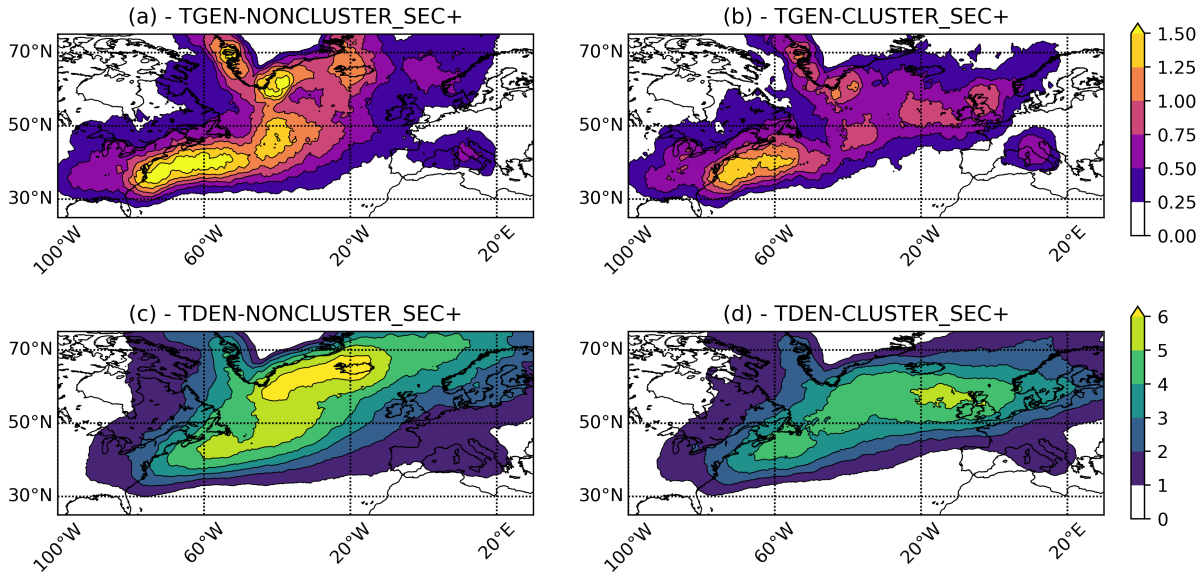

Figure 5.17: *Genesis density of Secondary+ cyclones forming over the North Atlantic that pass through the 55°N region (a) during non-clustered periods, and (b) those forming during clustered periods and three days prior. Track densities of the cyclones forming in (a) are shown in (c) and track densities of those forming in (b) are shown in (d). Units for all panels are number of cyclones per month per 5° spherical cap.*

region, which is consistent with the pattern of change for Secondary+ cyclones.

Therefore, this analysis shows that as clustering becomes more intense, the number of Secondary+ cyclones becomes larger, with approximately 50% of cyclones being Secondary+ cyclones during extreme periods of clustering. While there are slight increases in the amount of Secondary+ cyclogenesis near to the UK, there are actually less cyclones present (relative number per day) in the North Atlantic. The majority of the increase in the number of cyclones appears to be driven by the increased steering from the large-scale flow and RWB and a latitudinal shift of the main genesis region. This steering acts to concentrate all Secondary+ cyclones that form to travel along a similar track. The same is also true of the Primary and Solo cyclones. In Walz et al. (2018) the variability of clustering near the UK was shown to be associated with the different phases of the NAO and EA patterns, and the double-sided pattern of the RWB in figure 5.9e-5.9f has been shown to project onto the NAO (Messori and Caballero, 2015). Therefore, large-scale patterns such as the NAO/EA may play a role in modulating the occurrence of Secondary+ cyclones across the UK and other parts of western Europe.

5.5 Summary and Discussion

In this study the occurrence Secondary+ cyclones and the cyclone families which they are a part of, and how these phenomena contribute to the North Atlantic storm track are investigated. Despite the comprehensive

analysis of secondary cyclones by Schemm and Sprenger (2015) and Schemm et al. (2018) they did not objectively identify and compare the related primary cyclones, or quantify any differences in their preferential locations of genesis, track, and lysis. To identify Secondary+ cyclones and their associated Primary cyclones the method of Schemm and Sprenger (2015) is followed and applied to the cyclone identification and tracking algorithm of Murray and Simmonds (1991b). Three distinctly different cyclone classes are identified, these are: Primary, Secondary+, and Solo. The main results of this study are as follows:

- Primary and Secondary+ cyclone classes make up more than 50% of all cyclones across the North Atlantic ocean, therefore they are vital for the structure of the North Atlantic storm track. Primary cyclones tend to form over the Gulf stream and are commonly found close to the coast of North America and the western North Atlantic ocean. Secondary+ cyclones form over the Gulf stream, but also the central North Atlantic. Solo cyclones are most commonly found over continents, the Mediterranean, and the high latitude North Atlantic. The preferential locations of the Secondary+ cyclones across the central and eastern North Atlantic is a result of Primary cyclones propagating in a northeasterly direction from where they form near the Gulf stream with Secondary+ cyclones then most likely forming on their southern flank.
- Primary cyclones are associated with the development of an environment that is favourable for Secondary+ cyclone formation and downstream propagation toward Europe. The Primary cyclone development is associated with an increase in RWB on one or both flanks of the jet, which is generally zonally extended and strengthened toward Europe. The enhanced jet is associated with a reduction in low-level static stability on the poleward flank of the jet, hence making the environment surrounding Secondary+ cyclogenesis more favourable for cyclone formation and development.
- Secondary+ cyclones contribute approximately 50% of cyclones during clustered periods. There is also an increase in the number of Solo cyclones, with a minimal change in the number of Primary cyclones. The increase in the number of Secondary+ cyclones during clustered periods is mainly a result of the influence of the large-scale flow steering all cyclones along a similarly zonal path toward western Europe. The presence of the RWB acts to shift the main region of cyclogenesis further south to be at the same latitude as the region impacted by the clustering.

As Primary and Secondary+ cyclones are most commonly found over the western and central/eastern sectors of the North Atlantic, it is clear they are important for the overall structure of the North Atlantic storm track. The spatial separation of the two classes also illustrates the findings of Whittaker and Horn (1984) that individual cyclones rarely travel the entire length of the North Atlantic storm track, with those impacting Europe commonly forming very close the the continent (see also Hoskins and Hodges, 2002; Wernli and Schwierz, 2006; Dacre and Gray, 2009). The relative contributions of Secondary+ cyclones in the central North Atlantic are higher in this study than that found by Schemm et al. (2018). These

differences likely arise from the differences in the cyclone identification and tracking schemes applied, with the Wernli and Schwierz (2006) method used in the aforementioned study commonly identifying only half as many cyclones as the Murray and Simmonds (1991b) scheme used in this study (see figure 2 in Pinto et al., 2016).

Primary and Secondary+ cyclones follow different track orientations with Primary cyclones propagating more poleward and Secondary+ cyclones having a more zonal nature to their track. For Secondary+ cyclones impacting western Europe their latitude of genesis is modulated by the presence of an anomalously strong jet and RWB. These jet and RWB anomalies amplify with the downstream propagation of the preceding Primary cyclones. It might be possible that the differences in the jet/RWB response to the Primary cyclone are a result of differing baroclinic lifecycles of Primary cyclones (Thorncroft et al., 1993) and the differing momentum fluxes associated with the wave breaking from the two lifecycles. Based upon the jet/RWB pattern that is generated with the passage of these cyclones families into Europe it could be hypothesised that the passages of these families in specific locations are associated with various phases of the NAO or EA (see Messori and Caballero, 2015; Walz et al., 2018), with the Primary cyclones potentially playing a key role in modulating these large-scale patterns of variability on daily timescales (Rivière and Orlanski, 2007; Gómara et al., 2014b).

Secondary+ cyclones are also shown to form in regions of reduced low-level static stability, with the region of low stability being dictated by the latitude of the jet exit. These findings aligns with Schemm and Sprenger (2015), and also Wang and Rogers (2001) and Dacre and Gray (2009) who illustrated that cyclones forming in the eastern North Atlantic were more commonly associated with a lower stability environment. It is likely that the reduced stability is contributing to the faster growth or deeper cyclones and not additional genesis (Dacre and Gray, 2006).

There are several limitations to this study. Firstly, only one re-analysis product was utilised (ERA-Interim), and only 36 years of data from it. Future avenues of research could include investigating secondary cyclones in other re-analysis products, with the results from this study compared using consistent time periods from multiple products. In addition, just one cyclone identification and tracking algorithm has been used, and one method to identify synoptic-scale frontal features. Results may be sensitive to the choice of cyclone identification methodology, although most methods are consistent for mature phases of the cyclones' lifecycle, particularly for intense systems (Neu et al., 2013). Other frontal identification schemes are also available (e.g. Hewson, 1998; Simmonds et al., 2012), and it would be of interest to compare our results to results from Secondary+ cyclones identified using a different methodology.

Further directions for research could also include an investigation into the process of frontal-wave cyclogenesis for other oceanic basins such as the Pacific, as this process also occurs in other geographic regions (Schemm et al., 2018). In addition, a quantification of the role of the NAO, or other leading atmospheric patterns in controlling the density of Secondary+ cyclones would be of interest. Furthermore, with the database of cyclone types that has been created in this study, examination into the physical differences (e.g. lifecycle, intensity, deepening rate, structure, etc.) of the different classes would be of interest. Previous studies have shown differences in eastern and western North Atlantic cyclones and their evolution characteristics (e.g. Dacre and Gray, 2009; Čampa and Wernli, 2012), with the assumption that the two regional cyclones are systematically different, and performing the same analysis for Primary versus Secondary+ cyclones would be an interesting addition to this analysis.

With regards to the results presented in this study, further in-depth analysis of the processes driving our Secondary+ cyclones would be of interest, especially to build on the results of Schemm and Sprenger (2015) and investigating the role of the environment on specific cyclone features. It would be particularly interesting to perform idealised mesoscale simulations of these cyclogenesis events to examine the sensitivity to atmospheric conditions. Evidence of simulated Secondary+ cyclones has been demonstrated as an upstream response to the forcing of a Primary cyclone via an upper-level PV anomaly in some idealised channel simulations (Schemm et al., 2013). Furthermore, sensitivity experiments into drivers of the Primary and Secondary+ track orientation would also be an interesting avenue to pursue with the upper-level PV structure and moist processes being shown to be important for the poleward propagation of idealised mid-latitude cyclones (Coronel et al., 2015).

Chapter 6:

THE ROLE OF SERIAL EUROPEAN WINDSTORM CLUSTERING FOR EXTREME SEASONAL LOSSES AS DETERMINED FROM MULTI-CENTENNIAL SIMULATIONS OF HIGH RESOLUTION GLOBAL CLIMATE MODEL DATA

The clustering of extratropical cyclones across western Europe was clearly demonstrated as a feature of the winter season in chapters 3 and 4, and also in the wider literature (Mailier et al., 2006; Vitolo et al., 2009; Pinto et al., 2014). The intensity of clustering, and the magnitude of the overdispersion, is something that is variable, with a number of studies (Vitolo et al., 2009; Pinto et al., 2013; Cusack, 2016) finding that more intense extratropical cyclones have a tendency to cluster more and be more overdispersive. Furthermore, the study of Hunter et al. (2016) found that seasons with a greater number of extratropical cyclones were generally characterised by cyclones that had higher intensities. These studies suggest that clustering becomes larger for higher loss seasons. Some of these estimations are associated with large amounts of uncertainty due to the lack of data for high return period seasons (e.g. Cusack, 2016). The aim of this chapter of work is to first of all quantify the losses from extratropical cyclones across Europe at very high return period, and then attempt to understand how important clustering is for high loss seasons at these very high return periods. Subsequently, the research questions that will be addressed in this chapter are as follows:

Q4. Can windstorm losses associated with extratropical cyclones be represented in climate models

for seasonal losses with a return period of 200 years?

Q5. How important is clustering for the most severe seasons in terms of overall losses?

This text and figures that follow have been published in *Natural Hazards and Earth System Sciences* (Priestley et al., 2018).

Citation

Priestley, M. D. K., H. F. Dacre, L. C. Shaffrey, K. I. Hodges, and J. G. Pinto (2018), The role of serial European windstorm clustering for extreme seasonal losses as determined from multi-centennial simulations of high-resolution global climate model data, Natural Hazards and Earth System Sciences, 18, 2991-3006, doi: 10.5194/nhess-18-2991-2018.

Author Contributions

The concept for this study was developed MP, HD, LS, and JP, with KH providing assistance with the objective feature identification and tracking. The analysis, creation of figures, and writing of the text was completed by M. Priestley. The remainder of the authors provided feedback and comments to produce the final manuscript.

6.1 Abstract

Extratropical cyclones are the most damaging natural hazard to affect western Europe. Serial clustering occurs when many intense cyclones affect one specific geographic region in a short period of time which can potentially lead to very large seasonal losses. Previous studies have shown that intense cyclones may be more likely to cluster than less intense cyclones. We revisit this topic using a high resolution climate model with the aim to determine how important clustering is for windstorm related losses.

The role of windstorm clustering is investigated using a quantifiable metric (storm severity index, SSI) that is based on near-surface meteorological variables (10-metre wind speed) and is a good proxy for losses. The SSI is used to convert a wind footprint into losses for individual windstorms or seasons. 918 years of a present-day ensemble of coupled climate model simulations from the High-Resolution Global Environment Model (HiGEM) are compared to ERA-Interim re-analysis. HiGEM is able to successfully reproduce the wintertime North Atlantic/European circulation, and represent the large-scale circulation associated with the serial clustering of European windstorms. We use two measures to identify any changes in the contribution of clustering to the seasonal windstorm loss as a function of return period.

Above a return period of 3 years, the accumulated seasonal loss from HiGEM is up to 20% larger

than the accumulated seasonal loss from a set of random resamples of the HiGEM data. Seasonal losses are increased by 10-20% relative to randomised seasonal losses at a return period of 200 years. The contribution of the single largest event in a season to the accumulated seasonal loss does not change with return period, generally ranging between 25-50%.

Given the realistic dynamical representation of cyclone clustering in HiGEM, and comparable statistics to ERA-Interim, we conclude that our estimation of clustering and its dependence on the return period will be useful for informing the development of risk models for European windstorms, particularly for longer return periods.

6.2 Introduction

Extratropical cyclones are the dominant weather hazard that affects western Europe. On average extratropical cyclones cause over $2 billion (US $) of losses to the insurance industry per year in Europe (Schwierz et al., 2010) as a result of building damage and business interruption from severe wind gusts and large amounts of precipitation. The most severe individual storms can have much greater impacts than what may be observed in an average year, for example storms Daria (25/01/1990), Kyrill (18/01/2007), and Lothar (26/12/1999) caused $5.1, $5.8, and $6.2 billion of insured losses respectively (Munich Re, 2015). The most severe seasons, in terms of total windstorm loss, are often characterised by the recurrent influence of multiple cyclone events occurring in a short period of time, e.g. such as the winter of 2013/2014 (Matthews et al., 2014; Priestley et al., 2017b).

There have been several attempts to quantify losses associated with severe extratropical cyclones in re-analysis data and with data from General Circulation Models (GCMs) (e.g., Pinto et al., 2007; Leckebusch et al., 2007; Donat et al., 2011).These studies have primarily focussed on assessments of current climate loss potentials, and how these may alter under future climate conditions. These analyses commonly use loss proxies based on gridded meteorological data, such as the Storm Severity Index (SSI) (Klawa and Ulbrich, 2003). The SSI has been found to reproduce the inter-annual variability of windstorm losses in Germany with a correlation of r=0.96 (Klawa and Ulbrich, 2003). This analysis can be performed on a seasonal basis (Pinto et al., 2007; Leckebusch et al., 2007), but also for individual events (Della-Marta et al., 2009; Karremann et al., 2014b, 2016).

North Atlantic winter cyclones have a tendency to occur in groups that affect specific geographical regions within a given period of time. This process is known as serial clustering (Mailier et al., 2006). Serial clustering has been observed in re-analysis data sets in multiple studies (Mailier et al., 2006; Pinto et al., 2013), and is a prominent feature of the cyclones that affect western Europe. Vitolo et al. (2009), Pinto et al.

(2013), and Cusack (2016) provided evidence that the magnitude of serial clustering occurring over western and northwestern Europe may increase for more intense cyclones. Furthermore, a strong connection was found between the number of cyclones in a season and their intensities, particularly over the European sector (Hunter et al., 2016). Recent studies (Pinto et al., 2014; Priestley et al., 2017a) have been able to associate specific dynamical conditions with North Atlantic cyclone clustering events. Periods of clustering are associated with a strong and straight North Atlantic jet stream flanked by the presence of anomalous Rossby wave breaking (RWB) on one or both sides of the jet. The amount of RWB on each side of the jet determines the angle of the jet and hence the location of clustering. More RWB to the south (north) drives the jet and storms further north (south), whereas RWB on both sides keeps the jet and storms constrained to a more central latitude. When these dynamical conditions persist for an extended period of time, it drives many cyclones towards the same location in western Europe. Often these cyclones are members of a 'cyclone family', where cyclones form on the trailing cold fronts of mature cyclones further downstream (Bjerknes and Solberg, 1922). Clustering can have huge socio-economic impacts, for example the seasons of 1990, 1999 and 2013/14 were all characterised by this behaviour and resulted in insured losses of €20, €16, and €3.3 billion respectively, as well as numerous fatalities across Europe (Munich Re, 2015).

Despite previous studies assessing the return periods of European windstorm losses (Pinto et al., 2007; Leckebusch et al., 2007; Donat et al., 2011; Pinto et al., 2012) the importance of clustering to severe windstorm loss seasons across the whole of Europe has received less attention (notably Karremann et al., 2014b,a). In this study, we will further explore how clustering is associated with windstorm losses for Europe. With this aim, the historical reanalysis datasets provide a comprehensive spatial coverage and are typically around 40-100 years in length. Due to the temporal limitations of reanalysis, accurate estimations of high return period storms (1 in 200 year events) are therefore not possible. Assessments of European wind storm losses for longer return periods using general circulation models (GCMs) have been performed (Pinto et al., 2012; Karremann et al., 2014b,a). However, the aforementioned studies were mainly interested in investigating changes to windstorm losses under future climate conditions and all were performed with models with coarse horizontal resolution (ECHAM5/MPI-OM1, T63, $\sim$180 km in Europe (Roeckner et al., 2006)). In this study the High-Resolution Global Environment Model (HiGEM, Shaffrey et al. (2009)) is used since it has higher horizontal resolution compared to the GCMs used in previous studies. In addition, particular focus is placed on evaluating HiGEM's ability to represent the behaviour of clustering as identified in Priestley et al. (2017a).

The main science questions that will be addressed in this study are as follows:

1. Is HiGEM able to capture the upper-tropospheric large-scale dynamics associated with European cyclone clustering?

2. Does the SSI calculated using HiGEM output provide comparable results for individual windstorms and seasonal accumulations, to those obtained from the ERA-Interim re-analysis?
3. Does windstorm clustering contribute more to losses in Europe for winter seasons with large accumulated losses?

The paper continues as follows. The data and methods used are described in section 2. The results follow in section 3, which starts with an evaluation of HiGEM, then an analysis of the SSI as a suitable metric for comparing windstorms in HiGEM and ERA-Interim. Finally the importance of clustering for seasons with large accumulated European windstorm losses is addressed. The conclusions are presented in section 4.

6.3 Data & Methods

6.3.1 Datasets

The main data source for this work are simulations performed using HiGEM (Shaffrey et al., 2009), a fully coupled high resolution climate model based on the HadGEM1 configuration of the Met Office Unified Model (Johns et al., 2006b). The horizontal resolution of the HiGEM atmospheric component is 0.83° latitude x 1.25° longitude (N144) (∼90 km in mid-latitudes) with 38 vertical levels up to 39 km. The horizontal resolution of the ocean component is $\frac{1}{3}$° x $\frac{1}{3}$° (∼30 km) and is considered to be eddy-permitting. A total of 918 years of HiGEM data are available with a 6-hourly temporal resolution. This data comes from a series of 4-member ensemble decadal hindcasts initialised between 1960 and 2006, and also four 59 year transient experiments initialised in 1957. Full details of the data used are described in Shaffrey et al. (2017). HiGEM has been shown to have a good representation of the North Atlantic storm tracks, and also in the representation and distribution of extratropical cyclones (Catto et al., 2010, 2011).

For comparison, the re-analysis from the European Centre for Medium Range Weather Forecasts (ECMWF) ERA-Interim dataset (Dee et al., 2011) is used. ERA-Interim data is available at a 6-hourly resolution, starting from January 1979 and has a T255 spectral horizontal resolution (∼80 km) with 60 vertical eta levels up to 0.1 hPa. Therefore, the resolution of ERA-Interim is comparable to that of HiGEM. In total 36 years of ERA-Interim data are used, from 1979 to 2015. As the focus of this study is on wintertime losses resulting from extratropical cyclones our analysis will be constrained to the months of December, January, and February (DJF).

6.3.2 Cyclone Identification and Tracking

To identify extratropical cyclones in both datasets we use the tracking algorithm of Hodges (1994, 1995) applied in the same way as Hoskins and Hodges (2002). This method tracks features using maxima in the 850 hPa relative vorticity field in the Northern Hemisphere. Prior to tracking the vorticity field is spectrally

truncated to T42, which reduces the noise in the vorticity field. The large-scale background is also removed by removing total wavenumbers ≤ 5 in the spectral representation (Hoskins and Hodges, 2002). Maxima in the vorticity field (i.e. cyclonic features) are identified every 6 hours and formed into tracks. This is initially done by using a nearest neighbour approach to initialise the tracks, which are then refined by minimizing a cost function for track smoothness that is subject to adaptive constraints on the smoothness and displacement in a time step (Hodges, 1999). Pressure minima are also associated with the tracks using a minimization technique (Bengtsson et al., 2009) within a 5° radial cap. In order to exclude very small scale, noisy tracks, only tracks that travel at least 500 km and have a lifetime greater than 24 hours are retained. In previous dynamical clustering studies (Pinto et al., 2014; Priestley et al., 2017a) the method of Murray and Simmonds (1991a) has been applied. Both cyclone tracking methods perform similarly for the tracking and clustering of North Atlantic cyclones, though the Hodges (1994) method generally tends to produce lower clustering values over the North Atlantic/European sector (Pinto et al., 2016).

We follow the method of Priestley et al. (2017a) to calculate composite fields of RWB and the upper-level jet on clustered days. RWB is calculated using the 2-D Blocking Index method from Masato et al. (2013), which identifies overturning of potential temperature contours on the 2 PVU surface (dynamical tropopause; 1 PVU = 1×10^{-6} K m^2 kg^{-1} s^{-1}). The upper-level jet is identified as regions of high wind speed on the 250 hPa surface. These fields are composited for cyclones passing through three 700 km radii at different latitudes centred on 5°W; 45°N, 55°N, and 65°N, to focus on the impact for various locations in western Europe.

6.3.3 SSI Metric

The metric developed by Klawa and Ulbrich (2003) is used as a loss proxy for European windstorms. The SSI has been used in numerous other studies for similar purposes (Leckebusch et al., 2007; Pinto et al., 2007, 2012; Karremann et al., 2014b,a). It uses 10-metre wind speeds in its calculation of storm severity. We follow the approach of the population weighted SSI as used by Pinto et al. (2012) and Karremann et al. (2014b). The formulation of the SSI is defined in equation 6.1 and is constructed as follows:

- Losses due to wind occur on approximately 2% of all days (Palutikof and Skellern, 1991), therefore, for any losses to be produced the wind speed ($V_{i,j}$) must exceed the 98th percentile of the wind speed distribution.
- Buildings are generally constructed in such a way that they can sustain gusts that are expected locally. Hence, the 98th percentile is the local value ($V_{i,j}^{98}$). Following the method of Karremann (2015), if the 98th percentile is less than 9 m s^{-1}, the 98th percentile value is fixed at 9 m s^{-1}. Changing the value of $V_{i,j}^{98}$ provides a sensible threshold for regions where the actual $V_{i,j}^{98}$ is not a realistic threshold for the onset of damage, such as Southern Europe and Iberia.

- Losses do not occur if the wind speed does not exceed the local threshold ($I_{i,j}$).
- The value of $\frac{V_{i,j}}{V_{i,j}^{98}}$ is cubed as this is proportional to the kinetic energy flux (Palutikof and Skellern, 1991; Lamb, 1991) and this introduces a realistic, strongly non-linear wind-loss relationship (Klawa and Ulbrich, 2003).
- Winds exceeding the 98th percentile that do not occur over land are ignored as they will not contribute to losses ($L_{i,j}$).
- Insured losses from windstorms are dependent on the location of insured property, which are proportional to the local population density. The SSI is scaled by the 2015 global population density at the corresponding grid-box ($pop_{i,j}$, (Center for International Earth Science Information Network - CIESIN - Columbia University, 2017)).

$$SSI = \sum_{i=1}^{N_i} \sum_{j=1}^{N_j} \left(\frac{V_{i,j}}{V_{i,j}^{98}} - 1 \right)^3 \cdot I_{i,j} \cdot L_{i,j} \cdot pop_{i,j} \tag{6.1}$$

$$V_{i,j} = \begin{cases} max\left(V_{i,j,t}\right) & \text{if } V_{i,j} \geq 9\ ms^{-1} \\ 9\ ms^{-1} & \text{if } V_{i,j} < 9\ ms^{-1} \end{cases}, \ t = \text{time period}$$

$$I_{i,j} = \begin{cases} 0 \text{ if } V_{i,j} < V_{i,j}^{98} \\ 1 \text{ if } V_{i,j} \geq \mathrm{V}_{i,j}^{98} \end{cases}$$

$$L_{i,j} = \begin{cases} 0 \text{ over seas} \\ 1 \text{ over land} \end{cases}$$

$$pop_{i,j} = \text{Population density per grid-box}$$

The SSI is calculated at every land grid point and is used in two different forms for the main analysis in this study. Following insurance industry naming conventions, the first approach will be to calculate the maximum loss event in a year (herein referred to as the Occurrence Exceedance Probability (OEP)), and the second will calculate the total loss for an entire DJF season (herein referred to as the Annual Exceedance Probability (AEP)).

The OEP is calculated as the spatial sum of the maximum SSI within a 72-hour period (i.e. the maximum SSI calculated from the 6-hourly wind speeds in a 72-hour period, per grid point). The 72-hour time window is consistent with that used by re-insurance companies for defining a particular event (Mitchell-Wallace et al., 2017). The region used to calculate the OEP is an adapted version of the Meteorological Index (MI) box applied by Pinto et al. (2012). Our OEP region extends from $10°W - 20°E, 35°N - 60°N$ and covers all of western Europe and most of central Europe. Our region differs from that of Pinto et al. (2012) as it extends further south to $35°N$, in order to encompass the Iberian

peninsula and also all of Italy (shown by the black box in Figure 6.5b).

The AEP is calculated in the same way as the OEP, except that instead of using the single 72-hour maximum wind footprint, it sums all the individual 72-hour maximum wind speed footprints in the 90-day winter period. In the calculation of the AEP all events are retained. The sensitivity to retaining all events is tested later.

6.3.4 Clustering Measures

There are several ways to assess the clustering of windstorms, which give different information and perspectives. Described below are the three methods which will be used in this study.

6.3.4.1 Dispersion Statistic

The first measure is the dispersion statistic (ψ). This is a measure of the regularity of cyclone passages at a particular gridpoint (equation 6.2) (Mailier et al., 2006). This relates the variance (σ^2) in storm track density (average number of storms per month in a single DJF season) to the mean (μ) storm track density, with positive (negative) values indicating that cyclones are more likely to occur in groups (regularly). Near-zero values indicate a more random occurrence of cyclones (corresponding to a Poisson distribution).

$$\psi = \left(\frac{\sigma^2}{\mu}\right) - 1 \tag{6.2}$$

This statistical measure is the base quantification of where the dynamical clustering of cyclones is occurring. When done on a grid-point by grid-point basis it illustrates where cyclone passages are more regular, or more clustered and has been applied in numerous studies for this purpose (Mailier et al., 2006; Vitolo et al., 2009; Pinto et al., 2013). Moreover, Karremann et al. (2014b,a) estimated clustering of European storm series of different intensities and frequencies by approximating the data with a negative binomial distribution, thus estimating the deviation from a random Poisson distribution.

6.3.4.2 AEP/AEP_random

Another measure for assessing the impact of the clustering of cyclones is to examine the ratio of the AEP to an AEP that is calculated when all the storms have been randomised in time (this will herein be referred to as AEP_random). The randomisation re-orders all of the 72-hour SSI periods in the 918 DJF periods from HiGEM. Artificial DJF seasons are constructed by randomly sampling thirty 72-hour periods into a new order to remove any dynamical clustering between events that may be present in the HiGEM climate model. The AEP/AEP_random measure of clustering is particularly important for re-insurers as it provides information on how having dynamically consistent years (e.g. from the HiGEM model) provides different

AEPs relative to a set of random (stochastic) model year.

A value of AEP/AEP_random larger than 1 suggests that the dynamically consistent clustering and the severity of cyclones in HiGEM result in a larger AEP, relative to that expected from a randomly sampled set of events. Similarly, a value less than 1 suggests that the consistent grouping of cyclones gives a lower AEP than would be expected at that particular return period.

6.3.4.3 OEP/AEP

The final measure used to assess clustering is the ratio of the OEP to the AEP. If the total loss in a season were characterised by just one single 72-hour cyclone event then, by definition, the AEP and OEP would be identical. However, if the OEP were much smaller than the AEP then this would suggest there are many cyclone events contributing to the AEP. The OEP/AEP ratio therefore quantifies the dominance of a single loss event in a season. The OEP/AEP ratio is calculated using the OEP and AEP in the same season.

It should be noted that all the above measures provide different interpretations of the occurrence of clustering. The dispersion statistic is a measure of how grouped storms are in time relative to a Poisson distribution. This can be physically interpreted as measuring the seriality of clustering. The ratio of AEP to AEP_random provides information on the dynamically consistent grouping of cyclones affects the accumulated seasonal losses (e.g. that produced from a climate model) compared to a completely random series of cyclones. The OEP to AEP ratio gives information on the dominance of the largest loss event in the overall seasonal losses. One of the additional objectives of this study is to ascertain how consistent the different measures of clustering are for seasonal losses.

6.3.5 Return Periods and Statistical Methods

A majority of the results in this paper will be expressed in terms of return period. The return period provides a period of time in which an event of a certain magnitude is expected to occur. Return periods have been allocated in a way such that the maximum AEP year is assigned a return period of the length of the dataset divided by its rank (for the maximum event the rank is 1). Therefore the maximum AEP year from ERA-Interim has a return period of 36 years, the highest AEP year in HiGEM has a return period of 918 years, as they both occur once in their total time period respectively. The second largest events then have return periods of 18 years and 459 years for ERA-Interim and HiGEM respectively. This continues until the lowest ranked year, which has a return period of 1 year. For a majority of our analysis we rank the OEP in the order of descending AEP. This ensures we maintain a temporal connection between the OEP and AEP at all return periods and means that the largest OEP may not necessarily occur in the highest AEP year. Some analysis is performed on independently ordered AEP and OEP, which removes the connection

between maximum events and the years in which they occur.

The return periods of the most extreme events are estimated using a generalized Pareto distribution (GPD) that is fitted to the AEP and OEP data above a specified threshold ('peak over threshold' method). The GPD is fit using the maximum-likelihood method, following Della-Marta and Pinto (2009), and Pinto et al. (2012). Uncertainties at the 95% level are calculated using the delta method (Coles, 2001).

6.4 Results

6.4.1 Evaluation of Cyclone Clustering in HiGEM

HiGEM has a good representation of the large-scale tropospheric circulation (Shaffrey et al., 2009; Woollings, 2010) and also extratropical cyclone shape, structure, and distribution (Catto et al., 2010, 2011). Several other studies have demonstrated that the model has skill in seasonal to decadal predictions, particularly in the North Atlantic (Shaffrey et al., 2017; Robson et al., 2017). HiGEM provides a good representation of both the structure and amplitude of the DJF North Atlantic storm track (Figures 6.1a, c, e). The characteristic tilt of the North Atlantic storm track is evident as cyclones in HiGEM (Figure 6.1c) follow the SW-NE path found in ERA-Interim (Figure 6.1a). In addition the maxima in storm numbers off the coast of Newfoundland and also over the Irminger Sea agree (anomalies within $\pm$ 2 cyclones per month) with ERA-Interim (Figure 6.1e). There is an anomalous extension of the storm track in its exit region in HiGEM across Denmark and northern Germany, however the amplitude of the anomaly is small ($<$ 2 cyclones per month). On the larger scale there are minimal biases present across the entire basin and the European continent. There are localised errors that are mostly below 2 cyclones per month when compared to 36 years of ERA-Interim re-analysis (consistent with Catto et al. (2011)). The structure and amplitude of the Mediterranean storm track is also well captured. Stippling in Figure 6.1e indicates where HiGEM and ERA-Interim are different at the 95% level (performed using a two-tailed Student's t-test). These differences are only present around the coast of Greenland and are associated with the minima in the Labrador Sea and Davis Strait, and also the maxima across the east coast of Greenland. None of the anomalies across the rest of the North Atlantic or Europe are statistically significant.

The dispersion of cyclones in the North Atlantic for ERA-Interim and HiGEM is shown in Figures 6.1b and 6.1d respectively. The pattern of the dispersion is consistent for the two datasets with both being characterised by a more regular behaviour in the entrance of the storm track (western North Atlantic) where storms have their main genesis region (Hoskins and Hodges, 2002) and baroclinic processes are dominant. Both datasets show overdispersive (clustered) behaviour in the exit of the storm track, e.g. the UK and Iceland. The pattern of under/overdispersion in the exit/entrance region of the storm track is comparable

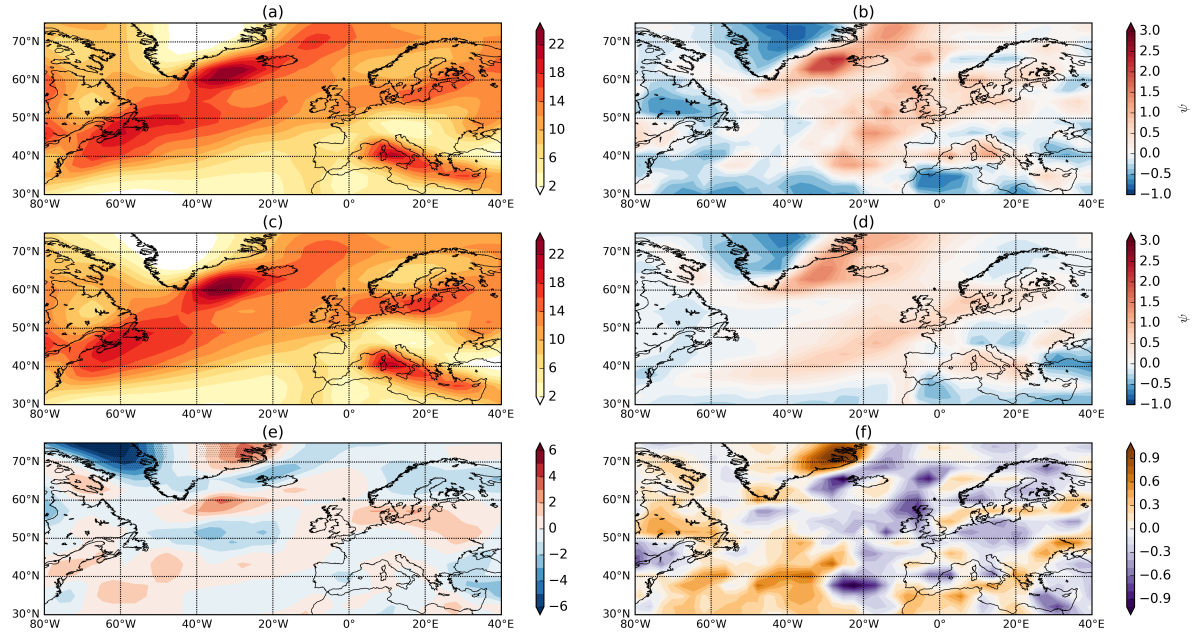

Figure 6.1: *Track density (a) and associated dispersion (b) for ERA-Interim DJF storm track.(c), (d) same as (a), (b) but for HiGEM. (e) is the difference in track density (HiGEM-ERA-Interm), stippling indicates where the two datasets are different at the 95% level. (f) is the difference in dispersion (HiGEM-ERA-Interim). Units for (a), (c), and (e) are cyclones per month per 5° spherical cap.*

with the studies of Mailier et al. (2006); Pinto et al. (2013). There are discrepancies in the magnitude of the dispersion (Figure 1f), however, the large-scale pattern and sign of the dispersion is consistent between the two datasets.

It was shown in Priestley et al. (2017a) that clustering events occurring at different latitudes of western Europe are associated with a specific set of dynamical conditions (as discussed in section 1). The clustering periods identified are characterised by a strong and extended upper-level jet that was associated with anomalous RWB on one or both flanks, which acts to drive the jet further north or further south and then anchor it in position. These persistent conditions allow the cyclones to track in similar directions and leads to clustering over different regions of western Europe. This analysis has been repeated for all 918 years of HiGEM data in order to assess how well HiGEM dynamically represents these events (Figure 6.2). The same analysis of ERA-Interim is shown in the supplementary material (Figure 6.3). Figure 6.2a shows that for cyclones clustering at 65°N, the jet is extended toward the northern United Kingdom with speeds in excess of 40 m s^{-1}. The jet is associated with large amounts of RWB on its southern flank. For clustered days at 55°N (Figure 6.2b), the extended jet is more zonal than for events at 65°N. The strong jet has anomalous RWB on the northern and southern flanks, however the RWB on the southern flank is of a smaller magnitude than that seen in ERA-Interim (Figure 6.3b). The clustered events at 45°N show a very zonal upper-level jet with a dominance of RWB on the northern flank.

All of the composites of clustered days (Figure 6.2a-c) show a marked departure from the climatology

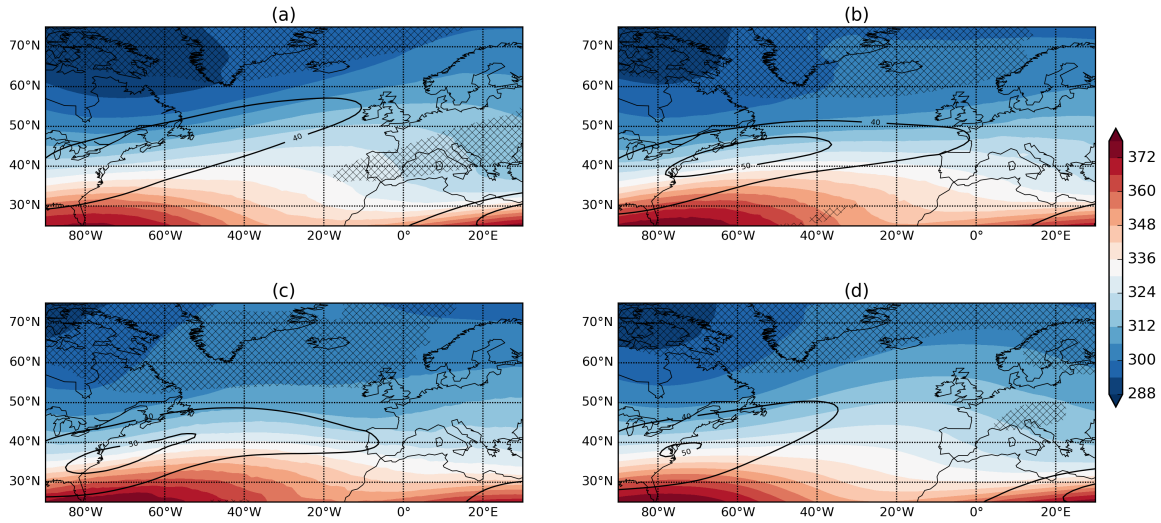

Figure 6.2: *Dynamical composites of clustered days at (a) 65°N, (b) 55°N, and (c) 45°N. (d) Climatology. For all panels the colored contours are θ on the 2 PVU surface (K). Black contours are the 250 hPa wind speed, starting at 40 m s^{-1} and increasing by 10 m s^{-1}. The crossed hatchings are where RWB was occurring on at least 30% of days.*

(Figure 6.2d). The jet is stronger and more zonally extended than the climatology for all three cases, and each features anomalous amounts of RWB on one or both flanks of the upper-level jet, all of which are comparable to ERA-Interim. The climatological state of the jet and RWB in HiGEM (Figure 6.2d) is comparable with ERA-Interim (Figure 6.3d), with a slightly reduced amount of RWB across central Europe. Hence, clustering events in HiGEM appear dynamically consistent with those in ERA-Interim, albeit with a lower frequency of anticyclonic RWB on the southern flank of the jet.

HiGEM has been found to have a good representation of North Atlantic extratropical cyclones and cyclone clustering, as well as the large-scale circulation driving this behaviour. This demonstrates the suitability of using HiGEM to investigate clustered windstorm related losses.

6.4.2 Comparison of SSI in ERA-Interim and HiGEM

The SSI is widely used for quantifying losses related to windstorms. We now compare the SSI for both HiGEM and ERA-Interim. The characteristic of the SSI is that it is calculated above a set threshold, the 98th percentile of the local distribution of 10-metre wind speed ($V_{i,j}^{98}$). The structure of $V_{i,j}^{98}$ for ERA-Interim, HiGEM, and the difference between the two datasets is shown in Figure 6.4. Both datasets show a similar large scale structure with maxima over the North Atlantic ocean and minima over the high orography of the Alps and Pyrenees. However, HiGEM values are systematically lower than ERA-Interim across almost all of Europe by 1-3 m s^{-1} (Figure 6.4c), whereas across the North Atlantic ocean the bias is smaller and

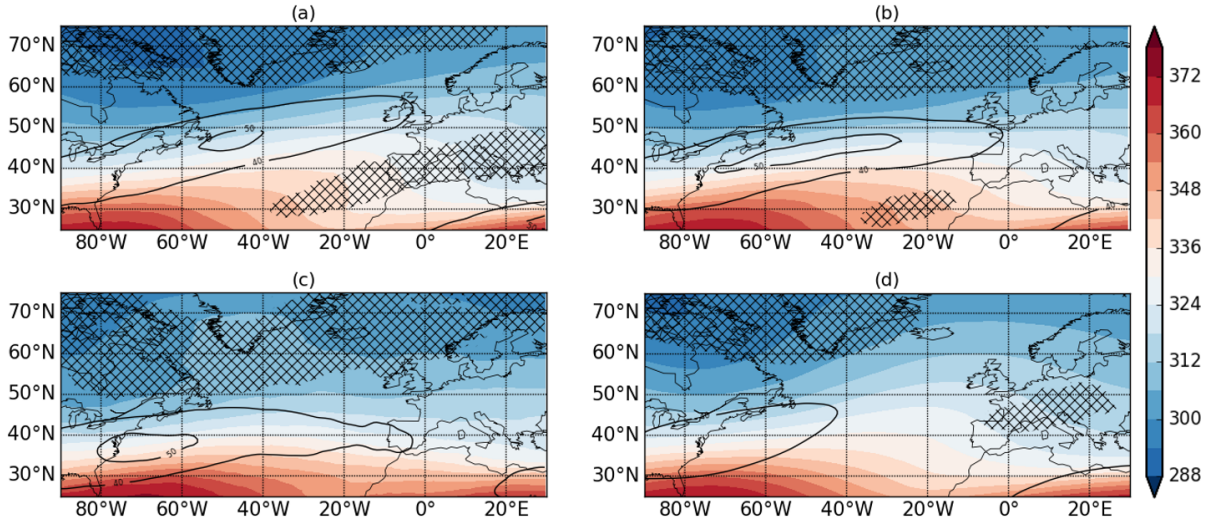

Figure 6.3: *Composites of clustered days from ERA-Interim at (a) 65°N, (b) 55°N, (c) 45°N and (d) Climatology. Contours and hatchings are the same as figure 6.2.*

slightly positive. This systematic difference suggests there may be differences in the boundary layer scheme of HiGEM compared to ERA-Interim as this bias is not present for wind speed at 850 hPa or higher (not shown). Similar differences have also been found in the biases of 10-metre and 925 hPa wind speeds in four reanalysis datasets (Hodges et al., 2011).

To address the lower European wind speeds, a simple bias correction is applied to the 10-metre wind speeds in HiGEM. This is done by correcting the 10-metre wind speeds by the spatially averaged offset in the $V_{i,j}^{98}$ field between ERA-Interim ($\overline{V_{i,j}^{98\,ERA-I}}$) and HiGEM ($\overline{V_{i,j}^{98\,HiGEM}}$) for all land grid points within our area of interest (black box in Figure 6.5b). As a result all HiGEM wind speeds are uniformly increased by 18.75% over land. The resulting bias-corrected HiGEM 10-metre wind speeds will be called HiGEM_bc herein and its formulation is shown in equation 6.3. The corrected $V_{i,j}^{98}$ wind field (difference relative to ERA-Interim) is shown in Figure 6.4d and shows much reduced differences across our core European region. In some regions (northern Germany, Benelux, northern and northwestern France) the differences have changed sign and are now positive, there are also some regions that still have negative anomalies, resulting in an overall neutral anomaly compared to ERA-Interim.

$$HiGEM\_bc = HiGEM * \frac{\overline{V_{i,j}^{98\,ERA-I}}}{\overline{V_{i,j}^{98\,HiGEM}}} \tag{6.3}$$

Spatial maps of the DJF average SSI are shown in Figure 6.5 and are consistent between ERA-Interim and HiGEM across large parts of northern and northwestern Europe. Both datasets show a peak in SSI across northwestern Europe from London across to northern and northwestern Germany, as would be expected

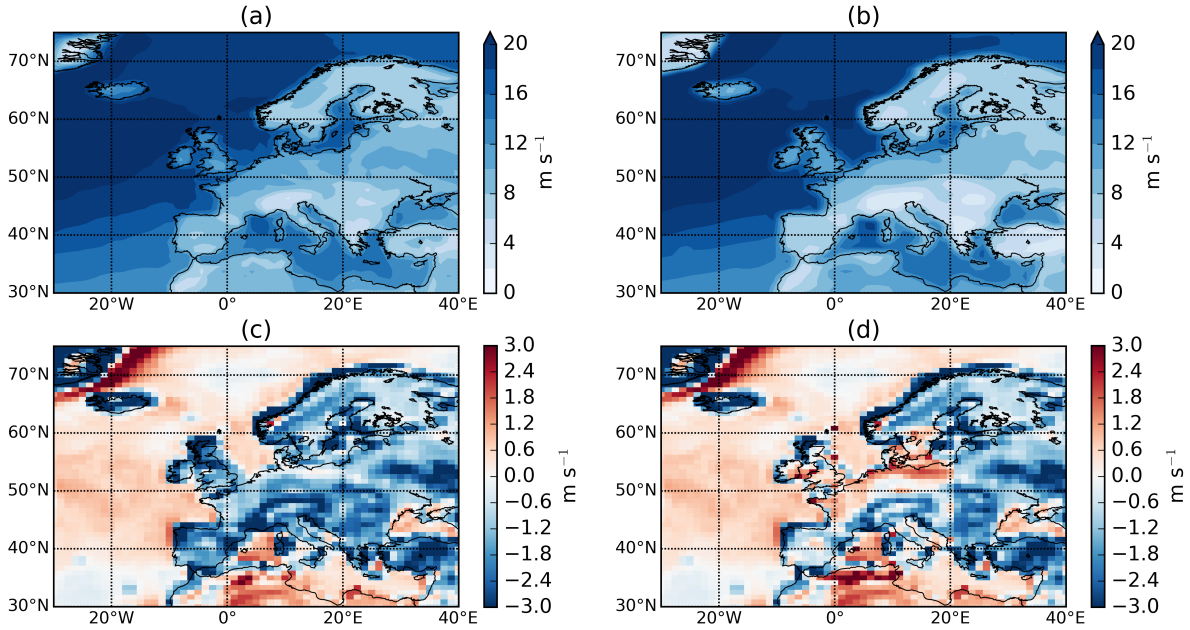

Figure 6.4: *98th percentile of 10-metre wind speed (m s^{-1}) for the DJF climatology of ERA-Interim (a) and HiGEM (b). (c) is HiGEM-ERA-Interim using the raw HiGEM wind speeds. (d) is HiGEM-ERA-Interim using the HiGEM winds that have been scaled by 18.75%.*

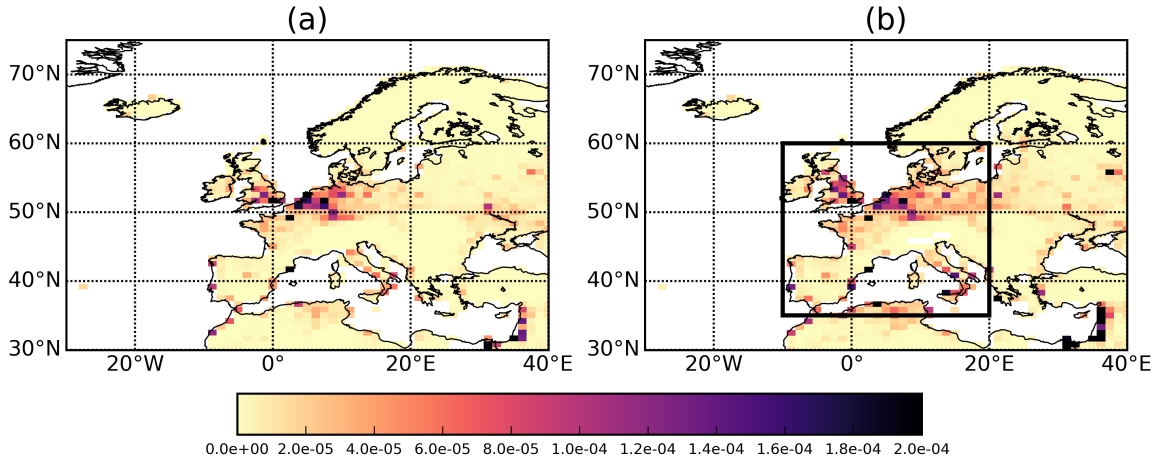

Figure 6.5: *DJF average of 6-hourly SSI for ERA-Interim (a) and HiGEM (b). The black box region in (b) is our SSI calculation region.*

from the population weighting. Other densely populated regions are also identifiable. There are further regions of noticeable SSI across Germany and extending east toward Russia. There are also peaks in SSI across the Iberian peninsula and Italy.

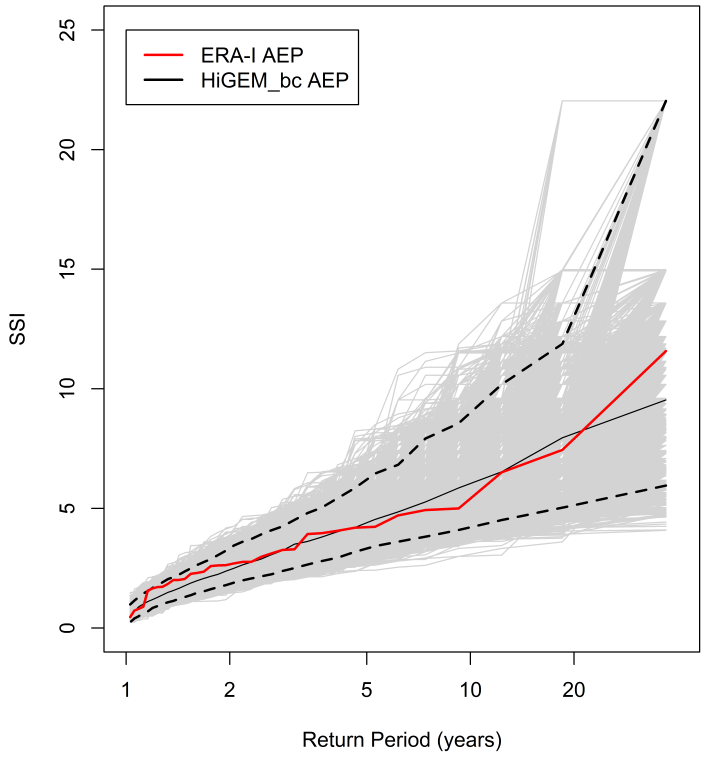

Figure 6.6: *Return periods of AEP for ERA-Interim (red line). The light grey lines are the 10,000 bootstrap samples of the HiGEM_bc AEP. The black dashed lines are the associated 95% confidence intervals of the HiGEM_bc AEP and the black solid line is the median.*

Figure 6.6 shows the AEP from ERA-Interim and HiGEM as a function of return period, up to a maximum return period of 36 years. Also shown in Figure 6.6 are 10,000 bootstrap samples of the 918 years of HiGEM_bc AEP data in 36 year samples, and the associated 95% confidence intervals. The AEP from ERA-Interim is within the confidence intervals of the HiGEM_bc samples at all return periods, with ERA-Interim being at the upper-end of the spread at the lowest return periods of 1-2 years, and in the middle of the spread for the remaining return periods. Figure 6.6 suggests that HiGEM_bc can capture the variation of AEP as a function of return period that is found in ERA-Interim.

In Figure 6.7 we have ordered the AEP and OEP independently by return period in order to assess how the SSI from ERA-Interim and HiGEM directly compare in magnitude at varying return periods. Also shown in Figure 6.7 are the GPD fits of the ERA-Interim AEP and OEP, and associated confidence intervals (non-filled). The GPD provides a good estimation of the data above a 5 year return period, however due to the small amount of data used to fit the distribution, uncertainties start to become very large above a return period of 20 years. By a return period of 50 years they have diverged greatly.

Also shown in Figure 6.7 are the 95% confidence intervals for the GPD fits (shaded regions) of the

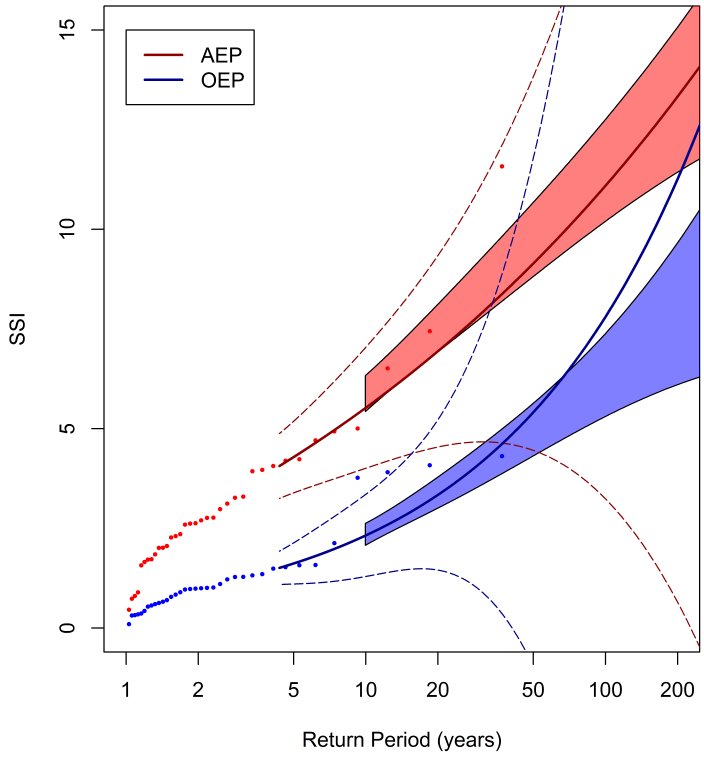

Figure 6.7: *Return periods of the AEP (red points) and OEP (blue points) of ERA-Interim. The solid red and blue lines are GPD fits applied to the AEP and OEP using an 70th percentile threshold. The dashed red and blue regions are the associated 95% confidence intervals. The shaded red and blue regions are the 95% confidence intervals of the HiGEM_bc AEP and OEP GPD fits. The OEP and AEP are sorted independently for both ERA-Interim and HiGEM. The GPD fits and confidence intervals are only plotted only above the GPD threshold of the 90th percentile.*

HiGEM_bc AEP and OEP (ordered independently). These are shown above a return period of 10 years. The confidence intervals for HiGEM_bc are much narrower than ERA-Interim, which is to be expected as there is considerably more data being used in the GPD fit (consistent with Karremann et al. (2014b)). For return periods for which both datasets have data ($<$ 36 years) the GPD fit of the HiGEM_bc AEP and OEP are within the confidence intervals of the ERA-Interim AEP and OEP. This is also the case for return periods greater than 36 years for the AEP and the OEP, although the confidence intervals for the GPD fit for ERA-Interim become extremely large for return periods greater than 50 years. HiGEM_bc is therefore consistent with the accumulated seasonal losses and the individual events found in ERA-Interim. This suggests HiGEM is a useful climate model for investigating AEP and OEP for large return periods.

6.4.3 Large Return Period Losses in HiGEM_bc

Figure 6.8 shows the AEP and OEP for HiGEM_bc. Both the AEP and OEP curves of HiGEM_bc extend beyond the respective maxima from ERA-Interim, suggesting that more severe windstorm seasons and also

single cyclone events may be possible than those seen in the ERA-Interim period. For example, the 918 year return period season in HiGEM is approximately twice the magnitude of the 1 in 36 year season in ERA-Interim. There is more noise in the ERA-Interim curves compared to their HiGEM_bc counterparts due to the smaller number of years. The OEP and AEP of HiGEM_bc are sorted by AEP magnitude in Figure 6.8. Consequently, there is substantially more spread in the OEP values than seen in Figure 6.7. However, a general increase in OEP with return period is still found, with low AEP years generally having a lower OEP and high AEP years having a higher OEP, but there are some specific deviations from this (for example, note the four very high OEP years between return periods 40 and 100).

To test the sensitivity of Figure 6.7 and Figure 6.8 to the default definition of AEP as the sum of all events, we repeated the analysis, but only retaining on average the top 3 events of each year. This equates to an order of magnitude reduction in the number of events (see Figure 6.9). The magnitudes of the reduced event AEPs are marginally lower than the original AEPs, as would be expected with the filtering of events, but the main features of the curves in Figure 6.9 are very similar.

(Hunter et al., 2016) previously showed how the number of cyclones within a winter is strongly related to their intensities. Similarly, earlier results (Fig. 6.1e) showed that cyclones in HiGEM tend to occur in groups. To quantify the contribution of windstorm clustering to the large AEP values we compare the HiGEM AEPs to randomised series of loss events. The ratio between the AEP and the AEP_random may be particularly important for the insurance industry as it characterises the importance of the clustering of cyclones in seasonal losses.

We have performed a non-replacement randomisation of the 72-hour periods that make up the HiGEM_bc AEP with 10,000 samples and this randomisation ensures that each random sample contains the exact same data as the original 918 years. This randomisation allows us to assess how the intensity of losses and the associated number of cyclones acts to influence the AEP in HiGEM_bc, compared to a timeseries where windstorms are occurring randomly. The mean of these random samples is shown by the black line in Figure 6.8, with the grey shading indicating the 95% confidence interval of these samples. Below a return period of $\sim$3 years the AEP_random is greater than that from the HiGEM_bc AEP and above the 3 year return period the AEP_random is consistently less than the AEP. Therefore, low (high) return period loss years tend to have a lower (higher) AEP than random.

The ratio of AEP to AEP_random is shown in Figure 6.10. Values >1 (<1) indicate a higher (lower) AEP in the actual HiGEM_bc years compared to the AEP_random years. Above a return period of 3 years the realistic, dynamically consistent, representation of the grouping of events in HiGEM_bc tends to generate

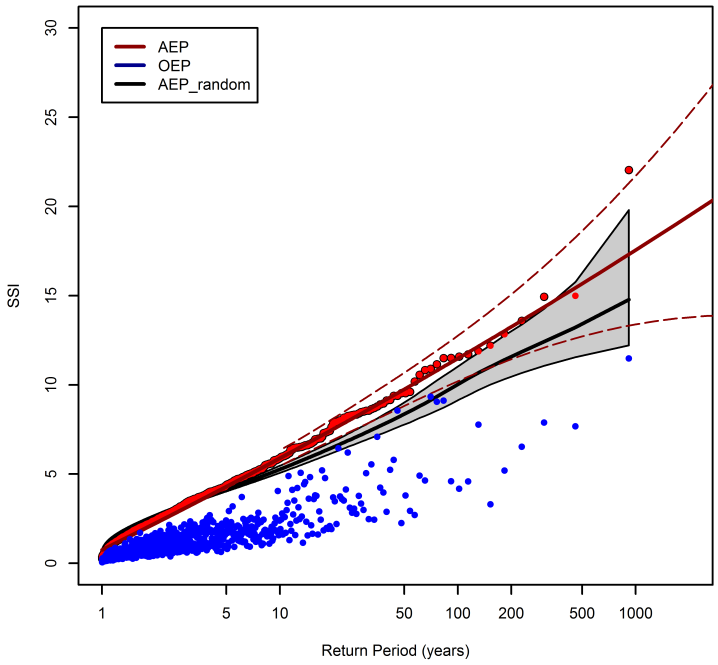

Figure 6.8: *Return periods of the AEP (red points) and OEP (blue points) for HiGEM_bc. The OEP and AEP are sorted according to AEP magnitude. The solid red line is the GPD fit applied to the AEP using a 90th percentile threshold. The dashed red lines are the associated 95% confidence intervals. The black line represents the mean of 10,000 non-replacement random samples of the HiGEM_bc AEP data. The surrounding shaded grey region represents the 95% confidence interval of these 10,000 samples. The GPD fit and confidence intervals are only plotted above the GPD threshold.*

more losses and a greater AEP than the random grouping of events. The median contribution above the 3 year return period is generally in the range of 1.1 to 1.2 times the random AEP. At a return period of 200 years the 95% confidence intervals range from 1 to 1.3. For low return periods ($<$ 3 years) the occurrence of events in HiGEM_bc leads to a lower AEP than in the random realisations, with HiGEM_bc AEP values in the range of 0.6 to 1. This suggests that during low loss winters, there are a smaller number of windstorms and weather loss events occurring in HiGEM_bc than would be expected from considering a randomised series of events.

The difference can be interpreted physically by considering two recent DJF periods in the UK. Firstly, the winter of 2009/2010 was characterized by a strongly negative NAO and an absence of extratropical cyclones influencing the UK for this period (Osborn, 2011). Secondly, the winter of 2013/2014 was almost the complete opposite and was associated with the continuous presence of deep cyclones, occurring in groups, for almost the entire DJF period (Matthews et al., 2014; Priestley et al., 2017b). The nature of these two seasons would result in 2009/2010 having a very low AEP, and 2013/2014 having a very high AEP. Randomising these two seasons the result would be two synthetic seasons with AEP values between these two extremes. Hence the clustering of cyclones in 2013/2014 results in a higher AEP than expected from random and 2009/2010 having a lower AEP than expected.

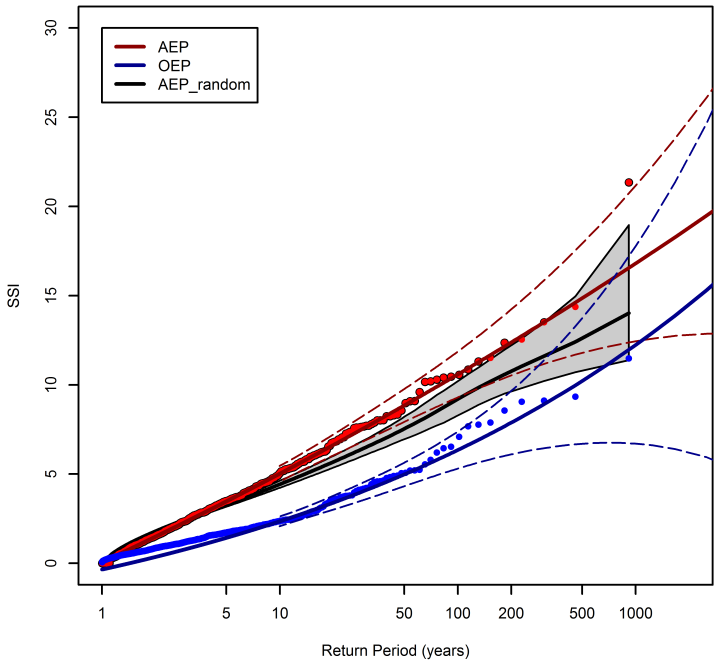

Figure 6.9: *As figure 6.5, but only retaining the top three events of every year.*

In Figure 6.10 it appears that the realistic, dynamically consistent, representation of clustering in HiGEM_bc causes higher losses above a 3 year return period with losses being 10-20% higher than random at all return periods. Despite the nearly constant value of AEP/AEP_random above a return period of 3 years, the absolute difference between the two values is increasing with return period (the AEP is more than 4 times larger at 918 year return period compared to a 3 year return period). Hence the physically consistent representation of clustering in HiGEM_bc is causing larger increases to the AEP with increasing return period.

A different view of clustering can be gained by examining how a single event can affect the accumulated seasonal losses through the ratio of the OEP to AEP. A high value implies that the single largest event is causing most of the losses in a season, and a lower value implies a contribution to the overall seasonal losses from many cyclones in that particular season. The results from ERA-Interim and HiGEM are compared in Figure 6.11a. This shows 10,000 random samples of 36 years of the HiGEM_bc OEP/AEP with associated confidence intervals as well as the ERA-Interim OEP/AEP. The values are sorted into return periods by order of descending AEP. There is considerable spread in the ERA-Interim OEP/AEP values, with minima of $\sim$ 0.2 at a return period of 1-2 years, and a maxima of $\sim$0.8 at a return period of 10 years. There is no clear systematic increase or decrease in the value of OEP/AEP in the ERA-Interim data, which is consistent with the median values and confidence intervals from the HiGEM_bc samples. The 95%

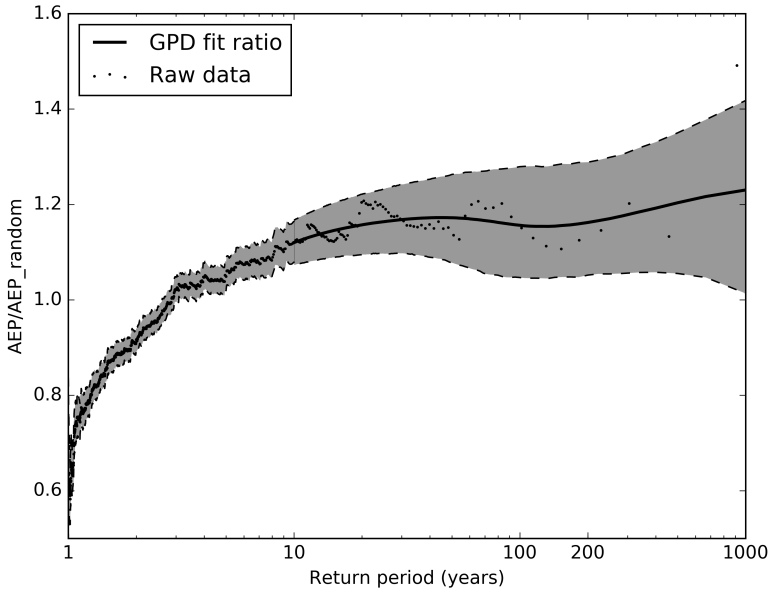

Figure 6.10: *The ratio of the model AEP to the 10,000 random samples of the AEP for increasing return period. Black dots are the raw data points. The dark grey region below 10 year return period indicates the 95% confidence interval of the raw AEP/AEP_random. Above 10 year return period the dark grey shaded region bounded by the black dashed lines is the 95% confidence interval using the fitted AEP (red line in figure 6) in the calculation and the black solid line is the median of the spread. Confidence intervals from the GPD fits are only shown above the GPD threshold.*

confidence intervals range from 0.15-0.65 at a return period of 1 year, and from 0.2-0.8 at a return period of 36 years. This suggests that there is a wide range of OEP/AEP values that may characterise a high or a low AEP season.

Figure 6.11b shows the OEP/AEP values for HiGEM_bc. As in Figure 6.11a there is considerable spread variation in the value of OEP/AEP at all return periods, with no clear systematic increase or decrease with return period. All return periods have a majority of the data with values of ∼0.25-0.5, with the extremes ranging from 0.15 to 0.9. This indicates that in terms of the contribution of a single event to the overall seasonal loss, there is no direct relationship with return period. At any return period it appears that 25-50% of losses will come from the largest event.

As with the ratio of AEP/AEP_random in Figure 6.10, the ratio of OEP/AEP in Figure 6.11b has a relatively constant value at all return periods and this suggests a constant relationship between the OEP and AEP. However, as the return period is increasing the OEP and AEP are also increasing, so despite the AEP/AEP_random ratio being constant at a return period of 5 years and 200 years, the absolute difference between OEP and AEP at the two return periods would be very different. The higher return periods have a higher absolute difference between the AEP and OEP, hence the additional losses that are not the OEP are increasing with return period. Hence the relative difference between the OEP and AEP is consistent with return period, but the absolute difference is continuing to increase with return period. This absolute increase

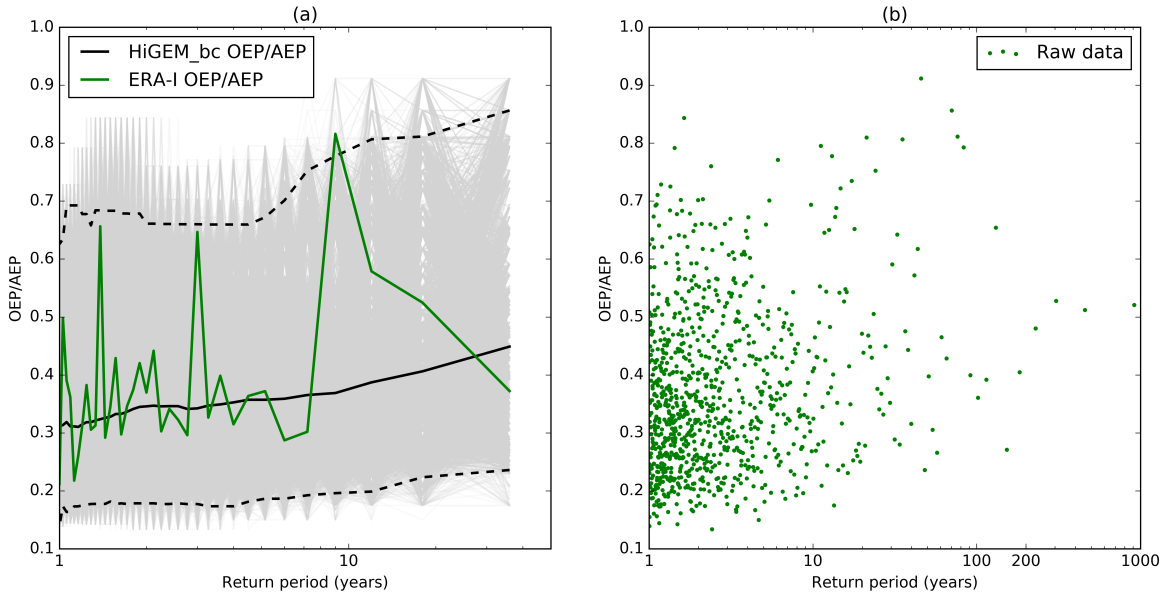

Figure 6.11: *(a) Return periods of OEP/AEP for ERA-Interim (green line). The light grey lines are the 10,000 bootstrap samples of the HiGEM_bc OEP/AEP. The black dashed lines are the associated 95% confidence intervals of the HiGEM AEP and the black solid line is the median. (b) Return periods of the OEP/AEP ratio for HiGEM_bc (green points).*

is likely a result of more severe events in the high return period AEP years.

6.5 Discussion & Conclusions

The aim of this study is to investigate the importance of serial clustering on seasonal timescales for high return period loss events caused by European windstorms. This is achieved using a GCM that is able to adequately capture the large-scale dynamics controlling cyclone clustering. This work has been performed using HiGEM, a high resolution fully coupled climate model. The performance of HiGEM has been evaluated using the ERA-Interim reanalysis. Losses from European windstorms have been estimated using a version of the SSI (Storm Severity Index) applied to European land grid points. The main conclusions of this work are as follows:

- HiGEM can successfully reproduce the large-scale dynamics associated with clustering of European cyclones that are seen in ERA-Interim. The biases in DJF storm track activity in HiGEM are small, with the tilt and intensity of the North Atlantic storm track being well represented. The pattern of dispersion in the North Atlantic is also consistent with ERA-Interim, with cyclones clustering more near the exit of the storm track, and an underdispersive and regular nature in the entrance region. The large scale circulation associated with clustering is also similar in HiGEM and ERA-Interim. Both show how clustering in different locations of western Europe is associated with a strong and extended upper-level jet that is flanked on one or both sides by anomalous RWB. Hence, extratropical cyclone clustering in HiGEM is occurring for the right dynamical reasons.

- SSI is used as a proxy to assess losses occurring from intense European windstorms. The SSI is applied to land points only and for an area than encompasses all of western and most of central Europe. It is found that HiGEM systematically underestimates 10-metre wind speed over European land regions. A simple bias correction (uniform increase by 18.75%) leads to a structure of the DJF SSI average that is consistent between the bias corrected HiGEM (HiGEM_bc) and ERA-Interim. The return periods of AEP and OEP are found to be consistent between HiGEM_bc and ERA-Interim for return periods less that 36 years. Therefore, HiGEM_bc appears to be a suitable model for assessing long return period losses from European windstorms.
- Compared to a random season of cyclones, the AEP from HiGEM_bc is larger at return periods greater than 3 years. The dynamically consistent representation of cyclone severity and clustering in HiGEM_bc results in values of AEP that are approximately 10-20% larger than AEP_random at a return period of 200 years. Therefore, not having a dynamically consistent representation of cyclone clustering appears to result in an underestimation of losses above a 3 year return period.
- The relative portion of the AEP that comes from the OEP is very variable across all return periods and there is no strong relationship between the two values. The contribution of the OEP to the AEP is found to be approximately 25-50% in HiGEM_bc. Therefore, the relative influence of the largest loss event in a season does not change with return period.

In this study we have shown that having a dynamically consistent representation of cyclone clustering and storm intensity causes the AEP to be approximately 10-20% higher (for return periods greater than three years) than that expected from a random selection of cyclones. Despite the near constant values of AEP/AEP_random above a 3 year return period, the absolute magnitude of the AEP relative to AEP_random is increasing with return period. This absolute increase suggests an increase in cyclone severity for higher return period loss seasons for cyclones of all magnitudes. This result has implications for loss modelling in the insurance industry and demonstrates that if a model does not adequately represent the clustering behaviour of cyclones then losses will be underestimated for larger return periods. Furthermore, as the wintertime average loss from windstorms in Europe is over $2 billion (Schwierz et al., 2010), this could result in an underestimation of losses by $200-400 million. In addition we have shown how the relative contribution of the largest event in contributing to the AEP does not change with return period and that the measure of OEP/AEP can be very variable from year to year. The measure of OEP/AEP is not a good measure for assessing any potential changes in the relative importance of a single storm, and hence any changes in clustering, with an increasing return period of a seasons AEP. It should also be noted that as these results come from just one single climate model more robust conclusions could be made from applying our methods to a greater number of climate models.

It has been shown in several studies (Leckebusch et al., 2007; Pinto et al., 2012) that loss potentials

associated with European windstorms would increase under future climate conditions. Based on low resolution ECHAM5 simulations, Karremann et al. (2014a) provided evidence that the combination of higher single losses and clustering in a warmer climate would lead to significantly shorter return periods for storm series affecting Europe. As in the present study we only focussed on windstorms under current climate conditions, it would be pertinent as a next step to evaluate if the tendency towards an increase in clustering holds true for the new high resolution CMIP6 climate projections.

Chapter 7:

DISCUSSION AND CONCLUSIONS

7.1 Overview of the Thesis

Extratropical cyclones pose a significant risk socio-economically to the European continent. They are the most damaging natural hazard for this part of the world (Della-Marta et al., 2010) and individual events can cause over $10 billion in economic losses (e.g. $11.5 billion from storm Lothar on 26/12/1999; Munich Re, 2016). Occasionally, intense cyclones occur in groups. This is known as clustering and losses can be even more severe due to the short period of time between damaging events (e.g. $18.7 billion in losses during December 1999; Munich Re, 2016).

Pinto et al. (2014) identified several episodes of clustering in recent years and associated a specific set of dynamical features with these periods of clustering. These features were also coupled with the common occurrence of cyclone families, with secondary cyclones forming on the trailing fronts of pre-existing cyclones. It was discussed in chapter 1, and by Economou et al. (2015), that there are three reasons why cyclones may cluster. The two dynamical reasons for this were either a modulation by the large scale flow (i.e. the North Atlantic Oscillation, NAO), or a dependence between successive storms (i.e. cyclone families and secondary cyclogenesis), with the third reason being that this may occur purely by chance. One aim of this thesis was to address the role of each of these two mechanisms through understanding how the large scale flow affects clustering and also the importance of cyclone families and secondary cyclogenesis during periods of clustering.

Intense cyclones have been shown to more likely occur in clusters than weaker cyclones (Mailier et al., 2006; Vitolo et al., 2009; Pinto et al., 2013), with the same being true for stormier seasons (Cusack, 2016). Hunter et al. (2016) also found that seasons with more cyclones tended to feature cyclones of a greater intensity. However, these studies have commonly been subject to significant uncertainty due to limitations with the size of the sample of data. One further aim of the work in this thesis was to understand

the role of clustering for winter seasons with high losses from wind damage (i.e. 1 in 200 year return period season).

These aims were summarised by 5 research questions presented in chapter 1. These questions are:

Q1. Are clustering events in different locations across western Europe associated with similar large-scale dynamical features?
Q2. What were the dynamical features that were associated with the clustered winter season of 2013/2014 across the UK?
Q3. To what extent do secondary cyclones contribute to periods of clustering that affect western Europe?
Q4. Can windstorm losses associated with extratropical cyclones be represented in climate models for seasonal losses with a return period of 200 years?
Q5. How important is clustering for the most severe seasons in terms of overall losses?

Section 7.2 is dedicated to addressing these questions based on the results presented in chapters 3 through 6. In section 7.3 the implications of the results in this thesis are discussed, with future avenues for work addressed in section 7.4. The concluding remarks of this thesis are in section 7.5

7.2 Key Findings

In this section the main findings of this thesis from chapters 3 to 6 are discussed. Each of the 5 research questions posed in chapter 1 are addressed individually.

7.2.1 Q1. Are clustering events in different locations across western Europe associated with similar large-scale dynamical features?

Key Result: Periods of clustering for different latitudes of western Europe are all associated with a zonally extended and strong jet that is flanked on one or both sides by Rossby wave breaking. For clustering at 55°N there is RWB on both sides of the jet, fixing the jet in this central latitude. For clustering occurring at 45°N and 65°N there is anomalous RWB on the northern and southern flanks of the jet respectively. The presence of the RWB on either flank acts to shift the jet further north or south through eddy momentum fluxes and results in cyclones tracking further to the north or south.

The results in chapter 3 (Priestley et al., 2017a) presented a dynamical characterisation of extratropical cyclone clustering for several regions of western Europe using objectively identified periods of clustering in the ERA-Interim re-analysis for the winters of 1979/1980 - 2014/2015. The study of Pinto et al. (2014) demonstrated how several select cases of clustering at 55°N were associated with RWB that flanked an

extended and strong jet stream. Periods of clustering identified in chapter 3 were identified in several locations, not just the 55°N region that was previously studied (Pinto et al., 2014; Priestley et al., 2017b). Clustering was identified for regions of the same size as previous, but located 10° to the north and south of the previously used region and centred at 45°N, 5°W and 65°N, 5°W.

It was found that for clustering of intense cyclones at 55°N a consistent picture with the previous case studies is found, with anomalous RWB on the northern and southern flanks of a zonally extended and strong jet at 250 hPa. This pattern is also consistent with case studies of severe individual cyclones toward Europe (Gómara et al., 2014a; Messori and Caballero, 2015), with the persistence in these features appearing crucial for the recurrent influence of multiple, intense cyclones during clustering events. Differences emerge when looking at clustering for the 45°N and 65°N regions, with the more southerly region having large RWB anomalies to the north of the jet, and the more northerly region having large RWB anomalies to the south of the jet. These opposing locations of RWB act to alter that angle of the jet at 250 hPa, with a more tilted jet for clustering at 65°N, and a more zonal jet for clustering at 45°N. RWB therefore appears to play a vital role in controlling the angle of the jet and hence the subsequent impact location of the cyclones. These results are consistent with previous studies that looked at the influence of RWB on jet latitude (Woollings et al., 2010a; Franzke et al., 2011).

For the three regions of clustering, the area the cyclones must pass through to be clustered is closely located to the left exit of the jet streak. The left exit is a vital region for the intensification of cyclones via the divergence that it provides (Rivière and Joly, 2006a,b) and it is very likely that this plays a role in the intensification of the cyclones that are identified in these episodes of clustering. This setup has been shown to project strongly onto the pattern of the North Atlantic Oscillation (NAO; Messori and Caballero, 2015), with the NAO also being linked to the occurrence of severe cyclones in Europe (Pinto et al., 2009; Donat et al., 2010). Furthermore, Mailier et al. (2006) and Walz et al. (2018) linked numerous large scale patterns such as the NAO, East Atlantic (EA) pattern, and Scandinavian (SCA) pattern to the inter-annual variability of cyclone numbers, and their observed overdispersion. Complimentary to this, the pattern of RWB for clustering at 55°N has been shown to project strongly to the pattern of the NAO (Messori and Caballero, 2015), it is therefore highly likely that the phase of the NAO is a key driver in the variability of the number of cyclones impacting Europe, and the intensity of clustering across the continent.

Further results show how anomalies in the jet and RWB develop relative to the time of clustering. RWB anomalies peak around 2 days prior to peak in the jet anomalies, which is consistent with the flux of momentum by the RWB in driving the acceleration of the jet (Barnes and Hartmann, 2012). Furthermore, the intensity of clustering (the total number of cyclones in a 7 day period) is positively correlated with the

amount of RWB on one or both flanks of the jet, and is also positively correlated with the strength of the jet, for clustering occurring at all latitudes. These relationships are associated with a large amount of spread and variability, indicating that the presence of RWB and an enhanced jet is very associated with periods of clustering, but that there may also be occasions when these features are present and clustering is not occurring, and vice versa. Therefore the presence of the extended jet and anomalous RWB is a necessary but not sufficient criteria for clustering over western Europe. Reasons for the spread in these relationships could be because there are processes that are important for clustering that were not considered in this study. For example, secondary cyclogenesis has been shown to be important for clustering (Pinto et al., 2014; Priestley et al., 2017b), and frontal waves commonly do not develop into secondary cyclones (Parker, 1998). This means that if secondary cyclogenesis is an important factor for contributing to clustering, there may be occasions when the large scale set up is favourable, but processes on the cyclone scale, or on the mesoscale could be inhibiting cyclogenesis (e.g. excessive frontal strain; Renfrew et al., 1997; Dacre and Gray, 2006). Furthermore, studies such as Gómara et al. (2014b) and Messori and Caballero (2015) have found a strong link between double-sided RWB and an extended jet for individual destructive windstorms, and not a series/cluster of cyclones. Therefore there may be several occasions that there are the necessary conditions observed for clustering but with only a singular cyclone occurrence, or with cyclones that are not deep enough to satisfy the intensity criteria. Finally, as periods of clustering require at least 4 intense cyclones in a 7-day period there may often be occasions when a clustered day is not associated with a presence of a cyclone (as the 4 cyclones occur on other dates in the surrounding 7 days) or the associated dynamics, hence providing further variability in these relationships.

7.2.2 Q2. What were the dynamical features that were associated with the clustered winter season of 2013/2014 across the UK?

Key Result: The winter season of 2013/2014 was found to have numerous periods of clustering across the UK, with nearly 3 times as many clustered days as the seasonal average. One particular period from 6-14 February 2014 featured numerous cyclones all connected as a cyclone family. The dynamical set up during this period was very consistent with the findings from chapter 3 and featured a zonally extended and strong jet with large areas of RWB on both the northern and southern flanks, maintaining its zonal state and tilt.

In chapter 4, the season of 2013/2014 was assessed from a clustering perspective (Priestley et al., 2017b). The results of chapter 3 and the previous studies of Pinto et al. (2014); Priestley et al. (2017a) highlighted a specific set of dynamical conditions associated with episodes of clustering for western Europe. It was hypothesised in their study that these periods of high clustering were associated with Rossby wave breaking (RWB) on both sides of an anomalously strong and zonally extended jet stream. The presence and persistence of these features would then allow for multiple cyclones to form and track along the same path,

between the two regions of RWB. These cyclones were often found to be part of a cyclone family, with each subsequent cyclone forming on the trailing front of the one preceding it. Analysis showed how the season of 2013/2014 was associated with 57 intense cyclones that passed over the UK in a 90 day period, with 37 of these exceeding the intensity threshold of the local 95th percentile of mean sea level pressure (MSLP). 32 clustered days were identified in this season using the metric for identifying clustering by Pinto et al. (2014), which is considerably higher than the climatological average of 11 days per season. One highlighted period of this season, from 6-14 February 2014, was associated with one large cyclone family of 9 cyclones.

Throughout this period of clustering, the upper troposphere of the North Atlantic was characterised by a very strong 250 hPa jet stream with maximum wind speeds of over 70 ms^{-1}, that was flanked by the occurrence of RWB on both the northern and southern edges of the jet. These large-scale conditions are consistent with the hypothesis introduced by Pinto et al. (2014). The zonal extension of the jet toward western Europe is likely driven by the presence of the RWB, which converges momentum into the core of the jet (Barnes and Hartmann, 2012). The location of the cyclones in this clustered period relative to that of the jet and RWB is of interest as most appear to cross the jet axis during their lifetime and are associated with the left exit region of the jet just before they reach the UK. This region is a common area for the intensification of cyclones (Rivière and Joly, 2006a,b) and likely played a role in there being so many intense cyclones passing over the UK during this season.

This analysis of the 2013/2014 season further confirms the the findings from chapter 3 and the hypothesis of Pinto et al. (2014) that periods of clustered over western Europe are associated with a specific set of dynamical conditions in the North Atlantic, which act to increase the number of cyclones that are tracking over the same location. Furthermore, it was demonstrated that cyclone families and secondary cyclogenesis appear to play an important role in these clustering periods, with 9 cyclones in 8 days all being connected as one cyclone family.

7.2.3 Q3. To what extent do secondary cyclones contribute to periods of clustering that affect western Europe?

Key Result: Secondary+ cyclones make up approximately 50% of all cyclones during severely clustered periods. The increase in Secondary+ cyclones during these periods of clustering is shown to be a result of enhanced steering by the large-scale flow, causing all cyclones to follow a more similar, zonal track across western Europe. Secondary+ cyclones and Primary cyclones have different preferential geographical locations in the North Atlantic. Primary cyclones are more common over the western North Atlantic, with Secondary+ cyclones more common over the central and eastern North Atlantic.

In chapter 5, an objective identification of secondary cyclones and cyclone families was presented with further analysis on the structure of the environment surrounding different classes of cyclone at their time of genesis, and also the role Secondary+ cyclones play in periods of clustering (Priestley et al., 2019). Secondary cyclones were highlighted as an important factor in periods of clustering by Pinto et al. (2014), and also in chapter 3 (Priestley et al., 2017b), however their role and contribution to periods of clustering had not been quantified.

The climatological frequency of Primary, Secondary+, and Solo cyclones in 36 winter seasons in ERA-Interim was presented. Primary cyclones are those at the start of a cyclone family, Secondary+ cyclones are any that follow a Primary in a family, and Solo cyclones are those that are not part of cyclone families at all. Primary cyclones are most frequently found in the western North Atlantic. Secondary+ cyclones are most commonly found in the central and eastern North Atlantic, contributing up to 40% of the total cyclone numbers in these regions. Solo cyclones are commonly found across continental regions, the Mediterranean, and the high latitude North Atlantic. Previously, Schemm and Sprenger (2015) and Schemm et al. (2015) identified secondary cyclones across the North Atlantic and found lower relative numbers (peak 20-30%) compared to the results presented in chapter 5. This is likely a result of different cyclone identification methods, with the method of Murray and Simmonds (1991b) being applied in this study, which has shown increases in cyclone numbers compared to the scheme of Wernli and Schwierz (2006) that were used in the aforementioned studies. Primary and Secondary+ cyclones have their genesis in similar regions to that of Type B and Type C cyclones respectively (as defined by Petterssen and Smebye, 1971; Deveson et al., 2002; Gray and Dacre, 2006), and therefore are likely to be of these classes. It was also shown that Secondary+ cyclones that impact western Europe commonly form very close to the European continent in the eastern North Atlantic, with their associated Primary cyclone forming over the Gulf stream and tracking toward the high latitudes of the North Atlantic. Dependent on the tilt of the track density of the Primary cyclones, the latitude at which subsequent the Secondary+ cyclones impacts Europe is affected. If the associated track of the Primary cyclone is steeper (shallower), the latitude of the Secondary+ cyclone impacting Europe is more northward (southward).

Primary cyclones appear to be crucial in setting up and environment favourable for the development of Secondary+ cyclones. As the Primary cyclone propagates downstream, it is associated with an increase in RWB and an acceleration of the jet (as in chapter 4, Priestley et al., 2017a). This acceleration of the jet is associated with a reduction in static stability at low levels, which could aid the development and intensification of the Secondary+ cyclones. Secondary+ cyclones, and specifically those forming in the eastern North Atlantic have been shown to be associated with a reduced stability atmosphere (Wang and

Rogers, 2001; Gray and Dacre, 2006; Schemm and Sprenger, 2015), and these results indicate this may be due to the presence of the associated Primary cyclone. The formation the Primary cyclone is shown to be insensitive to changes in the low-level static stability as Primary cyclones mainly form over the Gulf stream where baroclinic instability dominates the genesis process and is a persistent feature.

Secondary+ cyclones contribute approximately 50% of cyclones during clustered periods. The number of Secondary+ cyclones is shown to increase during periods of clustering, with the number of Solo cyclones increasing at a similar rate. The number of Primary cyclones does not increase as fast, as it was shown how this class of cyclone rarely propagate as far as the European continent. The increase in Secondary+ cyclones is shown to mainly be a result of increased steering from the large-scale flow in the North Atlantic, and not through an increased rate of cyclogenesis. The presence of large-scale RWB acts to concentrate the region of cyclogenesis near to western Europe, but the main reason for the increase in the number of Secondary+ cyclones through the 55°N region is due to the tracks of the cyclones being steered along a similar track by the presence of the anomalous RWB. As the pattern of RWB for clustering at 55°N has been shown to project strongly to the pattern of the NAO (Messori and Caballero, 2015), it is likely that the phase of the NAO is a key driver in the variability of the number of Secondary+ cyclones impacting Europe.

7.2.4 Q4. Can windstorm losses associated with extratropical cyclones be represented in climate models for seasonal losses with a return period of 200 years?

Key Result: 918 years of HiGEM coupled climate model data are shown to represent the winter North Atlantic storm track well, particularly the pattern of over/underdispersion and also the dynamics associated with periods of clustering. A version of the storm severity index is used as a proxy for windstorm losses that uses the 10 metre wind speed from HiGEM. The spatial pattern of losses from HiGEM agrees well with those from ERA-Interim. The event and season loss magnitudes for all of Europe from HiGEM are comparable to ERA-Interim out to a 36 year return period.

In chapter 6 the contribution of clustering to seasonal losses was explored (Priestley et al., 2018). A large quantity of climate model data is used (918 years from HiGEM; Shaffrey et al., 2009, 2017). Using such a large amount of data from a climate model is useful for estimating extreme events in the tail of the distribution as they are represented physically by the model. However, there are still associated uncertainties as these are simulated events and there are only limited estimations of severe windstorms for validation due to the relatively short observational record. Using over 900 years of model data allows for estimations of events at a return period of over 100 years and a reduction in sampling variability, which was a problem highlighted by Cusack (2016) in their estimations of extreme seasons. Despite this reduction in sampling uncertainty, there is of course still model uncertainty as the estimations made were only using one model.

HiGEM was shown to have a good representation of the North Atlantic storm track for the 918 years of study, with previous work also finding the model to have a good representation of the northern hemisphere circulation and structure of extratropical cyclones (Shaffrey et al., 2009; Catto et al., 2010, 2011). HiGEM was also shown to capture the large-scale dynamics associated with clustering as described in chapter 4 (Priestley et al., 2017a).

The Storm Severity Index (SSI; Klawa and Ulbrich, 2003; Leckebusch et al., 2008) was applied to 10-metre wind speed data as a proxy of the impact of extratropical cyclones on insured property. The SSI has been shown to be comparable with a number of other insurance loss metrics for windstorms (Prahl et al., 2015) and was chosen for this purpose due to its ease of implementation and wide use in other studies (e.g. Pinto et al., 2007; Karremann et al., 2014a; Pantillon et al., 2017). Loss values were calculated as a total seasonal accumulation and also as the largest single event within a season, with these being compared for the 918 years of HiGEM data, and 36 years of ERA-Interim re-analysis. The average spatial footprint and the loss magnitudes in HiGEM were consistent with ERA-Interim following a uniform re-scaling of the HiGEM wind speeds. Fitting a generalised pareto distribution (GPD) to the seasonal loss data demonstrated that there was a good agreement between HiGEM and ERA-Interim for losses out to a 36 year return period, the maximum loss estimation available from ERA-Interim. Therefore, losses from HiGEM out to a return period of 200 years (and above) can be estimated using HiGEM, with the associated GPD estimation providing an uncertainty surrounding these estimates.

7.2.5 Q5. How important of a contribution does clustering make to the most severe seasons in terms of overall losses?

Key Result: Having a representation of clustering in HiGEM that is consistent with that of ERA-Interim results in seasonal losses that are 10-20% higher than seasonal losses that do not represent clustering above a return period of 30 years. The clustering is removed though randomising the events across all 918 years of HiGEM. Not representing clustering sufficiently in a loss model would lead to a large under-estimation of the losses on a seasonal basis.

Following the assessment of the ability of HiGEM to reproduce loss events on a comparable magnitude of those in ERA-Interim the question of the importance of clustering for losses could be addressed. There is evidence that as the severity of cyclones increases, they are more likely to occur in clusters, rather be individual events (Vitolo et al., 2009; Pinto et al., 2013; Cusack, 2016), and that stormier seasons are characterised by the passage of an increased number of cyclones (Hunter et al., 2016). The importance of clustering can be quantified by comparing seasons with clustering present, to seasons where clustering has

been removed. The data set with implicit clustering was simply the original HiGEM seasons, as HiGEM was shown to represent clustering and the variability of cyclones correctly. To remove clustering, the cyclone events in HiGEM were randomised to ensure that there are no dynamical connections between events.

The importance of clustering was assessed for seasons with a varying intensity and different return periods out to a one in 918 year season. Clustering is shown to positively contribute to seasonal losses for seasons that have a return period that is greater than 3 years. Above a 3 year return period, having a dynamical model that represents clustering properly leads to larger seasonal losses by an average of 10-20%. This relative increase of 10-20% is consistent out to a return period of 200 years, albeit with larger uncertainty. As the magnitude of the losses in a season is increasing with return period, the effect of clustering is also a larger absolute contribution to the intensity of a seasons loss. Below a 3 year return period, the absence of clustering in low loss years means that the randomised timeseries have larger losses.

These results indicate that clustering has a positive effect on the magnitude of seasonal losses, especially for larger return period seasons. This is consistent with Vitolo et al. (2009), Cusack (2016), and Hunter et al. (2016) and demonstrates how clustering has a larger effect on losses for those seasons that have higher total losses. It also stresses the necessity for windstorm loss models to accurately represent the dynamical process of clustering, as not doing so will lead to a large underestimation for severe seasons.

7.3 Implications and Limitations of the Thesis

7.3.1 Implications

This thesis has investigated the dynamics and associated impacts related to the clustering of extratropical cyclones across western Europe. The conclusions discussed above have several key implications. First of all, a characterisation of all objectively identifiable clustering events, and their large scale drivers, has been provided for the first time, with the largest importance being the structure of RWB on one or both flanks of the upper-level jet. This is consistent with the study of Pinto et al. (2014) but provides further information regarding the key features, and associated variability of these large-scale, upper-atmospheric drivers. This pattern of the RWB and jet structure projects strongly onto the NAO (Messori and Caballero, 2015) and recent work by Scaife et al. (2014) has shown that the NAO and resultant winter storminess is predictable on seasonal timescales (1 to 4 months). Furthermore Befort et al. (2019) found how windstorms and extreme cyclones across Europe have some predictability on seasonal timescales, with the NAO also being a good predictor of windstorm occurrence for northern Europe. As the studies of Scaife et al. (2014) and Befort et al. (2019) suggest that the NAO and European storminess have some sort of predictability,

this therefore implies there would be some skill in forecasting/predicting periods of clustering or above average storminess on a seasonal timescale, which would be of great importance considering the severe socio-economic impacts of these events.

Secondly, the investigation into Secondary+ cyclones yielded important results with regards to their importance in different regions of the storm track. Secondary+ cyclones were shown to be important for the central and eastern North Atlantic regions of the storm track, which is consistent with the previous studies of Schemm and Sprenger (2015) and Schemm et al. (2018). Secondary+ cyclones contribute around 50% of cyclones during clustering periods and play an important role in the elevated number of cyclones. This has implications for modelling studies as climate models commonly have biases with the representation of the North Atlantic storm track (Zappa et al., 2013a), and therefore it may be the case that the representation of Secondary+ cyclones (either in the number or location) and clustering may also be incorrect. This could be an issue due to the socio-economic impacts often associated with Secondary+ cyclones (Dacre and Gray, 2009) and periods of clustering (Mailier et al., 2006). Any potential misrepresentation of Secondary+ cyclones and clustering is also important for future climate change simulations as models are often uncertain with the response of the storm track and any potential changes in the number of severe cyclones under future forcings (Zappa et al., 2013b; Economou et al., 2015). Therefore, it is important that the development, location, and impacts of Secondary+ cyclones is correctly represented in numerical models.

Finally, it has been shown that a high-resolution climate model (HiGEM) has a good dynamical representation of periods of clustering for Europe. Based on cyclone track data or loss data, it was suggested in Pinto et al. (2013), Vitolo et al. (2009), and Cusack (2016) that clustering is stronger for seasons that have more intense storms and are at a higher return period. The results presented in chapter 6 further demonstrate this and illustrate that the dynamical connection between cyclones and the process of clustering as it acts to increase loss relative to a random series of cyclones, for all seasons above a 3 year return period in the case of HiGEM. This result clearly demonstrates the importance for clustering being accurately represented by catastrophe modellers who are estimating windstorm losses at high return period. Loss and catastrophe models should have a dynamical representation of events that is consistent with observations and not treat the passage of cyclones, or clustering, as random.

7.3.2 Limitations

There are several limitations to the analysis and results presented in this study. Firstly, the results presented in chapters 3-6 only represent analysis using the Murray and Simmonds (1991b) and Hodges (1994, 1995, 1999) tracking schemes. As the study of Pinto et al. (2014), which provides the introductory analysis for

the work in chapters 3-6, was done using the scheme of Murray and Simmonds (1991b), and thresholds developed to reflect the behaviour of this scheme, this was seen as the best choice for the analysis in these chapters. Comparisons of cyclone tracking schemes and of clustering by Neu et al. (2013) and Pinto et al. (2016) have shown some discrepancies between methods for individual cyclones and the pattern of the storm track for a winter season, but that the large-scale overdispersion pattern of clustering is generally consistent between schemes. Clustering as measured in chapters 3-5 of this thesis (counting of cyclones passing through geographic regions) has not been performed with other schemes, so any uncertainties/differences in this representation of clustering are not known.

The exploration of secondary cyclogenesis presented in chapter 5 was done using a different scheme to that first objective identification of secondary cyclones by Schemm and Sprenger (2015) and Schemm et al. (2018). Consequently, the relative proportion of secondary cyclones in the North Atlantic differs between the study in this thesis and that of Schemm et al. (2018). These differences could be due to differing numbers of cyclones identified by each scheme in the central and eastern North Atlantic (see Pinto et al., 2016, for details), therefore any differences could be quantified by repeating this analysis with a number of different cyclone tracking schemes.

Finally, the assessment of the importance of clustering for seasonal losses in chapter 6 uses a single model approach (HiGEM) for the quantification. The results are therefore limited as they do not present the uncertainty that could come from a misrepresentations of phenomena in the physics of HiGEM. Multi-model assessments of clustering under current climate conditions have been performed previously (Economou et al., 2015), with models presenting a general consensus on the pattern of dispersion in the North Atlantic. However, no multi-model approach of windstorm losses and clustering at return periods of more than 100 years has been performed. Following a multi-model approach would therefore allow for much more robust estimations to be made on the impact of clustering than the single model assessment presented in this thesis.

7.4 Future Work

The work completed in this thesis has opened up several avenues for interesting further research. These avenues are discussed below.

- A more robust evaluation of the dynamics associated with clustering in new extended re-analyses would be of interest. With the availability of ERA5 back to 1950, and an extension to the most recent complete DJF season of 2018/19, this would present a near doubling in the amount of data used in the analysis of chapter 4-5. Moreover, additional dynamical analysis on clustering in different storm

tracks (e.g. Pacific, Southern Hemisphere) would be of interest to investigate if any events were associated with similar dynamical conditions as in the North Atlantic.

- Idealised or case study simulations of periods of clustering could present an interesting pathway for future research. Sensitivities to the jet strength and structure of RWB could be fully assessed. Furthermore, this would allow for the formation process of Secondary+ cyclones to be investigated further to see how sensitive the formation is to the stability anomalies identified in chapter 5 and also other environmental factors. The surrounding environment was explored by Schemm and Sprenger (2015) in part, but sensitivities of formation to parameters such as the vertical PV structure, surface latent heat flux, and low-level moisture content would be of interest.
- An assessment of Secondary+ cyclones in other storm tracks and oceanic basins would be of interest. Repeating the analysis of chapter 4 and focussing on the preferential locations of each cyclone class would be of interest. Schemm et al. (2018) provided an initial assessment of this, however, with the observed discrepancies in Secondary+ cyclone magnitude between the results in chapter 5 and their study, it would be fruitful to pursue this further and quantify any differences between the methods. Furthermore, a full intercomparison of the representation of Secondary+ cyclones with different cyclone identification and tracking algorithms applied would be interesting to assess the sensitivity of their relative importance for the storm track.
- The methodology of evaluating the importance of clustering from chapter 6 could easily be applied on a country basis to assess the impact over smaller geographical regions. Karremann et al. (2014a) and Cusack (2016) have performed assessments on the intensity of clustering for different countries, however there have been no studies to assess the impact of clustering on these smaller regions. This would be of interest particularly for loss modellers, insurance, and re-insurance companies with more restricted portfolios that do not focus on the entirety of Europe. It would perhaps be expected that larger countries in terms of geographic size would be more influenced by the occurrence of clustering (i.e. Vitolo et al., 2009), and this is something that could be quantified in this framework.
- A caveat of the results presented in chapter 6 is that they are just from one model. Therefore a multi-model assessment of the analysis presented in chapter 6 would allow for further uncertainty regarding the importance of clustering on seasonal losses to be addressed even further. Assessment of clustering in terms of the storm track dispersion has been performed across models (Economou et al., 2015), and re-analyses (Pinto et al., 2013), with most re-producing the correct pattern of dispersion in the North Atlantic. This is something that could also be achieved with the new generation of fully coupled atmosphere-ocean models that are part of the CMIP6 ensemble.
- A final avenue for further research would be to assess how clustering and the associated dynamical features would change in future climates. Using the new generation of CMIP6 models would be a great tool to perform this analysis and would provide a strong assessment as to projected changes in

this behaviour of the storm track. It would be of interest to see if the new high-resolution models can capture the dynamical features relevant for clustering (i.e. RWB, strong extended jet, Secondary+ cyclones in the eastern North Atlantic) and their associated variability. With projected changes to the storm track in the next century, and a possible reduction in the total number of cyclones (Zappa et al., 2013b) this would be of great interest. There are suggestions for an increase in severe cyclones for western Europe (Bengtsson et al., 2006) and an enhanced wind risk associated with this (Leckebusch et al., 2007; Pinto et al., 2007; Donat et al., 2011). Changes in the clustering of cyclones (as measured by dispersion) has shown to be uncertain in future climates (Economou et al., 2015), mainly due to issues with under-sampling of events and a lack of data for an accurate assessment. In addition, Karremann et al. (2014a) indicated that multi-event seasons (i.e. clustering) would occur at shorter return periods under future climate conditions. Therefore, a quantification of clustering as defined in chapter 3 and chapter 4 and the controlling dynamics in these models would be of great interest, as well as the impact of these events on the potentially increased wind risk for western Europe as in chapter 6.

7.5 Key Conclusions

Overall, this thesis has provided an assessment of the occurrence of extratropical cyclone clustering in western Europe and identified the various dynamical phenomena associated with these events. The contribution of cyclone families and secondary cyclones to periods of clustering has been explored, something that has been only previously hypothesised based on a small sample of observed cases. Finally, a high-resolution climate model has been used to investigate the role of clustering for extremely stormy winter seasons (1 in 200 year return period) across Europe. From these research avenues, several key conclusions have been found. The key messages are stated below.

- All periods of clustering occurring over three regions of western Europe were identified in the ERA-Interim re-analysis. The dynamical features associated with these events were identified with it being found that RWB preferentially occurs on one side, or both sides of a zonally extended and anomalously strong upper-level jet. The presence of RWB on each side of the jet determines that latitude at which cyclones are clustering for western Europe.
- Secondary+ cyclones have been quantified with regards to their preferential locations in the North Atlantic, and especially their differences compared to Primary cyclones. Secondary+ cyclones occur over the central and eastern North Atlantic, with Primary cyclones generally being found over the western North Atlantic. Secondary+ cyclones are shown to contribute to the increase in cyclone numbers during periods of clustering in western Europe, with this generally being shown to be a result of enhanced steering from the large scale flow, with only minimal increases in the rate of cyclogenesis.

- The contribution of clustering to seasonal wind losses across Europe was assessed in 918 years of fully coupled climate model data from HiGEM. By comparing the dynamically consistent model data with a randomised version of itself with clustering removed it was shown that dynamically representing clustering results in an increase in losses compared to that expected in a random year. This increase occurs for seasons above a 3 year return period and the magnitude of the increase ranges between 10% and 20% for a 200 year return period season.

Appendix A:

CHANGES IN STATIC STABILITY BASED ON THERMAL WIND BALANCE

Thermal Wind Balance formulated in terms of potential temperature (θ) in pressure (p) co-ordinates can be expressed as follows:

$$\frac{\partial u}{\partial p} = -\frac{1}{f\rho\theta}\left(\frac{\partial \theta}{\partial y}\right)_p \tag{A1}$$

Equation A1 can be simplified further by treating the Coriolis parameter (f), density (ρ), and the potential temperature (θ) as constant. Thereby giving:

$$\frac{\partial u}{\partial p} \approx -\left(\frac{\partial \theta}{\partial y}\right)_p \tag{A2}$$

In equation 5.1, the low-level static stability is formulated in pressure co-ordinates. By treating p, g, R, T, and $\bar{\theta}$ as approximately constant, this can be expressed as:

$$N^2 \approx \frac{\partial \theta}{\partial p} \tag{A3}$$

Through differentiating equation A2 with respect to p, the following relationship is obtained:

$$\frac{\partial^2 u}{\partial p^2} \approx -\frac{\partial}{\partial p}\left(\frac{\partial \theta}{\partial y}\right)_p \approx -\frac{\partial^2 u}{\partial p \partial y} \approx -\frac{\partial}{\partial y}\left(\frac{\partial \theta}{\partial p}\right) \tag{A4}$$

Using the relationship in equation A3 substituted into equation A4 it therefore states that as the second derivative of u with respect to p increases, the meridional gradient of the static stability will become more negative.

From figure A1 it can be seen that the anomalies in the jet are throughout the depth of the atmosphere with a peak between 200 and 350 hPa. These changes in jet speed with height imply that the value of $\frac{\partial u}{\partial p}$ will be positive below the jet maximum and have a value of zero at the height of the jet core and then being

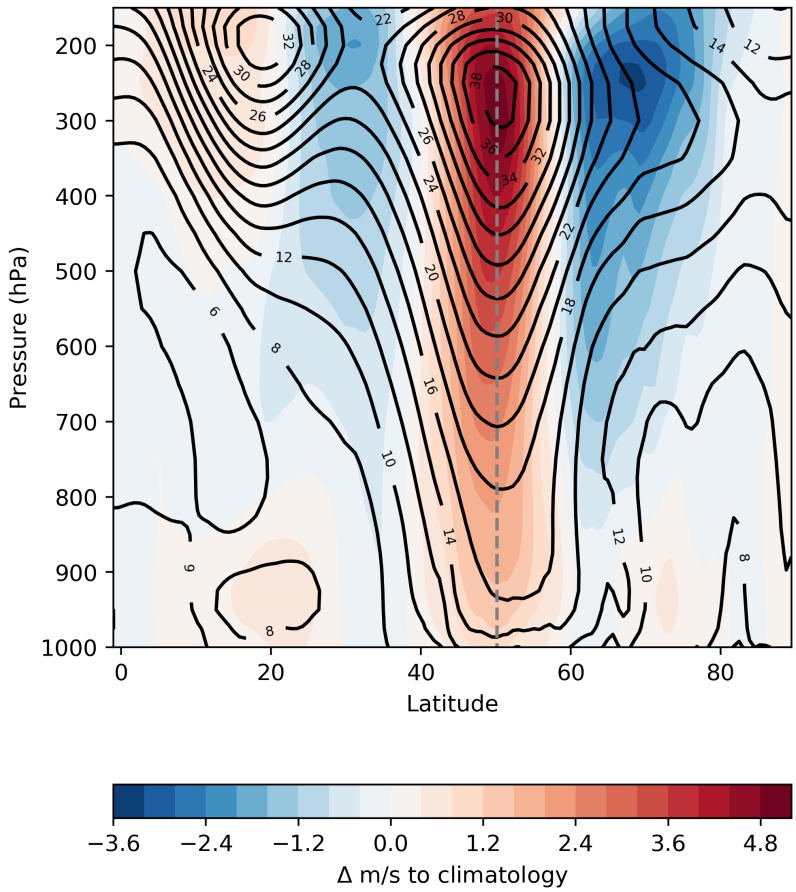

Figure A1: *Composite image of zonal mean wind at the time of Secondary+ cyclogenesis for Secondary+ cyclones passing through 55°N. Zonal mean from 40-0°W. Black contours are the full field at the time of cyclogenesis and the coloured filled contours are the anomalies relative to the long-term climatology in m s^{-1}. The grey dashed line represents the mid-latitude jet axis.*

negative above this. The maxima in $\frac{\partial u}{\partial p}$ will subsequently be in the middle troposphere. Through equation A2 this tells us that the gradient of θ will be increasing more across the jet in a northerly direction.

As $\frac{\partial u}{\partial p}$ will have a positive gradient in the lower troposphere, and a negative gradient in the upper troposphere this tells us that through equation A4 that $\frac{\partial^2 u}{\partial p^2}$ will be positive in the lower troposphere, negative in the upper troposphere, and have its minimum at the height of the jet maximum. The large values of $\frac{\partial^2 u}{\partial p^2}$ in the lower troposphere relate to a strong negative meridional N^2 (through equation A4) and the large negative values at the height of the jet maximum result in a positive meridional gradient of N^2 at that height. These patterns are seen in figure A2 with the stability gradients across the jet peaking at lower and upper levels, with negative N^2 anomalies on the poleward flank of the jet below 800 hPa.

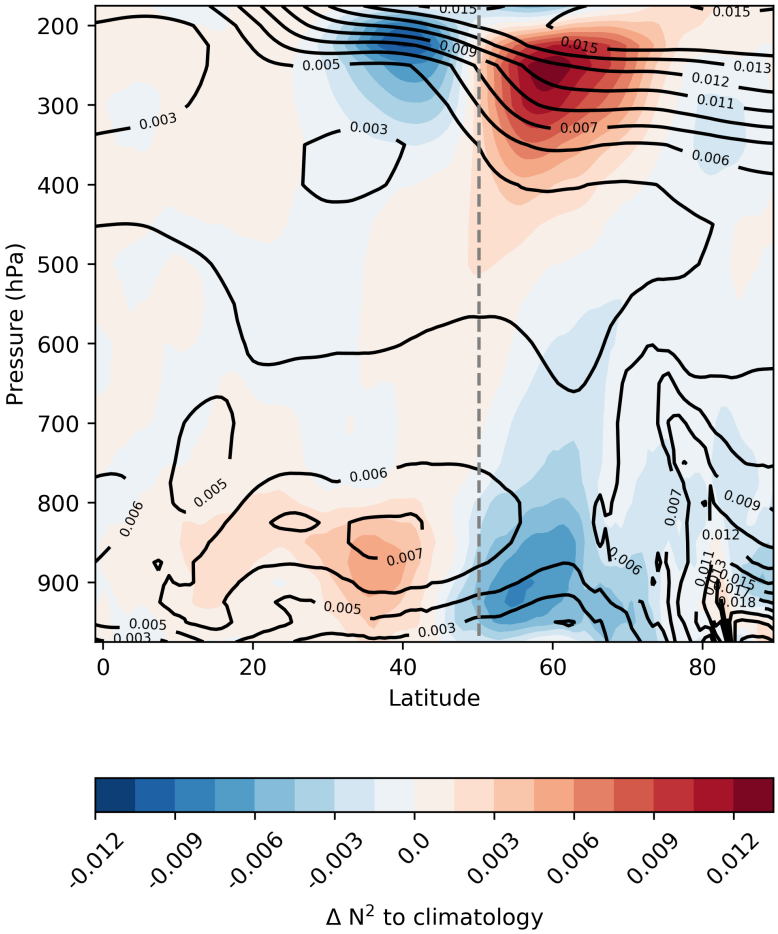

Figure A2: *Composite image of zonal mean static stability (N^2) at the time of Secondary+ cyclogenesis for Secondary+ cyclones passing through 55°N. Zonal mean from 40-0°W. Black contours are the full field at the time of cyclogenesis and the coloured filled contours are the anomalies relative to the long-term climatology. The grey dashed line represents the mid-latitude jet axis.*

Appendix B:

CLARIFICATIONS TO THE TEXT

In this section some clarifications and comments to the text and discussions in this thesis will be presented. These comments and clarifications have arisen as a result of the viva exam. Each clarification will be discussed on a point-by-point basis with the relevant references and figures stated in the text, as well as the location of the clarified text in the thesis.

- Through the thesis, and particularly in chapter 4, the winter season of 2013/2014 is discussed as a result of the record-breaking number of storms impacting the UK in this season. In chapter 4 the paper of Slingo et al. (2014) is referenced, which hypothesises that the high cyclone activity could be associated with the warm tropical west Pacific sea surface temperatures (SST) in this season. They hypothesise that the warm SSTs could trigger a Rossby wave train, which would result in higher than average pressure in the region of the Aleutian Low and as a result would cause lower than average temperatures across North America (which were observed). It is then hypothesised that these cold North American surface temperatures increase the baroclinicity in the region of the eastern coast of North America, generating an environment that is more favourable for cyclone growth and propagation downstream toward Europe. This hypothesis from Slingo et al. (2014) was tested by Wild et al. (2015) through correlations between a number of large-scale patterns. These were the number of European storms, the 2-metre temperature anomaly over North America, the rate of storms in the North Pacific, and OLR over the tropical western Pacific (as a proxy for the SSTs). It was found that the number of European storms was significantly negatively correlated with the 2-metre temperature anomaly over North America, and that the 2-metre North American temperature anomaly was significantly positively correlated with the tropical western Pacific OLR. However, the tropical western Pacific OLR was not significantly correlated with the number of European storms, indicating no direct relationship. A link remains possible between the western Pacific OLR and number of European storms, indirectly via the connections with 2-metre North American temperature anomaly.

Furthermore, Wild et al. (2015) found a strong relationship between the near surface temperature gradient near the eastern coast of North America, and the number of European storms, indicating that this may play a more direct role on the clustering observed in the winter of 2013/2014.

- One of the major conclusions of this thesis is that periods of clustering are associated with Rossby wave breaking (RWB) on one or both flanks of the jet, with this being double-sided for clustering occurring over the UK (specifically the 55°N, 5°W region). This is summarised by the composites first shown in figure 3.3. However, in figure 3.2d a timeseries of RWB is shown for the 2013/2014 season where the double-sided nature of the RWB is less apparent and which may contradict the results presented in figure 3.3. The discrepancies between these two figures can be explained via the method used to calculate the RWB. The method used is from Masato et al. (2013), and in figure 3.2d, calculates the RWB as the difference in the gradient of potential temperature (θ) and uses the absolute difference in the gradient for the calculations. This method was later adapted (sections 3.6 and 5.3.4) to be based on anomalies in the frequency of RWB relative to the climatological occurrence at that location. This different way applying this method is shown in figures 3.5 and 5.9f, which clearly highlight the double-sided nature of the RWB much more clearly than in figure 3.2d. Consequently, the RWB field from figure 3.2d has been re-calculated using the adapted method and is shown in figure B1. In figure B1 the occurrence of RWB is much clearer on the southern flank of the jet compared to the original figure 3.2d. Any apparent contradiction is a result of the way that the RWB has been plotted.

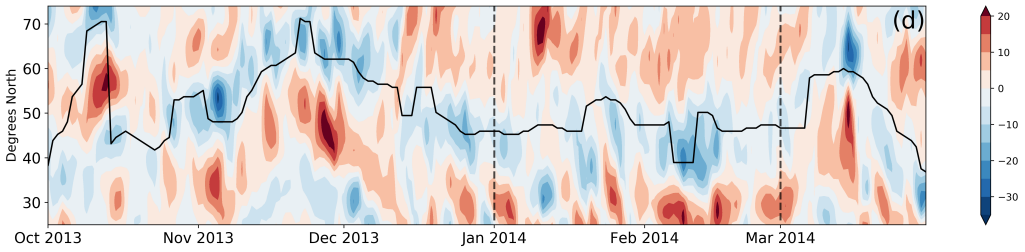

Figure B1: *Evolution of Rossby wave breaking throughout the 2013/2014 winter season from October 1 to March 31. The Rossby wave breaking field is plotted as an anomaly of the frequency relative to the background climatology. The black line is the jet latitude.*

- Throughout this thesis the term *'non-clustered'* is often used. In the context of the work presented in this thesis these non-clustered periods refer to any time when the clustering metric is not satisfied. The clustering metric requires at least 4 intense storms passing through a pre-defined region in a 7-day period. Therefore, a non-clustered period is when there is not 4 intense storms in 7-days. This could mean there are 0 storms, or 6 weak storms, but as neither satisfy the clustering criteria these would both be classed as non-clustered periods.
- At various points in this thesis windstorm losses are commonly quoted as being in dollars ($). In all instances this use refers to US Dollars.

- In chapter 3, the discussion in section 3.6 around figures 3.5 - 3.7 analyses the temporal relationship between RWB and the upper-level jet. The analysis concludes that the RWB peaks at lag -2, with the jet peaking at lag 0, although it would be difficult to ascertain which feature amplified first. It has been well documented in multiple studies (Rivière and Orlanski, 2007; Rivière et al., 2010; Barnes and Hartmann, 2012) that the presence of RWB causes shifts/accelerations of the jet on daily timescales through the differing momentum fluxes from cyclonic and anticyclonic RWB. Therefore, the conclusion from figures 3.5 - 3.7 that the jet is accelerating in response to the RWB anomalies can be given with strong confidence.
- In chapter 4 it is stated that seasons such as 2013/2014, 1990/1991, and 1999/2000 are clustered. Based upon the definition of clustering employed here and those previously (Mailier et al., 2006) it should be clarified that an entire season cannot be clustered and instead it should be stated that those seasons are characterised by more periods of clustering, that last longer than average, than would be expected.
- In the analysis of the winter of 2013/2014 in chapter 4 some precipitation data from ERA-Interim are presented (figures 4.2 and 4.3). In chapter 4 no verification or uncertainty estimates associated with this data are discussed. The ERA-Interim precipitation field does not provide any uncertainty around the output as it is produced by the model as a forecast field (Dee et al., 2011). There have been studies that have evaluated ERA-Interim precipitation over the UK (Rhodes et al., 2015; de Leeuw et al., 2015), which indicate that ERA-Interim tends to under-estimate precipitation totals by approximately 22%. Despite this under-estimation the ERA-Interim timeseries does correlate well with that from observations (0.91 de Leeuw et al., 2015), although the hit-rate for extreme events is only 40-65% (Rhodes et al., 2015). Despite this, for the purpose the data was used in chapter 4 (figure 4.2 and 4.3), it was decided that this product was fit for purpose.
- In chapter 4, in figure 4.3 and the surrounding text the difference in precipitation between non-clustered and clustered days is discussed. Herein it is discussed that clustered and non-clustered days receive significantly different amounts of precipitation. A histogram of the two distributions is shown in figure B2. Clustered and non-clustered days receive a mean of 6.25mm and 3.78mm respectively. Further to this the standard deviations are 5.52mm and 3.82mm respectively, with variances of 30.44m and 14.58mm. Using a Welch's t-test these two distributions give p=0.03. This therefore indicates they are significantly different at the 95% level. The reason for the very large variances is due to the long tail associated with precipitation data and both distributions being skewed toward low accumulations.
- In chapter 3 and chapter 4, it is stated that secondary cyclones play a role in contributing to the periods of clustering for western Europe. In chapter 5, this question to answered through the objective identification and tracking of frontal features and secondary cyclones. In chapter 5 it is discussed

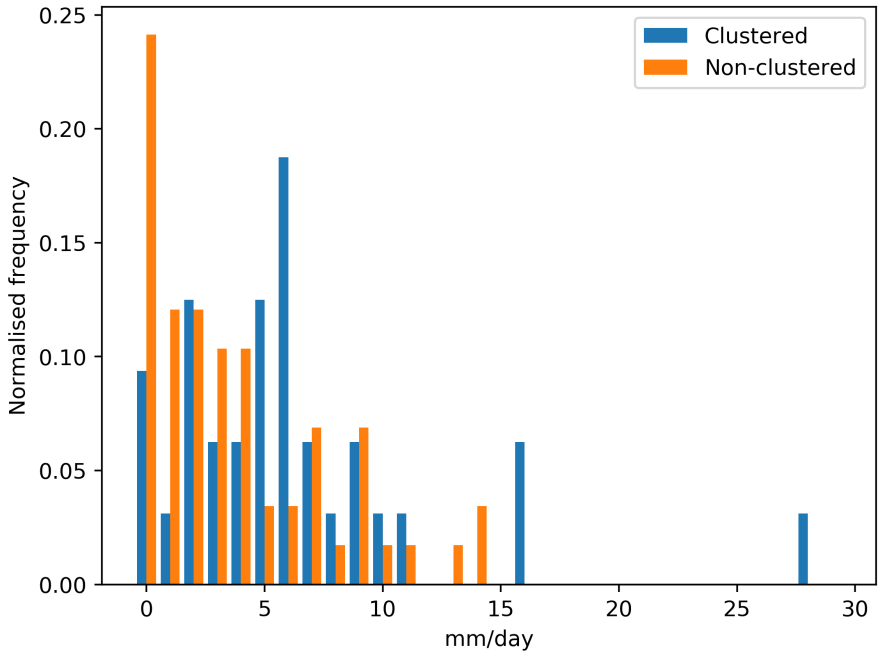

Figure B2: *A histogram of daily precipitation from EWP HadUKP (Alexander and Jones, 2001). Clustered days are in blue and non-clustered days in orange.*

that secondary cyclones contribute approximately 50% of cyclones to periods of clustering, however despite this there are actually relatively more cyclones forming during non-clustered periods than in clustered periods.

- Chapter 5 discusses the importance of Secondary+ cyclones for clustering that impacts on western Europe. Figure 5.16 investigates how the total number of each cyclone class changes with an increasing intensity of clustering. The conclusion reached is that Secondary+ cyclones contribute approximately 50% of cyclones during periods of clustering and that Secondary+ cyclones, along with Solo cyclones, contribute the most and increase their numbers with clustering intensity. One question that is not answered in chapter 5 is how the relative fraction of each cyclone class changes with the intensity of clustering. Figure B3 addresses this and shows the relative fraction of each cyclone class. There is a slight increase in the mean fraction of Secondary+ cyclones with clustering, however, this relationship is marred by large uncertainties. There is a slight decrease in the mean fraction of Solo cyclones, although again there is a lot of spread in this relationship. There is minimal change in Primary cyclones. This figure was not included in chapter 5 due to the large amounts of spread on these relationships that do not present a clear relationship between changes in the cyclone classes with clustering intensity. Whereas in figure 5.16 there is a clear, identifiable relationship.
- In chapter 6 the Storm Severity Index (SSI) is used to quantify losses from windstorms across Europe. In section 6.3.3 it is stated that the SSI was developed by Klawa and Ulbrich (2003). This is incorrect as the SSI was first introduced by Leckebusch et al. (2007) as a development from the original cubic

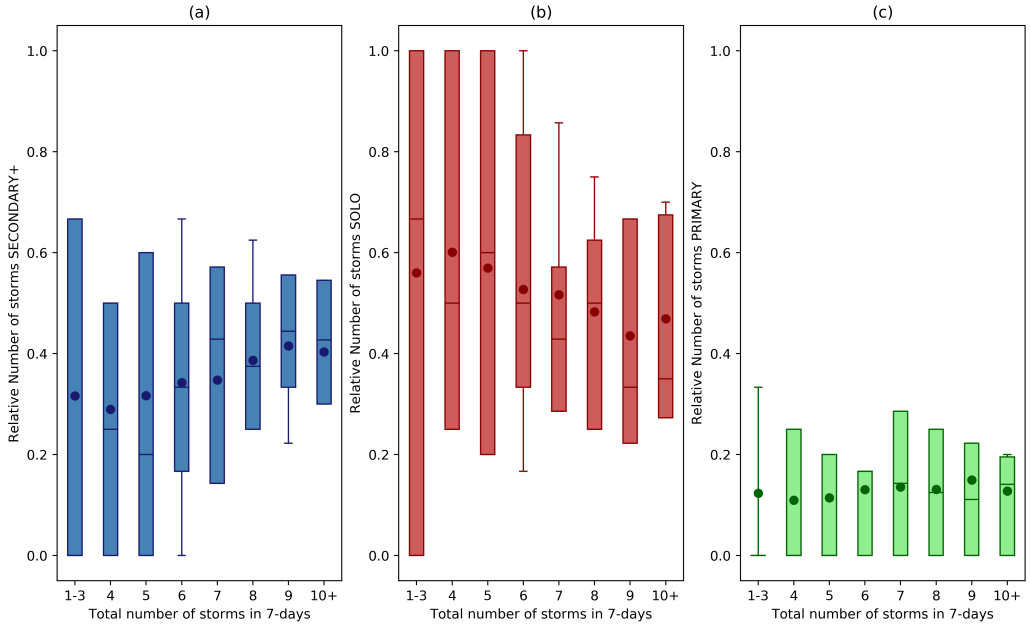

Figure B3: *The relative fractions of each class of cyclone relative to the total number of cyclones passing through the 55°N region. (a) Secondary+, (b) Solo, (c) Primary cyclones.*

loss relationship of Klawa and Ulbrich (2003). Furthermore, the application of the SSI more closely follows the Area-SSI (ASSI) from Leckebusch et al. (2007) as the SSI is calculated without tracking cyclones and is not specific to one event. This differs from the Event-SSI (ESSI), which specifically calculates the severity for winds associated with one individual tracked windstorm. In chapter 6, the SSI is calculated as a sum over the entire European area, and without tracking cyclones.

- In order to use the HiGEM data to calculate losses in chapter 6 a bias correction was applied in order to match the wind distribution more closely to that of ERA-Interim (figure 6.4). The bias correction applied was a simple uniform scaling of the HiGEM 10-metre winds by a factor of 1.1875 in order to match the distribution of the tail from ERA-Interim. As there are only 36 years of ERA-Interim and many realisations of this period from the HiGEM data, there is a chance that the HiGEM data is being over-fit to this particular realisation of history present in ERA-Interim. This correction assumes that this version of history provided by ERA-Interim is correct and fully representative of the historical period simulated by HiGEM. This is of course unlikely to be true. A further quantification of the bias correction could have been made using information from other re-analyses such as MERRA2 (Gelaro et al., 2017b), or JRA-55 (Kobayashi et al., 2015b), both of which provide further coverage of the ERA-Interim period. Furthermore, ERA5 (Hersbach and Dee, 2016) will soon provide data back to 1950, which would give a further estimation of the bias of HiGEM for its entire simulation period.
- When creating the randomised versions of HiGEM in chapter 6 to ascertain the importance of clustering on seasonal losses (figure 6.10) the randomisation is done across all years in the timeseries

and events are not limited to remain in the original year. Each of the 10,000 samples contains only one of each of the years with no repeat re-sampling within a single sampled timeseries.

References

Ackerman, S. A. and J. A. Knox, 2007: *Meteorology: understanding the atmosphere. 2nd ed*. Brooks/Cole.

Adamson, D., S. E. Belcher, B. J. Hoskins, R. S. Plant, et al., 2006: Boundary-layer friction in midlatitude cyclones. *Quarterly Journal of the Royal Meteorological Society*, **132**, 101–124.

Ahmadi-Givi, F., G. C. Graig, and R. S. Plant, 2004: The dynamics of a midlatitude cyclone with very strong latent-heat release. *Quarterly Journal of the Royal Meteorological Society*, **130**, 295–323, doi:10.1256/qj.02.226.

Alexander, L. V. and P. D. Jones, 2001: Updated precipitation series for the U.K. and discussion of recent extremes. *Atmospheric Science Letters*, **1**, 142–150, doi:10.1006/asle.2000.0016.

Barnes, E. A., 2013: Revisiting the evidence linking Arctic amplification to extreme weather in midlatitudes. *Geophysical Research Letters*, **40**, 4734–4739, doi:10.1002/grl.50880.

Barnes, E. A. and D. L. Hartmann, 2012: Detection of Rossby wave breaking and its response to shifts of the midlatitude jet with climate change. *Journal of Geophysical Research: Atmospheres*, **117**, 1–17, doi:10.1029/2012JD017469.

Befort, D. J., S. Wild, J. R. Knight, J. F. Lockwood, H. E. Thornton, L. Hermanson, P. E. Bett, A. Weisheimer, and G. C. Leckebusch, 2019: Seasonal forecast skill for extratropical cyclones and windstorms. *Quarterly Journal of the Royal Meteorological Society*, **145**, 92–104, doi:10.1002/qj.3406.

Befort, D. J., S. Wild, T. Kruschke, U. Ulbrich, and G. C. Leckebusch, 2016: Different long-term trends of extra-tropical cyclones and windstorms in ERA-20C and NOAA-20CR reanalyses. *Atmospheric Science Letters*, **17**, 586–595, doi:10.1002/asl.694.

Benedict, J. J., S. Lee, and S. B. Feldstein, 2004: Synoptic view of the North Atlantic oscillation. *Journal of the atmospheric sciences*, **61**, 121–144.

Bengtsson, L., K. I. Hodges, and N. Keenlyside, 2009: Will Extratropical Storms Intensify in a Warmer Climate? *Journal of Climate*, **22**, 2276–2301, doi:10.1175/2008JCLI2678.1.

Bengtsson, L., K. I. Hodges, and E. Roeckner, 2006: Storm Tracks and Climate Change. *Journal of Climate*, **19**, 3518–3543, doi:10.1175/JCLI3815.1.

Berry, G., M. J. Reeder, and C. Jakob, 2011: A global climatology of atmospheric fronts. *Geophysical Research Letters*, **38**, doi:10.1029/2010GL046451.

Bishop, C. H. and A. J. Thorpe, 1994a: Frontal Wave Stability during Moist Deformation Frontogenesis. Part I: Linear Wave Dynamics. *Journal of the Atmospheric Sciences*, **51**, 852–873, doi:10.1175/1520-0469(1994)051¡0852:FWSDMD¿2.0.CO;2.

— 1994b: Frontal Wave Stability during Moist Deformation Frontogenesis. Part II: The Suppression of Nonlinear Wave Development. *Journal of the Atmospheric Sciences*, **51**, 874–888, doi:10.1175/1520-0469(1994)051¡0874:FWSDMD¿2.0.CO;2.

Bjerknes, J., 1919: On the structure of moving cyclones. *Monthly Weather Review*, **47**, 95–99, doi:10.1175/1520-0493(1919)47¡95:OTSOMC¿2.0.CO;2.

Bjerknes, J. and H. Solberg, 1922: Life cycle of cyclones and the polar front theory of atmospheric circulation. *Geophysisks Publikationer*, **3**, 3–18.

Blackmon, M. L., 1976: A Climatological Spectral Study of the 500 mb Geopotential Height of the Northern Hemisphere. *Journal of the Atmospheric Sciences*, **33**, 1607–1623, doi:10.1175/1520-0469(1976)033¡1607:ACSSOT¿2.0.CO;2.

Bloomfield, H. C., L. C. Shaffrey, K. I. Hodges, and P. L. Vidale, 2018: A critical assessment of the long-term changes in the wintertime surface Arctic Oscillation and Northern Hemisphere storminess in the ERA-20C reanalysis. *Environmental Research Letters*, **13**, 094004, doi:10.1088/1748-9326/aad5c5.

Brayshaw, D. J., B. Hoskins, and M. Blackburn, 2009: The Basic Ingredients of the North Atlantic Storm Track. Part I: Land–Sea Contrast and Orography. *Journal of the Atmospheric Sciences*, **66**, 2539–2558, doi:10.1175/2009JAS3078.1.

— 2011: The Basic Ingredients of the North Atlantic Storm Track. Part II: Sea Surface Temperatures. *Journal of the Atmospheric Sciences*, **68**, 1784–1805, doi:10.1175/2011JAS3674.1.

Browning, K. A., 1986: Conceptual Models of Precipitation Systems. *Weather and Forecasting*, **1**, 23–41, doi:10.1175/1520-0434(1986)001¡0023:CMOPS¿2.0.CO;2.

— 1997: The dry intrusion perspective of extra-tropical cyclone development. *Meteorological Applications*, **4**, 317–324.

— 2004: The sting at the end of the tail: Damaging winds associated with extratropical cyclones. *Quarterly Journal of the Royal Meteorological Society*, **130**, 375–399, doi:10.1256/qj.02.143.

Browning, K. A. and N. M. Roberts, 1994: Structure of a frontal cyclone. *Quarterly Journal of the Royal Meteorological Society*, **120**, 1535–1557, doi:10.1002/qj.49712052006.

Carlson, T. N., 1980: Airflow Through Midlatitude Cyclones and the Comma Cloud Pattern. *Monthly Weather Review*, **108**, 1498–1509, doi:10.1175/1520-0493(1980)108¡1498:ATMCAT¿2.0.CO;2.

Catto, J. L., E. Madonna, H. Joos, I. Rudeva, and I. Simmonds, 2015: Global Relationship between Fronts and Warm Conveyor Belts and the Impact on Extreme Precipitation. *Journal of Climate*, **28**, 8411–8429, doi:10.1175/JCLI-D-15-0171.1.

Catto, J. L. and S. Pfahl, 2013: The importance of fronts for extreme precipitation. *Journal of Geophysical Research: Atmospheres*, **118**, 10,791–10,801, doi:10.1002/jgrd.50852.

Catto, J. L., L. C. Shaffrey, and K. I. Hodges, 2010: Can Climate Models Capture the Structure of Extratropical Cyclones? *Journal of Climate*, **23**, 1621–1635, doi:10.1175/2009JCLI3318.1.

— 2011: Northern hemisphere extratropical cyclones in a warming climate in the HiGEM high-resolution climate model. *Journal of Climate*, **24**, 5336–5352, doi:10.1175/2011JCLI4181.1.

Center for International Earth Science Information Network - CIESIN - Columbia University, 2017: Gridded Population of the World, Version 4 (GPWv4): Population Density, Revision 10.

Chaboureau, J.-P. and A. J. Thorpe, 1999: Frontogenesis and the development of secondary wave cyclones in FASTEX. *Quarterly Journal of the Royal Meteorological Society*, **125**, 925–940, doi:10.1002/qj.49712555509.

Chang, E. K. M., Y. Guo, and X. Xia, 2012: CMIP5 multimodel ensemble projection of storm track change under global warming. *Journal of Geophysical Research: Atmospheres*, **117**, doi:10.1029/2012JD018578.

Charney, J. G., 1947: The dynamics of long waves in a baroclinic westerly current. *Journal of Meteorology*, **4**, 136–162, doi:10.1175/1520-0469(1947)004¡0136:TDOLWI¿2.0.CO;2.

Chung, Y.-S., K. D. Hage, and E. R. Reinelt, 1976: On Lee Cyclogenesis and Airflow in the Canadian Rocky Mountains and the East Asian Mountains. *Monthly Weather Review*, **104**, 879–891, doi:10.1175/1520-0493(1976)104¡0879:OLCAAI¿2.0.CO;2.

Clark, P. A., K. A. Browning, and C. Wang, 2005: The sting at the end of the tail: Model diagnostics of fine-scale three-dimensional structure of the cloud head. *Quarterly Journal of the Royal Meteorological Society*, **131**, 2263–2292, doi:10.1256/qj.04.36.

Coles, S., 2001: *An Introduction to Statistical Modelling of Extreme Values*. Springer, London.

Coronel, B., D. Ricard, G. Rivière, and P. Arbogast, 2015: Role of Moist Processes in the Tracks of Idealized Midlatitude Surface Cyclones. *Journal of the Atmospheric Sciences*, **72**, 2979–2996, doi:10.1175/JAS-D-14-0337.1.

Cox, D. R. and V. Isham, 1980: *Point Processes*. Chapman and Hall/CRC.

Cusack, S., 2016: The observed clustering of damaging extratropical cyclones in Europe. *Natural Hazards and Earth System Sciences*, **16**, 901–913, doi:10.5194/nhess-16-901-2016.

Dacre, H. F. and S. L. Gray, 2006: Life-cycle simulations of shallow frontal waves and the impact of deformation strain. *Quarterly Journal of the Royal Meteorological Society*, **132**, 2171–2190.

— 2009: The spatial distribution and evolution characteristics of North Atlantic cyclones. *Monthly Weather Review*, **137**, 99–115.

Dacre, H. F., M. K. Hawcroft, M. A. Stringer, and K. I. Hodges, 2012: An Extratropical Cyclone Atlas: A Tool for Illustrating Cyclone Structure and Evolution Characteristics. *Bulletin of the American Meteorological Society*, **93**, 1497–1502, doi:10.1175/BAMS-D-11-00164.1.

Davis, C. A. and K. A. Emanuel, 1991: Potential Vorticity Diagnostics of Cyclogenesis. *Monthly Weather Review*, **119**, 1929–1953, doi:10.1175/1520-0493(1991)119¡1929:PVDOC¿2.0.CO;2.

de Leeuw, J., J. Methven, and M. Blackburn, 2015: Evaluation of ERA-Interim reanalysis precipitation products using England and Wales observations. *Quarterly Journal of the Royal Meteorological Society*, **141**, 798–806, doi:10.1002/qj.2395.

Dee, D., S. Uppala, A. Simmons, P. Berrisford, P. Poli, S. Kobayashi, U. Andrae, M. Balmaseda, G. Balsamo, P. Bauer, et al., 2011: The ERA-Interim reanalysis: Configuration and performance of the data assimilation system. *Quarterly Journal of the Royal Meteorological Society*, **137**, 553–597.

Della-Marta, P. M., M. a. Liniger, C. Appenzeller, D. N. Bresch, P. KöLlner-Heck, and V. Muccione, 2010: Improved estimates of the European winter windstorm climate and the risk of reinsurance loss using climate model data. *Journal of Applied Meteorology and Climatology*, **49**, 2092–2120, doi:10.1175/2010JAMC2133.1.

Della-Marta, P. M., H. Mathis, C. Frei, M. A. Liniger, J. Kleinn, and C. Appenzeller, 2009: The return period of wind storms over Europe. *International Journal of Climatology*, **29**, 437–459, doi:10.1002/joc.1794.

Della-Marta, P. M. and J. G. Pinto, 2009: Statistical uncertainty of changes in winter storms over the North Atlantic and Europe in an ensemble of transient climate simulations. *Geophysical Research Letters*, **36**, doi:10.1029/2009GL038557, l14703.

Deveson, A. C. L., K. A. Browning, and T. D. Hewson, 2002: A classification of FASTEX cyclones using a height-attributable quasi-geostrophic vertical-motion diagnostic. *Quarterly Journal of the Royal Meteorological Society*, **128**, 93–117, doi:10.1256/00359000260498806.

Donat, M. G., G. C. Leckebusch, J. G. Pinto, and U. Ulbrich, 2010: Examination of wind storms over Central Europe with respect to circulation weather types and NAO phases. *International Journal of Climatology*, **30**, 1289–1300, doi:10.1002/joc.1982.

Donat, M. G., G. C. Leckebusch, S. Wild, and U. Ulbrich, 2011: Future changes in European winter storm losses and extreme wind speeds inferred from GCM and RCM multi-model simulations. *Natural Hazards and Earth System Sciences*, **11**, 1351–1370, doi:10.5194/nhess-11-1351-2011.

Dorland, C., R. S. J. Tol, and J. P. Palutikof, 1999: Vulnerability of the Netherlands and Northwest Europe to Storm Damage under Climate Change. *Climatic Change*, **43**, 513–535, doi:10.1023/A:1005492126814.

Duchon, C. E., 1979: Lanczos Filtering in One and Two Dimensions. *Journal of Applied Meteorology*, **18**, 1016–1022, doi:10.1175/1520-0450(1979)0182.0.CO;2.

Eady, E. T., 1949: Long Waves and Cyclone Waves. *Tellus*, **1**, 33–52, doi:10.3402/tellusa.v1i3.8507.

Easterling, D. R., G. A. Meehl, C. Parmesan, S. A. Changnon, T. R. Karl, and L. O. Mearns, 2000: Climate Extremes: Observations, Modeling, and Impacts. *Science*, **289**, 2068–2074, doi:10.1126/science.289.5487.2068.

Eckhardt, S., A. Stohl, H. Wernli, P. James, C. Forster, and N. Spichtinger, 2004: A 15-Year Climatology of Warm Conveyor Belts. *Journal of Climate*, **17**, 218–237, doi:10.1175/1520-0442(2004)017¡0218:AYCOWC¿2.0.CO;2.

Economou, T., D. B. Stephenson, J. G. Pinto, L. C. Shaffrey, and G. Zappa, 2015: Serial clustering of extratropical cyclones in a multi-model ensemble of historical and future simulations. *Quarterly Journal of the Royal Meteorological Society*, **141**, 3076–3087, doi:10.1002/qj.2591.

Eliassen, A. and E. Keinschmidt, 1957: *Dynamic Meteorology. In: Bartels J. (eds) Geophysik II / Geophysics II*. Springer.

Emanuel, K. A., M. Fantini, and A. J. Thorpe, 1987: Baroclinic Instability in an Environment of Small Stability to Slantwise Moist Convection. Part I: Two-Dimensional Models. *Journal of the Atmospheric Sciences*, **44**, 1559–1573, doi:10.1175/1520-0469(1987)044¡1559:BIIAEO¿2.0.CO;2.

Emanuel, K. A. and R. Rotunno, 1989: Polar lows as arctic hurricanes. *Tellus A: Dynamic Meteorology and Oceanography*, **41**, 1–17, doi:10.3402/tellusa.v41i1.11817.

Field, P. R. and R. Wood, 2007: Precipitation and Cloud Structure in Midlatitude Cyclones. *Journal of Climate*, **20**, 233–254, doi:10.1175/JCLI3998.1.

Fink, A. H., T. Brücher, V. Ermert, A. Krüger, and J. G. Pinto, 2009: The European storm Kyrill in January 2007: synoptic evolution, meteorological impacts and some considerations with respect to climate change. *Natural Hazards and Earth System Sciences*, **9**, 405–423, doi:10.5194/nhess-9-405-2009.

Fink, A. H., S. Pohle, J. G. Pinto, and P. Knippertz, 2012: Diagnosing the influence of diabatic processes on the explosive deepening of extratropical cyclones. *Geophysical Research Letters*, **39**, doi:10.1029/2012GL051025.

Franzke, C., T. Woollings, and O. Martius, 2011: Persistent circulation regimes and preferred regime transitions in the North Atlantic. *Journal of the Atmospheric Sciences*, **68**, 2809–2825.

Gelaro, R., W. McCarty, M. J. Suárez, R. Todling, A. Molod, L. Takacs, C. A. Randles, A. Darmenov, M. G. Bosilovich, R. Reichle, K. Wargan, L. Coy, R. Cullather, C. Draper, S. Akella, V. Buchard, A. Conaty, A. M. da Silva, W. Gu, G.-K. Kim, R. Koster, R. Lucchesi, D. Merkova, J. E. Nielsen, G. Partyka, S. Pawson, W. Putman, M. Rienecker, S. D. Schubert, M. Sienkiewicz, and B. Zhao, 2017a: The Modern-Era Retrospective Analysis for Research and Applications, Version 2 (MERRA-2). *Journal of Climate*, **30**, 5419–5454, doi:10.1175/JCLI-D-16-0758.1.

— 2017b: The Modern-Era Retrospective Analysis for Research and Applications, Version 2 (MERRA-2). *Journal of Climate*, **30**, 5419–5454, doi:10.1175/JCLI-D-16-0758.1.

Gibson, J. K., P. Kållberg, S. Uppala, A. Hernandez, A. Nomura, and E. Serrano, 1997: ERA description. ECMWF Re-Analysis Project Report Series 1, ECMWF. *European Centre for Medium-Range Weather Forecasts*, 77.

Gill, A. E., 1982: *Atmosphere-Ocean Dynamics*. Academic Press.

Gómara, I., J. G. Pinto, T. Woollings, G. Masato, P. Zurita-Gotor, and B. Rodríguez-Fonseca, 2014a: Rossby wave-breaking analysis of explosive cyclones in the Euro-Atlantic sector. *Quarterly Journal of the Royal Meteorological Society*, **140**, 738–753.

Gómara, I., B. Rodríguez-Fonseca, P. Zurita-Gotor, and J. G. Pinto, 2014b: On the relation between explosive cyclones affecting Europe and the North Atlantic Oscillation. *Geophysical Research Letters*, **41**, 2182–2190, doi:10.1002/2014GL059647.

Gray, S. L. and H. F. Dacre, 2006: Classifying dynamical forcing mechanisms using a climatology of extratropical cyclones. *Quarterly Journal of the Royal Meteorological Society*, **132**, 1119–1137, doi:10.1256/qj.05.69.

Hand, W. H., N. I. Fox, and C. G. Collier, 2004: A study of twentieth-century extreme rainfall events in the United Kingdom with implications for forecasting. *Meteorological Applications*, **11**, 15–31, doi:10.1017/S1350482703001117.

Hanley, J. and R. Caballero, 2012: The role of large-scale atmospheric flow and Rossby wave breaking in the evolution of extreme windstorms over Europe. *Geophysical Research Letters*, **39**, doi:10.1029/2012GL053408.

Harrold, T. W., 1973: Mechanisms influencing the distribution of precipitation within baroclinic disturbances. *Quarterly Journal of the Royal Meteorological Society*, **99**, 232–251, doi:10.1002/qj.49709942003.

Hawcroft, M., L. Shaffrey, K. Hodges, and H. Dacre, 2012: How much Northern Hemisphere precipitation is associated with extratropical cyclones? *Geophysical Research Letters*, **39**.

Hawcroft, M. K., L. C. Shaffrey, K. I. Hodges, and H. F. Dacre, 2016: Can climate models represent the precipitation associated with extratropical cyclones? *Climate Dynamics*, **47**, 679–695, doi:10.1007/s00382-015-2863-z.

Haylock, M. R., 2011: European extra-tropical storm damage risk from a multi-model ensemble of dynamically-downscaled global climate models. *Natural Hazards and Earth System Sciences*, **11**, 2847–2857, doi:10.5194/nhess-11-2847-2011.

Haynes, P. H. and M. E. McIntyre, 1987: On the Evolution of Vorticity and Potential Vorticity in the Presence of Diabatic Heating and Frictional or Other Forces. *Journal of the Atmospheric Sciences*, **44**, 828–841, doi:10.1175/1520-0469(1987)044¡0828:OTEOVA¿2.0.CO;2.

Heneka, P., T. Hofherr, B. Ruck, and C. Kottmeier, 2006: Winter storm risk of residential structures - model development and application to the German state of Baden-Württemberg. *Natural Hazards and Earth System Sciences*, **6**, 721–733, doi:10.5194/nhess-6-721-2006.

Heneka, P. and B. Ruck, 2008: A damage model for the assessment of storm damage to buildings. *Engineering Structures*, **30**, 3603 – 3609, doi:https://doi.org/10.1016/j.engstruct.2008.06.005.

Heo, K.-Y., Y.-W. Seo, K.-J. Ha, K.-S. Park, J. Kim, J.-W. Choi, K. Jun, and J.-Y. Jeong, 2015: Development mechanisms of an explosive cyclone over East Sea on 3–4 April 2012. *Dynamics of Atmospheres and Oceans*, **70**, 30 – 46, doi:https://doi.org/10.1016/j.dynatmoce.2015.03.001.

Hersbach, H. and D. Dee, 2016: ERA5 reanalysis is in production. *ECMWF newsletter*, **147**, 5–6.

Hewson, T. D., 1998: Objective fronts. *Meteorological Applications*, **5**, 37–65.

Hewson, T. D. and U. Neu, 2015: Cyclones, windstorms and the IMILAST project. *Tellus A: Dynamic Meteorology and Oceanography*, **67**, 27128, doi:10.3402/tellusa.v67.27128.

Hodges, K. I., 1994: A General Method for Tracking Analysis and Its Application to Meteorological Data. *Monthly Weather Review*, **122**, 2573–2586, doi:10.1175/1520-0493(1994)122¡2573:AGMFTA¿2.0.CO;2.

— 1995: Feature Tracking on the Unit Sphere. *Monthly Weather Review*, **123**, 3458–3465, doi:10.1175/1520-0493(1995)123¡3458:FTOTUS¿2.0.CO;2.

— 1999: Adaptive Constraints for Feature Tracking. *Monthly Weather Review*, **127**, 1362–1373, doi:10.1175/1520-0493(1999)127¡1362:ACFFT¿2.0.CO;2.

Hodges, K. I., B. J. Hoskins, J. Boyle, and C. Thorncroft, 2003: A Comparison of Recent Reanalysis Datasets Using Objective Feature Tracking: Storm Tracks and Tropical Easterly Waves. *Monthly Weather Review*, **131**, 2012–2037, doi:10.1175/1520-0493(2003)131¡2012:ACORRD¿2.0.CO;2.

Hodges, K. I., R. W. Lee, and L. Bengtsson, 2011: A Comparison of Extratropical Cyclones in Recent Reanalyses ERA-Interim, NASA MERRA, NCEP CFSR, and JRA-25. *Journal of Climate*, **24**, 4888–4906, doi:10.1175/2011JCLI4097.1.

Holton, J., 2004: *An Introduction to Dynamic Meteorology, Fourth Edition*. Elsevier Academic Press.

Hope, P., K. Keay, M. Pook, J. Catto, I. Simmonds, G. Mills, P. McIntosh, J. Risbey, and G. Berry, 2014: A Comparison of Automated Methods of Front Recognition for Climate Studies: A Case Study in Southwest Western Australia. *Monthly Weather Review*, **142**, 343–363, doi:10.1175/MWR-D-12-00252.1.

Hoskins, B. and P. Berrisford, 1988: A Potential Vorticity perspective of the storm of 15–16 October 1987. *Weather*, **43**, 122–129, doi:10.1002/j.1477-8696.1988.tb03890.x.

Hoskins, B. J. and K. I. Hodges, 2002: New Perspectives on the Northern Hemisphere Winter Storm Tracks. *Journal of the Atmospheric Sciences*, **59**, 1041–1061, doi:10.1175/1520-0469(2002)059¡1041:NPOTNH¿2.0.CO;2.

Hoskins, B. J., M. E. McIntyre, and A. W. Robertson, 1985: On the use and significance of isentropic potential vorticity maps. *Quarterly Journal of the Royal Meteorological Society*, **111**, 877–946, doi:10.1002/qj.49711147002.

Hunter, A., D. B. Stephenson, T. Economou, M. Holland, and I. Cook, 2016: New perspectives on the collective risk of extratropical cyclones. *Quarterly Journal of the Royal Meteorological Society*, **142**, 243–256, doi:10.1002/qj.2649.

Huntingford, C., T. Marsh, A. A. Scaife, E. J. Kendon, J. Hannaford, A. L. Kay, M. Lockwood, C. Prudhomme, N. S. Reynard, S. Parry, J. A. Lowe, J. A. Screen, H. C. Ward, M. Roberts, P. A. Stott, V. A. Bell, M. Bailey, A. Jenkins, T. Legg, F. E. L. Otto, N. Massey, N. Schaller, J. Slingo, and M. R. Allen, 2014: Potential influences on the United Kingdom's floods of winter 2013/14. *Nature Climate Change*, **4**, 769–777, doi:10.1038/nclimate2314.

Hurrell, J. W., Y. Kushnir, G. Ottersen, and M. Visbeck, 2003: An overview of the North Atlantic Oscillation. *The North Atlantic Oscillation: Climatic Significance and Environmental Impact (eds J. W. Hurrell, Y. Kushnir, G. Ottersen and M. Visbeck)*, American Geophysical Union, Washington, D. C.

Iwabe, C. M. N. and R. P. da Rocha, 2009: An event of stratospheric air intrusion and its associated secondary surface cyclogenesis over the South Atlantic Ocean. *Journal of Geophysical Research: Atmospheres*, **114**, doi:10.1029/2008JD011119.

Jenkner, J., M. Sprenger, I. Schwenk, C. Schwierz, S. Dierer, and D. Leuenberger, 2010: Detection and climatology of fronts in a high-resolution model reanalysis over the Alps. *Meteorological Applications*, **17**, 1–18, doi:10.1002/met.142.

Johns, T. C., C. F. Durman, H. T. Banks, M. J. Roberts, A. J. McLaren, J. K. Ridley, C. A. Senior, K. D. Williams, A. Jones, G. J. Rickard, S. Cusack, W. J. Ingram, M. Crucifix, D. M. H. Sexton, M. M. Joshi, B.-W. Dong, H. Spencer, R. S. R. Hill, J. M. Gregory, A. B. Keen, A. K. Pardaens, J. A. Lowe, A. Bodas-Salcedo, S. Stark, and Y. Searl, 2006a: The New Hadley Centre Climate Model (HadGEM1): Evaluation of Coupled Simulations. *Journal of Climate*, **19**, 1327–1353, doi:10.1175/JCLI3712.1.

— 2006b: The New Hadley Centre Climate Model (HadGEM1): Evaluation of Coupled Simulations. *Journal of Climate*, **19**, 1327–1353, doi:10.1175/JCLI3712.1.

Joly, A. and A. J. Thorpe, 1990a: Frontal instability generated by tropospheric potential vorticity anomalies. *Quarterly Journal of the Royal Meteorological Society*, **116**, 525–560.

— 1990b: Frontal instability generated by tropospheric potential vorticity anomalies. *Quarterly Journal of the Royal Meteorological Society*, **116**, 525–560, doi:10.1002/qj.49711649302.

Karremann, M. K., 2015: *Return periods and clustering of potential losses associated with European windstorms in a changing climate*. Ph.D. thesis, Universität zu Köln.

Karremann, M. K., M. L. R. Liberato, P. Ordóñez, and J. G. Pinto, 2016: Characterization of synoptic conditions and cyclones associated with top ranking potential wind loss events over Iberia. *Atmospheric Science Letters*, **17**, 354–361, doi:10.1002/asl.665.

Karremann, M. K., J. G. Pinto, M. Reyers, and M. Klawa, 2014a: Return periods of losses associated with European windstorm series in a changing climate. *Environmental Research Letters*, **9**, 124016, doi:10.1088/1748-9326/9/12/124016.

Karremann, M. K., J. G. Pinto, P. J. von Bomhard, and M. Klawa, 2014b: On the clustering of winter storm loss events over Germany. *Natural Hazards and Earth System Sciences*, **14**, 2041–2052, doi:10.5194/nhess-14-2041-2014.

Kaspi, Y. and T. Schneider, 2013: The Role of Stationary Eddies in Shaping Midlatitude Storm Tracks. *Journal of the Atmospheric Sciences*, **70**, 2596–2613, doi:10.1175/JAS-D-12-082.1.

Kendon, M. and M. McCarthy, 2015: The UK's wet and stormy winter of 2013/2014. *Weather*, **70**, 40–47, doi:10.1002/wea.2465.

Klawa, M. and U. Ulbrich, 2003: A model for the estimation of storm losses and the identification of severe winter storms in Germany. *Natural Hazards and Earth System Sciences*, **3**, 725–732, doi:10.5194/nhess-3-725-2003.

Kobayashi, S., Y. Ota, Y. Harada, A. Ebita, M. Moriya, H. Onoda, K. Onogi, H. Kamahori, C. Kobayashi, H. Endo, K. Miyaoka, and K. Takahashi, 2015a: The JRA-55 Reanalysis: General Specifications and Basic Characteristics. *Journal of the Meteorological Society of Japan. Ser. II*, **93**, 5–48, doi:10.2151/jmsj.2015-001.

— 2015b: The JRA-55 Reanalysis: General Specifications and Basic Characteristics. *Journal of the Meteorological Society of Japan*, **93**, 5–48, doi:10.2151/jmsj.2015-001.

Kunz, T., K. Fraedrich, and F. Lunkeit, 2009: Synoptic scale wave breaking and its potential to drive NAO-like circulation dipoles: A simplified GCM approach. *Quarterly Journal of the Royal Meteorological Society*, **135**, 1–19, doi:10.1002/qj.351.

Kuo, Y.-H., M. A. Shapiro, and E. G. Donall, 1991: The Interaction between Baroclinic and Diabatic Processes in a Numerical Simulation of a Rapidly Intensifying Extratropical Marine Cyclone. *Monthly Weather Review*, **119**, 368–384, doi:10.1175/1520-0493(1991)119¡0368:TIBBAD¿2.0.CO;2.

Kvamstø, N. G., Y. Song, I. A. Seierstad, A. Sorteberg, and D. B. Stephenson, 2008: Clustering of cyclones in the ARPEGE general circulation model. *Tellus, Series A: Dynamic Meteorology and Oceanography*, **60 A**, 547–556, doi:10.1111/j.1600-0870.2008.00307.x.

Lamb, H. H., 1991: *Historic Storms of the North Sea, British Isles and Northwest Europe*. Cambridge University Press.

Leckebusch, G. C., B. Koffi, U. Ulbrich, J. G. Pinto, T. Spangehl, and S. Zacharias, 2006: Analysis of frequency and intensity of European winter storm events from a multi-model perspective, at synoptic and regional scales. *Climate Research*, **31**, 59–74, doi:10.3354/cr031059.

Leckebusch, G. C., D. Renggli, and U. Ulbrich, 2008: Development and application of an objective storm severity measure for the Northeast Atlantic region. *Meteorologische Zeitschrift*, **17**, 575–587, doi:doi:10.1127/0941-2948/2008/0323.

Leckebusch, G. C., U. Ulbrich, L. Fröhlich, and J. G. Pinto, 2007: Property loss potentials for European midlatitude storms in a changing climate. *Geophysical Research Letters*, **34**, doi:10.1029/2006GL027663, l05703.

Ludwig, P., J. G. Pinto, S. A. Hoepp, A. H. Fink, and S. L. Gray, 2015: Secondary Cyclogenesis along an Occluded Front Leading to Damaging Wind Gusts: Windstorm Kyrill, January 2007. *Monthly Weather Review*, **143**, 1417–1437, doi:10.1175/MWR-D-14-00304.1.

Mailier, P. J., 2007: *Serial clustering of extratropical cyclones*. Ph.D. thesis, University of Reading.

Mailier, P. J., D. B. Stephenson, C. A. T. Ferro, and K. I. Hodges, 2006: Serial Clustering of Extratropical Cyclones. *Monthly Weather Review*, **134**, 2224–2240, doi:10.1175/MWR3160.1.

Martin, G. M., M. A. Ringer, V. D. Pope, A. Jones, C. Dearden, and T. J. Hinton, 2006: The Physical Properties of the Atmosphere in the New Hadley Centre Global Environmental Model (HadGEM1). Part I: Model Description and Global Climatology. *Journal of Climate*, **19**, 1274–1301, doi:10.1175/JCLI3636.1.

Martínez-Alvarado, O., L. H. Baker, S. L. Gray, J. Methven, and R. S. Plant, 2014: Distinguishing the Cold Conveyor Belt and Sting Jet Airstreams in an Intense Extratropical Cyclone. *Monthly Weather Review*, **142**, 2571–2595, doi:10.1175/MWR-D-13-00348.1.

Masato, G., B. J. Hoskins, and T. Woollings, 2013: Wave-Breaking Characteristics of Northern Hemisphere Winter Blocking: A Two-Dimensional Approach. *Journal of Climate*, **26**, 4535–4549, doi:10.1175/JCLI-D-12-00240.1.

Matthews, T., C. Murphy, R. L. Wilby, and S. Harrigan, 2014: Stormiest winter on record for Ireland and UK. *Nature Climate Change*, **4**, 738–740, doi:10.1038/nclimate2336.

McGinley, J., 1982: A Diagnosis of Alpine Lee Cyclogenesis. *Monthly Weather Review*, **110**, 1271–1287, doi:10.1175/1520-0493(1982)110¡1271:ADOALC¿2.0.CO;2.

McIntyre, M. E. and T. Palmer, 1983: Breaking planetary waves in the stratosphere. *Nature*, **305**, 593.

Messori, G. and R. Caballero, 2015: On double Rossby wave breaking in the North Atlantic. *Journal of Geophysical Research: Atmospheres*, **120**.

Messori, G., P. Davini, M. C. Alvarez-Castro, F. S. R. Pausata, P. Yiou, and R. Caballero, 2018: On the low-frequency variability of wintertime Euro-Atlantic planetary wave-breaking. *Climate Dynamics*, doi:10.1007/s00382-018-4373-2.

Mitchell-Wallace, K., M. Jones, J. Hilier, and M. Foote, 2017: *Natural Catastrophe Risk Management and Modelling: A Practitioners Guide*. John Wiley and Sons Ltd.

Munich Re, 1993: Winter storms in Europe (I): Analysis of 1990 losses and future loss potential. Technical report, München: Münchener Rückversicherungs-Gesellschaft.

— 2002: Winter storms in Europe (II): Analysis of 1999 losses and loss potentials. Technical report, München: Münchener Rückversicherungs-Gesellschaft.

— 2015: Loss events in Europe 1980-2014: 10 costliest winter storms ordered by insured losses. Technical report, Münchener Rückversicherungs-Gesellschaft, Geo Risks Research, NatCatSERVICE.

— 2016: Loss events in Europe 1980-2015: 10 costliest winter storms ordered by insured losses. Technical report, Münchener Rückversicherungs-Gesellschaft, Geo Risks Research, NatCatSERVICE.

Murnane, R. J. and J. B. Elsner, 2012: Maximum wind speeds and US hurricane losses. *Geophysical Research Letters*, **39**, doi:10.1029/2012GL052740.

Murray, R. J. and I. Simmonds, 1991a: A numerical scheme for tracking cyclone centres from digital data. Part 2: application to January and July general circulation models. *Australian Meteorological Magazine*, **39**, 167–180.

— 1991b: A numerical scheme for tracking cyclone centres from digital data. Part I: Development and operation of the scheme. *Australian Meteorological Magazine*, **39**, 155–166, doi:10.1175/JCLI4203.1.

Nakamura, M. and R. A. Plumb, 1994: The Effects of Flow Asymmetry on the Direction of Rossby Wave Breaking. *Journal of the Atmospheric Sciences*, **51**, 2031–2045, doi:10.1175/1520-0469(1994)051¡2031:TEOFAO¿2.0.CO;2.

Neu, U., M. G. Akperov, N. Bellenbaum, R. Benestad, R. Blender, R. Caballero, A. Cocozza, H. F. Dacre, Y. Feng, K. Fraedrich, J. Grieger, S. Gulev, J. Hanley, T. Hewson, M. Inatsu, K. Keay, S. F. Kew, I. Kindem, G. C. Leckebusch, M. L. R. Liberato, P. Lionello, I. I. Mokhov, J. G. Pinto, C. C. Raible, M. Reale, I. Rudeva, M. Schuster, I. Simmonds, M. Sinclair, M. Sprenger, N. D. Tilinina, I. F. Trigo, S. Ulbrich, U. Ulbrich, X. L. Wang, and H. Wernli, 2013: Imilast: A community effort to intercompare extratropical cyclone detection and tracking algorithms. *Bulletin of the American Meteorological Society*, **94**, 529–547, doi:10.1175/BAMS-D-11-00154.1.

Novak, L., M. H. P. Ambaum, and R. Tailleux, 2015: The Life Cycle of the North Atlantic Storm Track. *Journal of the Atmospheric Sciences*, **72**, 821–833, doi:10.1175/JAS-D-14-0082.1.

Osborn, T. J., 2011: Winter 2009/2010 temperatures and a record-breaking North Atlantic Oscillation index. *Weather*, **66**, 19–21, doi:10.1002/wea.660.

Palutikof, J. P. and A. R. Skellern, 1991: Storm severity over Britain: a report to Commercial Union. Technical report, Climatic Research Unit, University of East Anglia, Norwich.

Pantillon, F., P. Knippertz, and U. Corsmeier, 2017: Revisiting the synoptic-scale predictability of severe European winter storms using ECMWF ensemble reforecasts. *Natural Hazards and Earth System Sciences*, **17**, 1795–1810, doi:10.5194/nhess-17-1795-2017.

Papritz, L., S. Pfahl, I. Rudeva, I. Simmonds, H. Sodemann, and H. Wernli, 2014: The Role of Extratropical Cyclones and Fronts for Southern Ocean Freshwater Fluxes. *Journal of Climate*, **27**, 6205–6224, doi:10.1175/JCLI-D-13-00409.1.

Parker, D. J., 1998: Secondary frontal waves in the North Atlantic region: A dynamical perspective of current ideas. *Quarterly Journal of the Royal Meteorological Society*, **124**, 829–856, doi:10.1002/qj.49712454709.

Pearce, R., D. Lloyd, and D. McConnell, 2001: The post-Christmas 'French' storms of 1999. *Weather*, **56**, 81–91, doi:10.1002/j.1477-8696.2001.tb06541.x.

Peixoto, J. P. and A. H. Oort, 1992: Physics of climate.

Pelly, J. and B. Hoskins, 2003: A New Perspective on Blocking. *Journal of the Atmospheric Sciences*, **60**, 743–755.

Petterssen, S., G. E. Dunn, and L. L. Means, 1955: Report of an Experiement in Forecasting of Cyclone Development. *Journal of Meteorology*, **12**, 58–67, doi:10.1175/1520-0469(1955)012¡0058:ROAEIF¿2.0.CO;2.

Petterssen, S. and S. J. Smebye, 1971: On the development of extratropical cyclones. *Quarterly Journal of the Royal Meteorological Society*, **97**, 457–482, doi:10.1002/qj.49709741407.

Pfahl, S. and H. Wernli, 2012: Quantifying the Relevance of Cyclones for Precipitation Extremes. *Journal of Climate*, **25**, 6770–6780, doi:10.1175/JCLI-D-11-00705.1.

Pinto, J. G., N. Bellenbaum, M. K. Karremann, and P. M. Della-Marta, 2013: Serial clustering of extratropical cyclones over the North Atlantic and Europe under recent and future climate conditions. *Journal of Geophysical Research: Atmospheres*, **118**, 12476–12485, doi:10.1002/2013JD020564.

Pinto, J. G., E. Fröhlich, G. Leckebusch, and U. Ulbrich, 2007: Changing European storm loss potentials under modified climate conditions according to ensemble simulations of the ECHAM5/MPI-OM1 GCM. *Natural Hazards and Earth System Science*, **7**, 165–175.

Pinto, J. G., I. Gómara, G. Masato, H. F. Dacre, T. Woollings, and R. Caballero, 2014: Large-scale dynamics associated with clustering of extratropical cyclones affecting Western Europe. *Journal of Geophysical Research: Atmospheres*, **119**, 13,704–13,719, doi:10.1002/2014JD022305.

Pinto, J. G., M. K. Karremann, K. Born, P. M. Della-Marta, and M. Klawa, 2012: Loss potentials associated with European windstorms under future climate conditions. *Climate Research*, **54**, 1–20, doi:10.3354/cr01111.

Pinto, J. G., T. Spangehl, U. Ulbrich, and P. Speth, 2005: Sensitivities of a cyclone detection and tracking algorithm: individual tracks and climatology. *Meteorologische Zeitschrift*, **14**, 823–838.

Pinto, J. G., S. Ulbrich, T. Economou, D. B. Stephenson, M. K. Karremann, and L. C. Shaffrey, 2016: Robustness of serial clustering of extratropical cyclones to the choice of tracking method. *Tellus A: Dynamic Meteorology and Oceanography*, **68**, 32204, doi:10.3402/tellusa.v68.32204.

Pinto, J. G., S. Zacharias, A. H. Fink, G. C. Leckebusch, and U. Ulbrich, 2009: Factors contributing to the development of extreme North Atlantic cyclones and their relationship with the NAO. *Climate dynamics*, **32**, 711–737.

Plant, R., G. C. Craig, and S. Gray, 2003: On a threefold classification of extratropical cyclogenesis. *Quarterly Journal of the Royal Meteorological Society*, **129**, 2989–3012.

Powell, M. D. and T. A. Reinhold, 2007: Tropical Cyclone Destructive Potential by Integrated Kinetic Energy. *Bulletin of the American Meteorological Society*, **88**, 513–526, doi:10.1175/BAMS-88-4-513.

Prahl, B. F., D. Rybski, O. Burghoff, and J. P. Kropp, 2015: Comparison of storm damage functions and their performance. *Natural Hazards and Earth System Sciences*, **15**, 769–788, doi:10.5194/nhess-15-769-2015.

Prahl, B. F., D. Rybski, J. P. Kropp, O. Burghoff, and H. Held, 2012: Applying stochastic small-scale damage functions to German winter storms. *Geophysical Research Letters*, **39**, doi:10.1029/2012GL050961.

Prettenthaler, Franz and Albrecher, Hansjörg and Köberl, Judith and Kortschak, Dominik, 2012: Risk and insurability of storm damages to residential buildings in austria. *The Geneva Papers on Risk and Insurance - Issues and Practice*, **37**, 340–364, doi:10.1057/gpp.2012.15.

Priestley, M. D. K., H. F. Dacre, L. C. Shaffrey, K. I. Hodges, and J. G. Pinto, 2018: The role of serial European windstorm clustering for extreme seasonal losses as determined from multi-centennial simulations of high-resolution global climate model data. *Natural Hazards and Earth System Sciences*, **18**, 2991–3006, doi:10.5194/nhess-18-2991-2018.

Priestley, M. D. K., H. F. Dacre, L. C. Shaffrey, S. Schemm, and J. G. Pinto, 2019: The Role of Secondary Cyclones and Cyclone Families for the North Atlantic Storm Track and Clustering over Western Europe. *Quarterly Journal of the Royal Meteorological Society*.

Priestley, M. D. K., J. G. Pinto, H. F. Dacre, and L. C. Shaffrey, 2017a: Rossby wave breaking, the upper level jet, and serial clustering of extratropical cyclones in western Europe. *Geophysical Research Letters*, **44**, 514–521, doi:10.1002/2016GL071277.

— 2017b: The role of cyclone clustering during the stormy winter of 2013/2014. *Weather*, **72**, 187–192, doi:10.1002/wea.3025.

Raible, C. C., P. M. Della-Marta, C. Schwierz, H. Wernli, and R. Blender, 2008: Northern Hemisphere Extratropical Cyclones: A Comparison of Detection and Tracking Methods and Different Reanalyses. *Monthly Weather Review*, **136**, 880–897, doi:10.1175/2007MWR2143.1.

Raschke, M., 2015: Statistical detection and modeling of the over-dispersion of winter storm occurrence. *Natural Hazards and Earth System Sciences*, **15**, 1757–1761, doi:10.5194/nhess-15-1757-2015.

Reed, R. J., 1955: A study of a characteristic type of upper-level frontogenesis. *Journal of Meteorology*, **12**, 226–237, doi:10.1175/1520-0469(1955)012¡0226:ASOACT¿2.0.CO;2.

Renard, R. J. and L. C. Clarke, 1965: Experiments in Numerical Objective Frontal Analysis. *Monthly Weather Review*, **93**, 547–556, doi:10.1175/1520-0493(1965)093¡0547:EINOFA¿2.3.CO;2.

Renfrew, I. A., A. J. Thorpe, and C. H. Bishop, 1997: The role of the environmental flow in the development of secondary frontal cyclones. *Quarterly Journal of the Royal Meteorological Society*, **123**, 1653–1675.

Revell, M. J. and R. N. Ridley, 1995: The origin and evolution of low-level potential vorticity anomalies during a case of Tasman Sea cyclogenesis. *Tellus A*, **47**, 779–796, doi:10.1034/j.1600-0870.1995.00120.x.

Rhodes, R. I., L. C. Shaffrey, and S. L. Gray, 2015: Can reanalyses represent extreme precipitation over England and Wales? *Quarterly Journal of the Royal Meteorological Society*, **141**, 1114–1120, doi:10.1002/qj.2418.

Rivals, H., J.-P. Cammas, and I. A. Renfrew, 1998: Secondary cyclogenesis: The initiation phase of a frontal wave observed over the eastern Atlantic. *Quarterly Journal of the Royal Meteorological Society*, **124**, 243–268.

Rivière, G., P. Arbogast, K. Maynard, and A. Joly, 2010: The essential ingredients leading to the explosive growth stage of the European wind storm Lothar of Christmas 1999. *Quarterly Journal of the Royal Meteorological Society*, **136**, 638–652, doi:10.1002/qj.585.

Rivière, G. and A. Joly, 2006a: Role of the low-frequency deformation field on the explosive growth of extratropical cyclones at the jet exit. Part I: Barotropic critical region. *Journal of the atmospheric sciences*, **63**, 1965–1981.

— 2006b: Role of the low-frequency deformation field on the explosive growth of extratropical cyclones at the jet exit. Part II: Baroclinic critical region. *Journal of the atmospheric sciences*, **63**, 1982–1995.

Rivière, G. and I. Orlanski, 2007: Characteristics of the Atlantic Storm-Track Eddy Activity and Its Relation with the North Atlantic Oscillation. *Journal of the Atmospheric Sciences*, **64**, 241–266, doi:10.1175/JAS3850.1.

Rivière, G. and I. Orlanski, 2007: Characteristics of the Atlantic Storm-Track Eddy Activity and Its Relation with the North Atlantic Oscillation. *Journal of the Atmospheric Sciences*, **64**, 241–266, doi:10.1175/JAS3850.1.

Roberts, J. F., A. J. Champion, L. C. Dawkins, K. I. Hodges, L. C. Shaffrey, D. B. Stephenson, M. A. Stringer, H. E. Thornton, and B. D. Youngman, 2014: The XWS open access catalogue of extreme European windstorms from 1979 to 2012. *Natural Hazards and Earth System Sciences*, **14**, 2487–2501, doi:10.5194/nhess-14-2487-2014.

Robson, J., I. Polo, D. L. R. Hodson, D. P. Stevens, and L. C. Shaffrey, 2017: Decadal prediction of the North Atlantic subpolar gyre in the HiGEM high-resolution climate model. *Climate Dynamics*, doi:10.1007/s00382-017-3649-2.

Roeckner, E., R. Brokopf, M. Esch, M. Giorgetta, S. Hagemann, L. Kornblueh, E. Manzini, U. Schlese, and U. Schulzweida, 2006: Sensitivity of Simulated Climate to Horizontal and Vertical Resolution in the ECHAM5 Atmosphere Model. *Journal of Climate*, **19**, 3771–3791, doi:10.1175/JCLI3824.1.

Saha, S., S. Moorthi, H.-L. Pan, X. Wu, J. Wang, S. Nadiga, P. Tripp, R. Kistler, J. Woollen, D. Behringer, H. Liu, D. Stokes, R. Grumbine, G. Gayno, J. Wang, Y.-T. Hou, H.-y. Chuang, H.-M. H. Juang, J. Sela, M. Iredell, R. Treadon, D. Kleist, P. Van Delst, D. Keyser, J. Derber, M. Ek, J. Meng, H. Wei, R. Yang, S. Lord, H. van den Dool, A. Kumar, W. Wang, C. Long, M. Chelliah, Y. Xue, B. Huang, J.-K. Schemm, W. Ebisuzaki, R. Lin, P. Xie, M. Chen, S. Zhou, W. Higgins, C.-Z. Zou, Q. Liu, Y. Chen, Y. Han, L. Cucurull, R. W. Reynolds, G. Rutledge, and M. Goldberg, 2010: The NCEP Climate Forecast System Reanalysis. *Bulletin of the American Meteorological Society*, **91**, 1015–1058, doi:10.1175/2010BAMS3001.1.

Scaife, A. A., A. Arribas, E. Blockley, A. Brookshaw, R. T. Clark, N. Dunstone, R. Eade, D. Fereday, C. K. Folland, M. Gordon, L. Hermanson, J. R. Knight, D. J. Lea, C. MacLachlan, A. Maidens, M. Martin, A. K. Peterson, D. Smith, M. Vellinga, E. Wallace, J. Waters, and A. Williams, 2014: Skillful long-range prediction of European and North American winters. *Geophysical Research Letters*, **41**, 2514–2519, doi:10.1002/2014GL059637.

Schär, C. and H. C. Davies, 1990: An Instability of Mature Cold Fronts. *Journal of the Atmospheric Sciences*, **47**, 929–950, doi:10.1175/1520-0469(1990)047¡0929:AIOMCF¿2.0.CO;2.

Schemm, S., I. Rudeva, and I. Simmonds, 2015: Extratropical fronts in the lower troposphere–global perspectives obtained from two automated methods. *Quarterly Journal of the Royal Meteorological Society*, **141**, 1686–1698, doi:10.1002/qj.2471.

Schemm, S. and M. Sprenger, 2015: Frontal-wave cyclogenesis in the North Atlantic – a climatological characterisation. *Quarterly Journal of the Royal Meteorological Society*, **141**, 2989–3005, doi:10.1002/qj.2584.

Schemm, S., M. Sprenger, and H. Wernli, 2018: When during Their Life Cycle Are Extratropical Cyclones Attended by Fronts? *Bulletin of the American Meteorological Society*, **99**, 149–165, doi:10.1175/BAMS-D-16-0261.1.

Schemm, S., H. Wernli, and L. Papritz, 2013: Warm Conveyor Belts in Idealized Moist Baroclinic Wave Simulations. *Journal of the Atmospheric Sciences*, **70**, 627–652, doi:10.1175/JAS-D-12-0147.1.

Schultz, D. M., 2001: Reexamining the Cold Conveyor Belt. *Monthly Weather Review*, **129**, 2205–2225, doi:10.1175/1520-0493(2001)129¡2205:RTCCB¿2.0.CO;2.

Schultz, D. M., D. Keyser, and L. F. Bosart, 1998: The Effect of Large-Scale Flow on Low-Level Frontal Structure and Evolution in Midlatitude Cyclones. *Monthly Weather Review*, **126**, 1767–1791, doi:10.1175/1520-0493(1998)126¡1767:TEOLSF¿2.0.CO;2.

Schultz, D. M. and P. N. Schumacher, 1999: The Use and Misuse of Conditional Symmetric Instability. *Monthly Weather Review*, **127**, 2709–2732, doi:10.1175/1520-0493(1999)127¡2709:TUAMOC¿2.0.CO;2.

Schwierz, C., P. Köllner-Heck, E. Z. Mutter, D. N. Bresch, P. L. Vidale, M. Wild, and C. Schär, 2010: Modelling European winter wind storm losses in current and future climate. *Climatic Change*, **101**, 485–514, doi:10.1007/s10584-009-9712-1.

Serreze, M. C., F. Carse, R. G. Barry, and J. C. Rogers, 1997: Icelandic Low Cyclone Activity: Climatological Features, Linkages with the NAO, and Relationships with Recent Changes in the Northern Hemisphere Circulation. *Journal of Climate*, **10**, 453–464, doi:10.1175/1520-0442(1997)010¡0453:ILCACF¿2.0.CO;2.

Shaffrey, L. C., D. Hodson, J. Robson, D. Stevens, E. Hawkins, I. Polo, I. Stevens, R. T. Sutton, G. Lister, A. Iwi, et al., 2017: Decadal predictions with the HiGEM high resolution global coupled climate model: description and basic evaluation. *Climate Dynamics*, **48**, 297–311, doi:10.1007/s00382-016-3075-x.

Shaffrey, L. C., I. Stevens, W. A. Norton, M. J. Roberts, P. L. Vidale, J. D. Harle, A. Jrrar, D. P. Stevens, M. J. Woodage, M. E. Demory, J. Donners, D. B. Clark, A. Clayton, J. W. Cole, S. S. Wilson, W. M. Connolley, T. M. Davies, A. M. Iwi, T. C. Johns, J. C. King, A. L. New, J. M. Slingo, A. Slingo, L. Steenman-Clark, and G. M. Martin, 2009: U.K. HiGEM: The new U.K. high-resolution global environment model - Model description and basic evaluation. *Journal of Climate*, **22**, 1861–1896, doi:10.1175/2008JCLI2508.1.

Shapiro, M. A. and D. Keyser, 1990: Fronts, jet streams and the tropopause. *Extratropical Cyclones, The Erik Palmen Memorial Volume*, 167–191.

Shutts, G. J., 1990: Dynamical aspects of the october storm, 1987: A study of a successful fine-mesh simulation. *Quarterly Journal of the Royal Meteorological Society*, **116**, 1315–1347, doi:10.1002/qj.49711649604.

Sibley, A., 2010: Analysis of extreme rainfall and flooding in Cumbria 18–20 November 2009. *Weather*, **65**, 287–292, doi:10.1002/wea.672.

Simmonds, I., K. Keay, and J. A. Tristram Bye, 2012: Identification and Climatology of Southern Hemisphere Mobile Fronts in a Modern Reanalysis. *Journal of Climate*, **25**, 1945–1962, doi:10.1175/JCLI-D-11-00100.1.

Simmons, A. J. and B. J. Hoskins, 1978: The Life Cycles of Some Nonlinear Baroclinic Waves. *Journal of the Atmospheric Sciences*, **35**, 414–432, doi:10.1175/1520-0469(1978)035¡0414:TLCOSN¿2.0.CO;2.

Sinclair, M. R., 1994: An objective cyclone climatology for the Southern Hemisphere. *Monthly Weather Review*, **122**, 2239–2256.

Slingo, J., S. Belcher, A. Scaife, M. McCarthy, A. Saulter, K. McBeath, A. Jenkins, C. Huntingford, T. J. Marsh, J. Hannaford, and S. Parry, 2014: The Recent Storms and Floods in the UK. *Met Office UK*, 1–27, doi:10.1038/scientificamerican04051913-315.

Smart, D. J. and K. A. Browning, 2014: Attribution of strong winds to a cold conveyor belt and sting jet. *Quarterly Journal of the Royal Meteorological Society*, **140**, 595–610, doi:10.1002/qj.2162.

Swiss Re, 2016: Misfortune seldom comes alone: Winter Storm clusters in Europe. Technical report, Swiss Reinsurance Company: Zurich.

Thomas, C. M. and D. M. Schultz, 2019: What are the Best Thermodynamic Quantity and Function to Define a Front in Gridded Model Output? *Bulletin of the American Meteorological Society*, **100**, 873–895, doi:10.1175/BAMS-D-18-0137.1.

Thorncroft, C. D. and B. J. Hoskins, 1990: Frontal Cyclogenesis. *Journal of the Atmospheric Sciences*, **47**, 2317–2336, doi:10.1175/1520-0469(1990)047¡2317:FC¿2.0.CO;2.

Thorncroft, C. D., B. J. Hoskins, and M. E. McIntyre, 1993: Two paradigms of baroclinic-wave life-cycle behaviour. *Quarterly Journal of the Royal Meteorological Society*, **119**, 17–55, doi:10.1002/qj.49711950903.

Trenberth, K. E., J. T. Fasullo, and J. Mackaro, 2011: Atmospheric Moisture Transports from Ocean to Land and Global Energy Flows in Reanalyses. *Journal of Climate*, **24**, 4907–4924, doi:10.1175/2011JCLI4171.1.

Turner, A. G. and H. Annamalai, 2012: Climate change and the South Asian summer monsoon. *Nature Climate Change*, **2**, doi:10.1038/nclimate1495.

Čampa, J. and H. Wernli, 2012: A PV Perspective on the Vertical Structure of Mature Midlatitude Cyclones in the Northern Hemisphere. *Journal of the Atmospheric Sciences*, **69**, 725–740, doi:10.1175/JAS-D-11-050.1.

Ulbrich, U., T. Brücher, A. H. Fink, G. C. Leckebusch, A. Krüger, and J. G. Pinto, 2003: The central European floods of August 2002: Part 2 –Synoptic causes and considerations with respect to climatic change. *Weather*, **58**, 434–442, doi:10.1256/wea.61.03B.

Ulbrich, U., A. H. Fink, M. Klawa, and J. G. Pinto, 2001: Three extreme storms over Europe in December 1999. *Weather*, **56**, 70–80, doi:10.1002/j.1477-8696.2001.tb06540.x.

Uppala, S. M., P. W. KÅllberg, A. J. Simmons, U. Andrae, V. D. C. Bechtold, M. Fiorino, J. K. Gibson, J. Haseler, A. Hernandez, G. A. Kelly, X. Li, K. Onogi, S. Saarinen, N. Sokka, R. P. Allan, E. Andersson, K. Arpe, M. A. Balmaseda, A. C. M. Beljaars, L. V. D. Berg, J. Bidlot, N. Bormann, S. Caires, F. Chevallier, A. Dethof, M. Dragosavac, M. Fisher, M. Fuentes, S. Hagemann, E. Hólm, B. J. Hoskins, L. Isaksen, P. A. E. M. Janssen, R. Jenne, A. P. Mcnally, J.-F. Mahfouf, J.-J. Morcrette, N. A. Rayner, R. W. Saunders, P. Simon, A. Sterl, K. E. Trenberth, A. Untch, D. Vasiljevic, P. Viterbo, and J. Woollen, 2005: The ERA-40 re-analysis. *Quarterly Journal of the Royal Meteorological Society*, **131**, 2961–3012, doi:10.1256/qj.04.176.

Vitolo, R., D. B. Stephenson, L. M. Cook, and K. Mitchell-Wallace, 2009: Serial clustering of intense European storms. *Meteorologische Zeitschrift*, **18**, 411–424, doi:10.1127/0941-2948/2009/0393.

Volonté, A., P. A. Clark, and S. L. Gray, 2018: The role of mesoscale instabilities in the sting-jet dynamics of windstorm Tini. *Quarterly Journal of the Royal Meteorological Society*, **144**, 877–899, doi:10.1002/qj.3264.

Walz, M. A., D. J. Befort, N. O. Kirchner-Bossi, U. Ulbrich, and G. C. Leckebusch, 2018: Modelling serial clustering and inter-annual variability of European winter windstorms based on large-scale drivers. *International Journal of Climatology*, **38**, 3044–3057, doi:10.1002/joc.5481.

Walz, M. A., T. Kruschke, H. W. Rust, U. Ulbrich, and G. C. Leckebusch, 2017: Quantifying the extremity of windstorms for regions featuring infrequent events. *Atmospheric Science Letters*, **18**, 315–322, doi:10.1002/asl.758.

Wang, C.-C. and J. C. Rogers, 2001: A Composite Study of Explosive Cyclogenesis in Different Sectors of the North Atlantic. Part I: Cyclone Structure and Evolution. *Monthly Weather Review*, **129**, 1481–1499, doi:10.1175/1520-0493(2001)129¡1481:ACSOEC¿2.0.CO;2.

Wernli, H., 1997: A lagrangian-based analysis of extratropical cyclones. II: A detailed case-study. *Quarterly Journal of the Royal Meteorological Society*, **123**, 1677–1706, doi:10.1002/qj.49712354211.

Wernli, H. and H. C. Davies, 1997: A lagrangian-based analysis of extratropical cyclones. I: The method and some applications. *Quarterly Journal of the Royal Meteorological Society*, **123**, 467–489, doi:10.1002/qj.49712353811.

Wernli, H., S. Dirren, M. A. Liniger, and M. Zillig, 2002: Dynamical aspects of the life cycle of the winter storm 'Lothar' (24–26 December 1999). *Quarterly Journal of the Royal Meteorological Society*, **128**, 405–429, doi:10.1256/003590002321042036.

Wernli, H. and C. Schwierz, 2006: Surface Cyclones in the ERA-40 Dataset (1958–2001). Part I: Novel Identification Method and Global Climatology. *Journal of the Atmospheric Sciences*, **63**, 2486–2507, doi:10.1175/JAS3766.1.

Whittaker, L. M. and L. H. Horn, 1984: Northern Hemisphere extratropical cyclone activity for four mid-season months. *Journal of Climatology*, **4**, 297–310, doi:10.1002/joc.3370040307.

Wild, S., D. J. Befort, and G. C. Leckebusch, 2015: Was the Extreme Storm Season in Winter 2013/14 Over the North Atlantic and the United Kingdom Triggered by Changes in the West Pacific Warm Pool? *Bulletin of the American Meteorological Society*, **96**, S29–S34, doi:10.1175/BAMS-D-15-00118.1.

Woollings, T., 2010: Dynamical influences on European climate: an uncertain future. *Philosophical Transactions of the Royal Society of London A: Mathematical, Physical and Engineering Sciences*, **368**, 3733–3756, doi:10.1098/rsta.2010.0040.

Woollings, T., A. Hannachi, and B. Hoskins, 2010a: Variability of the North Atlantic eddy-driven jet stream. *Quarterly Journal of the Royal Meteorological Society*, **136**, 856–868, doi:10.1002/qj.625.

Woollings, T., B. Hoskins, M. Blackburn, and P. Berrisford, 2008: A New Rossby Wave–Breaking Interpretation of the North Atlantic Oscillation. *Journal of the Atmospheric Sciences*, **65**, 609–626, doi:10.1175/2007JAS2347.1.

Woollings, T., B. Hoskins, M. Blackburn, D. Hassell, and K. Hodges, 2010b: Storm track sensitivity to sea surface temperature resolution in a regional atmosphere model. *Climate Dynamics*, **35**, 341–353, doi:10.1007/s00382-009-0554-3.

Zahn, M. and H. von Storch, 2008: A long-term climatology of North Atlantic polar lows. *Geophysical Research Letters*, **35**, doi:10.1029/2008GL035769.

Zappa, G., L. Shaffrey, and K. Hodges, 2014: Can Polar Lows be Objectively Identified and Tracked in the ECMWF Operational Analysis and the ERA-Interim Reanalysis? *Monthly Weather Review*, **142**, 2596–2608, doi:10.1175/MWR-D-14-00064.1.

Zappa, G., L. C. Shaffrey, and K. I. Hodges, 2013a: The Ability of CMIP5 Models to Simulate North Atlantic Extratropical Cyclones. *Journal of Climate*, **26**, 5379–5396, doi:10.1175/JCLI-D-12-00501.1.

Zappa, G., L. C. Shaffrey, K. I. Hodges, P. G. Sansom, and D. B. Stephenson, 2013b: A multimodel assessment of future projections of north atlantic and european extratropical cyclones in the CMIP5 climate models. *Journal of Climate*, **26**, 5846–5862, doi:10.1175/JCLI-D-12-00573.1.